2018

EXPERIMENTAL AND COMPUTATIONAL INVESTIGATION OF DUAL FUEL DIESEL- NATURAL GAS RCCI COMBUSTION IN A HEAVY-DUTY DIESEL ENGINE

Mufaddel Dahodwala
Michigan Technological University, mzdahodw@mtu.edu

EXPERIMENTAL AND COMPUTATIONAL INVESTIGATION OF DUAL FUEL DIESEL- NATURAL GAS RCCI COMBUSTION IN A HEAVY-DUTY DIESEL ENGINE

By

Mufaddel Z. Dahodwala

A DISSERTATION

Submitted in partial fulfillment of the requirements for the degree of

DOCTOR OF PHILOSOPHY

In Mechanical Engineering–Engineering Mechanics

MICHIGAN TECHNOLOGICAL UNIVERSITY

2018

This dissertation has been approved in partial fulfillment of the requirements for the Degree of DOCTOR OF PHILOSOPHY in Mechanical Engineering–Engineering Mechanics.

Department of Mechanical Engineering–Engineering Mechanics

Dissertation Advisor:	*Dr. Jeffrey Naber*
Committee Member:	*Dr. Dean Tomazic*
Committee Member:	*Dr. Mahdi Shahbhakti*
Committee Member:	*Dr. Darrell Robinette*
Department Chair:	*Dr. William Predebon.*

Dedication

I would like dedicate this dissertation to my family, especially my wife Fatema, my beautiful children – Jumana and Insiyah, and my parents Zohar and Nafisa Dahodwala, for their unconditional support and encouragement throughout this challenging yet exciting journey. They have all played a key role in completion of this dissertation. Words cannot express my gratitude for their love and support.

Table of Contents

List of figures

List of tables

Author contribution statement

I would like to acknowledge the contribution of my colleagues from FEV North America Inc., Erik Koehler and Satyum Joshi in writing and review of two SAE papers - 2014-01-1308 and 2015-01-0849, which are part of this dissertation. I would also like to thank the other co-authors and all FEV colleagues who took the time to review the two SAE papers and provided valuable feedback.

Acknowledgements

I would like to take this opportunity to thank all individuals and institutions that have supported me in completing my dissertation.

To begin with I would like to express my deepest appreciation and gratitude to my advisor Dr. Jeffrey Naber for providing me with the opportunity and continuous support to pursue this online PhD degree. Without his guidance and support this thesis would not have been possible. I would also like to thank Dr. Dean Tomazic for his support and inputs through the research process. I would like to thank Dr. Mahdi Shahbhakti and Dr. Darrell Robinette for being part of my research committee.

I would also like to thank FEV North America, Inc. management for encouraging this research effort and providing the resources necessary to accomplish the testing and computational studies. Special appreciation goes out to my colleagues from FEV North America Inc., Erik Koehler, Satyum Joshi and Vinay Nagaraju for devoting their time and effort in developing and executing test plans along with their support in review and analysis of testing data.

I would also like to acknowledge the support that was received from Converge Science in developing the CFD models for the computational studies along with the opportunity to present some of the computational results in a user group conference held in Wisconsin Madison in 2014. Again special mention goes out to my colleague Satyum Joshi who also helped in development of the baseline CFD models for this study.

I would also like to take this opportunity to acknowledge the guiding influence of my previous advisor Dr. Naeim Henein under whom I completed my Master's Thesis at Wayne State University. His guidance during my early research days laid the foundation on which I have been able to complete this dissertation.

Finally I would like thank my family members and friends for their continuous support and encouragement.

List of abbreviations

AC	Alternating Current
AHRR	Apparent Heat Release Rate
AMR	Adaptive Mesh Refinement
BMEP	Brake Mean Effective Pressure
BSFC	Brake Specific Fuel Consumption
BTE	Brake Thermal Efficiency
bTDC	Before Top Dead Center
CA	Crank Angle
CH4	Methane
CA10	Crank Angle for 10 % mass fraction burned
CA50	Crank Angle for 50 % mass fraction burned
CA10-90	10-90% mass fraction burned
CI	Compression Ignition
CFD	Computational Fluid Dynamics
CNG	Compressed Natural Gas
CR	Compression Ratio
CO	Carbon Monoxide
CO2	Carbon Dioxide
COV	Coefficient of Variance
DOC	Diesel Oxidation Catalyst
DPF	Diesel Particulate Filter
ECU	Engine Control Unit
EGR	Exhaust Gas Recirculation
EIA	Energy Information Administration
EPA	Environmental Protection Agency
FTP	Federal Test Procedure
GHG	Green House Gas
HD	Heavy-Duty
HRR	Heat Release Rate
IMEP	Indicated Mean Effective Pressure
MIRA	Motor Industry Research Association
MPRR	Maximum Pressure Rise Rate
NMHC	Non-Methane Hydrocarbon
NTC	Negative Temperature Coefficient
NO_x	Nitrogen Oxides
LTC	Low Temperature Combustion
OBD	On Board Diagnostics
PCP	Peak Cylinder Pressure
PM	Particulate Matter
RCCI	Reactivity Controlled Compression Ignition
RCP	Rapid Controller Prototyping

RMC	Ramped Modal Cycle
SCR	Selective Catalytic Reduction
SI	Spark Ignited
TDC	Top Dead Center
THC	Total Hydrocarbons
VCR	Variable Compression Ratio
WN	Wobbe Number

Abstract

Among the various alternative fuels, natural gas is considered as a leading candidate for heavy-duty applications due to its availability and applicability in conventional internal combustion diesel engines. Compared to their diesel counterparts natural gas fueled spark-ignited engines have a lower power density, reduced low-end torque capability, limited altitude performance, and ammonia emissions downstream of the three-way catalyst. The dual fuel diesel/natural gas engine does not suffer with the performance limitations of the spark-ignited concept due to the flexibility of switching between different fueling modes. Considerable research has already been conducted to understand the combustion behavior of dual fuel diesel/natural gas engines. As reported by most researchers, the major difficulty with dual fuel operation is the challenge of providing high levels of natural gas substitution, especially at low and medium loads.

In this study extensive experimental and simulation studies were conducted to understand the combustion behavior of a heavy-duty diesel engine when operated with compressed natural gas (CNG) in a dual fuel regime. In one of the experimental studies, conducted on a 13 liter heavy-duty six cylinder diesel engine with a compression ratio of 16.7:1, it was found that at part loads high levels of CNG substitution could be achieved along with very low NO_x and PM emissions by applying reactivity controlled compression ignition (RCCI) combustion. When compared to the diesel-only baseline, a 75% reduction in both NO_x and PM emissions was observed at a 5 bar BMEP load point along with comparable fuel consumption values.

Further experimental studies conducted on the 13 liter heavy-duty six cylinder diesel engine have shown that RCCI combustion targeting low NO_x emissions becomes progressively difficult to control as the load is increased at a given speed or the speed is reduced at a given load. To overcome these challenges a number of simulation studies were conducted to quantify the in-cylinder conditions that are needed at high loads and low to medium engine speeds to effectively control low NO_x RCCI combustion. A number of design parameters were analyzed in this study including exhaust gas recirculation (EGR) rate, CNG substitution, injection strategy, fuel injection pressure, fuel spray angle and compression ratio. The study revealed that lowering the compression ratio was very effective in controlling low NO_x RCCI combustion. By lowering the base compression ratio by 4 points, to 12.7:1, a low NO_x RCCI combustion was achieved at both 12 bar and 20 bar BMEP load points. The NO_x emissions were reduced by 75% at 12 bar BMEP while fuel consumption was improved by 5.5%. For the 20 BMEP case, a 2% improvement in fuel consumption was achieved with an 87.5% reduction in NO_x emissions. At both load points low PM emissions were observed with RCCI combustion.

A low NO_x RCCI combustion system has multiple advantages over other combustion approaches, these include; significantly lower NO_x and PM emission which allows a reduction in aftertreatment cost and packaging requirements along with application of higher CNG substitution rates resulting in reduced CO_2 emissions.

1 Introduction

The majority of the world's primary energy demand is currently being satisfied by fossil fuels. It is well known that fossil fuels, such as the conventional petroleum based liquid fuels, will become scarce within the next few decades [1]. Awareness of limitations of fossil fuels reserves and the fact that burning of fossil fuels is a major contribution to the greenhouse gas (GHG) emission, has led to a growing interest in the use of alternative energy resources for the operation of internal combustion engines. Heavy-duty applications are one of the largest consumers of liquid fuel and the exhaust gas emissions from heavy-duty applications have become an important environmental issue. As such the heavy-duty industry is steadily moving towards alternative fuels to address the issue of dwindling fossil fuel resources. Climate change from increase in GHG emissions along with health problems in populated cities and increasingly stringent emission regulations are also major contributors in the push towards adoption of alternate fuels.

Natural gas is identified as a leading candidate for heavy-duty applications among other alternative fuels. The use of CNG in heavy-duty applications has seen a sharp growth in the last couple of years as reported in studies conducted by the Energy Information Administration (EIA) [1]. EIA studies project CNG consumption in heavy-duty applications to increase at 11.4% per year through 2040. The growth is mainly seen in the off-road market, but other sectors such as on-highway, marine and locomotive are also embracing a switch to CNG. The reasons are its availability and its applicability in conventional internal combustion diesel engines. In addition to an operating cost savings due to a lower price of natural gas relative to diesel, there is also an opportunity to reduce emissions, such as Particulate Matter (PM) and Carbon Dioxide (CO_2) due to the nature of the combustion and the molecular makeup of the fuel – 0.257 gCO_2/kJ of diesel ($C_{12}H_{26}$) vs. 0.058 gCO_2/ KJ of methane (CH_4)

There are two main technology approaches through which CNG can be applied for heavy-duty engines. A common approach for existing diesel engines is to operate in a dual fuel regime where CNG is introduced in to the cylinder along with intake charge. The injected diesel fuel is used to ignite the CNG mixture to achieve the desired load. A second approach considers a dedicated CNG combustion system that requires the addition of an ignition source. The main technological challenges that apply to this type of engine conversion are studied in detail by Ribas [2] and Ouellette [3].

In the case of dual fuel diesel/CNG engines, two types of technologies are currently considered depending on the method used for CNG induction as shown in Figure 1. In the first type, both the diesel fuel and natural gas are directly injected into the combustion chamber using either two separate injectors or a special injector with a dual-concentric needle design [4]. In the second type, natural gas is either fumigated at a single point into the intake path of the engine before or after the turbocharger compressor. The natural gas is premixed with air and EGR or injected at multiple points in the intake port of the

engine. Intake fumigation at single point is the most widely used method of CNG induction for on-highway applications due to its simplicity and cost.

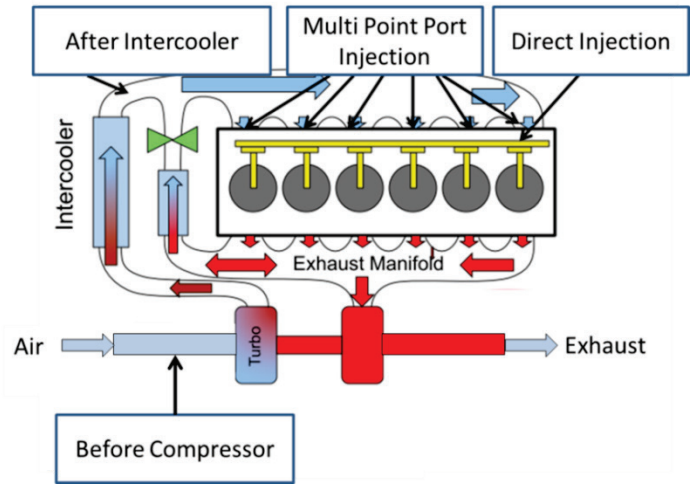

Figure 1 Pathways of Introducing CNG in a Diesel Engine

In dual fuel diesel/natural gas engines with intake fumigation or port injection, the air and natural gas mixture from the intake is drawn into the cylinder during the intake stroke and diesel fuel is injected near the end of the compression stroke. The diesel fuel auto ignites and the corresponding diesel combustion initiates the combustion of the natural gas. This approach is generally referred to as 'conventional' dual fuel combustion. For conventional dual fuel combustion researchers have concluded that a single diesel injection event is sufficient for effectively igniting the premixed natural gas-air mixture [5-11]. However, this approach suffers from very low combustion efficiency at low loads with an increase in CNG substitution. As shown in Figure 2, a deterioration in combustion efficiency from 99.9% to 50% is seen with increase in CNG substitution from 0% to 80% along with significant increase in hydrocarbon and methane (CH_4) emissions. An increase in NO_x emissions was also observed up to 40% CNG substitution, due to reduction in EGR, but then dropped as the combustion efficiency deteriorated. The EGR reduction can be attributed to the richer lambda values observed with increasing CNG substitution as the fresh air charge is displaced with CNG. The high levels of unburned hydrocarbon emissions limit the application of higher CNG substitution levels (>20%) at low loads.

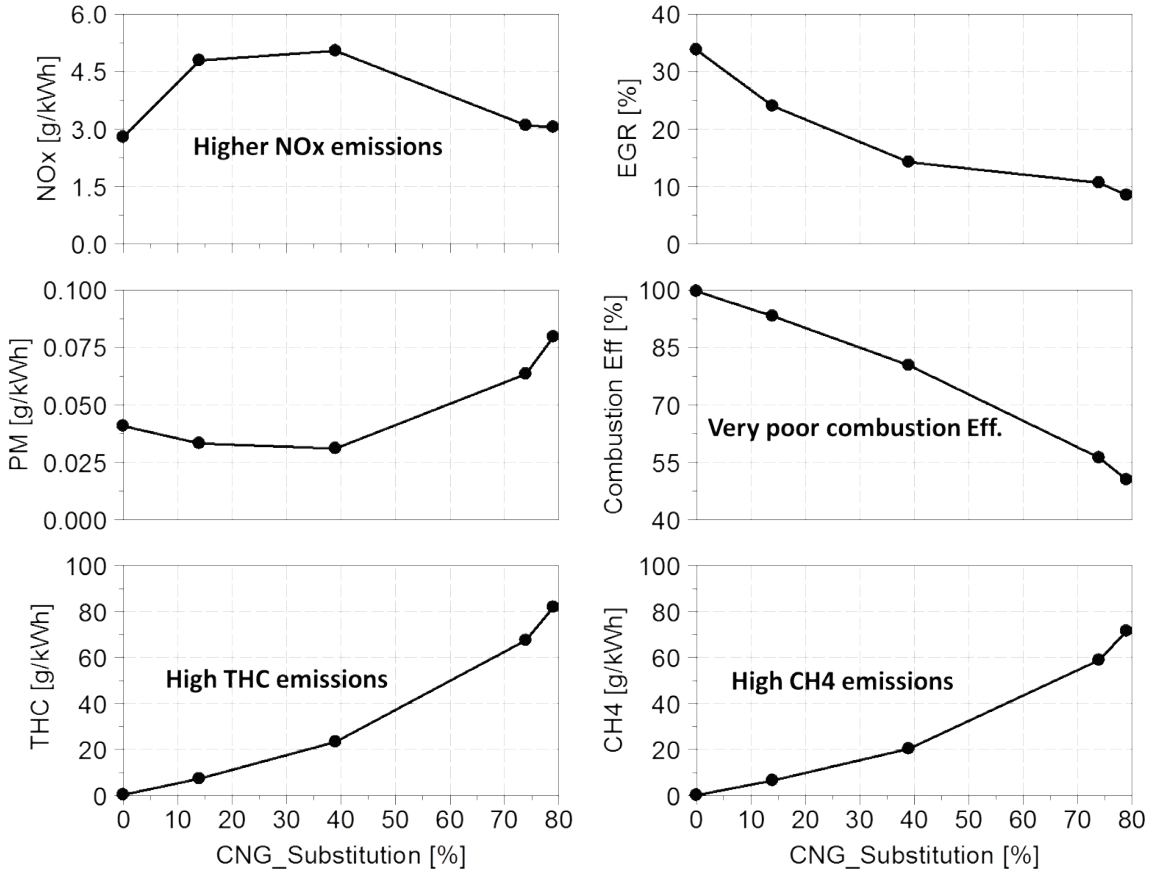

Figure 2 Emissions and performance parameters for dual fuel combustion at 1500 rpm and 5 bar BMEP, plotted against CNG substitution [12]

Recently, researchers [12-27] have explored the possibility of applying advanced diesel injection events to improve the combustion efficiency of the dual fuel diesel/natural gas engines at part load. This strategy has also been evaluated on diesel/gasoline engines and the type of combustion that is achieved has been termed reactivity controlled compression ignition, or RCCI, due to the nature of the reactivity (cetane) distribution achieved within the cylinder [12-27]. RCCI combustion specifically exploits the difference in reactivity between two fuels by introducing the low cetane fuel (natural gas) along with the air during the intake stroke and igniting the air-natural gas mixture by injecting the higher cetane fuel (diesel) later in the compression stroke. Figure 3 highlights the key difference in the combustion and emissions characteristics between conventional dual fuel and RCCI combustion as demonstrated on a heavy-duty diesel engine fueled with diesel and natural gas, as part of this PhD work [12, 17]. As the diesel injection timing is advanced from 7.6° bTDC to 32° bTDC, carbon monoxide (CO) and unburned hydrocarbon emissions increase while the peak cylinder pressure and temperature increase results in higher NO_x emissions. However, with further advancement in timing, beyond 32° bTDC, the heat release rate (HRR) moves closer to TDC. This results in lower peak combustion temperatures and pressures that provide a

sharp reduction in NO_x emissions. As observed by many researchers, this heat release trace is wider with a lower peak and clearly visible two-stage heat release associated with RCCI combustion [12-27].

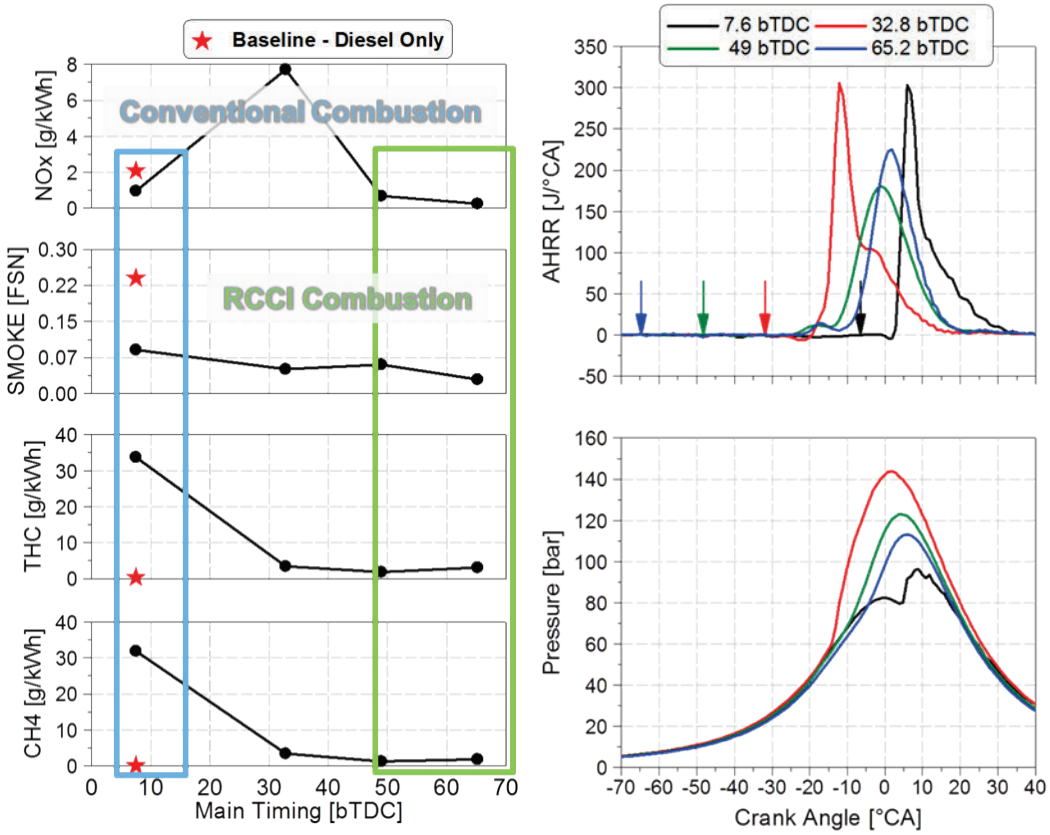

Figure 3 HRR, cylinder pressure, emissions and performance variables at 1500 rpm and 5 bar BMEP for four different main injection timings at 60% substitution [12]

2 Literature Review

A number of studies have been conducted to explore RCCI combustion with diesel natural gas in diesel engines. Table 1 summarizes the main RCCI research with alternative fuels. One of the first studies conducted to explore RCCI combustion in a heavy-duty (HD) compression ignited (CI) engine with diesel-CNG was done by Nieman et al. [13], using the multi-dimensional CFD code KIVA-3V in conjunction with the CHEMKIN chemistry tool, on a 2.44L single cylinder engine. The study was conducted at six operating points to cover the engine operation range, from 4 to 23 bar gross IMEP and 800-1800 rpm engine speed. They employed an in-house optimization algorithm to vary parameters including amount of CNG substitution, diesel injection events and quantity, and EGR rate. The authors demonstrated that, using RCCI combustion strategy low NO_x and soot emissions (below the US 2010 on-road HD certification limit) can be obtained in the complete engine operating map with high combustion efficiencies especially at the mid load points. At higher loads, the combustion efficiency deteriorated due to application of high levels of EGR (>30%) needed to increase ignition delay and at low loads, the low reactivity of CH_4 caused the combustion to be inefficient. Further the authors [13] reported that no EGR was required up to 13.5 bar IMEP to achieve RCCI combustion. However the CFD findings were not validated through experimental investigations.

Similar to the study of Nieman et al. [13], Zoldak et al. [14] explored the challenges of RCCI combustion at the rated power point, for a 15L HD diesel engine, by also conducting a computational study in KIVA -3V CFD code coupled with CHEMKIN II, as done by reference [13]. Authors in this study employed a dual injection strategy, and optimized the injection timing and quantity along with the overall NG substitution levels, similar to the work done by reference [13]. The authors demonstrated that efficient RCCI combustion can be achieved at the rated point, if the peak cylinder pressure limits are increased to 210 bar. The unburned hydrocarbon and CO emissions values were not reported by the authors even though CHEMKIN-II was used for the chemical reaction analysis.

Comparing the results of reference [14] to the results outlined by reference [13], at rated conditions, we see that the final NO_x emission reported by reference [14] is five times higher than the values reported by reference [13]. The diesel injection events for reference [13] are much earlier (-92.7 ATDC and -20.4 ATDC) utilizing higher EGR levels (48%) compared to the timing and EGR utilized by reference [14] (-55 ATDC and 6 ATDC, 36% EGR), which could likely explain the lower NO_x levels seen by reference [13]. It is interesting that even though both studies use significantly different injection timing and EGR rates, the total CNG substitution level remains relatively consistent in both studies (80-85%). This indicates that the combustion stability in dual fuel operation with diesel-NG is more dependent on the overall substitution level, whereas the injection events along with EGR percentage are primarily responsible for the final emissions outcome.

Table 1: Main RCCI research with diesel and CNG

Sr#	Authors	Research Objective	Methodology	Main Results
1	Dahodwala et al. [12]	Diesel-CNG combustion evaluation in a dual fuel regime and as an enabler to achieve RCCI combustion	2010 - 13L HD diesel engine with cooled HP EGR and CR: 16.5:1	RCCI combustion demonstrated at low loads, which allowed for application of higher CNG substitution and lower NO_x and PM emissions. CNG introduction without optimization of the base calibration can lead to high THC emissions.
2	Nieman et al. [13]	Evaluate the feasibility of using natural gas as the low reactivity fuel for RCCI combustion	KIVA-3V CFD code in conjunction with the CHEMKIN chemistry tool and the NSGA II algorithm	The use of natural gas as the low-reactivity fuel in RCCI combustion yielded clean, quiet, and efficient combustion throughout the speed-load range investigated - 4 to 23 bar gross IMEP and 800-1800 rpm engine speed.
3	Zoldak et al. [14]	Examine trade-offs of emissions, fuel consumption, PCP and MPRR in a RCCI engine using CNG-diesel fuel at the rated power point	KIVA-3V CFD code in conjunction with the CHEMKIN chemistry tool	RCCI combustion strategy showed 17.5% lower NO_x, 78% lower soot and a 24% reduced fuel consumption when compared to a conventional diesel combustion strategy using the same AFR and EGR rate, at the rated power point.

4	Doosje et al. [15]	Evaluate Diesel-CNG RCCI operation in a six-cylinder HD engine with cooled EGR in the 1200–1800 rpm range between 2 and 9 bar BMEP	Experimental evaluation of a Tier-4f 8L, six-cylinder HD diesel engine	RCCI operation with Euro-VI engine out NO_x and soot emissions was achieved between 2 and 9 bar BMEP without EGR in the 1200-1800 rpm range. Corresponding hydrocarbon levels were high. Thermal efficiency was comparable to or better than diesel operation.
5	Jia and Denbratt [16]	Experimental investigation of natural gas–diesel dual-fuel RCCI in a heavy duty engine using two different compression ratios	Single-cylinder DI diesel engine with CR: 17:1 and14:1	At CR 17:1, CA50 occurred mostly before TDC resulting in low indicated thermal efficiency. The desired CA50 phasing could be achieved by increasing the level of EGR at the expensive of higher THC emissions. Reducing the CR from 17:1 to 14:1 reduced NO_x emissions and delayed combustion (CA50) phasing but increased HC emissions.
6	Dahodwala et al. [17]	Evaluating in-cylinder mixture properties required in realizing dual-fuel diesel- CNG RCCI combustion at multiple speed and load points.	2010 - 13L HD diesel engine with cooled HP EGR and CR: 16.5:1 and CFD simulation using CONVERGE	At 5 bar BMEP with an increase in CNG substitution, the burn duration increased, leading to a retarded combustion phasing. Higher EGR rate retarded combustion phasing and increased

				the combustion duration. At 14 bar BMEP, it was observed that maximum pressure rise rates were more sensitive to boost pressure than higher EGR levels
7	Zoldak et al. [18]	Proposing DI-NG concept for RCCI combustion	Detailed CFD simulations using KIVA-CHEMKIN	The results indicated that DI-NG was successful in controlling the MPRR to below 10 bar/deg and PCP to less than 180 bar at 1800 rpm and 18 bar BMEP. The authors also demonstrated improvement in NO_x, HC and soot emissions to meet engine-out targets for engines equipped with modern after-treatment systems
8	Bekdemir et al. [19]	Application of multi-zone approach to NG-diesel RCCI combustion in a heavy-duty engine	8L six-cylinder DI diesel engine, CR 18:1	The trends for the control relevant characteristics, CA10, CA50, PCP, MPPR and NO_x emissions were predicted well for a variation of SOI, blend ratio and engine speed. Almost in all cases, the model over-predicted the ignition delay and combustion efficiency, leading to a consistent mismatch

				of the compared variables
9	Garcia et. al. [20]	Understand the most relevant characteristics and behaviors of a light duty dual fuel CNG-diesel engine operating under high substitution ratios	4-cylinder Volvo D4 2L diesel engine, modified for dual fuel operation.	Low load dual fuel operation with high diesel substitution ratios at highly diluted conditions is unacceptable, due to high methane emissions levels. Application of lower substitution ratios (maximum around 60%) at low loads results in acceptable emission levels with the possibility to apply alternative combustion modes like RCCI
10	Walker et al. [21]	Examine the operating range of the RCCI combustion strategy with methane–diesel fueling and compare against gasoline–diesel RCCI operation	Caterpillar SCOTE, CR 14.9:1	The experimental results showed a significant load extension of RCCI engine operation with methane–diesel fueling compared to gasoline–diesel fueling. For gasoline–diesel operation, the CA10–90 combustion duration shortened as the engine load was increased. Conversely, for methane–diesel operation, the CA10–90 combustion duration lengthened

				as the engine load was increased due to the lower reactivity of methane fuel.
11	Kakaee et al. [22]	Investigating effects of natural gas composition on combustion and emissions characteristics of an RCCI engine at load of 9 bar IMEP	Detailed CFD simulations	RCCI engine fueled with higher wobbe number (WN) displayed higher peak pressure and temperature, NO_x emissions and lower THC and CO emissions compared to the fuel with lower WN. Generally, from efficiency and emissions point of view, the gas with higher WN is favorable at higher engine speeds
12	May et al. [23]	Key speeds and loads were explored in order to determine where Premixed Dual-Fuel Combustion (PDFC) is effective at reducing engine-out methane emissions over conventional dual fuel combustion	Experimental investigations using a NG and diesel HD single cylinder research engine	In comparison with conventional natural gas-diesel combustion, PDFC shows significant reductions in methane slip as well as CO emissions at medium load. For most loads, PDFC lowers emissions simultaneously, but there are some cases where NO_x production is increased

13	Hanson et al. [24]	While typical RCCI studies focus on low engine-out NOx emissions, limited studies have been conducted to evaluate the maximum BTE potential with RCCI combustion targeting higher NO_x emissions	Experimental studies on RCCI combustion with diesel and natural gas were done on an 12.4L, 312kW HD diesel engine at 15 operating points with and without EGR	Authors report that peak BTE of 46.8% could be achieved along with extension of RCCI combustion to 20 bar BMEP with use of early pilot injection and near top dead center main injection with relaxed NOx emissions limit ($\geq$ 10 g/kWh). Similar to other RCCI studies, the authors reported higher THC and CH_4 emissions with RCCI combustion compared to conventional diesel combustion
14	Kakee et. al., [26]	Study explores the effects of three piston bowl geometry on natural gas/diesel RCCI performance and emissions at medium engine load	Detailed CFD simulations using Converge CFD tool and GRI mechanism	It was found that the bowl profile did not affect combustion of RCCI engine at low engine speeds, but it greatly affected it at higher engine speeds. Bowl profile considerably affected NO_x emissions, but it had negligible effect on THC and CO emissions.
15	Khatamnejad et al. [27]	Examine the effects of diesel injection timing, diesel/natural gas ratio and diesel fuel included spray angle on combustion and emissions formation at various engine loads and	CFD simulation coupled with chemical kinetics	Quantity and timing of direct injected diesel fuel is a critical factor to control combustion phasing. Increasing diesel fuel quantity leads to reduced THC and CO emissions. Diesel fuel targeting inside the

		speeds, in a heavy duty diesel engine		combustion chamber has a simultaneous beneficial effects on emissions formation and engine performance due to more homogeneous air fuel mixture
16	Poorghasemi et. al., [28]	Effect of diesel injection strategies on natural gas/diesel RCCI combustion characteristics in a light duty diesel engine	Experimental investigations on a 4-cylinder light duty diesel engine with CR:17:1 and CFD studies using Converge CFD with detailed reaction mechanism	The results show a reduction in NOx emission while limiting HC and CO emissions by increasing the NG fraction, advancing the first SOI with higher fuel fraction, lower injection pressure and employing a wider injector spray angle.

Referring to the table above one experimental study on RCCI combustion with diesel and CNG was done by Doosje et al. [15] on an 8L, 250kW HD diesel engine. The authors selected eight operating points for this study, from 3-9 bar BMEP and 1200-1800 rpm engine speed. The authors utilized a single injection strategy for their study with no EGR. The authors reported that, very low NO_x and PM emissions can be obtained with RCCI combustion only up to 10 bar BMEP, with no EGR. This conclusion is similar to the one made by reference [13], wherein they could demonstrate RCCI operation up to 13 bar gross IMEP without using EGR. Above 10 bar BMEP, the authors were limited by either the peak cylinder pressure limit, or the maximum pressure rise rates. These findings are contrary to those reported by reference [13] & [14], where RCCI combustion was demonstrated up to rated power conditions using CFD tools. A limiting factor could be the single injection strategy employed by reference [15] compared to the multiple injection strategy proposed by references [13] and [14]. Also as demonstrated by reference [13], as we start increasing load, EGR is needed in the system to increase ignition delay to control combustion phasing, which was not thoroughly investigated by the authors in reference [15]. The authors also reported high unburned hydrocarbon emissions, as seen by reference [13] for all load points.

Recent experimental studies on RCCI combustion with diesel and natural gas were done by Hanson et. al. [24, 25] on a 12.4L, 312 kW HD diesel engine. Investigations were carried out at 15 operating point's representative of the EPA 13 mode RMC. A peak

cylinder pressure limit of 250 bar was employed along with a combustion noise target of 92 dBA. Since the study was conducted as part of the Super Truck Project, a relaxed NO_x limit of 10 g/kWh was employed to achieve maximum possible brake thermal efficiency (BTE). The natural gas was port injected at a constant start of injection timing of -570°ATDC for all test cases. Double pulses were used for the diesel injections, with the pilot injection phased early in the compression stroke (-570°ATDC) and the main injection near top dead center. This strategy was employed to achieve RCCI combustion at high loads with maximum BTE however at the expense of very high NO_x emissions. The authors argued that while typical RCCI studies focus on low engine-out NO_x emissions, the current higher NO_x emissions results can still be considered RCCI combustion due to the use of in-cylinder fuel blending to create reactivity levels (i.e. early injections) similar to all previous RCCI combustion studies The investigation at all 15 operating points were done with and without EGR. The authors concluded that with relaxed NO_x targets, peak BTE of 46.8% would be achieved along with extension of RCCI combustion to 20 bar BMEP which was higher than previous experimental RCCI studies [13, 16] where the peak load was limited to below 10 bar BMEP. Similar to other RCCI studies, the authors reported that the unburned hydrocarbon and CH_4 emissions were higher with RCCI combustion compared to conventional diesel combustion. Authors in reference [24] and [25] have achieved RCCI combustion across the complete engine map but with higher NO_x emissions compared to base diesel operation. None of the experimental studies conducted so far have shown that RCCI combustion can be achieved along with low NO_x emissions across the complete engine map.

Experimental studies conducted as part of this PhD work and outlined in section 4, have shown that RCCI combustion becomes progressively difficult to control as the load is increased at a given speed or the speed is reduced at a given load. To control RCCI combustion a critical tradeoff exists between the reactivity level and ignition delay. At low engine speeds, with limited capability to increase EGR, the ignition delay time is shorter thereby making RCCI combustion difficult to control. On the other hand, the relatively larger quantity of diesel fuel (higher cetane fuel) injected at high loads makes the combustion phasing difficult to control.

In further review of the existing work, none of the CFD studies conducted to date to evaluate RCCI combustion with diesel/natural gas in heavy-duty diesel engines have provided a comprehensive comparison between the CFD predictions and test results for different control parameter settings. CFD studies conducted by Khatamnejad et al. [27] on a heavy duty diesel engine compare the cylinder pressure and heat release rate predictions between CFD and experimental results for four different diesel injection timings using detailed chemistry at 1500 rpm and 6 bar BMEP. The author report that compared to the experimental data the cylinder pressure predictions in CFD are lower for the most retarded timing (8 bTDC) and higher for the most advanced timing (35 bTDC) investigated. The best correlation was seen with the diesel SOI at 31 bTDC. The authors used this timing case for further investigations regarding the effect of CNG substitution and diesel fuel injection parameters. The discrepancy in cylinder pressure prediction with CFD for the timing sweep were not further investigated in this study. Also the authors

applied the CFD models to predict cylinder pressure at multiple CNG substitution levels however the model was only validated for a fixed CNG substitution level.

In order to address these gaps in the understanding of diesel/natural gas RCCI combustion, this research focuses on the following topics:

- Conducting experimental investigation of diesel/natural gas RCCI combustion in a heavy-duty diesel engine targeting low NO_x emissions (< 0.26 g/kWh meeting the US EPA HD on road 2010 NO_x emission limit)
- Validating the CFD predictions to the experimental RCCI data using a detailed chemical mechanism in Converge CFD software to establish a baseline correlation for future studies
- Examining trends and sensitivities in the experimental studies and apply the validated CFD model to quantify the in-cylinder conditions that are needed at higher loads (>10 bar BMEP) in order to effectively control a low NO_x RCCI combustion (< 0.26 g/kWh)

Through these efforts, the research aims to provide a comprehensive summary regarding the impact of key factors including reactivity level, dilution and degree of premixing in achieving a low NO_x RCCI combustion at medium engine speed (1500 rpm) and higher loads (>10 bar BMEP).

3 Test Cell Setup

A production heavy-duty diesel engine was used for this investigation. The 2010 inline 6-cylinder engine has a displacement of 13 liters, is rated at 425 HP and is On-Board Diagnostics (OBD) - II compliant. It is equipped with a high pressure common rail fuel injection system, cooled high pressure EGR, and a compression ratio of 16.7:1. CNG was introduced into the intake using eight CNG injectors located downstream of the charge air cooler. A mixer was installed downstream of the CNG introduction location to support equal distribution of the CNG in the intake manifold. Figure 4 outlines the test cell setup used in this investigation. A Rapid Controller Prototyping (RCP) system was used for controlling the amount of CNG induction. The production engine was equipped with a Diesel Oxidation Catalyst (DOC), Diesel Particulate Filter (DPF) and Selective Catalytic Reduction (SCR) catalyst, however for this investigation only a DOC was installed and the backpressure was adjusted via a back pressure valve to simulate the absent aftertreatment components. The aftertreatment module in the Engine Control Unit (ECU) was deactivated to prevent it from affecting the base engine performance.

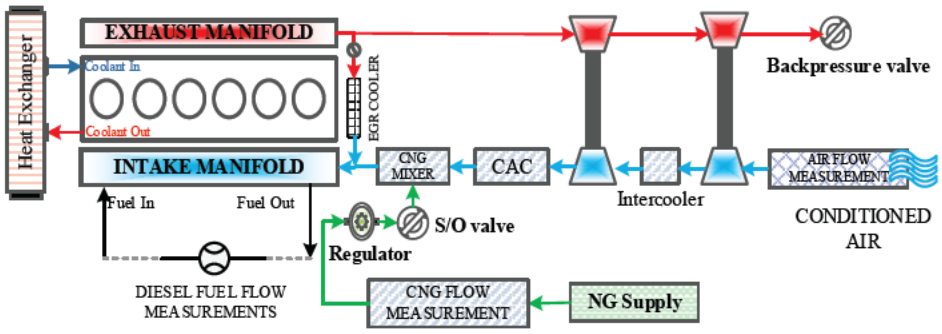

Figure 4 Test Cell Schematic (Update to show two stage T/C

The engine was coupled to a 560 kW Alternating Current (AC) dynamometer. CNG and diesel fuel flow measurements were accomplished using Micro Motion flow meters while the air flow was measured using an ABB air flow meter. Engine-out and tailpipe gaseous emissions were measured with a dual channel Horiba MEXA 7500 DEGR emission bench. The intake manifold was instrumented for CO_2 concentration measurement, which was used for calculation of the EGR rate. PM emission was determined through the Motor Industry Research Association (MIRA) calculation, which utilized data provided by a smoke meter drawing sample upstream of the DOC. The engine was instrumented with Kistler 6061B in-cylinder pressure transducers to allow cylinder pressure measurements on all six cylinders.

Based on operating points from the RMC, HD FTP and highway cycles for this engine, 12 specific test points were selected for this study as shown in Figure 5. The points were selected to provide a good balance between certification cycles and real-world operation. For the baseline substitution study, the CNG substitution was increased in 10% increments until the engine became unstable ((IMEP) Coefficient of Variation (COV)

less than 10%) or a limit of peak pressure (190 bar) or maximum turbine inlet temperature (720 degC) was reached.

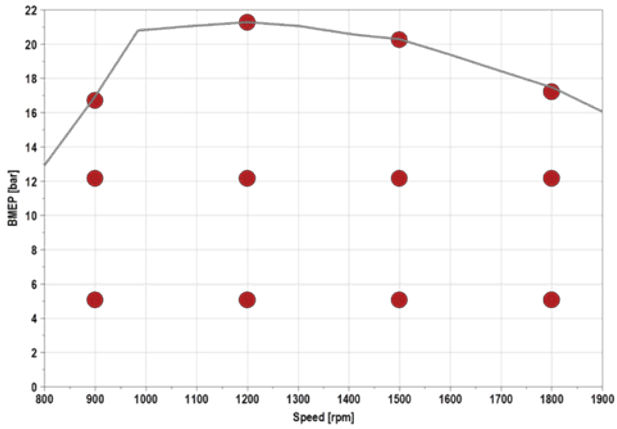

Figure 5 Test points used in the current investigation

For optimization studies, the effect of main injection timing and CNG substitution was studied at each of the selected operating points. Figure 6 shows an example test matrix for one particular engine speed. The main injection timing was swept at different substitution levels across the three load points. At high loads the timing could not be advanced because of peak pressure limitations, and it was found that higher substitution could only be achieved by retarding the main timing. RCCI combustion was evaluated at the part load points. The test matrix for RCCI combustion at part loads was an extension of the test matrix shown in Figure 6. The timings were advanced to 50-80 deg CA bTDC at substitution levels of 60-80%. The CNG substitution was calculated on an energy basis. The details of the calculation are outlined in Appendix A.1

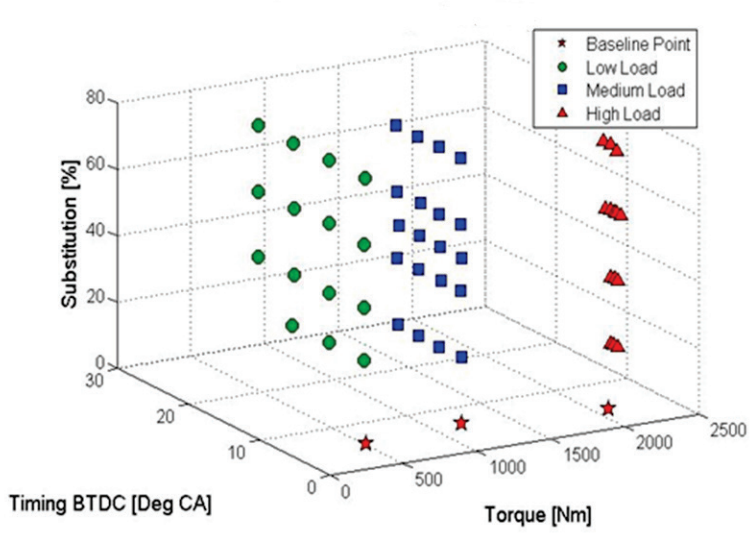

Figure 6 Test matrix applied for optimization at a fixed speed [12]

4 Test Results

The experimental investigations were conducted with the aim to answer three key questions:

- What is the impact of replacing diesel fuel with CNG on the performance and emissions of a 2010 on-highway heavy duty diesel engine?
- What are the potential improvements in CNG substitution percentages through calibration optimization?
- Can advanced combustion concepts like RCCI be implemented with dual fuel diesel/CNG operation and provide additional performance and emission benefits?

The sections below detail the experimental investigations that were conducted as part of this study that have previously being submitted as part of two SAE publications [12, 17].

4.1 Measurement Data Uncertainty Analysis

To evaluate the repeatability of the measurement data set, multiple reference points were measured during the course of the testing with diesel only operation. Figure 7 overviews the reference point summary for some of the key measurements including torque, peak cylinder pressure (cyl#1), AFR, EGR, NOx emissions and smoke numbers at the rated power point – 1700 rpm / 100% load. Also shown in the figure is the standard deviation value for each parameter along with the 2σ band (95% confidence interval). All test points are within the 2σ band for the measurements plotted in Figure 7. The relatively low standard deviation value for all parameters shown in Figure 7 indicates that the measurements were repeatable and the resulting conclusions drawn in the subsequent sections are reliable.

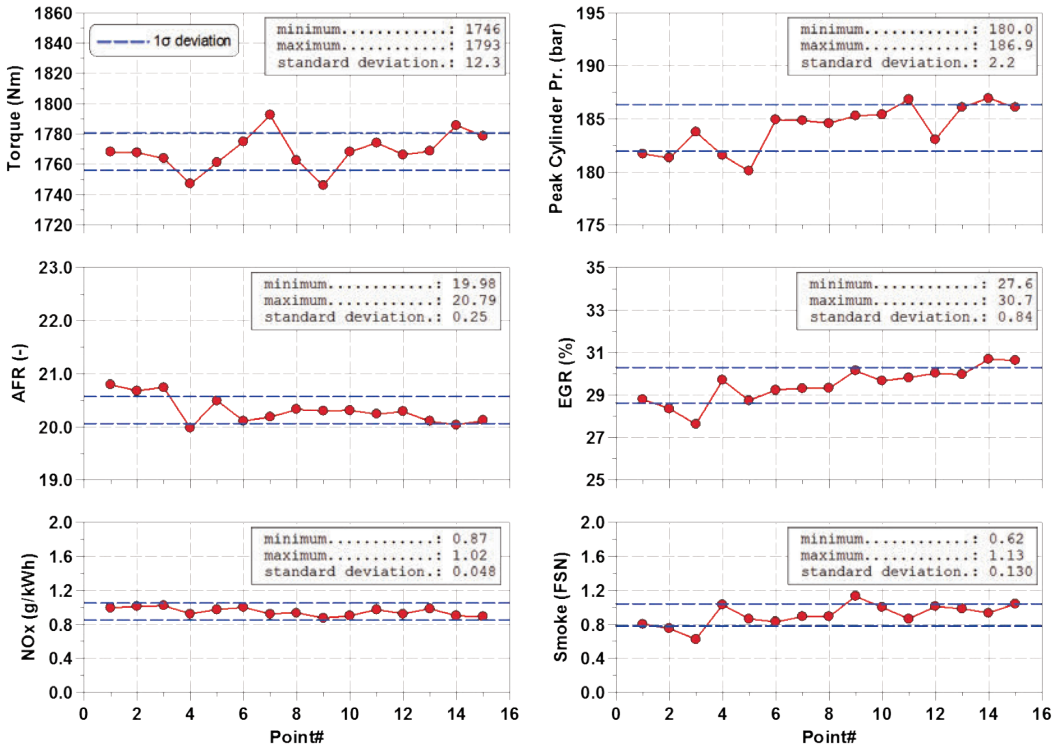

Figure 7 Reference point data analysis at 1700 rpm and 100% pedal with diesel only operation

4.2 Impact of Replacing Diesel Fuel with CNG

To evaluate the impact of substituting CNG without changes in the baseline calibration, diesel quantity was lowered by reducing the pedal demand and maintaining load by introducing CNG into the system. With this approach, the control parameter set points, including the injection events, EGR rates and rail pressures were controlled by the ECU based on the commanded fueling and the engine speed. The study was conducted at #12 different operating points as highlighted in Figure 5.

Figure 8 shows the apparent heat release rate (AHRR) and cylinder pressure traces for 5 bar BMEP at three different substitution levels along with the emission impact and corresponding control variables settings for different substitution levels. From these figures, deterioration in combustion efficiency can be seen with an increase in CNG substitution, possibly due to the reduction in injected diesel fuel leading to lower combustion chamber temperatures. This led to significant increase in hydrocarbon emissions and brake specific fuel consumption (BSFC). An increase in NO_x emissions was observed up to 40% CNG substitution, due to reduction in EGR, but then dropped as the combustion efficiency deteriorated. The EGR reduction can be attributed to the richer lambda values observed with increasing CNG substitution as the fresh air charge is displaced with CNG. Increased PM emissions at higher substitution were possibly due to the richer lambda value.

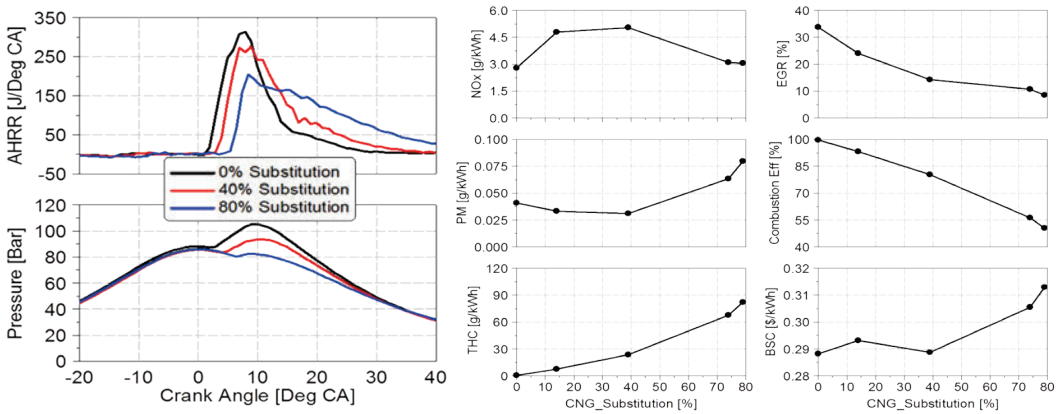

Figure 8 AHRR, cylinder pressure and performance parameters for 5 bar BMEP load at 1500 rpm at different CNG substitution levels [12]

A reduced peak in the heat release trace and a late burning of CNG, also observed by Maxey et al. [32], was clearly visible with an increase in substitution. Observations regarding the combustion behavior are in agreement with those of Maxey et al. [31]; wherein the reduction in diesel fuel quantity reduces the amount of diesel available to ignite the less reactive CNG [32].

Figure 9 outlines the AHRR and cylinder pressure trace for 12 bar BMEP along with emission impact with increasing CNG substitution at the same load. Similar trends for NO_x, PM and THC emissions were observed for 12 bar BMEP as seen at 5 bar BMEP, however, here the combustion efficiency remained above 90%. At this load, a maximum substitution of 98% could be reached where CNG was ignited by the diesel pilot injection and an SI type heat release trace was observed. A NO_x emission increase was closely coupled to a reduced EGR rate and an earlier heat release. In general, the combustion COV, as also observed by Sun et al. [33], was affected by CNG substitution percentage and the EGR quantity.

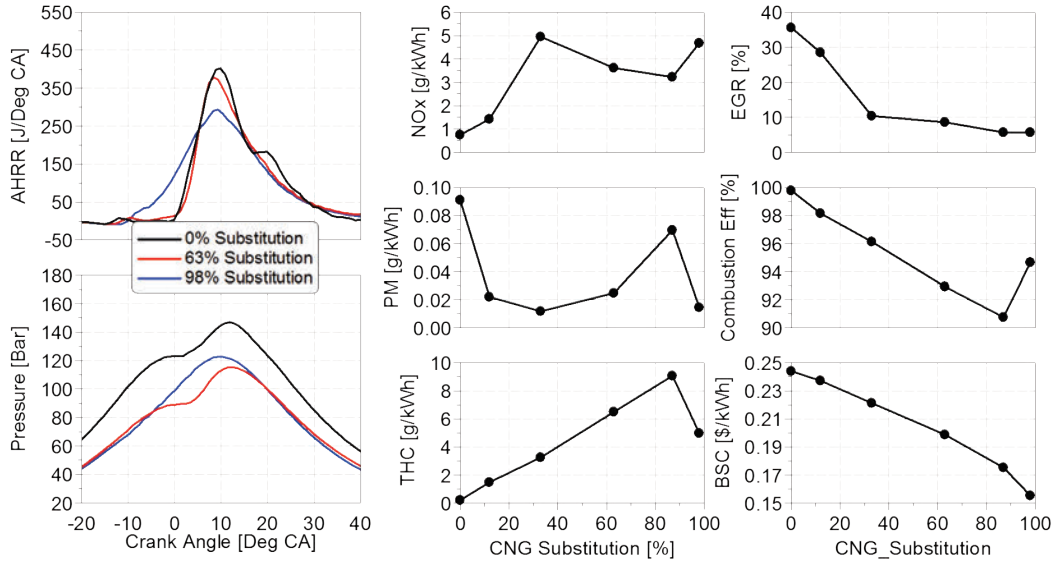

Figure 9 AHRR, cylinder pressure and performance parameters for 12 bar BMEP load at 1500 rpm at different CNG substitution levels [12]

The cylinder pressure rise rate and the peak cylinder pressure increased significantly at 20 bar BMEP as shown in Figure 10, due to the simultaneous combustion of diesel and CNG. This limited CNG substitution to 36% at this load point. Combustion efficiency remained above 98.8% due to the higher combustion temperatures. The NO_x, PM and THC emissions trends presented in Figure 10 for 20 bar BMEP are similar to those observed at 5 bar and 12 bar BMEP.

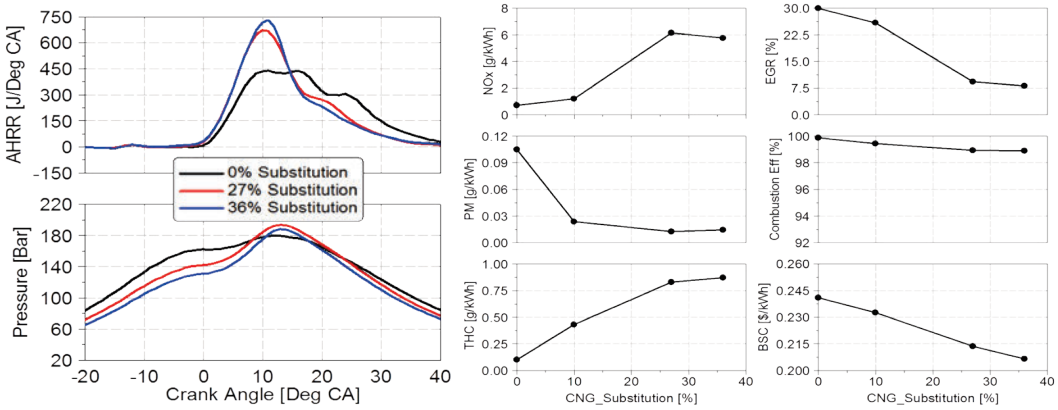

Figure 10 AHRR, cylinder pressure and performance parameters for 20 bar BMEP load at 1500 rpm [12]

Figure 11 shows the practical CNG substitution map when access to the calibration is not available and thus no calibration changes are applied. This map is determined by maintaining the engine-out emissions within a level that would allow the engine to meet US2010 emission legislation when conventional diesel aftertreatment is applied. The average NO_x emission for the baseline diesel calibration was approximately 2.0 g/bhp-hr,

therefore a NO_x limit of 2.0 g/bhp-hr, along with a NMHC limit of 0.238 g/bhp-hr, was applied as limiting criteria.

From Figure 11 we can see that the average substitution would be limited to less than 10% if the base calibration is carried over and no changes are applied. There are three major reasons for the limited substitution shown in Figure 11. First, at low loads the amount of unburned THC is very high. Second, at mid loads the NO_x emissions tend to increase due to a reduction in EGR caused by running richer lambda values. Lastly, the peak pressures increase with increase in CNG substitution at higher loads, leading to the necessity to observe mechanical limits.

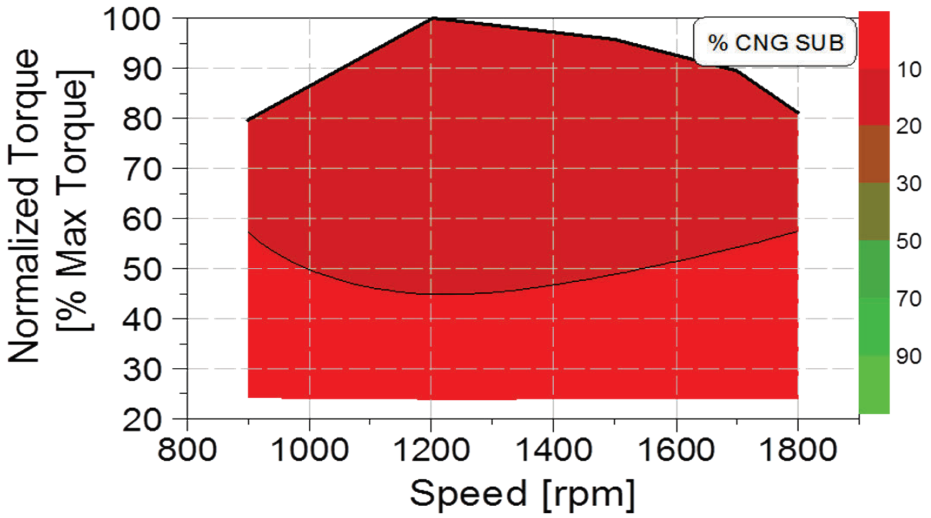

Figure 11 Practical CNG substitution map without base engine calibration changes and meeting US2010 emission standards [12]

4.3 Calibration Optimization

As detailed in the previous section, very low CNG substitution levels can be achieved when changes to the base diesel calibration are not considered. Therefore, to increase the CNG substitution levels, a modification of the base calibration is required. The base calibration used three injections along with EGR to reach the desired NO_x, PM and NMHC targets when operating on diesel fuel. To understand the effect of each injection event, a series of tests were conducted at 1500 rpm and 5 bar BMEP and multiple substitution levels. Three injection strategies were explored: main injection only, main + pilot injection and main + post injection. In order to eliminate the effect of EGR, the EGR rate was reduced and maintained at a near-zero level throughout modification of the base calibration. A summary of the injection strategy employed for each case is provided in Table 2.

Table 2 Overview of the three injection strategies employed at 1500 rpm, 5 bar BMEP and different CNG substitution

Strategy	Main Timing (bTDC)	Pilot Quantity (mg/hub)	Pilot Sep. (usec)	Post Timing (mg/hub)	Post Sep. (usec)	EGR (%)
Main injection only	7.85	0	0	0	0	0
Main + Pilot injection	7.75	2.04	1772	0	0	0
Main + Post injection	7.95	0	0	9	-1755	0
Main injection + EGR	7.58	0	0	0	0	34

Figure 12 shows the impact of each of these strategies on the NO_x and THC emissions at various CNG substitution levels. The NO_x emissions decrease with an increase in CNG substitution levels for all three strategies, but none of the strategies show a significant advantage in their ability to control THC emissions. Therefore, to simplify the diesel injection control, a main injection only strategy was applied for the calibration optimization. It was also realized that EGR was required to control the NO_x emissions, as shown in Figure 12.

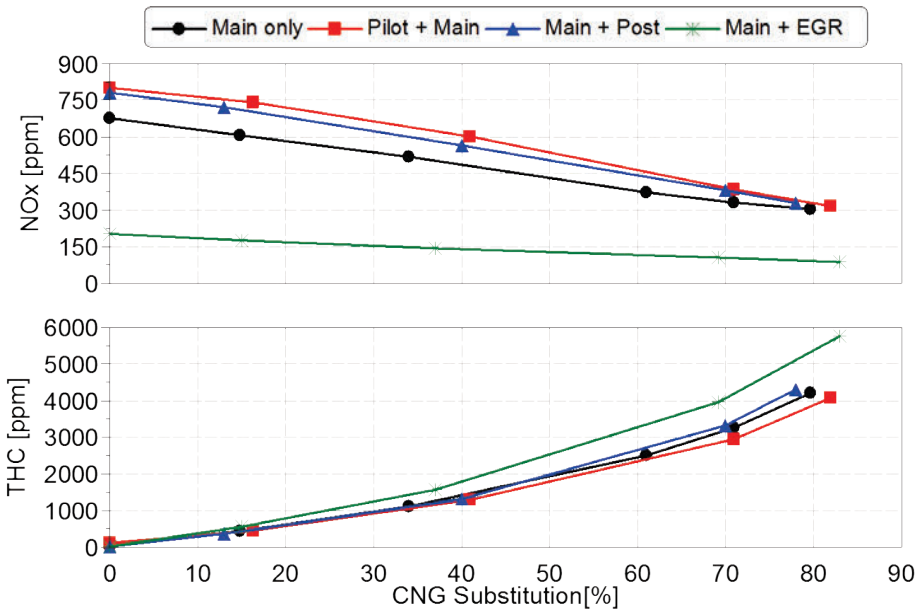

Figure 12 Comparison of NO_x and THC emission for multiple CNG substitution levels at 1500 rpm and 5 bar BMEP [12]

A study was then conducted with multiple CNG substitution levels and diesel injection timings for the main injection only case. At each speed and load point the EGR rate and injection pressure were held constant. The boost pressure was controlled by the ECU

based on the existing calibration. The diesel injection timing advance was restricted to 20 deg bTDC, above which the possibility of spraying the diesel fuel directly on the cylinder liner was high. The CNG substitution was limited to 80%; above this level the combustion was unstable and resulted in very high THC emissions. The optimization study was conducted at all 12 points as outlined in Figure 5. To describe the impact of injection timing and CNG substitution on emission and performance, the following text focuses on the results obtained at 1500 rpm and three different load points.

Figure 13 shows the effect of diesel injection timing and CNG substitution levels on the NO_x, PM and THC emissions at 1500 rpm and 5 bar BMEP. A decrease in NO_x emissions and an increase in THC emissions can be observed as CNG substitution levels are increased at constant injection timing.

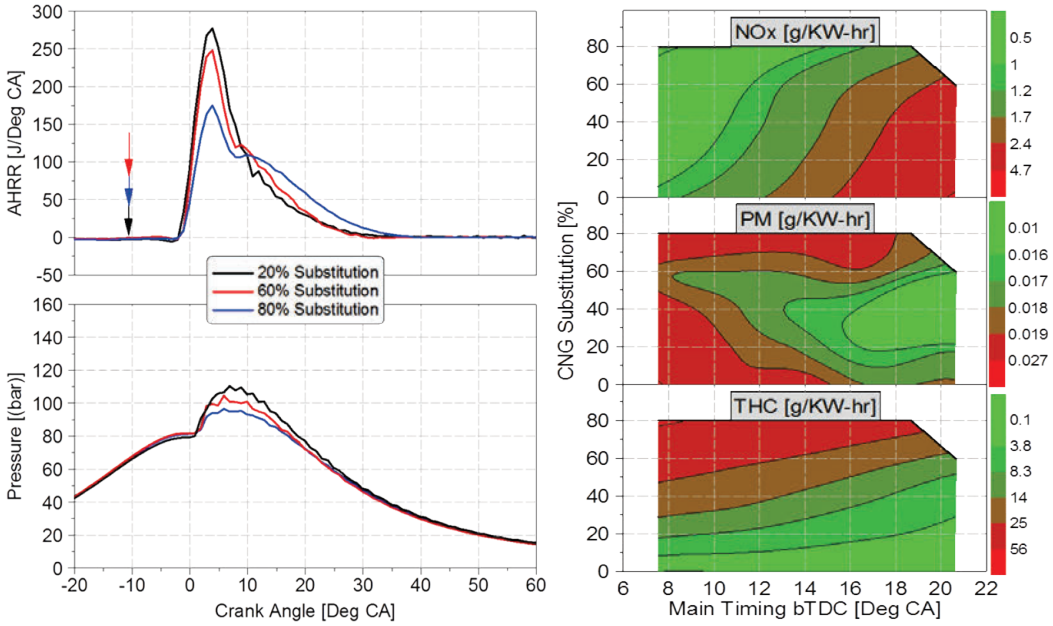

Figure 13 AHRR and cylinder pressure for 1500 rpm, 5 bar BMEP at 10bTDC injection timing with three different substution levels along with emissions for different injection timings and substitution levels [12]

Figure 13 compares the AHRR and pressure traces for three different substitution levels at a fixed injection timing of 11 deg bTDC. As shown in Figure 13, the initial peak of the AHRR trace reduces as CNG substitution is increased, while the longer burn durations lead to lower combustion temperatures and lower NO_x emissions. However, at a fixed substitution level the NO_x emissions increase as the injection timing is advanced, but the THC emissions decrease.

Comparing the AHRR traces in Figure 14, it can be observed that, as the injection timing is advanced, the AHRR traces move toward top dead center (TDC). This leads to higher in-cylinder temperatures causing higher NO_x emission formation but at the same time allowing more time for the CNG to burn at higher temperatures and reducing the THC

emissions. Although the best NO_x emission results are obtained between 60% and 80% substitution levels and approximately 12 deg bTDC injection timing, at this point, the unburned THC emissions are very high. Thus, a compromise must be identified between the maximum substitution and the allowable NO_x and THC emissions. The PM emissions, on the other hand, are very low across the complete optimization range, with a minimum achieved at 20 deg bTDC between 20% and 60% CNG substitution levels. Unfortunately, the NO_x emissions in this range are very high.

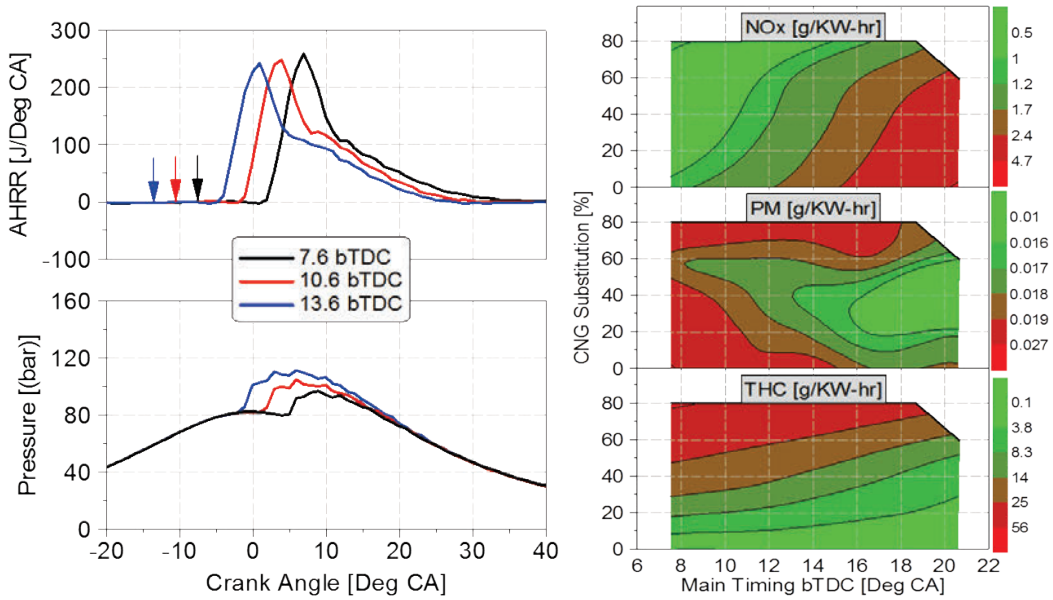

Figure 14 AHRR and cylinder pressure for 1500 rpm, 5 bar BMEP at 60% CNG substitution with three different injection timings along with emissions for different injection timings and substitution levels [12]

Figure 15 shows the NO_x, PM and THC emissions at 1500 rpm and 12 bar BMEP. The NO_x emission results are similar in terms of a decreasing trend with increase in CNG substitution levels at the same injection timing and an increase in NO_x emissions with injection timing advance at a constant substitution level. Again, as in the previous case, the regions where the NO_x emissions are lowest have very high THC emissions and vice-versa. Thus, at mid loads as well, the amount of CNG substitution is dependent upon the trade-off between NO_x and THC emissions.

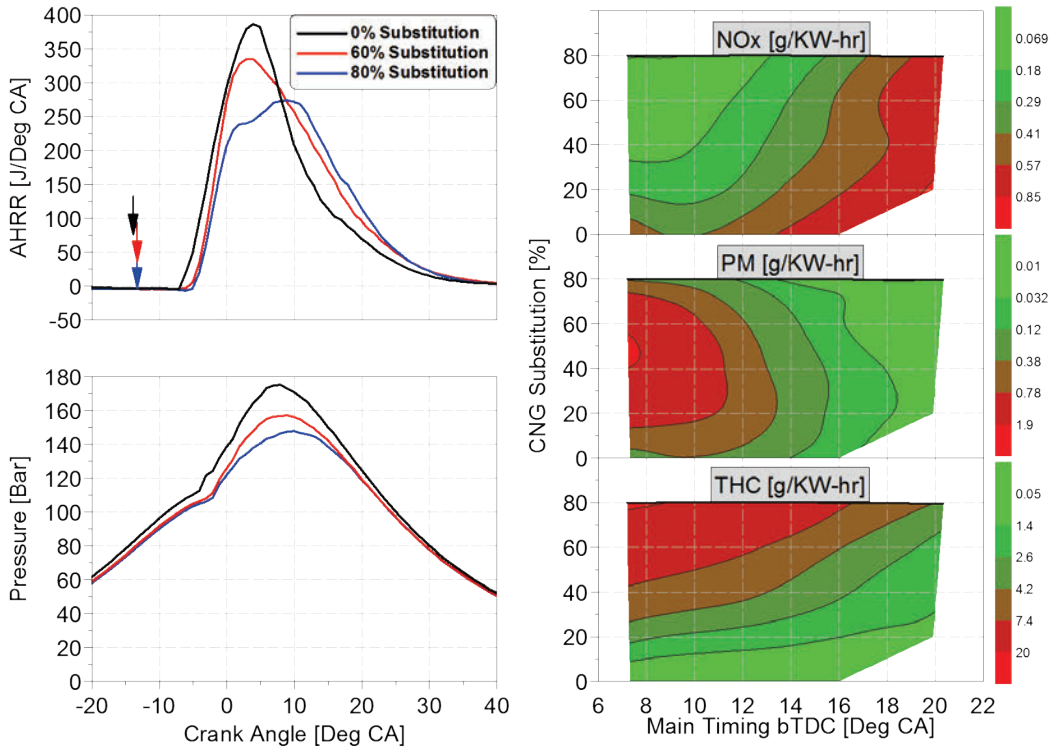

Figure 15 AHRR and cylinder pressure for 1500 rpm, 12 bar BMEP at 14bTDC injection timing with three different substution levels along with emissions for different injection timings and substitution levels [12]

Figure 16 shows the impact of injection timing at three different substitution levels for 20 bar BMEP. Contrary to the approach at the lower loads, the injection timing was retarded at high load to allow for higher CNG substitution levels. By retarding the injection timing, the mechanical limits of maximum cylinder pressure were avoided. As the injection timing was retarded with increasing CNG substitution levels, the NO_x and PM emissions were decreasing with a familiar increase in THC emissions. Comparing the AHRR traces in Figure 16, it is observed that as the CNG substitution is increased the peak of the AHRR trace moves away from TDC, matching the earlier finding of longer burn duration with less reactive CNG leading to reduced NO_x formation. At a fixed substitution level, a retarded timing reduced the NO_x emission as expected, but the THC emissions increased. The ability to further retard the injection timing is limited beyond a certain crank angle since the longer CNG burn duration leads to high THC emissions.

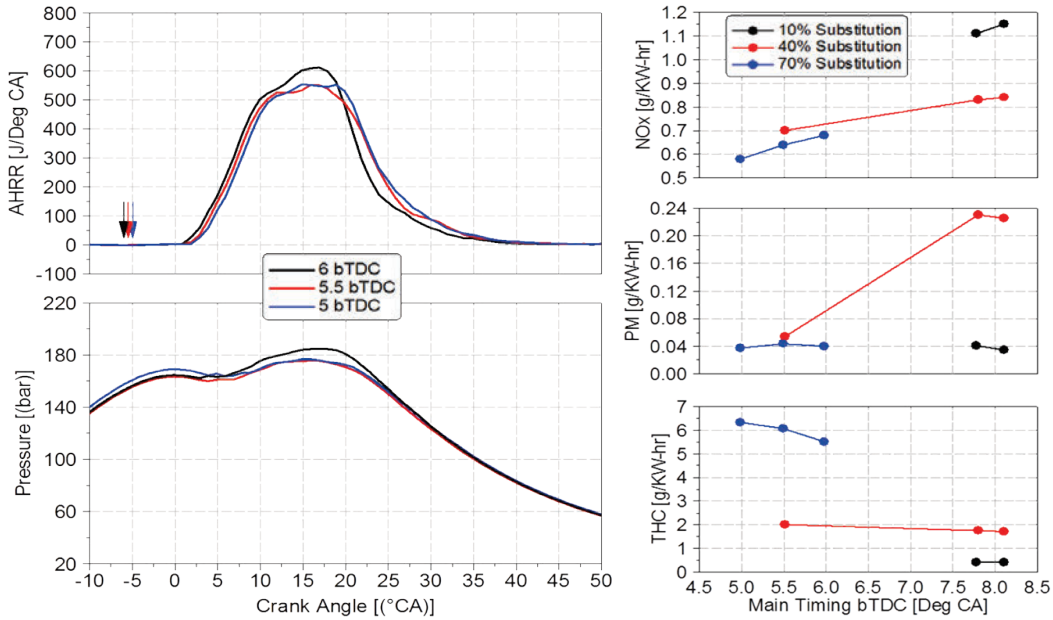

Figure 16 Injection timing study for different CNG substitution levels at 1500 rpm, 20 bar BMEP with 28% EGR [12]

Based on the main timing and CNG substitution studies conducted at the #12 speed and load points, a map was generated showing the maximum CNG substitution that is possible when allowing changes to the base calibration. The map is again determined by observing the limits imposed by the US2010 emission legislation. As shown in Figure 17 the average substitution achieved is approximately 50%, with higher substitution achieved at the higher load points where the retarded injection timing strategy was employed to control the pressure rise rates. With this substitution level, there was a penalty in the CH_4 emissions. At low loads the substitution is mainly limited by the unburned hydrocarbons due to a limited diesel quantity available for igniting the premixed CNG charge.

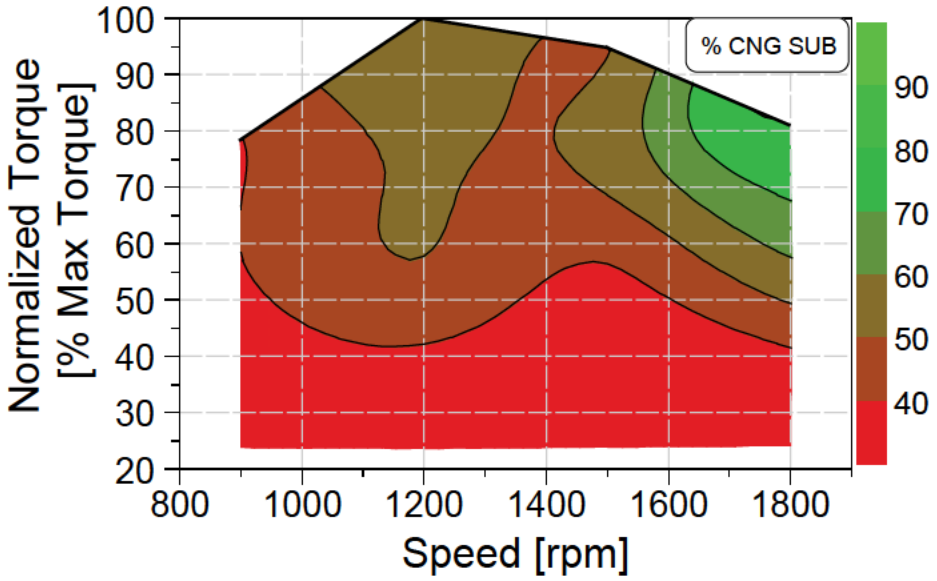

Figure 17 Optimized CNG substitution map with calibration changes and meeting US2010 emission standards [12]

4.4 Investigation of RCCI Combustion

The existence of very high hydrocarbon emissions at low loads impeded higher substitution levels during the optimization effort. As a step toward further optimization, it was considered that the higher fuel reactivity difference between CNG and diesel could potentially enable RCCI combustion, despite a relatively high compression ratio. To explore this concept, the main injection timing for diesel was advanced well beyond conventional diesel injection timings. Of the #12 test points RCCI was investigated experimentally at the eight operating points highlighted in Figure 18. The five full load operating points did not give an opportunity to investigate RCCI combustion due to the physical limitation of the test engine. RCCI combustion studies were performed at two different load points (5 and 12 bar BMEP) and four different engine speeds (900, 1200, 1500 and 1800 rpm).

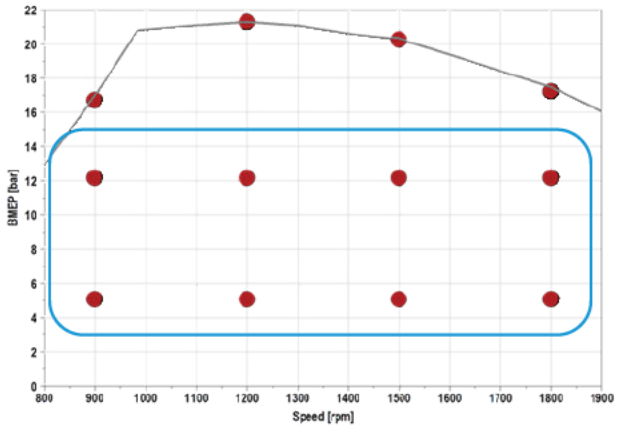

Figure 18 Test points for RCCI combustion evaluation

4.4.1 RCCI Combustion Evaluation at 5 bar BMEP

To identify the in-cylinder conditions favorable for RCCI combustion, three control variables – namely CNG substitution, EGR rate and the injection events were varied as outlined in Table 3. The identified combustion strategy was then applied to other engine speeds at 5 bar BMEP in an attempt to achieve RCCI combustion.

Table 3 Test parameters for RCCI combustion evaluation at 5 bar BMEP

Sensitivity Parameter	**Substitution**	**EGR Rate**	**Split Injection Quantity**	**Engine Speed**
Target Combustion Characteristic	**Reactivity Gradient**	**Dilution**	**Degree of Mixing**	**Residence Time**
Speed [rpm]	1500	1500	1800	1200-1800
EGR Rate [%]	35	9-37	40	Maximum Possible
Substitution [% CNG]	40-80	60	60	60

4.4.1.1 Effect of CNG Substitution

In order to study the impact of CNG substitution on RCCI, an injection timing sweep was conducted at three different CNG substitution level as shown in Figure 19. A combustion behavior change from conventional dual fuel combustion to RCCI combustion at overly advanced timings was observed. The trend was similar with different substitution levels

as shown in Figure 19. The engine load for each case was held constant by adjusting the total fueling according to the desired substitution level.

Initially, as the injection timing was advanced at 60% and 80% substitution, the combustion phasing advanced. However, after 25-35 °CA bTDC the combustion phasing retarded, indicating a change in combustion behavior. A sharp reduction in NO_x emission was also simultaneously observed as the combustion phasing was retarded. This behavior was not observed at 40% substitution. A possible reason could be that the higher diesel fueling at 40% substitution led to an overly stratified mixture with high reactivity which then was not able to achieve controlled auto-ignition.

THC and CO emissions reduced significantly at these advanced timings, as compared to near TDC timings, due to increased time for the high reactivity diesel fuel to mix with the premixed CNG-air mixture. However, an interesting observation was an increase in CO emissions as the combustion behavior changed from conventional dual fuel to RCCI combustion. Possibly, the advance in injection timing, which resulted in increased CH_4 conversion, led to a decrease in the oxygen availability for CO oxidation. The local combustion temperatures may also contribute to the decrease in CO oxidation as these temperatures are reduced with RCCI combustion. The higher CO emission linked to higher substitution rates can be attributed to the lower global lambda value associated with higher substitution levels. Combustion efficiency of 95% and above was only observed for 40% and 60% substitution levels at the most advanced timing.

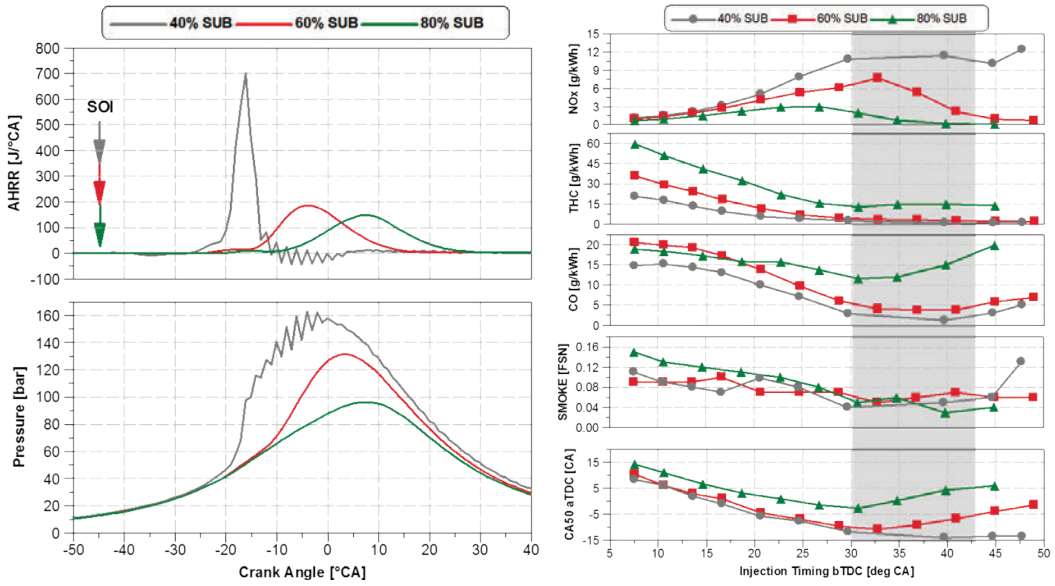

Figure 19 AHRR and cylinder pressure for three different substitution levels at injection timing of 45 bTDC along with injection timing sweep at three different substitution levels at 35% EGR for 1500 rpm 5 bar BMEP [17]

Figure 19 also shows the heat release rate and cylinder pressure profile for three substitution levels at a fixed timing of 45 bTDC. Substitution at 40% displays a very sharp heat release rate indicating that the diesel fuel auto-ignited all at once, while a controlled heat release rate could be observed at higher substitution levels due to reactivity gradient. At a fixed injection timing it was also observed that combustion phasing was more retarded at higher substitution levels, indicating that the combustion phasing was sensitive to injection timing as well as substitution level. This observation has also been reported by other researchers exploring RCCI combustion with different fuels. Higher substitution levels can enable optimum combustion phasing at the expense of higher THC and CO emissions.

4.4.1.1 Effect of EGR Rate

An EGR rate study was performed at 1500 rpm with two EGR levels, 9% and 37%, as shown in Figure 20. The CNG substitution was held constant at 60% for all test points. We can see in Figure 20 that, at a fixed injection timing, higher EGR rates resulted in increased combustion duration with a retarded heat release rate. There was no change in the ignition delay between the two heat release traces, but the low temperature reactions, especially the negative temperature coefficient (NTC) regime, are longer with higher EGR rates leading to an overall longer burn duration.

NO_x emissions reduced with increase in EGR rate and advanced injection timing at a fixed substitution level. Smoke number was reduced with an increase in EGR rate, possibly due to a longer ignition delay for the main heat release, which results in better mixing. THC and CO emissions were higher with 37% EGR due to lower global lambda values. However, the lower combustion efficiency was offset by higher thermal efficiency for the higher EGR case due to favorable combustion phasing. The results indicate that EGR was effective in controlling the burn duration and improving thermal efficiency at low load.

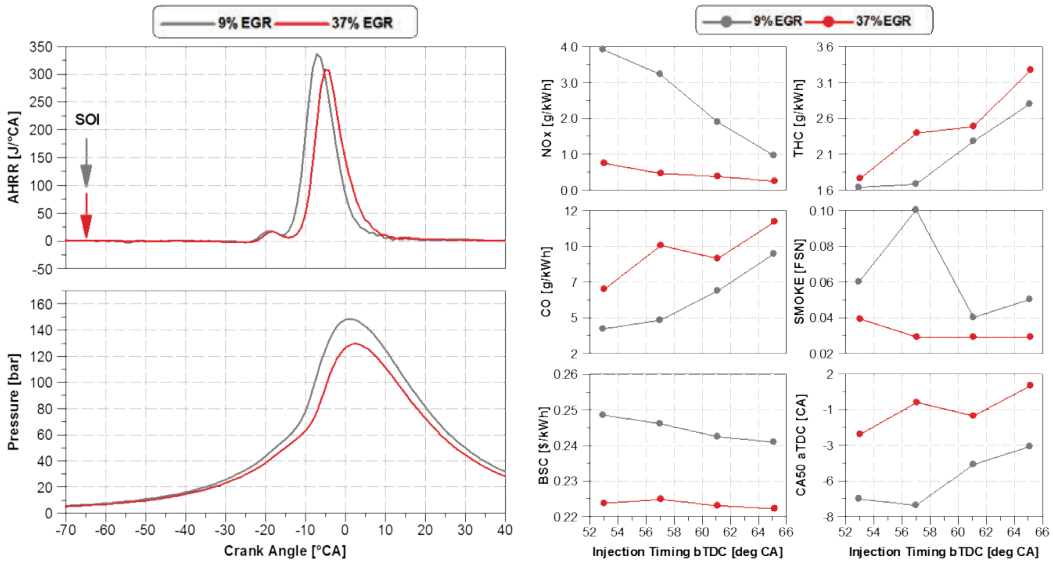

Figure 20 AHRR and cylinder pressure at 65 bTDC injection timing and 60% substitution along with injection timing sweep at two different EGR rates at 60% substitution and 1500 rpm 5 bar BMEP [17]

4.4.1.2 Effect of Injection Strategy

To investigate the effect of split injection, diesel injection quantity for the first injection was varied from 94% to 52% at 1800 rpm and 60% CNG substitution as shown in Figure 21. Figure 21 also provides the heat release trace for these test points. It was observed that with reduction in first injection quantity the burn duration reduced with higher peak heat release rate, resulting in higher NO_x emissions. THC emissions also increased due to less time available for mixing as the higher quantity of diesel fuel is injected later in the cycle.

It was noted in section 4.4.1.1 that CO emissions increased slightly as the combustion behavior changed with injection timings beyond 35 CA bTDC. In this case, the split injection quantity sweep simulated the effect of change in injection timing and hence a reduction in CO emissions was observed with reduction in first injection quantity. This trend in emissions and combustion phasing was observed with different injection timings for split injection quantity sweep.

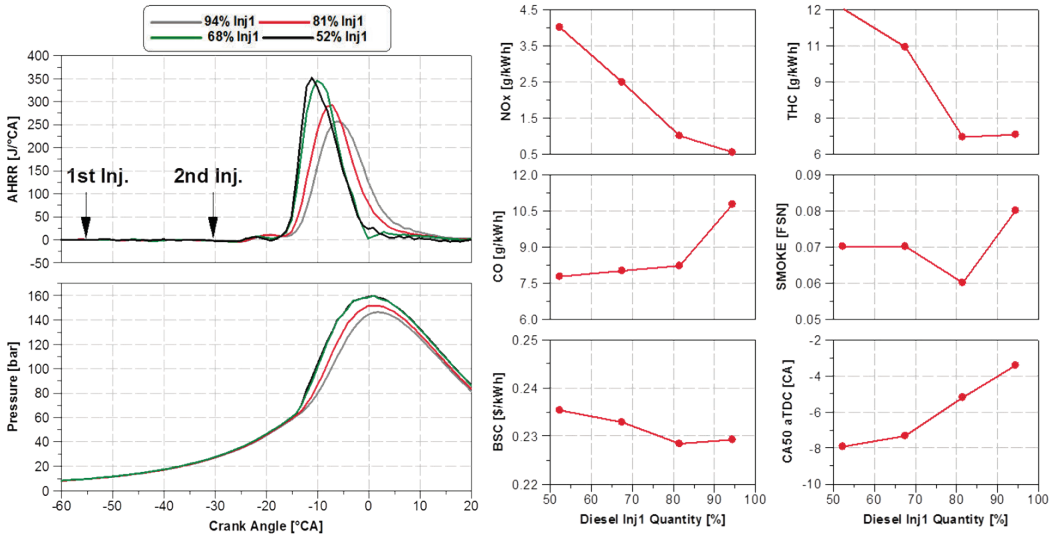

Figure 21 First-injection quantity sweep for a split injection with first injection at 56 bTDC and second injection at 31 bTDC, 1800 rpm 5 bar BMEP with 40% EGR and 60% CNG substitution [17]

4.4.1.3 Variation with Engine Speed

Based on the results of the substitution study at 1500 rpm and considering the observed NO_x and CO emissions tradeoff, 60% CNG substitution was used for further investigation at different engine speeds. Figure 22 summarizes the results obtained from a single injection timing sweep study conducted at 60% substitution for four different engine speeds. At each engine speed the maximum EGR achievable with the production hardware was applied.

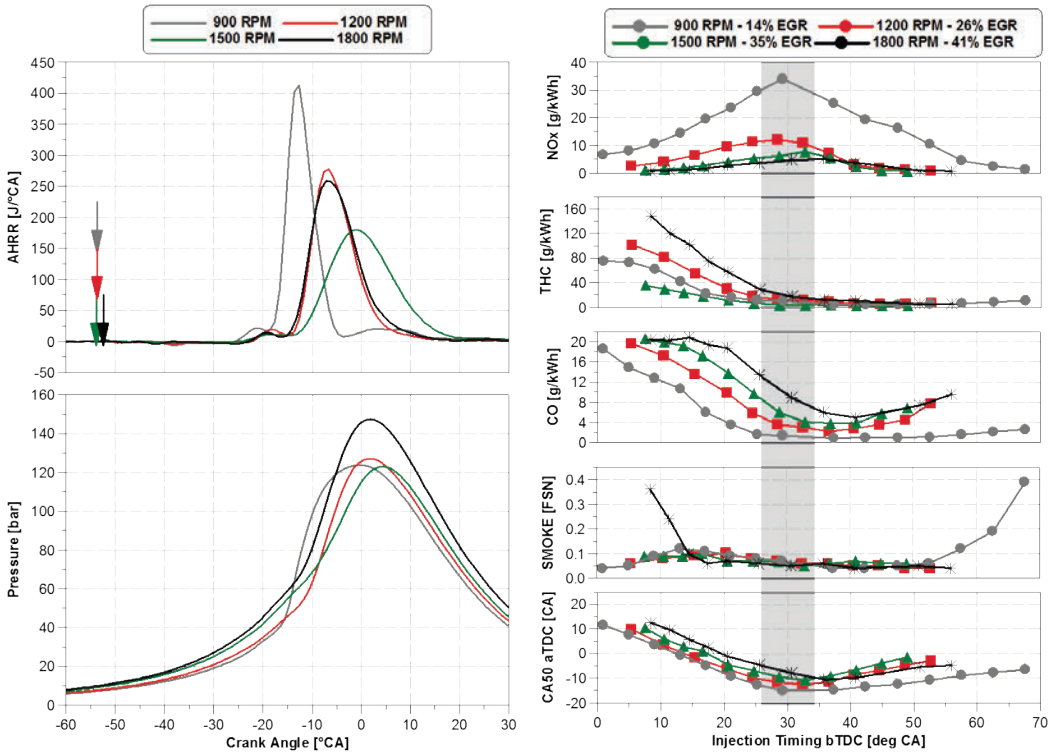

Figure 22 AHRR and cylinder pressure at 51-53 bTDC injection timing along with injection timing sweep at different engine speeds, 60% CNG substitution and 5 bar BMEP [17]

A similar change in combustion behavior, from conventional dual fuel to RCCI combustion, was observed at all engine speeds as shown in Figure 22. However, the injection timing at which the change in combustion behavior occurred advanced with an increase in engine speed, as can be seen in the NO_x and CA50 plot in Figure 22. The injection timing at which the combustion behavior changed was more advanced at 1800 rpm when compared to 1200 rpm.

As shown in Figure 22, at 60% substitution and fixed injection timing the ignition delay did not change significantly with an increase in engine speed. In general the lower residence time available at higher engine speed along with higher EGR rates leads to a more retarded and lower heat release peak with longer burn duration. This trend was observed from 900 rpm to 1500 rpm, however at 1800 rpm, the heat release rate advanced. This break in the trend can also be seen in the CA50 and NO_x plot shown in Figure 22. The cylinder pressure plot in Figure 22 shows that the in-cylinder pressure for the 1800 rpm case near the start of combustion is higher compared to the 1500 rpm case, which would imply that the in-cylinder temperatures near start of combustion would also be higher. This, coupled with the lower heat loses to the cylinder walls at higher speeds, might have resulted in the phasing for the 1800 rpm case to be earlier than the 1500 rpm case.

In general, for conventional injection timing, NO_x emissions were higher for lower engine speeds, due to an advanced combustion with a shorter duration and a higher peak heat release rate. Similar levels of NO_x could be achieved for all engine speeds by varying the injection timing. However, for RCCI combustion, the NO_x emissions for 1800 rpm are higher compared to the 1200 and 1500 rpm cases. This trend follows the earlier phasing seen with 1800 rpm as outlined in Figure 22. THC and CO emissions were reduced at lower engine speeds likely due to a higher residence time for combustion.

4.4.2 RCCI Combustion Evaluation at 12 bar BMEP

During investigation of RCCI combustion at 12 bar BMEP additional challenges, to those observed at 5 bar BMEP, were encountered. These include controlling maximum pressure rise rate, peak pressure, combustion phasing, air-fuel ratios, engine stability and higher THC emissions. This section overviews the results from the optimized RCCI combustion points at different engine speeds and further investigates the effect of certain key variables, such as boost pressure and rail pressure.

4.4.2.1 Variation with Engine Speed

Figure 23 overviews the emission and performance data for optimized RCCI combustion at three engine speeds. Both engine out and DOC out emission data are plotted in Figure 23, along with the comparison to the baseline diesel operation point. The DOC was a typical oxidation catalyst used on an on-highway truck diesel engine. RCCI combustion that provided significant reduction in engine out NO_x and PM emissions when compared to the baseline diesel operation could only be achieved at 1800 rpm. At 1200 and1500 rpm, peak pressures and maximum pressure rise rates limit the ability to achieve complete RCCI combustion. Table 4 summarizes the calibration parameters for these three operating points.

As seen in Figure 23, although the burn duration and phasing for the three engine speeds are similar, the residence time is quite different. At 1800 rpm, low levels of NO_x emissions could be achieved as compared to baseline diesel. However, at 1500 rpm, despite a lower peak heat release rate and similar combustion phasing compared to 1800 rpm, no significant reduction in NO_x emissions relative to baseline diesel operation was observed. The higher residence time available at lower engine speeds could be one reason for this behavior. In order to reduce NO_x emissions, a more retarded combustion phasing would be needed. This could be achieved by increasing the EGR rate, reducing boost pressure and/or increasing substitution.

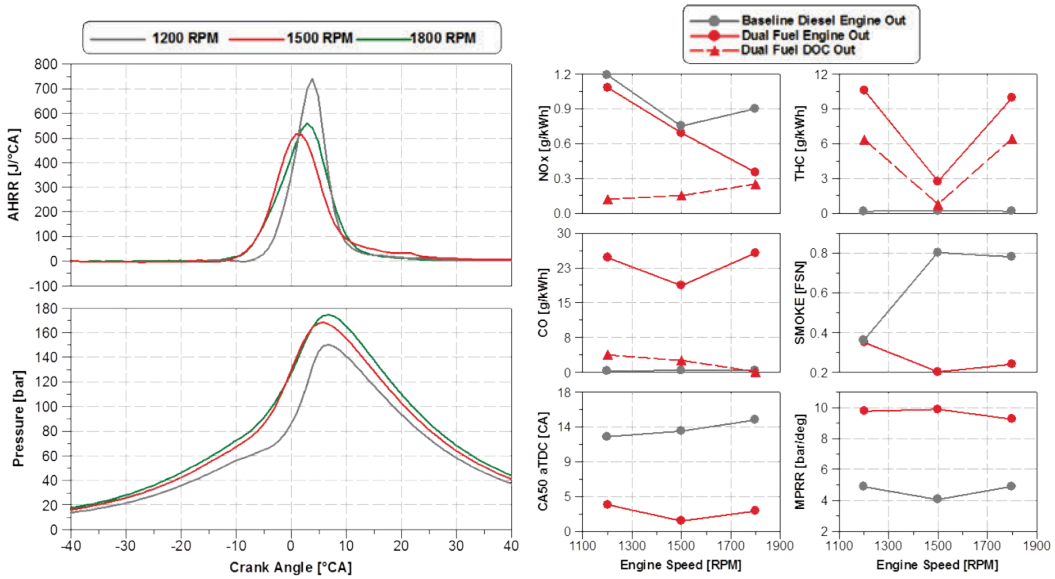

Figure 23 Comparison of baseline diesel and optimized dual fuel operating points at three different engine speeds at 12 bar BMEP [17]

At 12 bar BMEP, EGR rate and substitution could only be increased by increasing boost pressure as the engine was operating at stoichiometric conditions. However, increasing boost pressure had a counteracting effect and combustion phasing was advanced. It was observed that at stoichiometric conditions combustion phasing was more sensitive to changes in boost pressure as compared to higher EGR rate. This impact on combustion phasing is displayed in Figure 24. The combustion phasing and burn duration was later optimized at 1500 rpm to maintain MPRR within 10 bar/deg.

When compared to the baseline diesel combustion, THC and CO emissions were higher for dual fuel combustion, however most of THC emissions consisted of unburned CH_4. High CNG substitution levels inherently reduced the smoke emissions, with the exception of the 1200 rpm case, where higher EGR rates applied for dual fuel combustion resulted in smoke levels similar to baseline diesel. When operating at stoichiometric conditions, NO_x conversion was observed over DOC along with the THC and CO oxidation. At this lambda condition the DOC functioned as a three-way catalyst and a significant reduction in NO_x emissions was observed at the DOC outlet.

Table 4 Calibration parameters for dual fuel operating points at 14 bar BMEP load points

Engine Speed [rpm]	1200	1500	1800
Substitution [%]	83	86	81
EGR Rate [%]	30	34	38
Injection 1 Timing [bTDC Deg °CA]	44	80	65
Injection 2 Timing [bTDC Deg °CA]	16	40	33
Injection 1 Quantity [%]	51	52	48
Injection Pressure	1500	1000	1880
Boost Pressure [Bar]	1.6	1.8	1.9
Lambda [-]	0.95	1.01	0.97

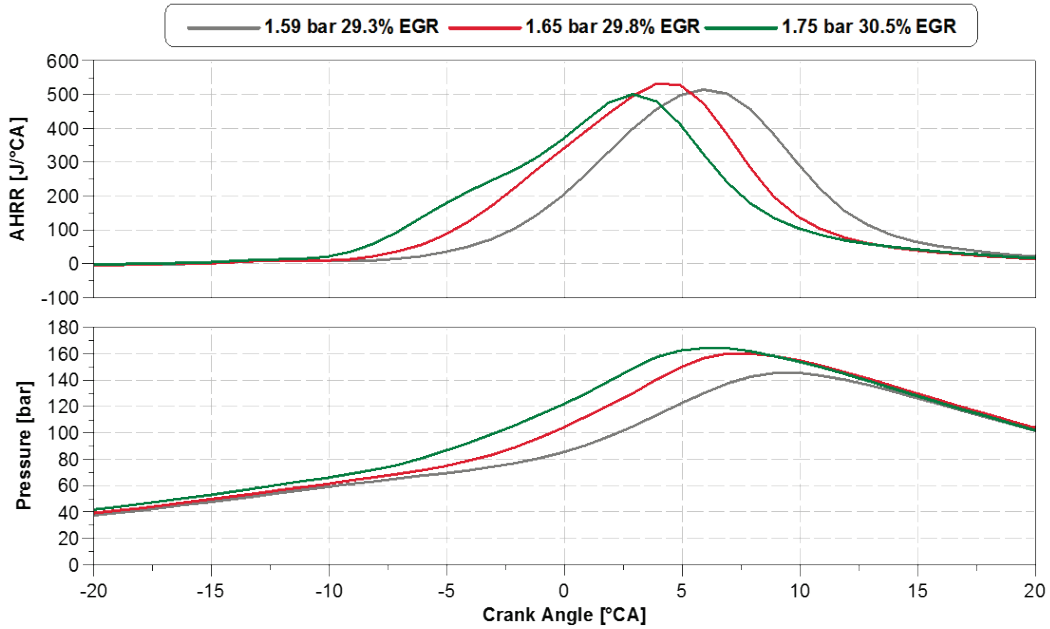

Figure 24 AHRR and cylinder pressure showing the effect of boost pressure at 1200 rpm and 12 bar BMEP with 30% EGR and 87% CNG substitution. Split injection timing fixed at 60-30 bTDC with a 50/50 quantity split [17]

4.4.2.2 Effect of Injection Strategy

Similar to the strategy explored at 5 bar BMEP, a split injection strategy was also evaluated at 12 bar BMEP to achieve RCCI combustion with advanced timings by varying the diesel injection quantity for the first injection from 94% to 47%. The main

and post injection timings were fixed and diesel quantity distribution between the two injections was varied as shown in Figure 25.

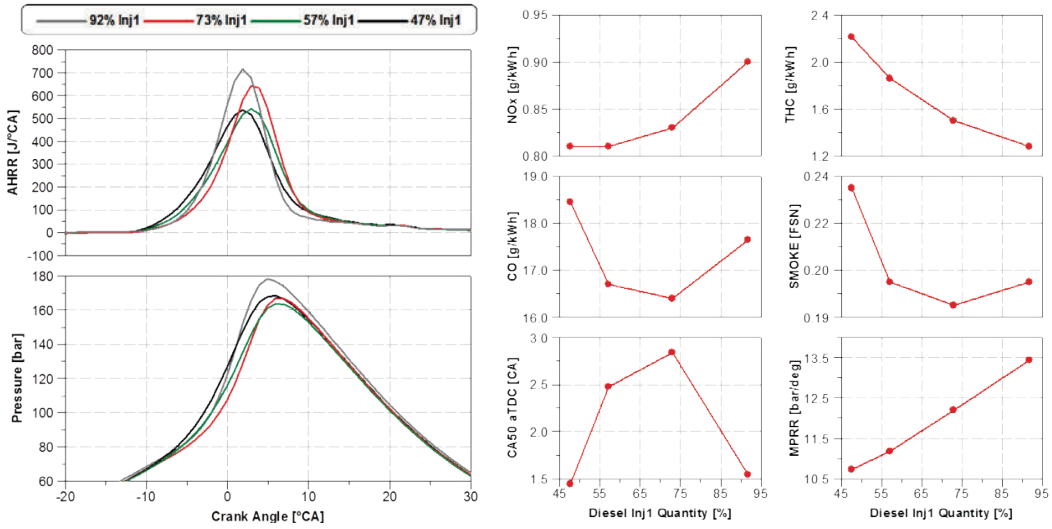

Figure 25 First injection quantity sweep for a split injection with first injection at 60 bTDC and second injection at 30 bTDC, 1500 rpm 12 bar BMEP with 34% EGR and 86% CNG substitution [17]

Figure 25 also provides the heat release and cylinder pressure curves for the four different split injection strategies. As the injection quantity in first injection was reduced the burn duration increased and the peak of heat release rate decreased due to better mixture stratification obtained through split injection. This is in contradiction to that observed at 5 bar BMEP with spilt injection, where the peak of heat release rate increased and the burn duration reduced with reduction in first injection quantity. At a lower substitution level, as in the case of 5 bar BMEP, split injection can over-stratify the mixture. This over-stratified mixture can then lead to simultaneous auto-ignition of a larger quantity of diesel, as opposed to a controlled heat release achieved through a spatial gradient of fuel reactivity.

The maximum pressure rise rates reduced with a reduction in quantity of the first diesel injection. A slight reduction in NO_x emissions was observed, possibly due to a better mixture stratification obtained through split injection. The increase in quantity of the second injection reduced the mixing time and led to higher smoke, THC and CO emissions for a 47% injection 1 diesel quantity when compared to a 92% injection 1 quantity.

4.4.2.3 Effect of Rail Pressure Variation

One of the limitations to achieve RCCI combustion at 1500 rpm was the high cylinder pressure rise rates. To control the pressure rise rates rail pressure was varied from 1800 bar to 1000 bar as shown in Figure 26. Once again, looking at the heat release rate and cylinder pressure curves in Figure 26, it can be observed that with reduced rail pressure

the peak of the heat release rate is reduced and the burn duration is increased. This is likely a result of increased mixture stratification due to a larger diesel droplet size associated with the lower injection pressure and thus more time for mixing when compared to higher injection pressure. Maximum pressure rise rates and NO_x emissions reduced with lower injection pressure, however smoke, THC and CO emissions increased.

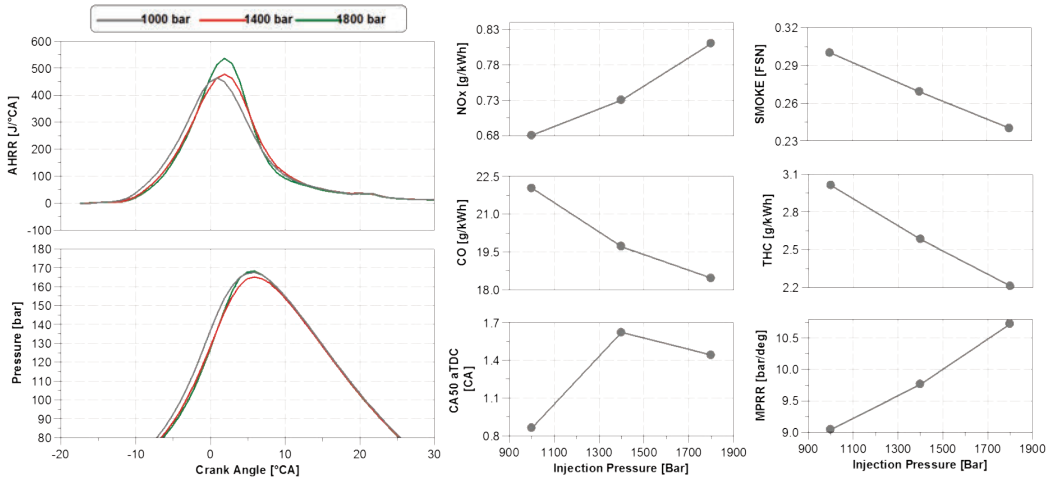

Figure 26 AHRR and cylinder pressure for injection pressure variation with 60-30 bTDC split injection along with injection pressure sweep with 60-30 bTDC split injection and 50/50 quantity split, at 1500 rpm 12 bar BMEP with 34% EGR and 86% CNG substitution [17]

4.4.3 Summary of RCCI Investigation at 5 bar and 12 bar BMEP

Based on the experimental results at 5 bar BMEP, we can conclude that with an increase in CNG substitution the burn duration increases, leading to a retarded combustion phasing. More favorable CA50 can be achieved by increasing substitution for a fixed timing, however at the expense of higher THC and CO emissions. Combustion phasing and burn duration at 5 bar BMEP could also be controlled through EGR rate. Higher EGR rate retarded combustion phasing and increased the combustion duration. Although combustion efficiency was lower for higher EGR rates, better fuel conversion efficiency was observed due to a higher thermal efficiency. Split injection, with a higher injection quantity in the second injection, advances combustion phasing due to a higher quantity of diesel fuel being injected later in the cycle and leading to an insufficiently mixed charge. The injection timing at which the change in combustion behavior occurred advances with an increase in engine speed. The THC and CO emissions were lower as the engine speed reduced.

At 12 bar BMEP RCCI combustion could be achieved at 1800 rpm, but at lower engine speeds maximum pressure rise rates limited the ability of achieving RCCI combustion with lower NO_x emissions. In order to control maximum pressure rise rates and combustion phasing, boost pressures had to be reduced. It was observed that maximum pressure rise rates were more sensitive to boost pressure than higher EGR levels. At 1500

rpm split injection and a reduction in injection pressure were effective in controlling maximum pressure rise rates and peak pressure. Figure 27 highlights the test points where RCCI combustion with low NO_x emissions was achieved and also highlights the challenges encountered in achieving low NO_x RCCI combustion at the remaining load points.

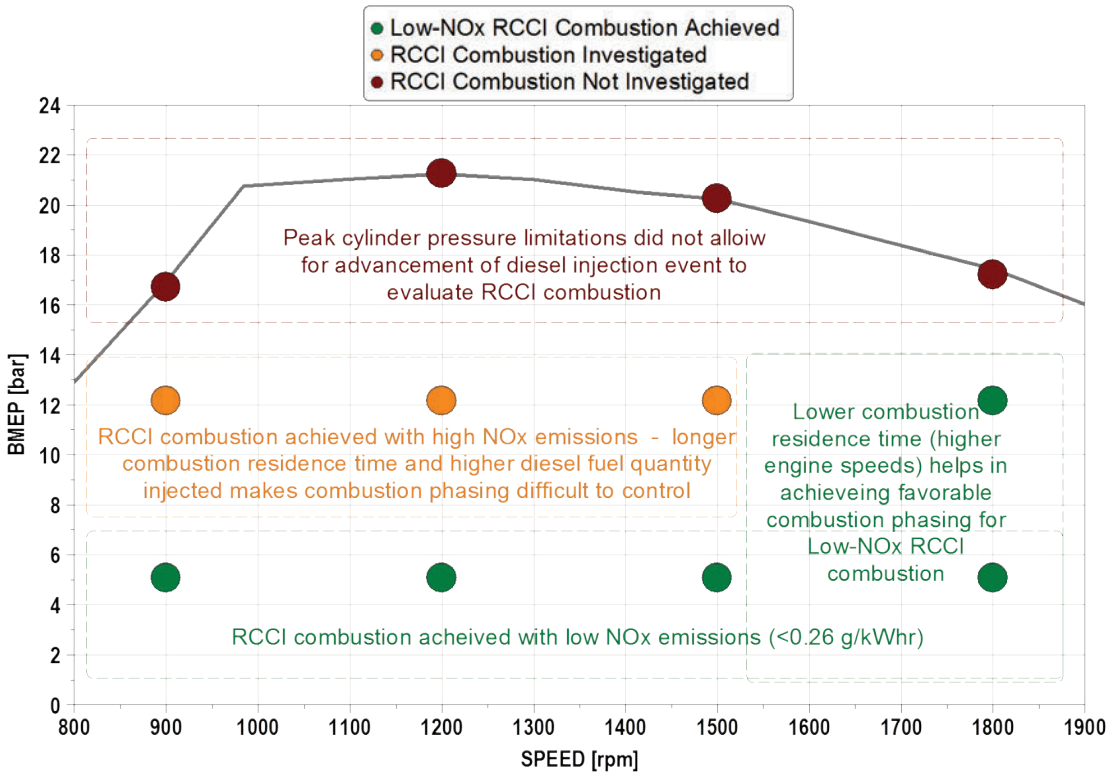

Figure 27 Overview of RCCI combustion investigation results at 12 specific test points

5 CFD Simulation setup

In order to better understand the behavior of RCCI combustion with diesel-CNG, computational studies were conducted using CONVERGE CFD software. The complete engine geometry, including the intake and exhaust ports, was modeled in CONVERGE as shown in Figure 28. Boundary conditions for the gas exchange simulations were obtained from a calibrated GT-Power model of the engine. Figure 29 provides a schematic of the GT-Power model used for generating the boundary conditions. The model was calibrated against the baseline diesel and dual fuel data with production turbocharger. For each operating point evaluated in CFD a measured pressure analysis was conducted in GT-Power to confirm accuracy of the measured data. Experimental measurements showed considerable in-cylinder pressure variation between cylinders as highlighted in Figure 30. The measured pressure analysis approach was used to identify the cylinder# that should be used for generating boundary conditions for CFD simulations as shown in Figure 31. The measured pressure analysis calculates the burn rate from the experimental cylinder pressure trace and specified fuel quantity. The analysis outputs two key variables – consistency check and LHV multiplier which are used to identify the appropriate cylinder pressure traces. As general guideline, for considering a cylinder pressure trace for generating boundary conditions, the consistency check needs to pass (1) and the LHV multiplier needs to be closer to 1 (±5%). Referring to Figure 31, for the 1500 rpm and 5 bar BMEP operating cylinder #5 was selected for generating boundary conditions as compared to cylinder #2. Another advantage of using a validated GT-Power model lies in the ability to quantify and compare boundary conditions at IVC between CFD simulations and test data. In the current study the IVC gas composition along with cylinder pressure and temperature predictions from the GT simulations were compared with the predictions from the gas exchange simulations in CFD to generate appropriate start conditions for subsequent CFD combustion simulations.

For the Converge CFD model setup the grid resolution in the cylinder was set to 1 mm. Further grid resolution was also added in the form of adaptive mesh refinement (AMR) on both velocity and temperature fields with a sub-grid criterion of 1m/s and 2.5K, respectively. AMR is a feature in CONVERGE which refines the mesh at every time-step as the difference between two adjacent cells falls below the sub-grid criterion. This feature enables greater resolution of relevant parameters in-cylinder.

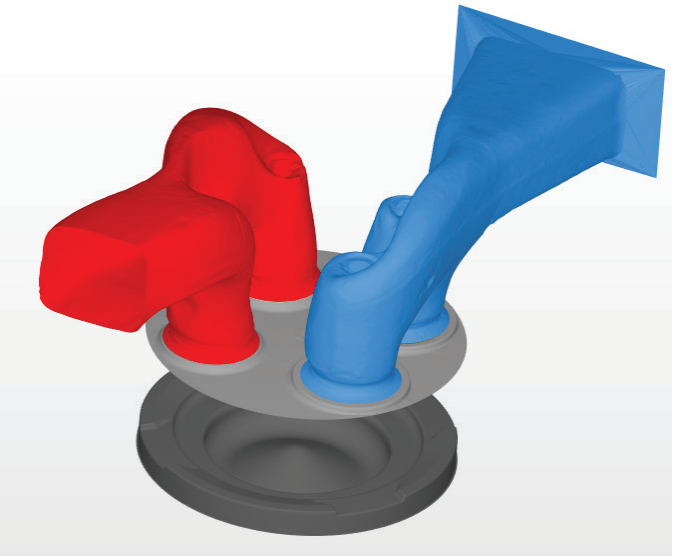

Figure 28 Model setup in CONVERGE CFD Software [17]

Initial combustion modeling was executed with the SAGE detailed chemistry solver using the Rahimi mechanism [38]. This is a reduced CNG-diesel mechanism that consists of 76 species and 464 reactions. Refer appendix B for additional details regarding the Rahimi mechanism. CNG as a fuel was modeled as methane (CH_4) and diesel fuel was modeled as n-heptane (C_7H_{16}). n-heptane was used in place of diesel fuel because its cetane number (CN~56) is relatively close to that of typical diesel fuels (CN~50).The injector consist of a 8-hole nozzle with an included spray angle of 146 deg and 0.19 mm nozzle hole diameter. The spray modeling was set up using a modified Kelvin Helmholtz (KH) – Rayleigh Taylor (RT) droplet breakup model without specifying the breakup length. The turbulence model used combines both RANS (Reynolds Averaged Navier-Stokes) and RNG (Re-Normalisation Group) theory-derived k-ε equations. Soot was predicted by the Hiroyasu soot model, which uses acetylene (C_2H_2) as a precursor for the soot species. NO_x emissions were predicted in terms of nitrogen oxide (NO) from the Rahimi mechanism and further multiplied by 1.533 to compute the NO_x emissions. The 1.533 factor corresponds to the ratio of the molecular weight of NO_2 (46 g/mole) and NO (30 g/mole).

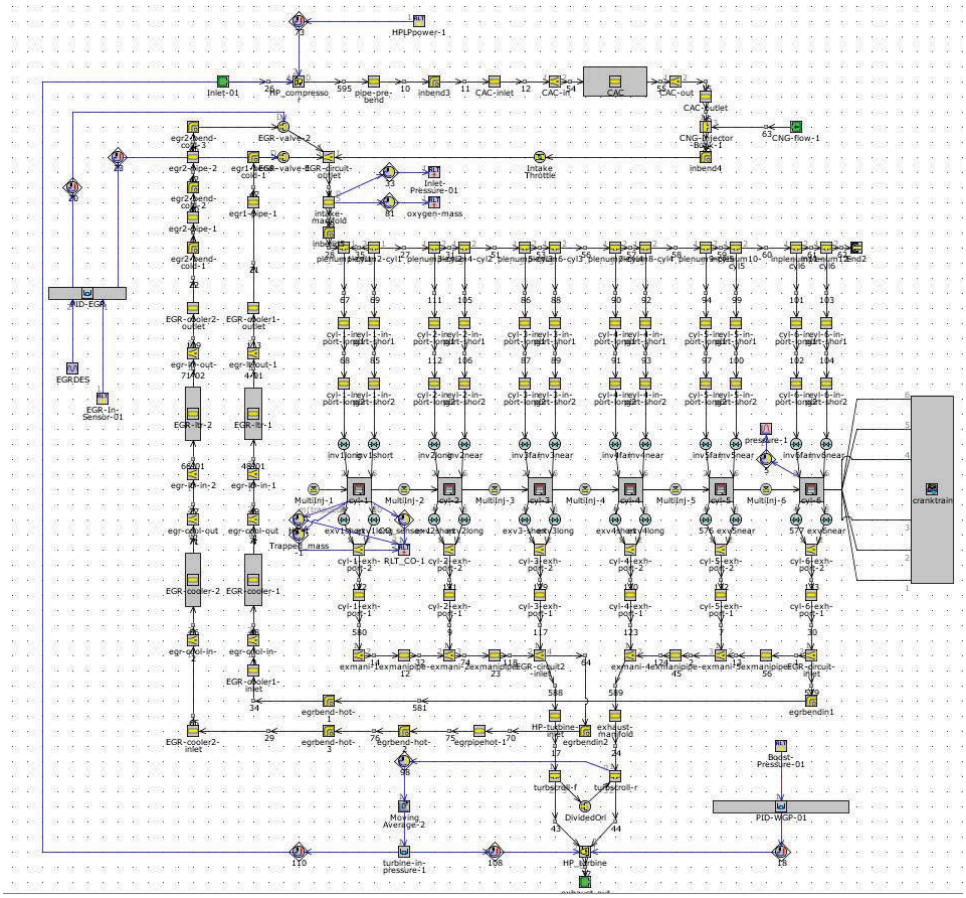

Figure 29 Overview of the GT-Power engine model used for generating boundary conditions for the CFD studies

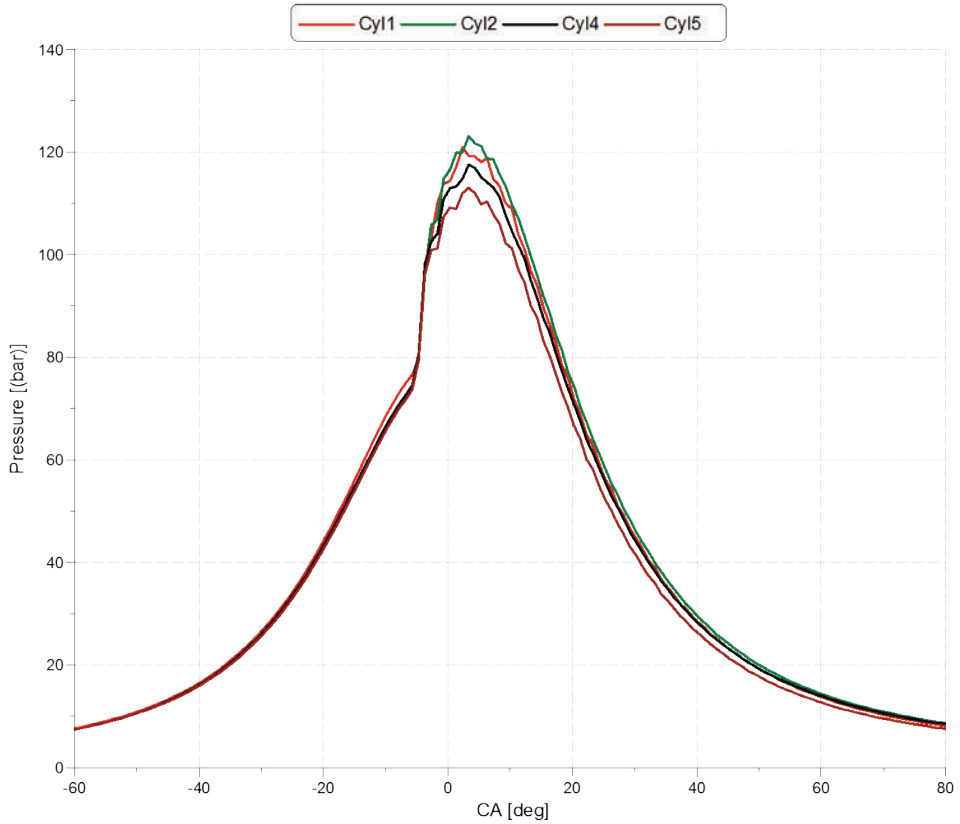

Figure 30 Experimental measurements showing cylinder to cylinder pressure variations for 40% CNG substitution and 36% EGR at 1500 rpm and 5 bar BMEP

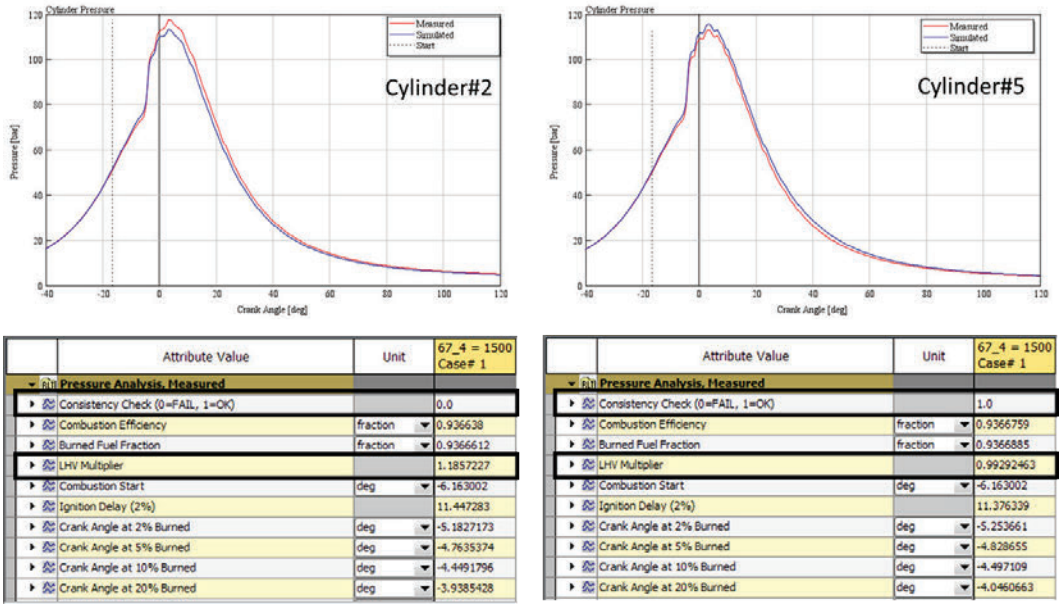

	Attribute Value	Unit	67_4 = 1500 Case# 1
	Pressure Analysis, Measured		
	Consistency Check (0=FAIL, 1=OK)		0.0
	Combustion Efficiency	fraction	0.936638
	Burned Fuel Fraction	fraction	0.9366612
	LHV Multiplier		1.1857227
	Combustion Start	deg	-6.163002
	Ignition Delay (2%)		11.447283
	Crank Angle at 2% Burned	deg	-5.1827173
	Crank Angle at 5% Burned	deg	-4.7635374
	Crank Angle at 10% Burned	deg	-4.4491796
	Crank Angle at 20% Burned	deg	-3.9385428

	Attribute Value	Unit	67_4 = 1500 Case# 1
	Pressure Analysis, Measured		
	Consistency Check (0=FAIL, 1=OK)		1.0
	Combustion Efficiency	fraction	0.9366759
	Burned Fuel Fraction	fraction	0.9366885
	LHV Multiplier		0.99292463
	Combustion Start	deg	-6.163002
	Ignition Delay (2%)		11.376339
	Crank Angle at 2% Burned	deg	-5.253661
	Crank Angle at 5% Burned	deg	-4.828655
	Crank Angle at 10% Burned	deg	-4.497109
	Crank Angle at 20% Burned	deg	-4.0460663

Figure 31 Example of measured pressure analysis set up in GT-Power using pressure traces from cylinder#2 and #5 for 40% CNG substitution and 36% EGR at 1500 rpm and 5 bar BMEP

6 CFD Study

The CFD study aims to summarize the impact of key control variables in achieving a low NO_x RCCI combustion at 1500 rpm and a mid-load (12 bar BMEP) and a high load (20 bar BMEP) operating points. The study was conducted in three parts. The first part of the study focused on determining the reaction mechanism that could be used for evaluating low temperature RCCI combustion with diesel and natural gas. The computational results were evaluated against experimental RCCI results at 5 bar BMEP for two different engine speeds and a range of control parameters including CNG substitution, EGR rate and injection timing. Once an appropriate reaction mechanism was identified the second part of the study involved determining the control parameters requirements for achieving a Low NO_x RCCI combustion at 12 bar BMEP and 1500 rpm. The following control parameters were evaluated as part of the CFD investigations at 12 bar BMEP:

- CNG substitution (Reactivity level)
- EGR rate (Dilution)
- Spray angle
- Rail pressure
- Compression ratio

The third part of the study focused on applying the control parameters identified at 12 bar BMEP to the 20 bar BMEP operating point for achieving a Low NO_x RCCI combustion. An additional parameter in terms of multiple injection (degree of premixing) was also evaluated at 20 bar BMEP.

6.1 Evaluation of Reaction Mechanism

Initial CFD simulations using the Rahimi mechanism [38] were conducted in Converge CFD software at 1500 rpm and 5 bar BMEP. This is a reduced CNG-diesel mechanism that consists of 76 species and 464 reactions and is recommended by Converge for diesel natural gas dual fuel applications. Details related to the specific test point evaluated in CFD are provided in Table 5.

Table 5 RCCI operating point evaluated in CFD

Engine Speed	1500 rpm
Engine Load	5 bar BMEP
CNG Substitution	60%
Injection Timing bTDC	42.5 CA bTDC
EGR	35%
Compression Ratio	16.7:1

Injection Pressure	1900 bar
Intake Pressure	1.7 bar
Lambda	2.26

Initial CFD investigations at 1500 rpm and 5 bar BMEP operating point using the Rahimi mechanism shows that there is a large discrepancy in the cylinder pressure predictions with CFD and those acquired from testing, as highlighted in Figure 32. The combustion efficiency predicted in the CFD is much lower in comparison to the experimental data, thus resulting in high levels of unburned hydrocarbon and CH_4 emissions; as shown in Figure 33.

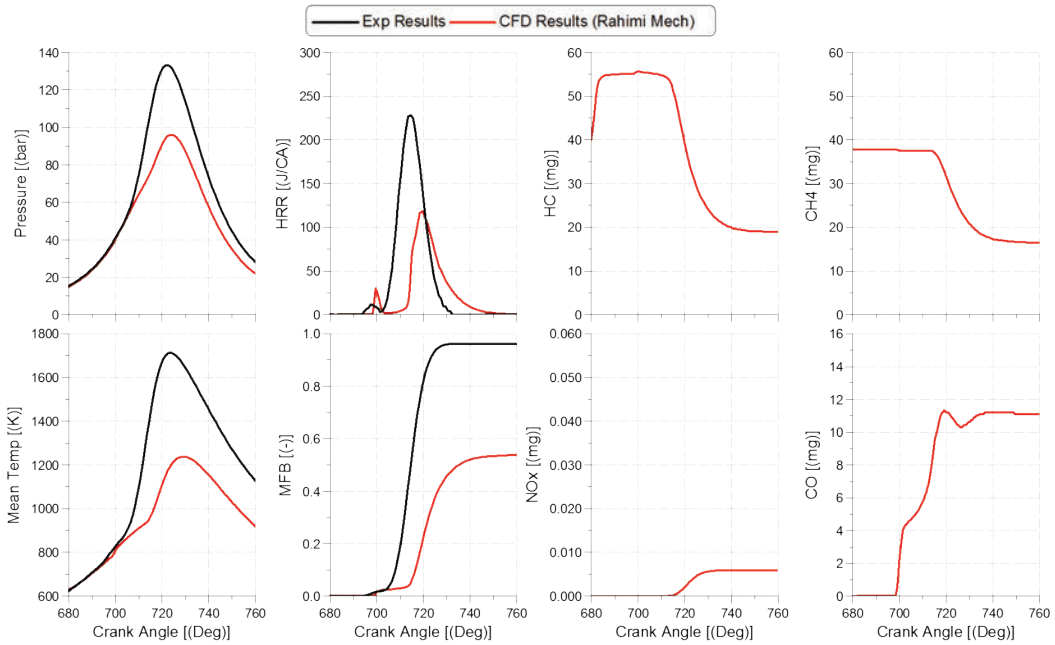

Figure 32 Comparison of CFD predictions vs. test results at 1500 rpm and 5 bar BMEP with 60% CNG substitution, 35% EGR and SOI: 42.5°bTDC

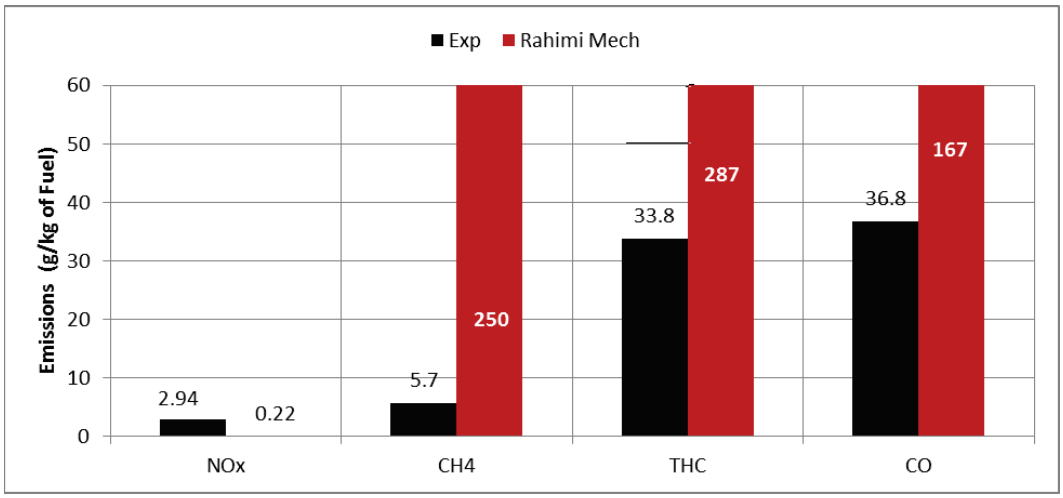

Figure 33 Comparison of emission predictions with CFD vs. test results at 1500 rpm and 5 bar BMEP with 60% CNG substitution, 35% EGR and SOI: 42.5°bTDC

Studies conducted by Zhang et al., [28] have shown that the gas temperature at IVC has a strong influence on the start of combustion for a premixed diesel CNG mixture. As shown in Figure 34, the cylinder pressure predictions in CFD improve with an offset of the initial gas temperature at intake valve closing (IVC). This also leads to improvements in combustion efficiency and lower CH_4 emissions as highlighted in Figure 35. A similar behavior was also observed by the authors in reference [29], for a conventional dual fuel combustion evaluation using Rahimi mechanism with Converge CFD software. However, no explanation was provided for the need to offset the gas temperature at IVC and for the final temperature offset that was used. In this study it was observed that an offset of the IVC gas temperatures helped to improve the methane oxidation. However, even after offsetting the IVC gas temperature by 22 K, or 6% compared to the base simulation, evaluating the HRR we see a 6-7 CA delay in start of main combustion event thereby leading to lower peak cylinder pressure predictions when compared to test data. Even if the temperature offset could be used to match test results there are two flaws in this approach with respect to the current study. First as outlined in section 5, a validated GT-Power model was used in this study to compare the in-cylinder pressure and temperature conditions at IVC between the GT model and CFD gas exchange simulations. Arbitrarily offsetting the IVC temp could violate this validation Second different temperature offset values might need to be applied based on the diesel SOI to match the test results which would then impose limitations on the predictive nature of the CFD simulations. Hence offsetting the IVC temperatures to speed up the reaction mechanism was deemed inappropriate for the current study.

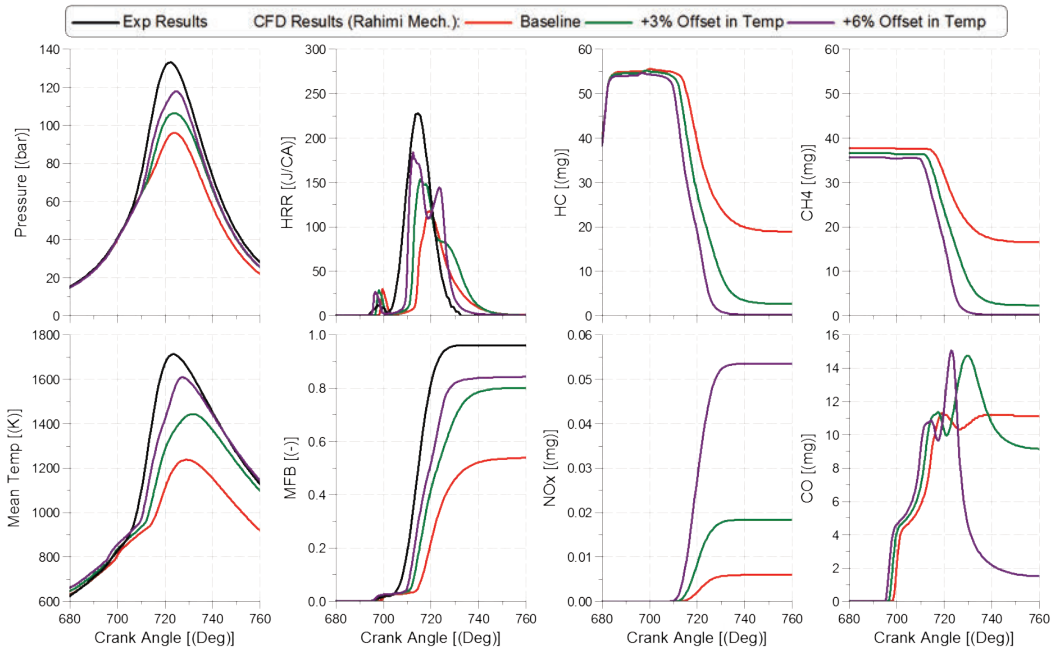

Figure 34 Comparison of CFD predictions with different offset on IVC gas temperatures at 1500 rpm and 5 bar BMEP with 60% CNG substitution, 35% EGR and SOI: 42.5°bTDC

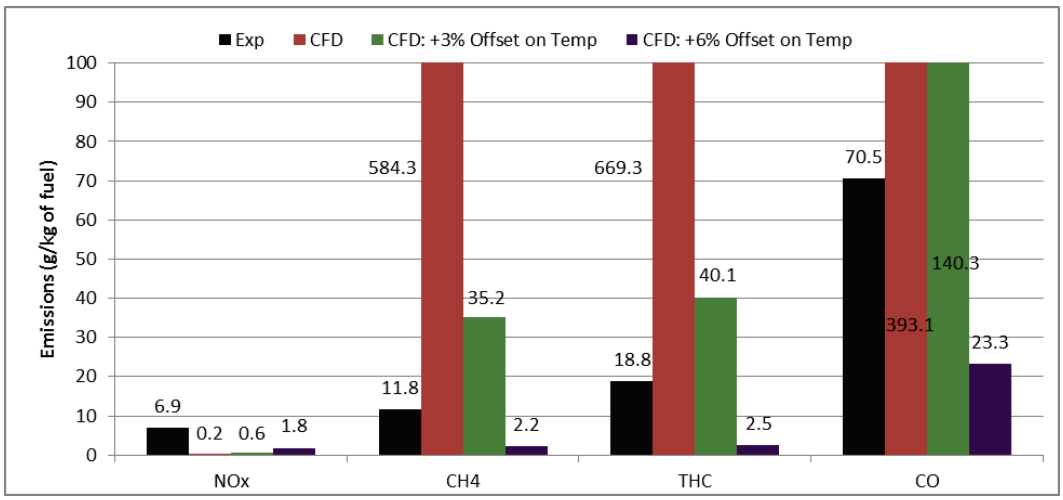

Figure 35 Comparison of emissions predictions with different offset on IVC gas temperatures at 1500 rpm and 5 bar BMEP with 60% CNG substitution, 35% EGR and SOI: 42.5°bTDC

Since the Rahimi mechanism over predicted the ignition delay, it was hypothesized that the low temperature reactions related to RCCI combustion with diesel and natural gas were not accurately represented in this mechanism. As part of this study three alternate

mechanisms were investigated using Converge CFD software to improve baseline predictions. The first mechanism involved using the original GRI 3.0 mechanism developed by researchers at Stanford University for methane [39]. The second mechanism involved using the well-established Chalmers mechanism for n-heptane which is used as a surrogate for diesel fuel [40]. The final mechanism evaluated consisted of combining the original GRI 3.0 mechanism with the Chalmers mechanism and was termed as the Combined mechanism. The Combined mechanism consisted of 76 species and 424 reactions, refer Appendix C for more details regarding the Combined mechanism. Initial simulations with the alternate mechanisms at 1500 rpm and 5 bar BMEP show a closer match in cylinder pressure with the Combined mechanism when compared to the test data; as highlighted in Figure 36. The cylinder pressure predictions from the GRI 3.0 mechanism are similar to the Rahimi mechanism whereas the predictions from the Chalmers mechanism are closer to the test results but the ignition delay is over predicted leading to a later combustion phasing. Referring to Figure 38 we see that for the combined mechanism the low temperature reactions start near the piston crown region closer to the liner at around 708 CA and then the flame front moves towards the center of the piston bowl. On the other hand the low temperature reactions for the Rahimi mechanism start near the step region of the piston bowl at a much later crank angle (around 718 CA) and then move towards the liner region. Since the diesel SOI for this case is very advanced it is expected that a significant amount of the injected fuel hits the piston crown region and stays in the crevice region. Hence it is not unexpected that the low temperature reactions start in the piston crown region as seen for the Combined mechanism compared to the Rahimi mechanism.

The NO_x emissions prediction from CFD is much closer to the experimental value with the Combined mechanism compared to all other mechanisms investigated; as highlighted in Figure 37. The unburned hydrocarbon and CH_4 emission predictions with the Combined and the Chalmers mechanism are much lower compared to the test data. In case of the Rahimi and GRI 3.0 mechanism where the cylinder pressure are under predicted, the unburned hydrocarbon and CH_4 emission are much higher compared to the test data. In conclusion the Combined mechanism does a better job in predicting the experimental combustion behavior and NO_x emissions compared to the other mechanisms investigated, however the absolute NO_x emission predictions from the Combined mechanism are still lower by 40% compared to the experimental results.

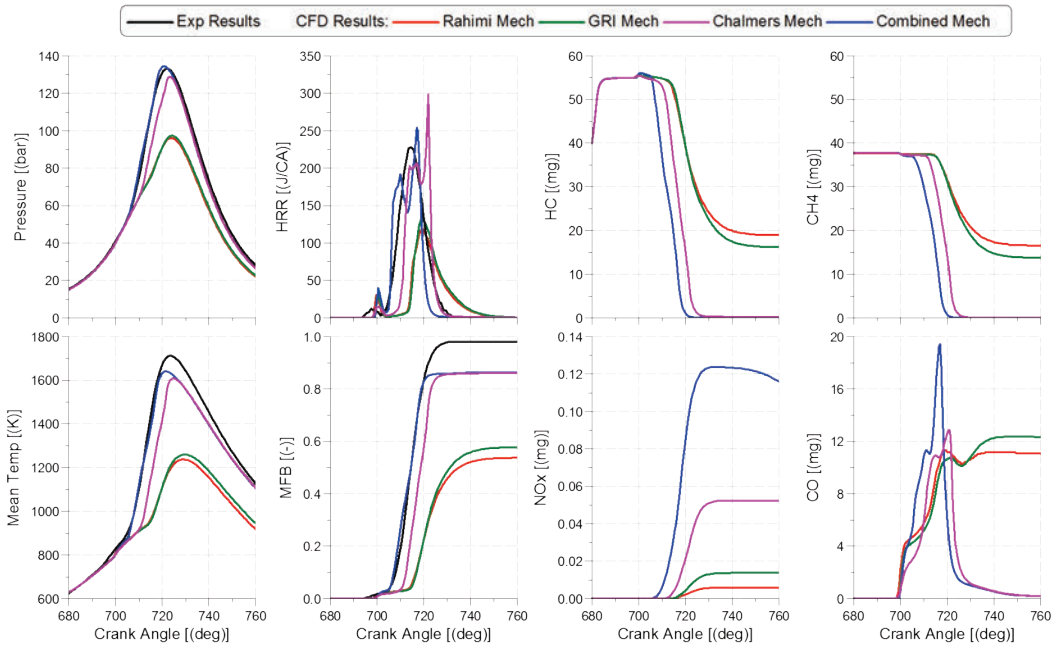

Figure 36 Comparison of performance and emissions predictions on a CA basis with four different mechanisms at 1500 rpm and 5 bar BMEP with 60% CNG substitution, 35% EGR and SOI: 42.5°bTDC

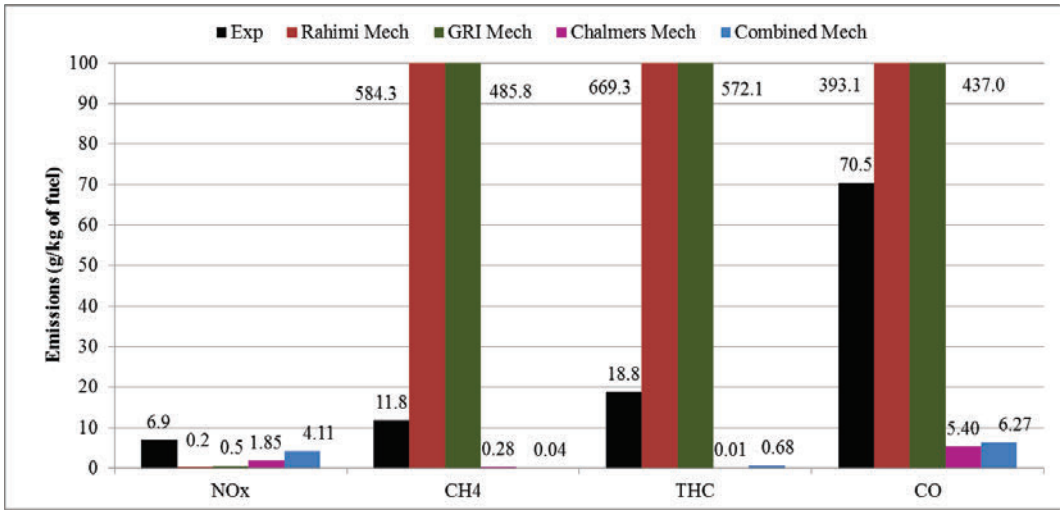

Figure 37 Comparison of emissions predictions with two different mechanisms at 1500 rpm and 5 bar BMEP with 60% CNG substitution, 35% EGR and SOI: 42.5°bTDC

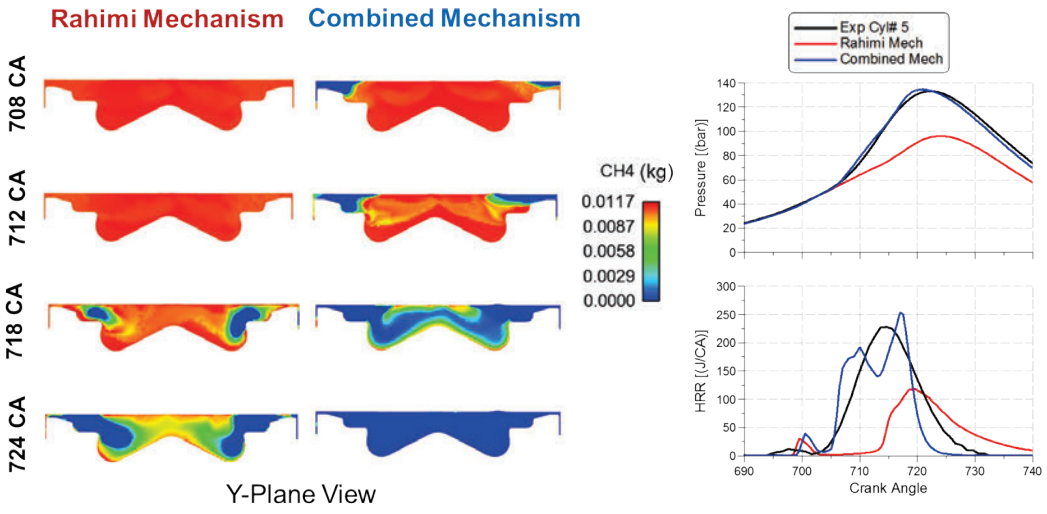

Figure 38 CFD plots comparing the low temperature heat release prediction between Combined and Rahimi mechanism at 1500 rpm and 5 bar BMEP with 60% CNG substitution, 35% EGR and SOI: 42.5°bTDC

With the aim to reduce computational time for the CFD investigations using Converge a 45 deg sector model ($1/8^{th}$ model) was created from the full geometry model. The sector model is used to simulate impact of one nozzle spray. The 45 deg sector angle corresponds to the area covered by one spray in an 8-hole nozzle as applied in the full geometry simulations. Figure 39 shows the correlation in cylinder pressure and HRR predictions between the full geometry model and the sector model while Figure 40 compares the emissions predictions between the full geometry and the sector model. The sector geometry predicts a shorter ignition delay compared to the full geometry model which results in earlier start of combustion as shown in Figure 39. However after the initial heat release peak the combustion slows down in the sector model compared to the full geometry model and then results in a higher second HRR peak. The slowdown in combustion could be attributed to the movement of the fuel within the sector model. One key assumption that is made while simulating a sector case is in regards to the fuel mass that leaves the boundary of the sector. This fuel mass is assumed to enter the sector geometry from the other end to mimic spray to spray interactions that would be seen in the full geometry case. This assumes that all sprays in the full geometry behave identical. This assumption has its limitation especially in the current situation where premixed methane is present in the cylinder and may lead to unfavorable fuel to fuel interaction resulting in fuel rich regions which, in the sector case, might have resulted in combustion slow down after the initial shorter ignition delay predictions.

The peak cylinder pressures between sector and full geometry cases are similar as shown in Figure 39. The shorter ignition delay along with the higher secondary HRR peak results in higher mean gas temperature. The NO_x emission predictions with the sector model are 30% higher compared to the full geometry model predictions due to the higher mean gas temperatures. However the NO_x emissions predictions from the sector case are

more closely matched (14% lower) with the experimental results compared to the full geometry results (40% lower). The unburned hydrocarbon and CO emissions predictions are higher with the sector case compared to the full geometry but still considerably lower compared to the test data. Overall the cylinder pressure and heat release trace from the sector model shows a reasonable correlation with the full geometry model predictions and also the NO_x emissions predictions in the sector model are closer to the experimental values, hence it was concluded that a sector model could be used for further evaluation to improve computational efficiency.

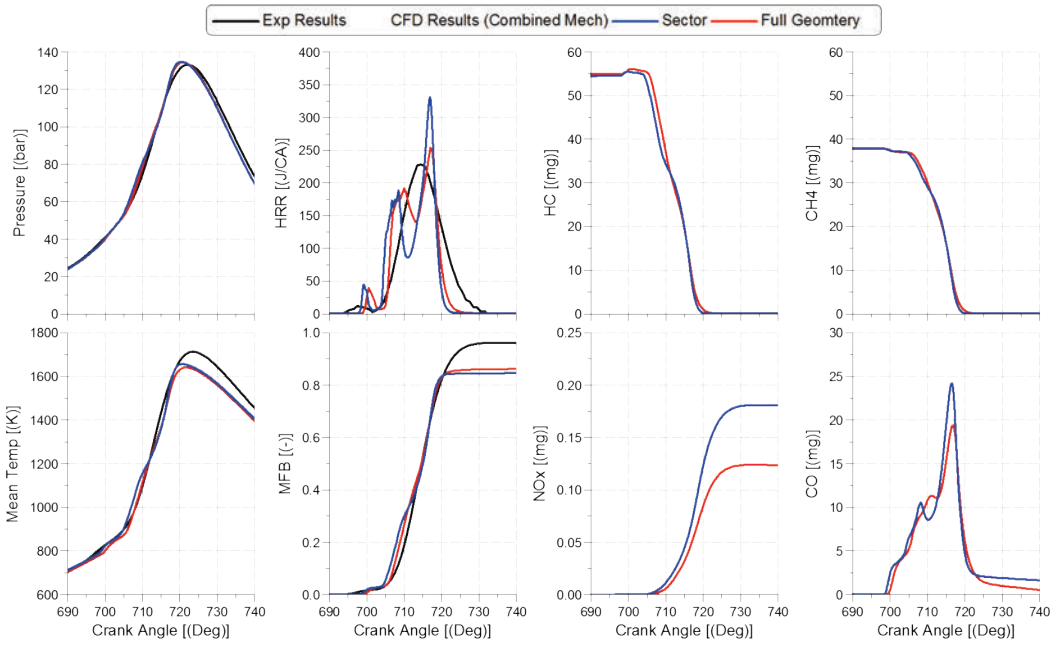

Figure 39 Comparison of performance and emission predictions for full geometry and sector case with modified reaction mechanisms at 1500 rpm and 5 bar BMEP with 60% CNG substitution, 35% EGR and SOI: 42.5°bTDC

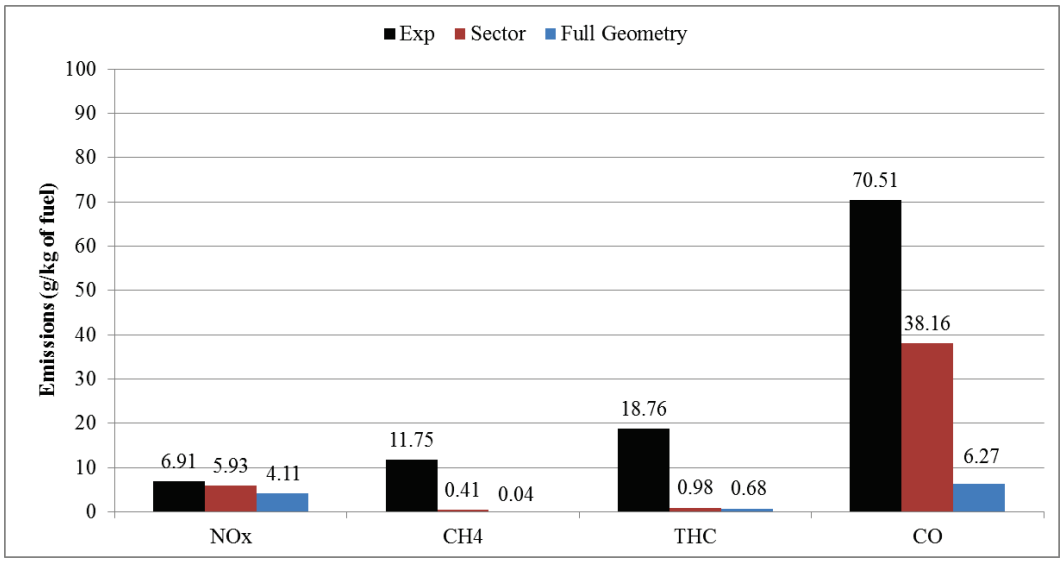

Figure 40 Comparison of emission predictions for full geometry and sector case with modified reaction mechanisms at 1500 rpm and 5 bar BMEP with 60% CNG substitution, 35% EGR and SOI: 42.5°bTDC

To validate the feasibility of using the Combined reaction mechanism at a higher load point, CFD simulations were performed with a sector model at 1500 rpm and 12 bar BMEP. The operating point considered 38% EGR and 60% CNG substitution along with a single diesel injection event close to the top dead center location (7.3 CA bTDC). The diesel injection timing used in the test case corresponds to the timing typically employed with conventional dual fuel combustion. Since low NO_x RCCI combustion was not achieved at the 1500 rpm and 12 bar BMEP during the experimental studies, an alternative test condition was required to validate the Combined reaction mechanism. Two factors favored the use of a diesel injection timing near TDC for this CFD investigation. First, the combination of EGR percentage and CNG substitution employed in the test case were similar to the conditions that would be employed to achieve low NO_x RCCI combustion. Second, the resultant NO_x emissions for the dual fuel case with timing near TDC (0.64 g/kWh) were lower than those observed with base diesel operation (1.02 g/kWh).

From Figure 41 we can see that the HRR and cylinder pressure predictions from CFD model are over predicted compared to the experimental results while Figure 42 shows that the corresponding NO_x emissions predictions from CFD are higher when compared to the experimental results. Overall, the predictions from the Combined mechanism do not show a good correlation with the experimental results for the test conditions evaluated at 1500 rpm and 12 bar BMEP.

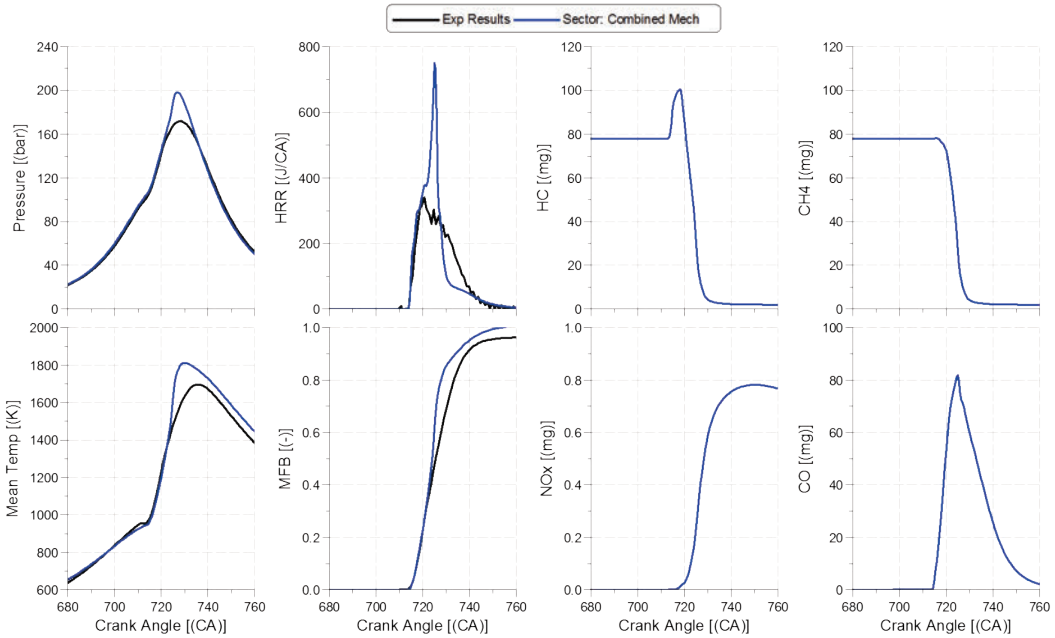

Figure 41 Comparison of performance and emissions predictions on a CA basis at 1500 rpm and 12 bar BMEP with 60% CNG substitution, 38% EGR and SOI: 7.3°bTDC

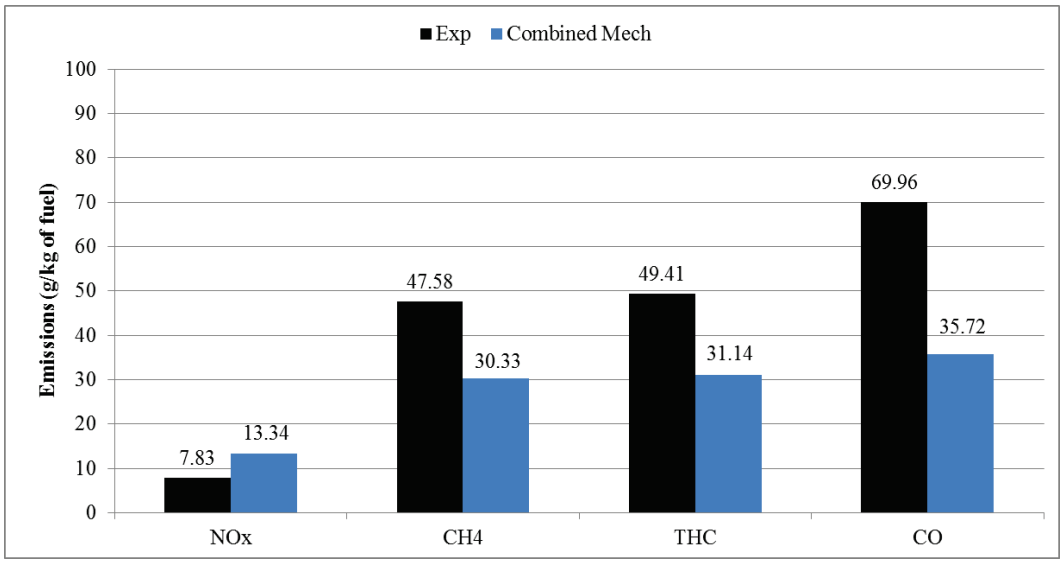

Figure 42 Comparison of emissions predictions at 1500 rpm and 12 bar BMEP with 60% CNG substitution, 38% EGR and SOI: 7.3°bTDC

To better understand the application of both Rahimi as well as Combined reaction mechanism, a study was conducted at six operating points as outlined in Table 6. The operating points were selected such that a range of injection timing and CNG substitutions could be evaluated with the two mechanisms at 1500 rpm and two load points – 5 bar and 12 bar BMEP. The aim of this study was to determine if certain control parameter settings favored a particular mechanism over the other.

Table 6 – Control parameter setting for six (6) operating points used for evaluation of Rahimi and Combined mechanism

Parameters	Units	1	2	3	4	5	6
Engine Speed	rpm	1500	1500	1500	1500	1500	1500
BMEP	bar	5	5	5	12	12	12
CNG Subs	%	40	60	80	40	60	80
EGR	%	35.6	35.0	35.7	37.7	37.9	29.7
SOI	bTDC	10.1	42.5	20.3	11.2	9.8	34.6
Rail Pressure	bar	1880	1879	1883	1958	1883	1888
NO_x	g/kWh	3.14	0.67	2.90	0.77	0.64	2.34
Lambda	-	2.20	1.94	2.24	1.40	1.33	0.99

For the 1500 rpm and 5 bar BMEP test point, referring Figure 43 and Figure 45, we see that the Rahimi mechanism does a better job of predicting the experimental ignition delay for the 40% and 80% CNG substitution cases where the diesel injection timings are closer to TDC, 10.1 bTDC and 20.3 bTDC respectively. The ignition delay predictions from the Combined mechanism is closer to the experimental results for the 60% CNG substitution case where the applied diesel injection timing is relatively advanced (42.5 bTDC) as seen in Figure 44. As can be seen in Figure 44 the measured cylinder pressure data as well as the heat release traces are well predicted by the Combined mechanism for the 60% CNG and 42.5 bTDC injection timing. Figure 45 shows that the cylinder pressure and heat release predictions are closer to the experimental results for the 80% CNG and 20.3 bTDC injection timing. Figure 43 reveals that even though the Rahimi mechanism does a better job for predicting the ignition delay the overall cylinder pressure trace is not well predicted with both mechanisms.

Figure 46, Figure 47 and Figure 48 compare the CFD predictions with both reaction mechanism to experimental results for the 1500 rpm and 12 bar BMEP operating points. Referring to Figure 46 and Figure 47, the ignition delay, in-cylinder pressure and overall heat release traces are well predicted with the Rahimi mechanism for the 40% and 60% CNG substitution cases where the diesel injection timing are closer to TDC, 11.2 and 9.8 bTDC respectively. When a more advanced injection timing is applied as is the case with 80% CNG substitution (34.6 bTDC), refer Figure 48, the Combined mechanism shows better predictions in terms of ignition delay, in-cylinder pressure and overall heat release

traces when compared to the experimental results. These observations with regards to diesel injection timing are similar to ones seen for the 1500 rpm and 5 bar BMEP cases. Table 7 summarizes the six operating points that have been evaluated and the corresponding reaction mechanism that shows reasonable predictions compared to the experimental results.

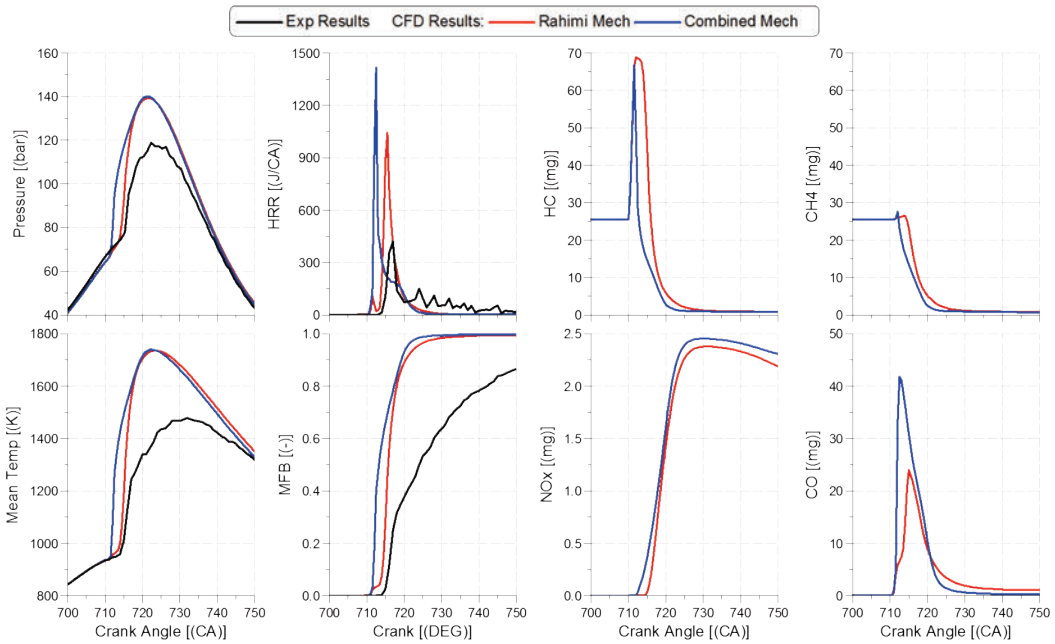

Figure 43 Comparison of performance and emissions predictions on a CA basis with two different mechanisms at 1500 rpm and 5 bar BMEP with 40% CNG Subs, 35.6% EGR and SOI: 10.1 bTDC

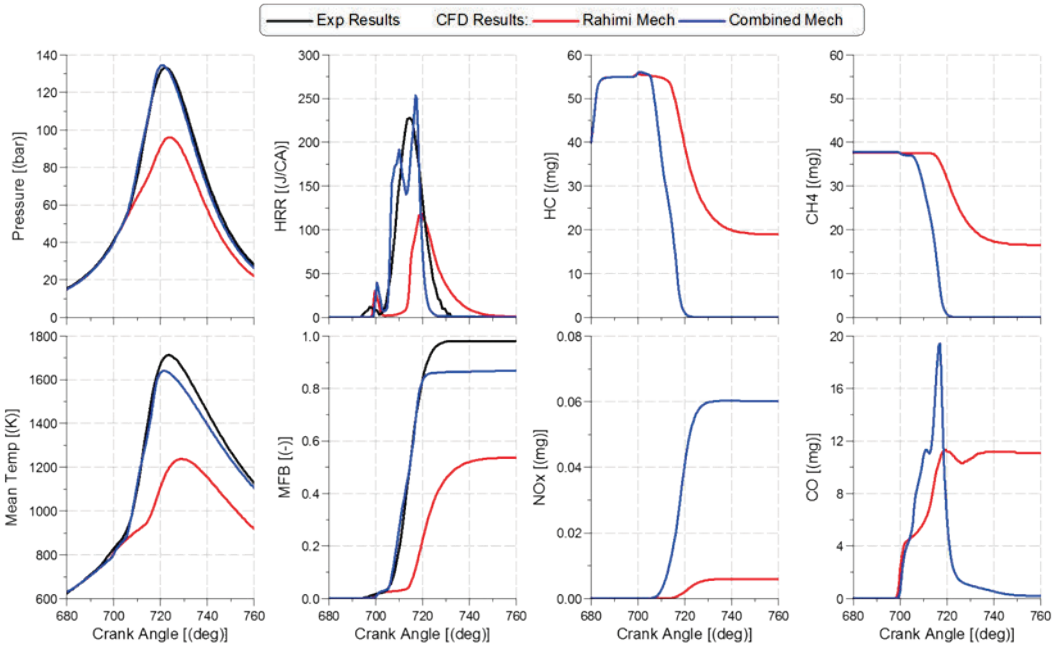

Figure 44 Comparison of performance and emissions predictions on a CA basis with two different mechanisms at 1500 rpm and 5 bar BMEP with 60% CNG Subs, 35% EGR and SOI: 42.5 bTDC

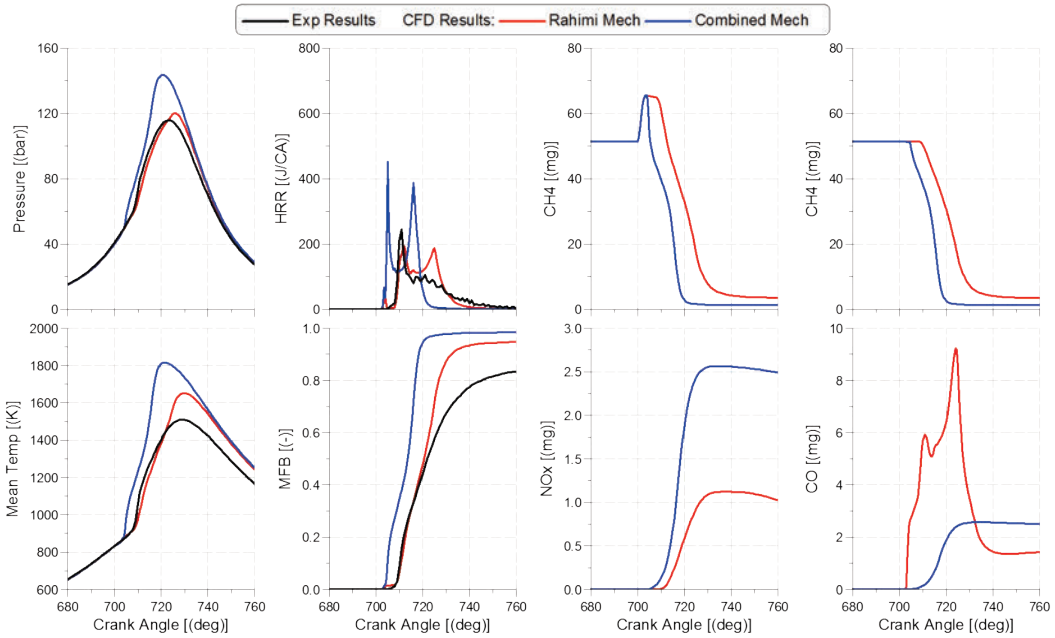

Figure 45 Comparison of performance and emissions predictions on a CA basis with two different mechanisms at 1500 rpm and 5 bar BMEP using 80% CNG Subs, 35.7% EGR and SOI: 20.3 bTDC

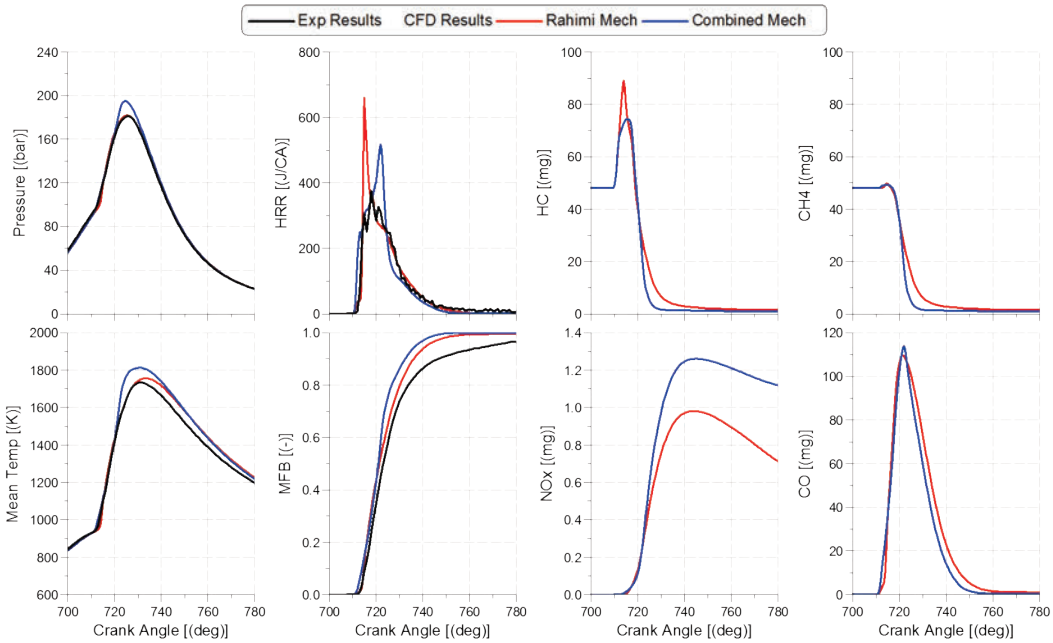

Figure 46 Comparison of performance and emissions predictions on a CA basis with two different mechanisms at 1500 rpm and 12 bar BMEP using 40% CNG Subs, 37.7% EGR and SOI: 11.2 bTDC

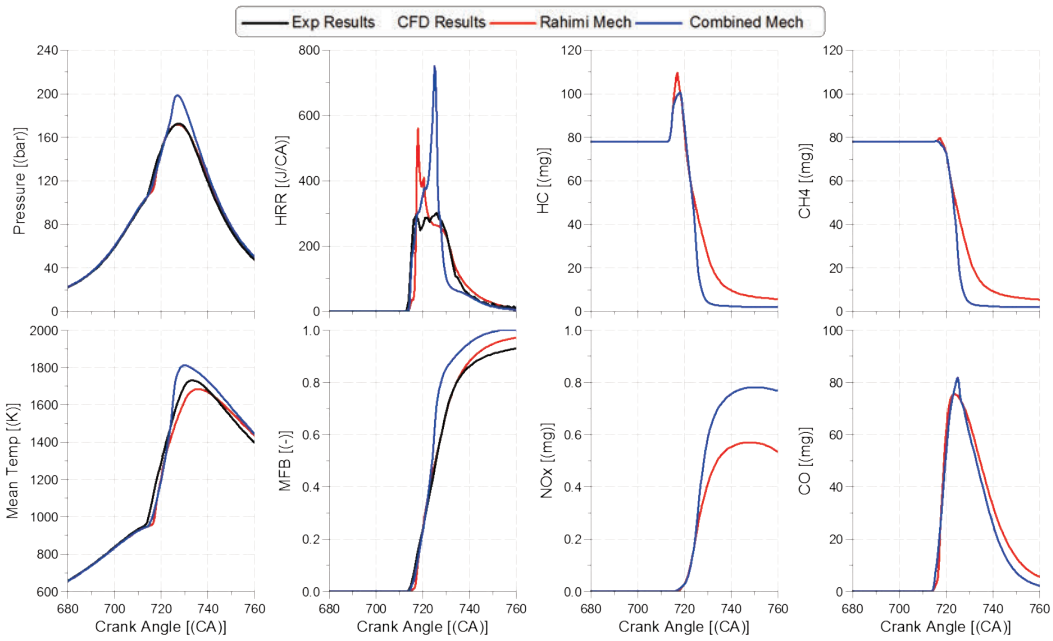

Figure 47 Comparison of performance and emissions predictions on a CA basis with two different mechanisms at 1500 rpm and 12 bar BMEP using 60% CNG Subs., 37.9% EGR and SOI: 9.8 bTDC

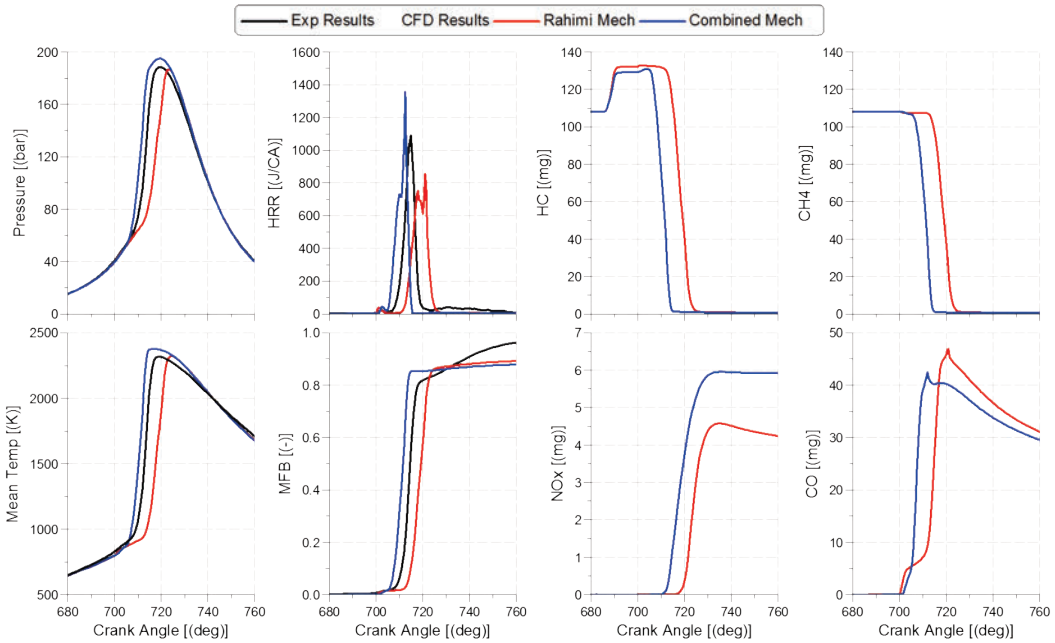

Figure 48 Comparison of performance and emissions predictions on a CA basis with two different mechanisms at 1500 rpm and 12 bar BMEP using 80% CNG Subs., 29.7% EGR and SOI: 34.6 bTDC

Table 7 Overview of reaction mechanism that shows good correlation for the six operating points evaluated with Rahimi and Combined Mechanism

CNG Subs	1500 rpm – 5 bar BMEP	1500 rpm – 12 bar BMEP
40%	None SOI: 10.1 bTDC	Rahimi Mech SOI: 11.2 bTDC
60%	Combined Mech SOI: 42.5 bTDC	Rahimi Mech SOI: 9.8 bTDC
80%	Rahimi Mech SOI: 20.3 bTDC	Combined Mech SOI: 34.6 bTDC

Referring to Table 7 we can observe that the Combined mechanism does a better job of predicting the test results when the timings are relatively advanced (> 30 bTDC) irrespective of the engine operating point and CNG substitution %. The Rahimi mechanism is more suited for operating conditions where the diesel injection timing are

closer to the TDC location. For the 1500 rpm and 5 BMEP test case at 40% CNG substitution both reaction mechanisms over predicted the cylinder pressure results. From the injection timings applied, the Rahimi mechanism should have been better suited to predict this operating point which we can see in terms of the ignition delay, refer Figure 43, but the reason for the subsequent higher heat release rate were not investigated in this study. From Table 7 it is evident that for a single diesel injection case, when advanced timing similar to those applied for RCCI combustion are used the low temperature reactions are well predicted by the Combined mechanism. When the injection timing is more retarded as would be the case with conventional dual fuel combustion the Combined mechanism predicts a shorter ignition delay and hence over predicts the cylinder pressure. For conventional dual fuel combustion timing the use of Rahimi mechanism is more suited were low temperature reactions are not as critical.

A subsequent CFD study was than conducted at 1500 rpm and 5 bar BMEP with the Rahimi mechanism as well as Combined mechanism where the diesel injection timing were varied from 1 bTDC to 42.5 bTDC. All test points selected were at a constant CNG substitution and EGR% with single diesel injection event as shown in Table 8.

Table 8 Overview of test points used for evaluating the Rahimi mechanism and Combined mechanism at 1500 rpm and 5 bar BMEP

Parameters	**Units**	**1**	**2**	**3**	**4**
Engine Speed	**rpm**	1500	1500	1500	1500
BMEP	**bar**	5	5	5	5
CNG Subs	**%**	60	60	60	60
EGR	**%**	35.3	35.3	34.5	35
SOI	**bTDC**	1	18.2	30.3	42.5
Rail Pressure	**bar**	1880	1880	1880	1880
NO_x	**g/kWh**	0.94	5.31	5.37	0.67

Figure 49 compares the cylinder pressure and HRR between experimental results and CFD predictions with both reaction mechanism at the diesel injection timing of 1 bTDC. The Rahimi mechanism predicts a longer initial ignition delay compared to the Combined mechanism. The ignition delay seen from the experimental results lies in between the predictions from the two mechanism. Both mechanisms predict similar peak cylinder pressures which are comparable to the experimental results. In terms of the heat release trace the peak is more closely matched with the combined mechanisms whereas the peak heat release rate is higher for the Rahimi mechanism with the longer ignition delay when compared to experimental results. The experimental NO_x emissions results are well

matched with both reaction mechanism as shown in Figure 50. Overall both reaction mechanism show a reasonable match with the experimental results for near TDC injection timings.

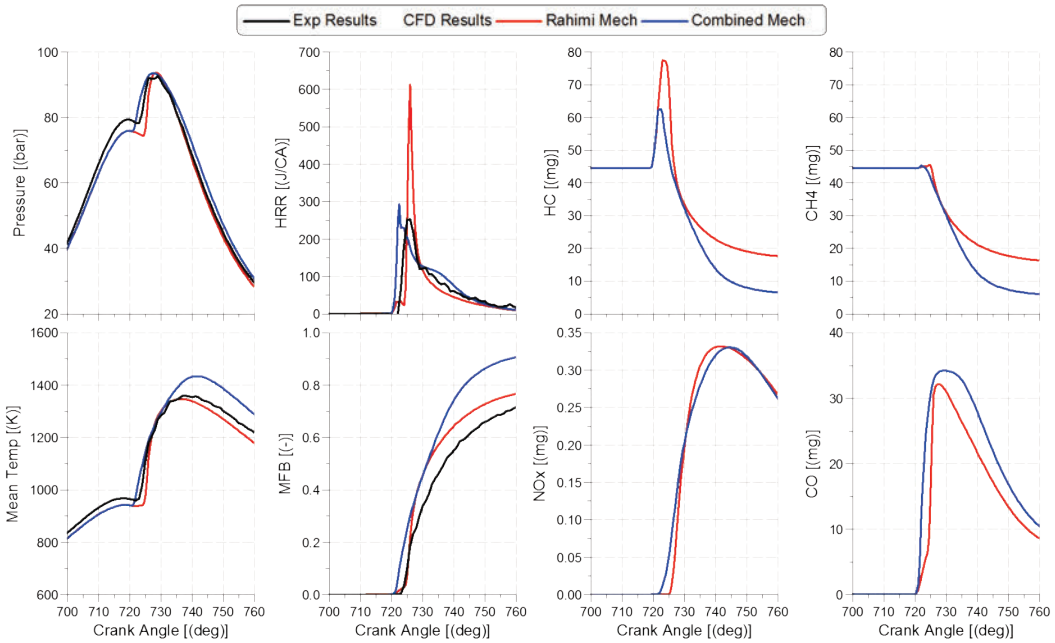

Figure 49 Comparison of performance and emissions predictions on a CA basis with two different mechanisms at 1500 rpm and 5 bar BMEP using 60% CNG Subs., 35% EGR and SOI: 1bTDC

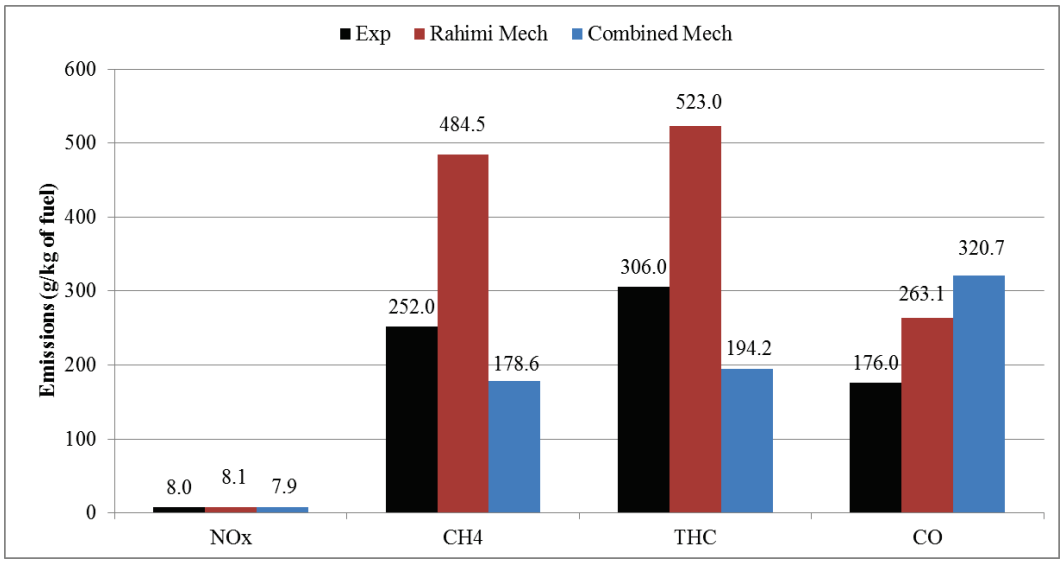

Figure 50 Comparison of emissions predictions with two different mechanisms at 1500 rpm and 5 bar BMEP using 60% CNG Subs., 35% EGR and SOI: 1 bTDC

Comparison of the cylinder pressure and HRR, at the diesel injection timing of 18.2 bTDC, between CFD simulations and experimental results are shown in Figure 51. For this case the Rahimi mechanism does a better job of predicting the initial ignition delay as well as the overall cylinder pressure trace compared to the Combined mechanism. The Combined mechanism predicts a shorter ignition delay resulting in higher initial heat release rate along with higher peak cylinder pressures compared to the test data. As expected, the NO_x emission are also better predicted with Rahimi mechanism compared to the Combined mechanism as shown in Figure 52.

Figure 53 and Figure 55 compare the cylinder pressure and HRR between experimental results and CFD predictions with both reaction mechanism at the diesel injection timing of 30.3 bTDC and 42.5 bTDC respectively. In both cases the ignition delay as well as the overall experimental cylinder pressure data is better predicted by the Combined mechanism compared to the Rahimi mechanism. The Rahimi mechanism under predicts the ignition delay leading to a relatively retarded combustion phasing compared to the test results and overall lower mass fraction burned (MFB) compared to the Combined mechanism. Although both reaction mechanisms under predict the NO_x emissions compared to the experimental results, the predictions are closer with the Combined mechanism compared to the Rahimi mechanism as highlighted in Figure 54 and Figure 56.

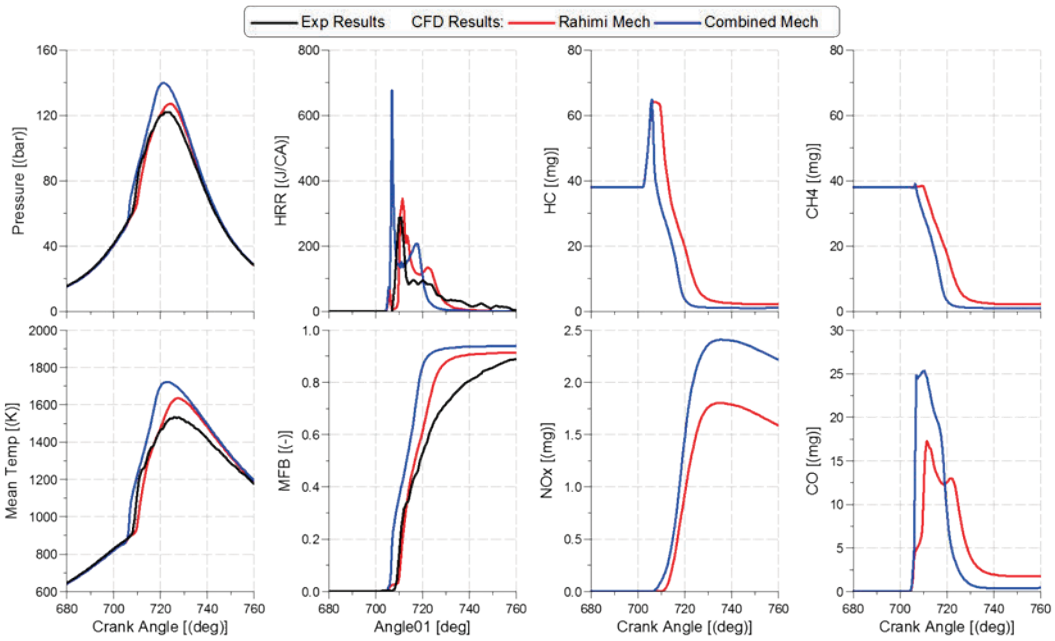

Figure 51 Comparison of performance and emissions predictions on a CA basis with two different mechanisms at 1500 rpm and 5 bar BMEP using 60% CNG Subs., 35% EGR and SOI: 18.2bTDC

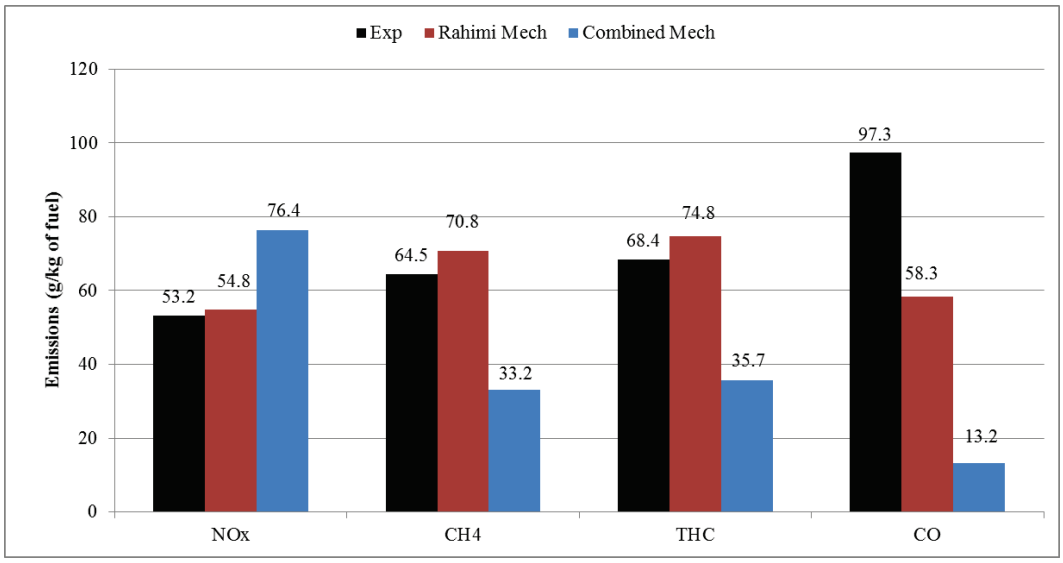

Figure 52 Comparison of emissions predictions with two different mechanisms at 1500 rpm and 5 bar BMEP using 60% CNG Subs., 35% EGR, and SOI: 18.2 bTDC

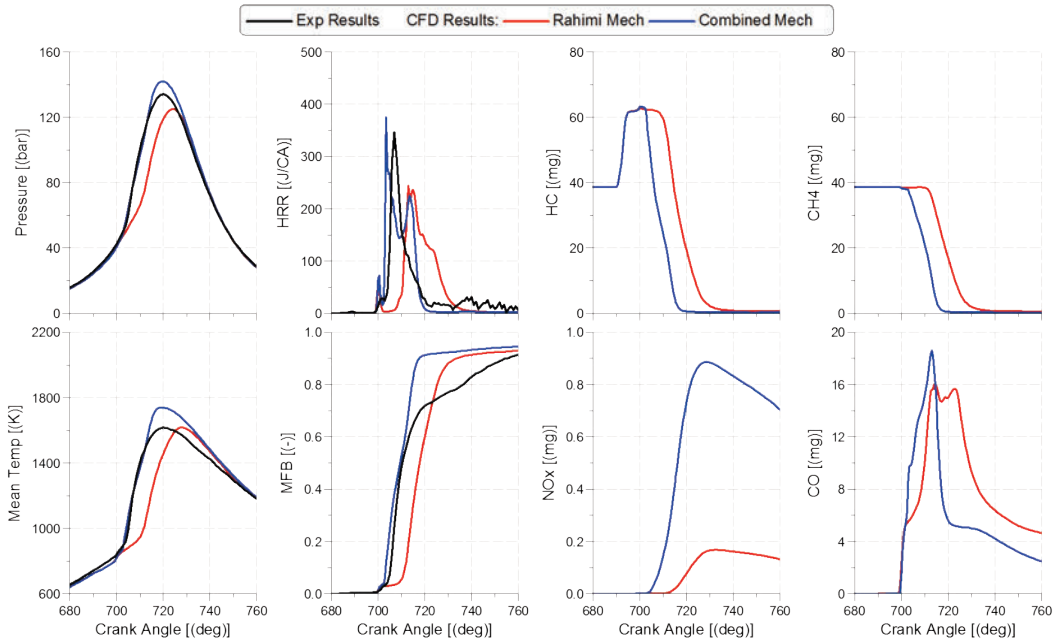

Figure 53 Comparison of performance and emissions predictions on a CA basis with two different mechanisms at 1500 rpm and 5 bar BMEP using 60% CNG Subs., 35% EGR and SOI: 30.3bTDC

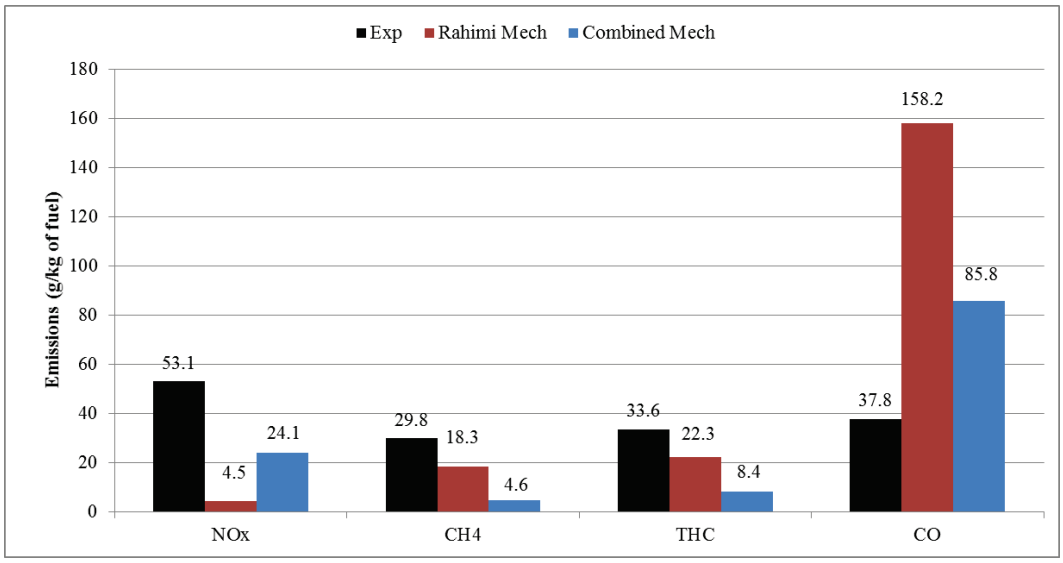

Figure 54 Comparison of emissions predictions with two different mechanisms at 1500 rpm and 5 bar BMEP using 60% CNG Subs., 35% EGR and SOI: 30.3 bTDC

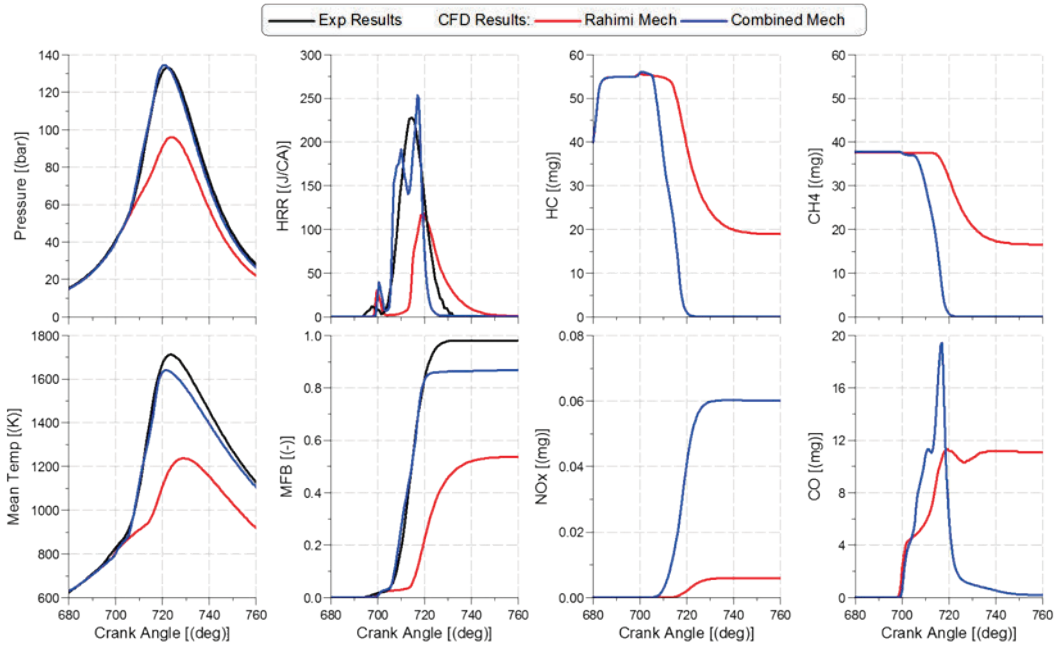

Figure 55 Comparison of performance and emissions predictions on a CA basis with two different mechanisms at 1500 rpm and 5 bar BMEP using 60% CNG Subs., 35% EGR and SOI: 42.5bTDC

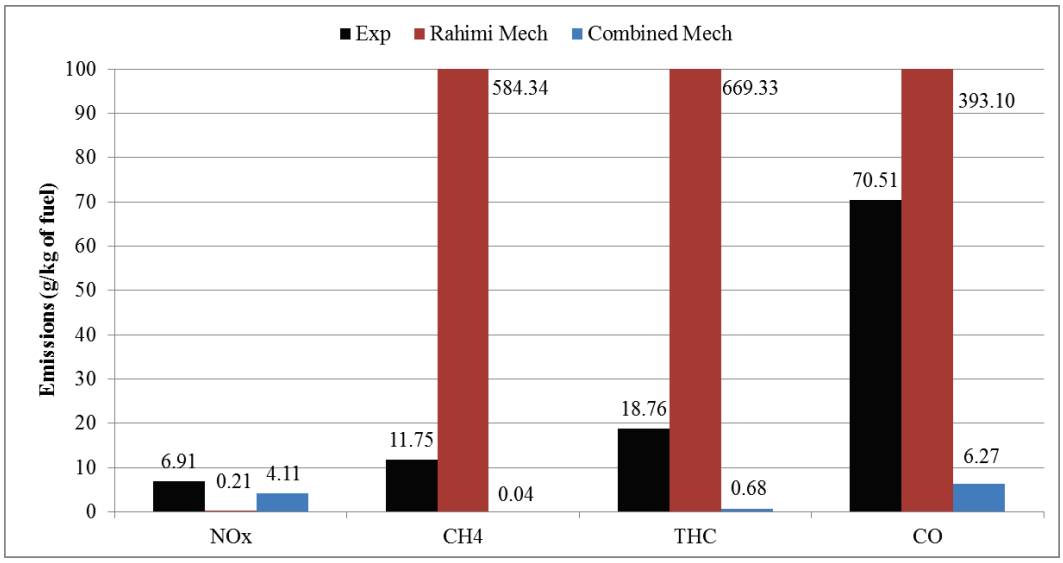

Figure 56 Comparison of emissions predictions with two different mechanisms at 1500 rpm and 5 bar BMEP using 60% CNG Subs., 35% EGR and SOI: 42.5 bTDC

From the results above it is clear that neither mechanism is capable of predicting the experimental results across the complete timing range shown in Table 8. However there exists a certain timing range where either mechanism shows a favorable prediction compared to the experimental results. The predictions from the Rahimi mechanism are well matched with experimental results when the diesel injection events are retarded (≤ 30 bTDC) whereas the Combined mechanism is better suited at predicting the experimental results with relatively advanced injection timing (>30 bTDC). For near TDC injection timings both mechanism show a reasonable correlation with experimental results in terms of peak cylinder pressure predictions and NO_x emissions. The fundamental difference in the both mechanism lies in the prediction of the ignition delay which than impacts the overall heat release and the resultant cylinder pressure and NO_x emission predictions. The Rahimi mechanism has a longer ignition delay and works better when the end temperature are higher as would be case with retarded diesel injection timings. The Combined mechanism on the other hand predicts much shorter ignition delay which works well when the end gas temperature are lower at start of combustion as would be case with advanced diesel injection timings.

In the subsequent CFD studies both reaction mechanism are applied depending on the diesel injection timing that is being investigated. For the parametric study discussed in following sections the Rahimi mechanism is applied for cases where at least one diesel injection event is closer to the TDC location (≤ 30 bTDC) whereas the Combined mechanism is applied where all diesel injection events are advanced beyond 30 bTDC.

6.2 Parametric Study at 1500 rpm and 12 bar BMEP

In order to evaluate the possibility of a low-NO_x RCCI combustion at 1500 rpm and 12 bar BMEP, a three variable DOE including CNG substitution, EGR and SOI was conducted at 1500 rpm – 12 bar BMEP using the Combined reaction mechanism as outlined below:

- CNG substitution (%): 60, 70, 85
- EGR (%): 40, 50, 60
- Diesel SOI (bTDC): 30, 45, 60

All test points were simulated using a single diesel injection event with a constant rail pressure of 1800 bar. The boundary conditions for each operating point were generated using a calibrated GT-Power engine model as outlined in section 5. The GT-Power engine model had to be updated with new turbocharger maps for generating boundary conditions for cases with high CNG substitution and EGR rates to maintain acceptable AFR (≥17:1). Table 9 overviews the boost pressure, exhaust pressure and AFR that we generated using the updated GT-Power engine model for 30 bTDC SOI. Cold flow CFD simulations were not conducted for each operating point listed in Table 9. However relevant IVC boundary conditions (pressure, temperature and composition) corresponding to the AFR and EGR listed in Table 9 were generated by modifying existing CFD cold flow results from the base simulation case. Boundary conditions generated with 30 bTDC SOI were than applied to evaluate CFD runs at 45 and 60 bTDC SOI.

Table 9 Overview of test points used for parametric study at 1500 rpm and 12 bar BMEP at 30 bTDC SOI and 1800 bar rail pressure using Combined mechanism

	Base	**1**	**2**	**3**	**4**	**5**	**6**	**7**	**8**	**9**
CNG Subs. (%)	80	60	60	60	70	70	70	85	85	85
EGR rate (%)	30	40	50	60	40	50	60	40	50	60
SOI (bTDC)	34.6	30	30	30	30	30	30	30	30	30
Boost Pr. (bar)	1.73	3.01	2.98	3.15	3.02	2.99	3.12	3.03	2.99	3.14
Exhaust Pr. (bar)	1.92	3.67	3.49	3.81	3.68	3.49	3.75	3.66	3.47	3.75
Air Fuel Ratio	16.5	25.8	21.4	17.2	26.0	21.7	17.2	26.4	22.0	17.5

Figure 57 compares the impact of EGR and CNG substitution at fixed injection timing of 30 bTDC. At all EGR%, higher gross indicated thermal efficiency (GITE) seen with 85% CNG substitution due to an improved CA50 location. However the CA50 for all cases is still before TDC. Further at all CNG substitutions % the following was observed

- MFB reduces with increase in EGR%
- Peak cylinder pressures and maximum pressure rise rates reduce with increase in EGR%
- NO_x emissions reduce while PM, CH4, THC and CO emissions increase with increase in EGR%
- At 60% EGR the NO_x emissions are relatively low however due to the advanced combustion phasing the overall peak cylinder pressures are considerable higher compared to the peak cylinder pressure limit of the baseline engine hardware (190 bar)
- No significant impact on wall film mass seen with changes in EGR % and CNG Substitution % at fixed injection timing

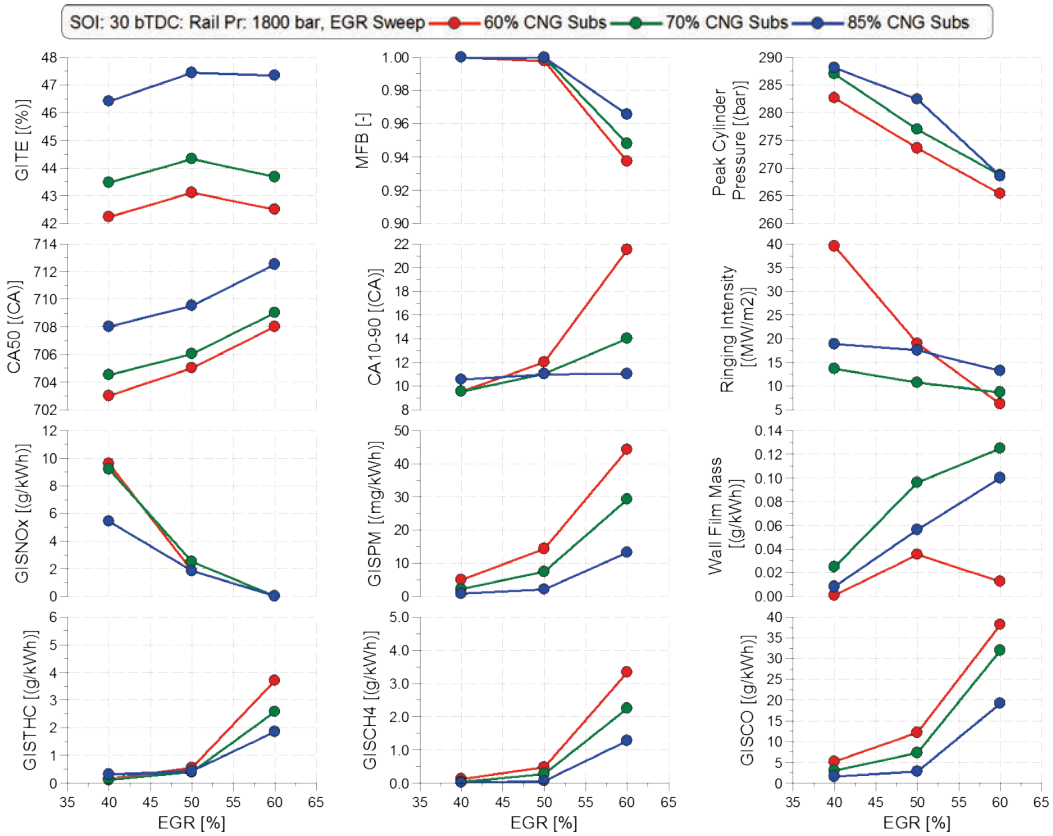

Figure 57 Impact of EGR and CNG substitution on performance parameters at 30 bTDC SOI for 1500 rpm and 12 bar BMEP using Combined mechanism

Referring to Figure 58 we can see a two peak heat release rate for the 60% CNG substitution case at 40% EGR and 30 bTDC SOI. As the CNG substitution is increased at constant EGR% and SOI, we see that the first peak of the heat release trace reduces while

the second peak increases in magnitude. It is evident that as the CNG substitution % is increased the amount of premixed diesel reduces which lowers the first peak of the heat release trace. Due to this the subsequent NO_x emissions are also lower with the increased CNG substitution as shown in Figure 57. Overall the study shows that a relatively high CNG substitution would be required to lower the first heat release peak to target a Low NO_x RCCI combustion. However the study also reveals that higher EGR% would be required to control the maximum pressure rise rate and NO_x emissions which leads to high levels of unburned HC and CH4 emissions. Also at all conditions the maximum peak cylinder pressures were much higher (260-280bar) than the baseline hardware limitations (190 bar).

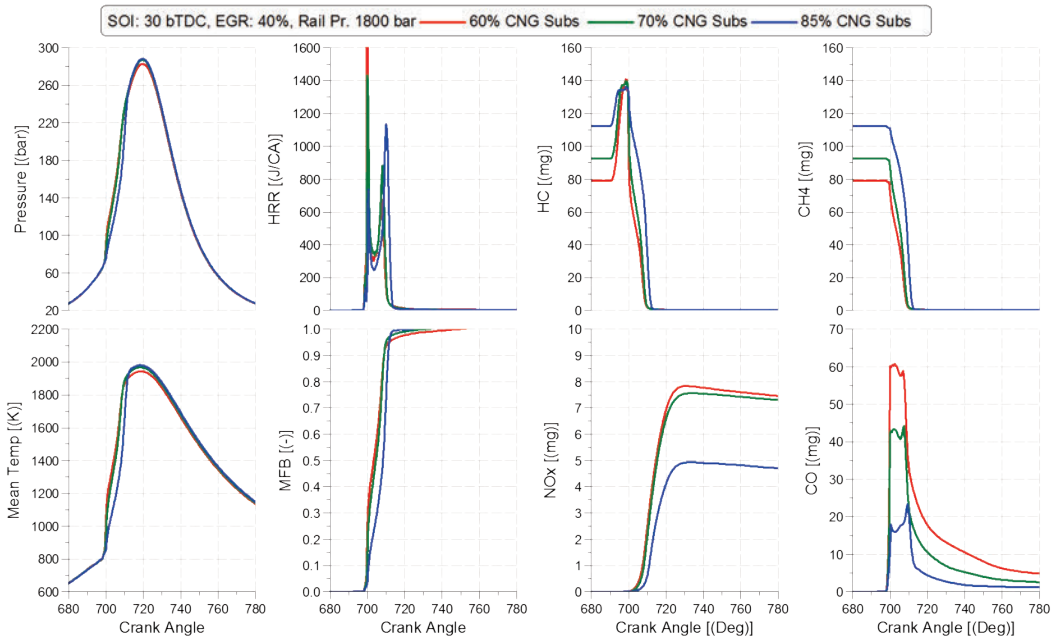

Figure 58 Comparison of performance and emission parameters on a CA basis for different CNG substitutions at 40% EGR and 30 bTDC SOI for 1500 rpm and 12 bar BMEP using Combined mechanism

To reduce the maximum pressure rise rate and NO_x emissions at lower EGR%, a SOI study was conducted at 40% and 50% EGR keeping the CNG substitution constant at 85%. Referring Figure 59 we observe that at both EGR levels, no significant impact is seen on GITE with advance in injection timing. With advancing injection timing the CA50 starts to retard however the MFB reduces due to increased wall film interaction leading to negligible improvement in GITE. Also the total burn duration reduces significantly with advancing SOI, resulting in higher pressure rise rates. It can be concluded that the larger ignition delay with advancing SOI results in more spontaneous combustion leading to higher pressure rise rates and peak cylinder pressures. Both NO_x and PM emissions reduce simultaneously with advancing SOI at both EGR levels. The lower NO_x emission are a result of the retarded combustion phasing which leads to lower in-cylinder temperatures as shown in Figure 60. The PM reduces as the injected diesel has a longer time to mix resulting in more complete combustion. There is also a reduction

in THC, CH4 and CO emissions with advancing SOI as shown in Figure 59. From this study we can conclude that the delayed combustion phasing with advanced timing helps in reducing NO_x emissions as the mass averaged temperatures are lower but increases the pressure rise rates as observed by the increase in ringing intensity. Also advancing of the injection timing does not resolve the issue of higher peak cylinder pressures compared to the baseline hardware limitation of 190 bar.

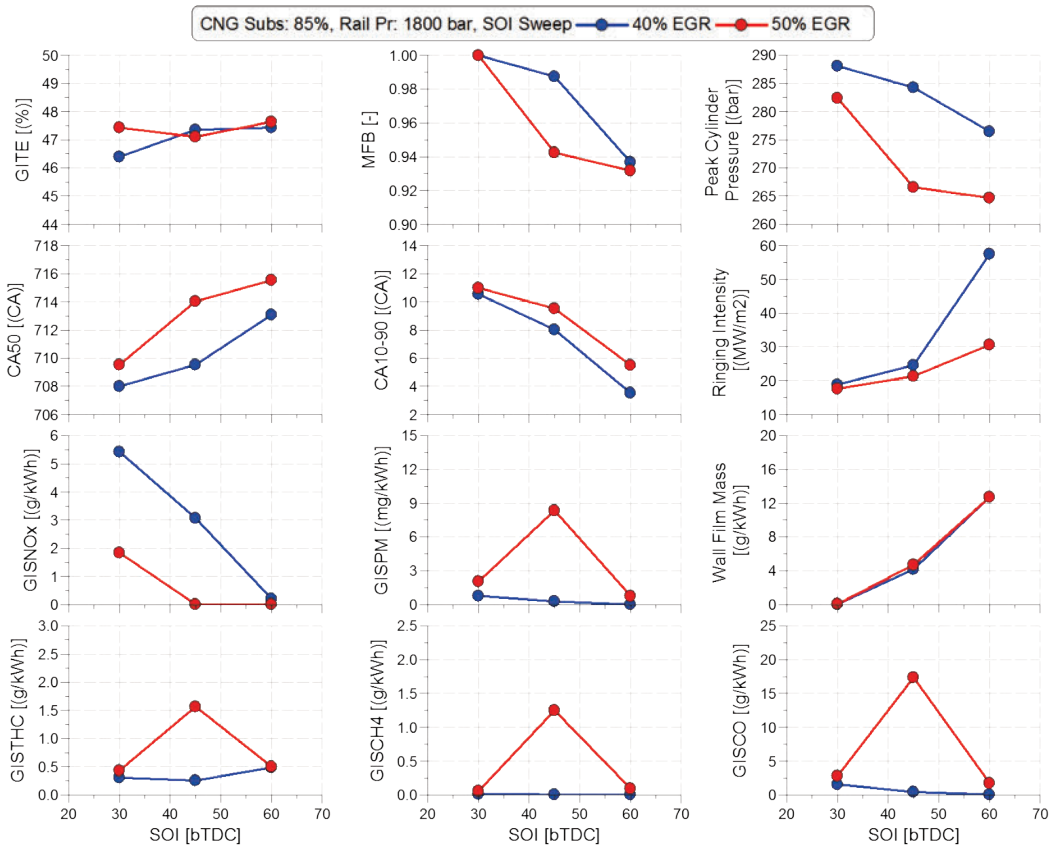

Figure 59 Impact of EGR and SOI at 85% CNG substitution for 1500 rpm and 12 bar BMEP using Combined mechanism

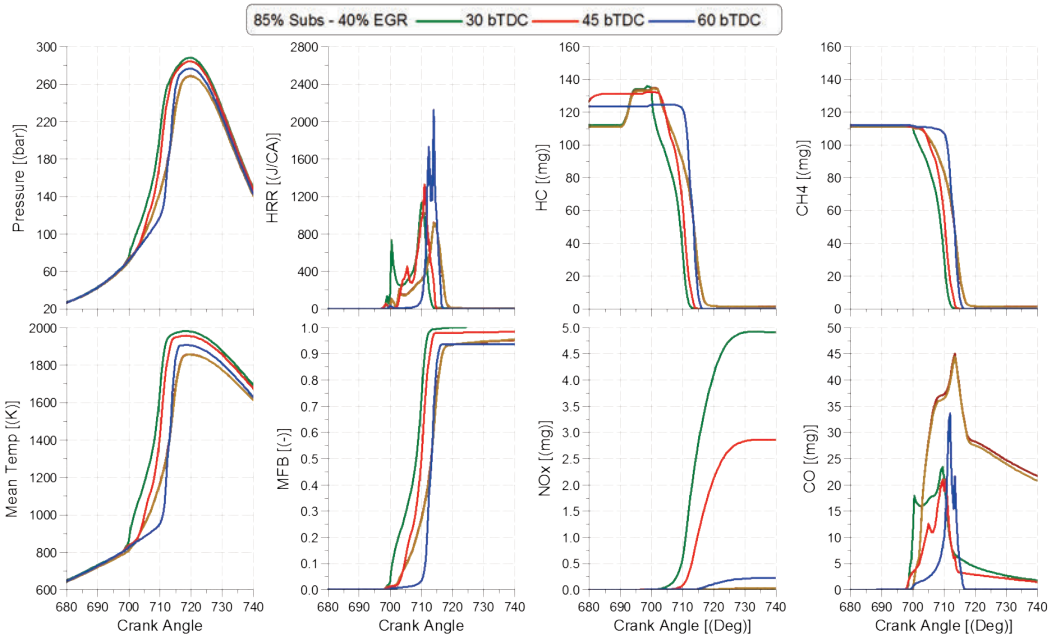

Figure 60 Comparison of performance and emission parameters on a CA basis for different SOI at 40% EGR and 85% CNG substitution for 1500 rpm and 12 bar BMEP using Combined mechanism

In order to reduce the pressure rise rates a rail pressure sweep was conducted at 85% CNG substitution, 40% EGR and 60 bTDC SOI as shown in Figure 61. Three different rail pressures were investigated in this study including 600, 1200 and 1800 bar. Marginal improvement in GITE were seen with reducing rail pressure from 1800 to 1200 bar. No improvement in GITE seen with lowering rail pressure from 1200 bar to 600 bar. With reducing rail pressure the MFB increases however the CA50 also advances which negates the efficiency gains resulting from the higher MFB. The advanced CA50 with lower rail pressure also results in higher peak cylinder pressure and NO_x emissions as shown in Figure 61. The lowering of rail pressure does help in extending the total burn duration with a two phase heat release which leads to lower pressure rise rates as seen in Figure 62. Lowering rail pressures also results in lower wall film mass which results in reduced HC emissions. However lowering rail pressure does results in increase of PM and CO emissions due to direct impact on diesel spray mixing. From this study it was observed that lowering rail pressure helped in reducing the max pressure rise rate but it also resulted in higher NO_x emissions. The issue of high peak cylinder pressures was still unresolved.

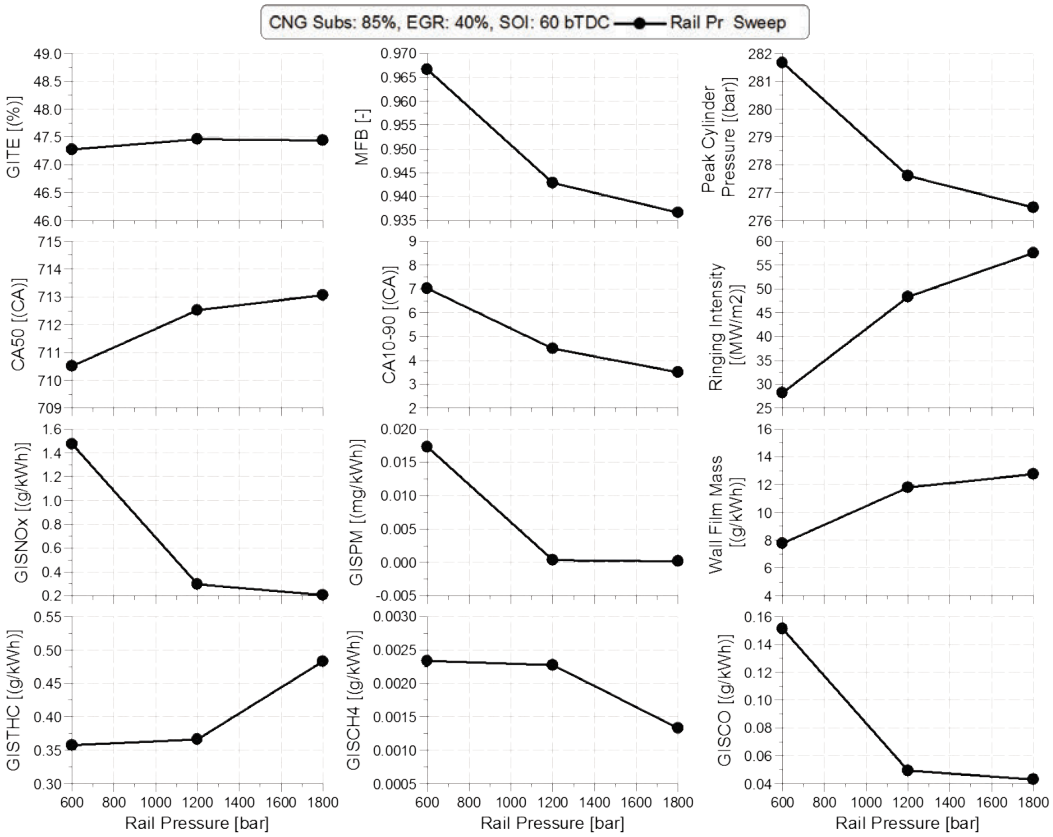

Figure 61 Impact of rail pressure on performance and emission parameters at 85% CNG substitution, 40% EGR and 60 bTDC SOI for 1500 rpm and 12 bar BMEP using Combined mechanism

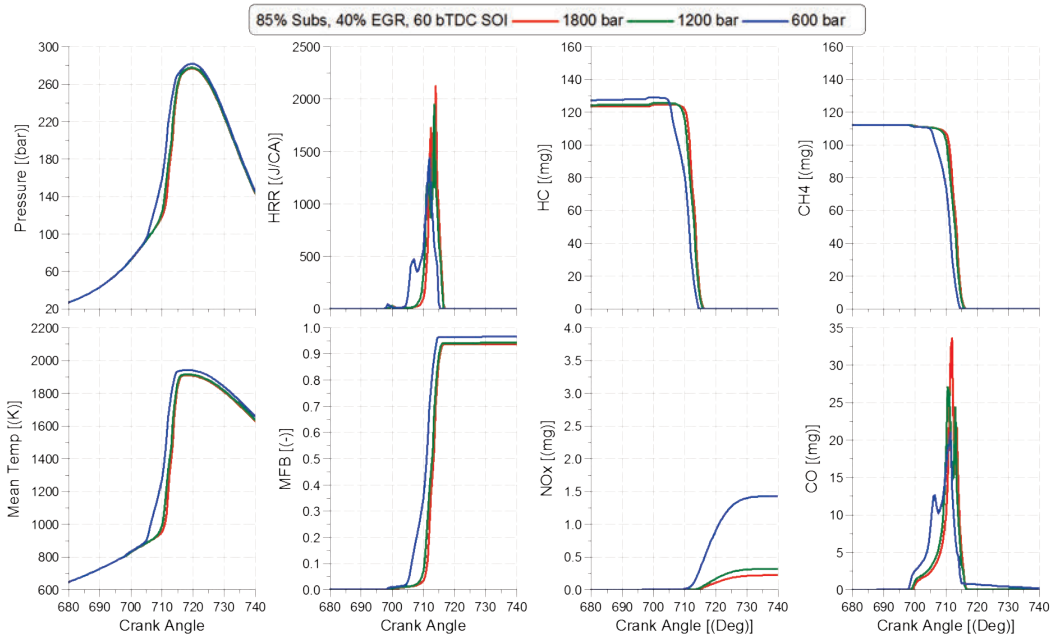

Figure 62 Comparison of performance and emission parameters on a CA basis for different rail pressures at 40% EGR, 85% CNG substitution and 60 bTDC SOI for 1500 rpm and 12 bar BMEP using Combined mechanism

Focusing on parameters that can reduce the maximum pressure rise rates and NO_x emissions at lower EGR%, a spray angle (injector included angle) sweep was conducted at 85% CNG substitution, 40% EGR, 60 bTDC SOI and 1800 bar rail pressure as shown in Figure 63. Four different spray angles were selected for this investigation: 146 (base), 120, 90 and 60 deg. It was hypothesized that the reduced spray angle would increase the ignition delay by creating a richer fuel mixture inside the piston bowl which would likely retard the CA50 leading to lower NO_x emission as well as increased burn duration with reduced maximum pressure rise rates. Referring Figure 63 it was observed that the GITE improves with reducing the spray angle which is largely driven by the improved MFB. The higher MFB was mainly achieved by avoiding liner impingement which results in lower wall film mass, refer Figure 63 and Figure 64. Contrary to the initial hypotheses the CA50 advances with reducing spray angle which results in higher peak cylinder pressures and corresponding higher NO_x emissions, as seen in Figure 63. A step change in NOx emissions is seen with reducing spray angle from 90 to 60 deg. Referring to Figure 65 we see that for the 60 deg spray angle the CH4 within the combustion bowl starts to oxidize much earlier compared to the 90 deg SA case where the CH4 starts to oxidize near the piston top surface closer to the liner at a later crank angle. This results in an earlier CA50 location along with higher NO_x emissions for the 60 deg SA case compared to the 90 deg spray angle case.

For the 60 deg spray angle case the maximum pressure rise rates are lower with a longer burn duration CA10-90. Referring Figure 66, for the 60 deg spray angle case the combustion occurs in two stage. An initial stage that is driven by the diesel fuel burning inside the piston bowl followed by a subsequent slower oxidation of methane within the

squish region. It is also interesting to observe that the CH4 emissions are highest for the case with 60 deg spray angle with the unburned CH4 located within the bowl as seen at the EVO location (864 CA) in Figure 65. The study overall revealed that the reduced spray angle leads to higher GITE since it avoids fuel impingement on the cylinder liner leading to more complete combustion along with lower pressure rise rates due to the longer burn durations. However the lower spray angle also results in increased NO_x emissions due to an earlier combustion phasing.

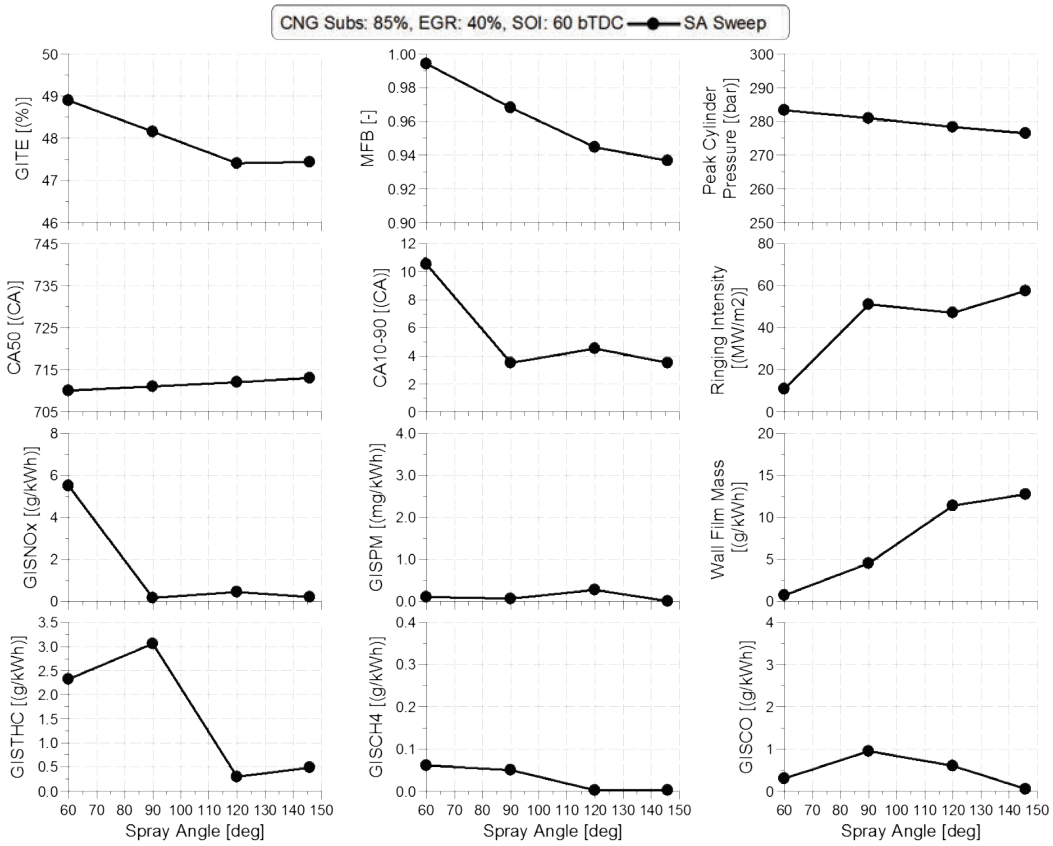

Figure 63 Impact of nozzle spray angle at 85% CNG substitution, 40% EGR and 60 bTDC SOI for 1500 rpm and 12 bar BMEP using Combined mechanism

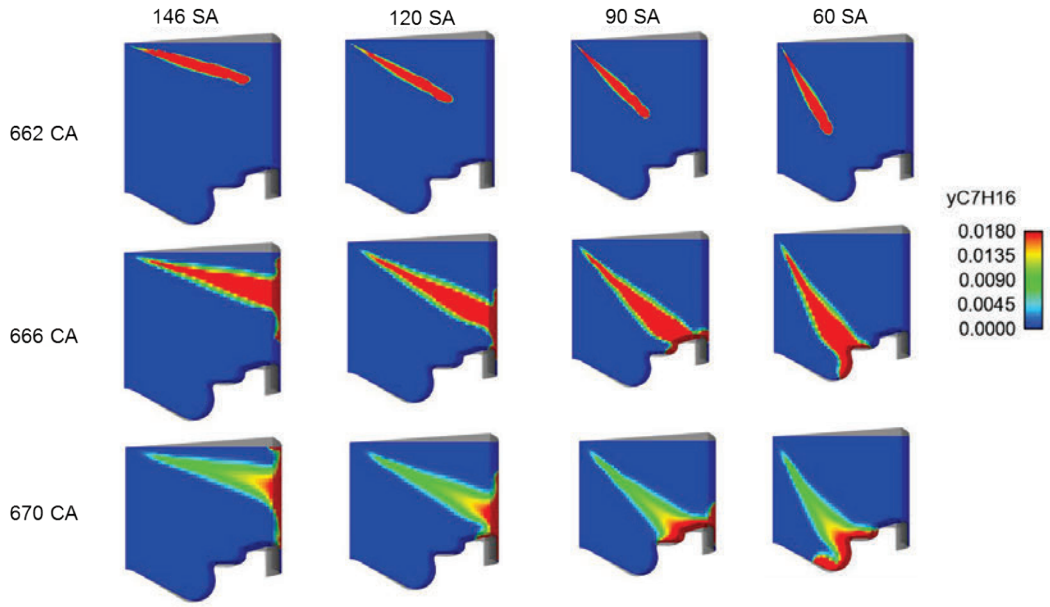

Figure 64 CFD plots comparing diesel spray interaction with liner and piston bowl for different nozzle spray angles at 40% EGR, 85% CNG substitution, 60 bTDC SOI and 1800 bar rail pressure for 1500 rpm and 12 bar BMEP using Combined mechanism

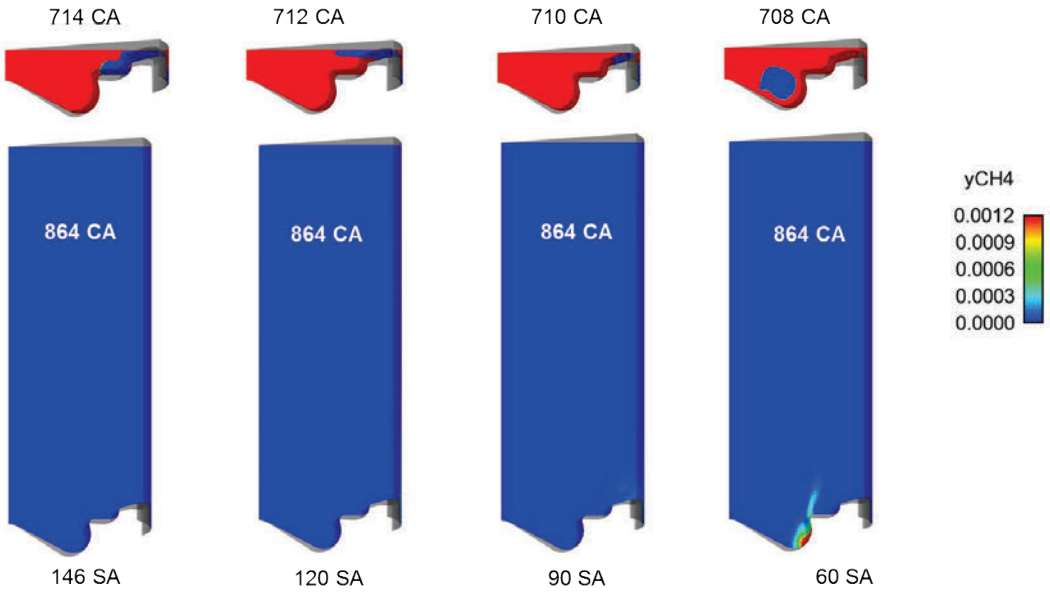

Figure 65 CFD plots comparing in-cylinder CH4 concentration for different nozzle spray angles at 40% EGR, 85% CNG substitution and 60 bTDC SOI for 1500 rpm and 12 bar BMEP using Combined mechanism

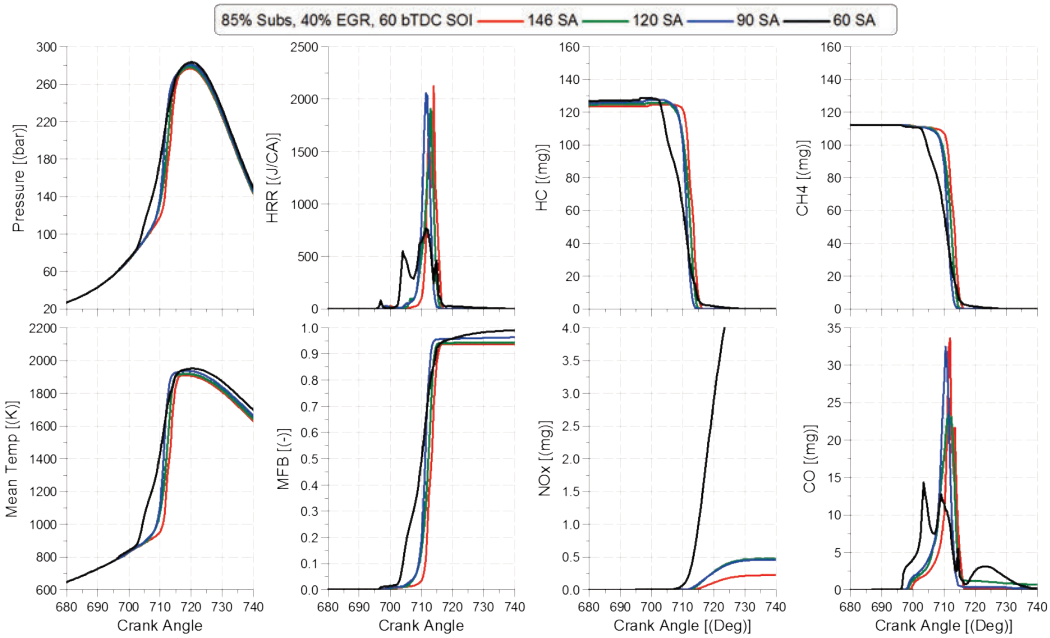

Figure 66 Comparison of performance and emission parameters on a CA basis for different nozzle spray angles at 40% EGR, 85% CNG substitution and 60 bTDC SOI for 1500 rpm and 12 bar BMEP using Combined mechanism

The next study conducted included varying the geometric compression ratio of the engine to lower compression temperature which would aid in increasing the ignition delay. The study was conducted at 85% CNG substitution, 40% EGR and 30 bTDC SOI. The study was initially conducted at two compression ratio: 16.7 and 13.7. This was based on the assumption that a two stage VCR system can achieve a step change in geometric compression ratio of 3 to 4 points [41]. Based on promising results seen at 13.7 compression ratio two lower compression ratio of 12.7 and 11.7 were selected for evaluation to determine compression ratio limits beyond which optimum combustion phasing would not be possible.

Referring Figure 67 it was found that GITE improves with reducing compression ratio to 12.7 beyond which the retarded combustion phasing leads to lower combustion efficiency. The retarded CA50 values and longer burn duration with reduced compression ratio results in significantly lower peak cylinder pressures and lower max pressure rise rates as seen in Figure 68. The retarded combustion phasing with lower compression ratio also results in significantly lower NO_x emissions. However all other emissions including PM. THC, CH4 and CO increase with reducing compression ratio. Overall the study revealed that lowering compression ratio is effective in controlling peak cylinder pressures, pressure rise rates as well as resultant NO_x emissions. However as we keep reducing compression ratio beyond a certain value the thermal efficiency begins to reduce as the combustion phasing (CA50) is retarded beyond an optimum location. For the current study a compression ratio of 12.7 was found to be optimum for the test conditions that were investigated. Figure 69 compares the CH4 oxidation at different CA's for 16.7 and 12.7 compression ratio. From the plots we can see that for both compression ratios

the overall combustion proceeds in an identical pattern once the CH4 oxidation starts. The lower compression ratio primarily results in a longer ignition delay which help in achieving the optimum combustion phasing. Even though the lower compression ratio of 12.7 resulted in lower peak cylinder pressures and retarded combustion phasing the $ISNO_x$ emissions were still higher compared to the target of a low NO_x RCCI combustion. A timing sweep study was than conducted at a compression ratio of 12.7 based on the earlier results from the timing study at compression ratio of 16.7 which showed that the $ISNO_x$ emissions reduced with advancing injection timing, refer Figure 59.

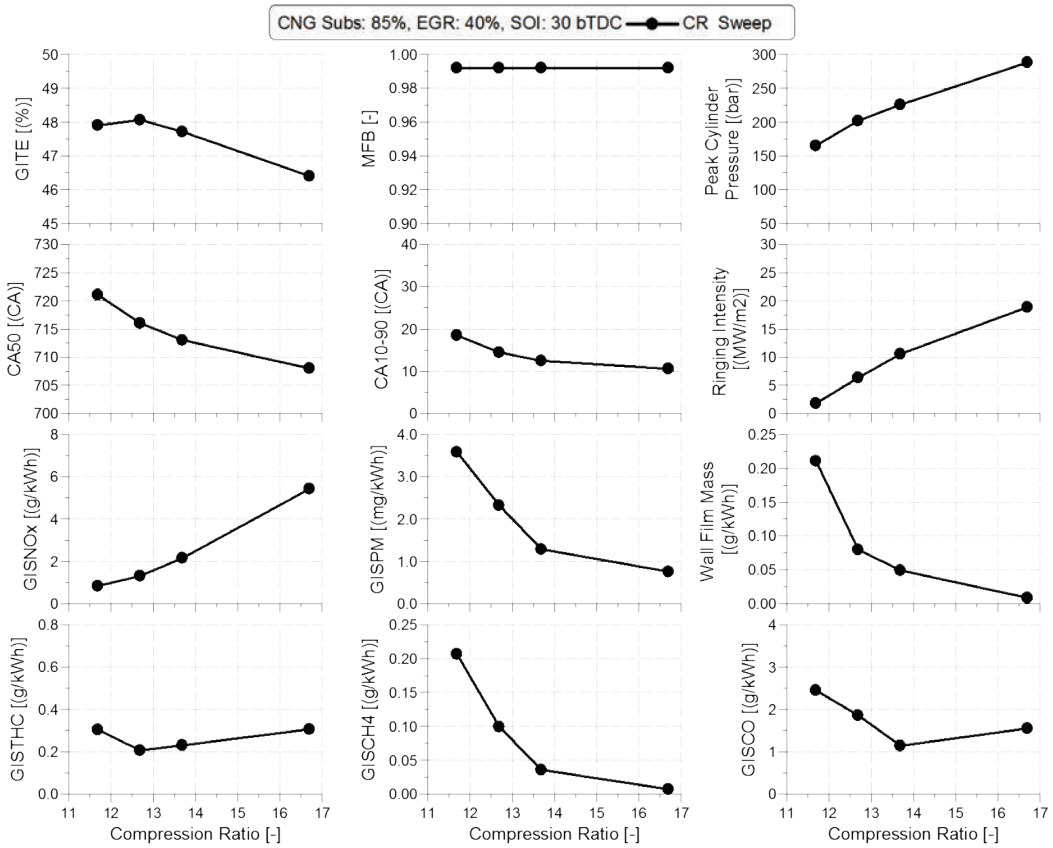

Figure 67 Impact of compression ratio on performance and emission parameters at 85% CNG substitution, 40% EGR and 30 bTDC SOI for 1500 rpm and 12 bar BMEP using Combined mechanism

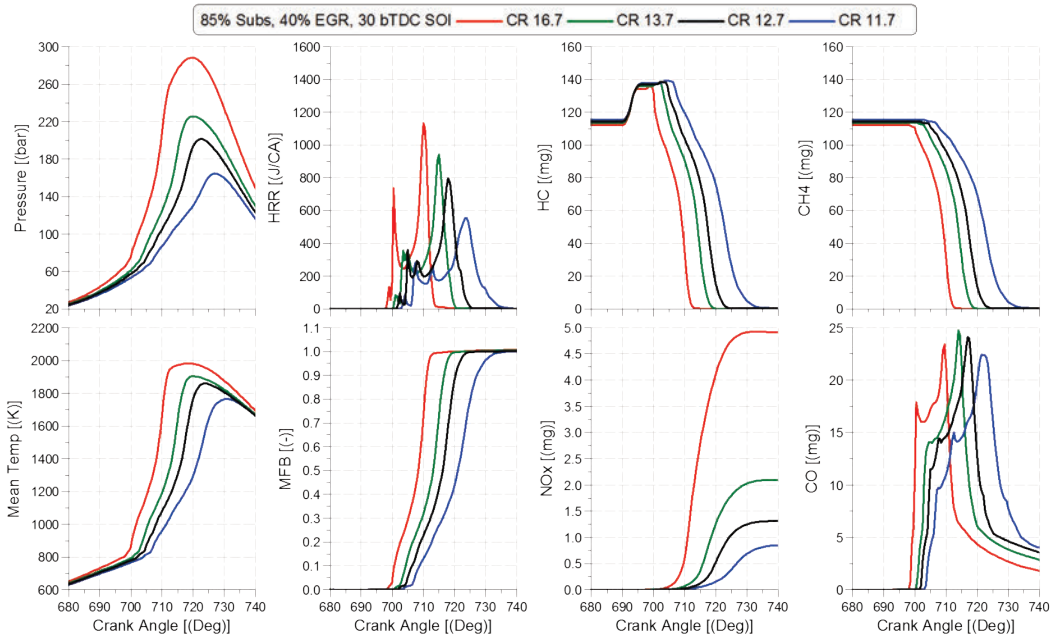

Figure 68 Comparison of performance and emission parameters on a CA basis for different compression ratios at 40% EGR, 85% CNG substitution and 30 bTDC SOI for 1500 rpm and 12 bar BMEP using Combined mechanism

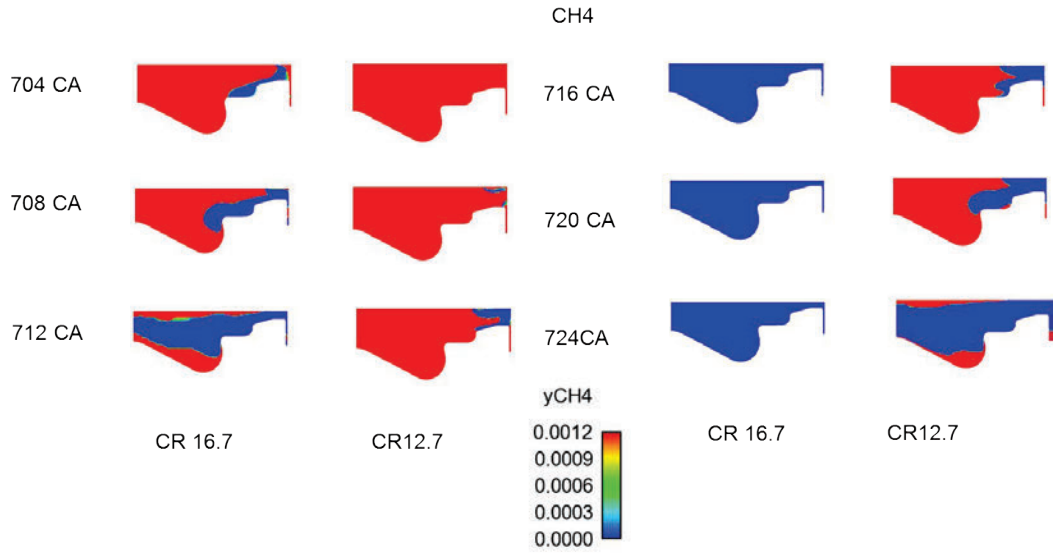

Figure 69 CFD plots comparing in-cylinder CH4 concentration for two different compression ratios (16.7 and 12.7) at 40% EGR, 85% CNG substitution and 30 bTDC SOI for 1500 rpm and 12 bar BMEP using Combined mechanism

Figure 70 compares the timing sweep study at compression ratio of 12.7 to the timing sweep study conducted at compression ratio of 16.7 with 40% EGR and 85% CNG substitution. At both compression ratios with advancing injection timing the CA50 starts to retard however the MFB reduces (due to increased wall film interaction) leading to

small improvements in GITE. At the lower compression ratio of 12.7 advancing the timing to 60 bTDC leads to partial combustion with very high levels of unburned THC and CO emissions as seen in Figure 71. Comparing the total burn duration with both compression ratios we see that the burn duration increases at the lower compression of 12.7 versus a reduced burn duration at the compression ratio of 16.7. This also leads to lower pressure rise rates with advancing of injection timing at the lower compression ratio of 12.7. The NO_x and PM emissions both reduce simultaneously with advancing SOI at both compression ratios due to the retarded combustion phasing. There is also a reduction in THC, CH4 and CO emissions with advancing SOI for both compression ratios except at 60 bTDC injection timing for compression ratio of 12.7 where partial combustion leads to higher unburned THC and CO emissions, refer Figure 70 and Figure 71. Based on this study it was concluded that, at the compression ratio of 12.7, with advancing of injection timing from 30 to 45 bTDC, the 90% reduction in $ISNO_x$ emissions (1.05 g/kWh @ 30 bTDC SOI vs 0.11 g/kWh @ 45 bTDC SOI) along with 0.5% improvement in GITE supports the development of a low NO_x RCCI strategy at higher loads.

With the control parameters defined for sustaining a Low NO_x RCCI combustion at 12 bar BMEP, a comparison was made of the results between the sector simulations that were applied to define this strategy and its impact when considered with full geometry simulations. The control parameter settings used for this comparison included 40% EGR, 85% CNG substitution and 45 bTDC SOI at a compression ratio of 12.7. Referring to Figure 72 we see a good match in the cylinder pressures, temperature and heat release traces between the sector and full geometry simulations. The MFB and the resultant HC, CH4 and CO emissions also correlate well between the sector and full geometry simulations. However the resultant NO_x emission predictions from the full geometry simulations are lower compared to the sector simulations as shown in Figure 72. This trend is not unexpected given the original observations that were made when the sector simulations results were compared to the full geometry and experimental results in section 6.1. Referring to Figure 40 it was observed that the NO_x emission predictions with the sector model were higher compared to the full geometry model predictions but closer to the experimental values. Given that the $ISNO_x$ emissions predictions from the full geometry simulations are lower compared to the sector simulations and the previous observations from Figure 40, it can be concluded that a Low NO_x RCCI at 12 bar BMEP operating point could be achieved using the control strategy defined with the sector simulations. When compared to the baseline experimental results at 12 bar BMEP with diesel only operation, it was found that the proposed low NO_x RCCI combustion strategy with diesel and natural gas resulted in 75% reduction in NO_x emissions while fuel consumption was improved by 5.5% as shown in Table 10. The PM emissions were lower by 67% compared to the baseline diesel case.

Referring to the previous CFD study conducted by Nieman et al., [13] they observed that at 1460 rpm and 13.5 bar gross IMEP, a low NO_x RCCI combustion would be achieved with CR of 16.1:1. They applied a split injection strategy with the timing of the first injection event at 79.5 bTDC and second injection event at 39.6 bTDC with 55% diesel

mass injected in the first injection event. They also applied 0% EGR for this operating point and reported low NO_x emissions (0.07 g/kWh) and relatively high GITE of 48.9%. In the current CFD study, the low NO_x RCCI combustion was achieved applying relatively high EGR rate of 40% along with lower compression ratio of 12.7:1 compared to the base compression ratio of 16.7:1. A single diesel injection event was used in the current study. Even with the application of a lower compression ratio the peak cylinder pressure were higher for optimized conditions compared to the baseline experimental results, refer Table 10.

In the current study evaluation of split injection timing was conducted as part of the experimental investigation at 12 bar BMEP using compression ratio of 16.7:1, as shown in Figure 25. For this study the first and second injection timing were held constant at 60 bTDC and 30 bTDC respectively while the mass of diesel fuel in the first injection was varied from 47% to 94%. For all test points the gross indicated NO_x emissions were relatively high (>0.6 g/kWh) along with maximum pressure rise rate above 10.5 bar/deg. The authors in ref [13] report a relatively low pressure rise rate of 4.4 bar/deg for their optimized results at 13.5 gross IMEP. Based on the experimental results conducted as part of the current study application of EGR rate below 40% was not considered for the subsequent CFD study.

To explain the discrepancy in the application of the control parameters between the current study (experimental and CFD) versus the CFD study conducted by authors in ref [13] we need to examine the reaction mechanism that were applied for both CFD studies. Referring to section 6.1, it is evident that RCCI combustion with diesel and natural gas is difficult to predict with a single set of reaction mechanism across the complete range of injection timing that are typically investigated. If the reaction mechanism used in the study by ref [13] behaves similar to the Rahimi mechanism than based on the injection timing applied this would over predict the injection delay and hence leads to favorable combustion phasing. If the current control parameters setting that are recommended by reference [13] were applied, the results would be very similar to the SOI investigation conducted at 45 bTDC for the current CFD study. Also the authors in ref [13] do not provide validation of the simulation results with test data in their study whereas in the current study this validation is considered before the detailed CFD evaluation is undertaken.

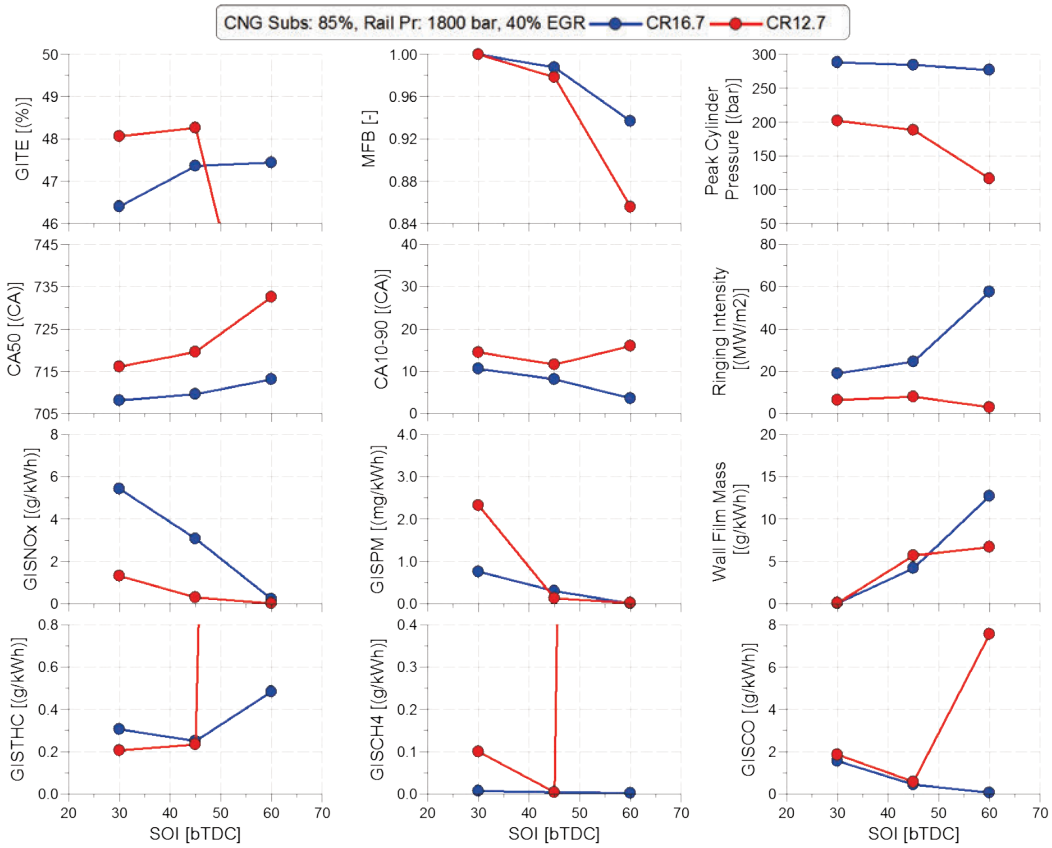

Figure 70 Impact of compression ratio and SOI on performance and emission parameters at 85% CNG substitution, 40% EGR and 1800 bar injection pressure for 1500 rpm and 12 bar BMEP using Combined mechanism

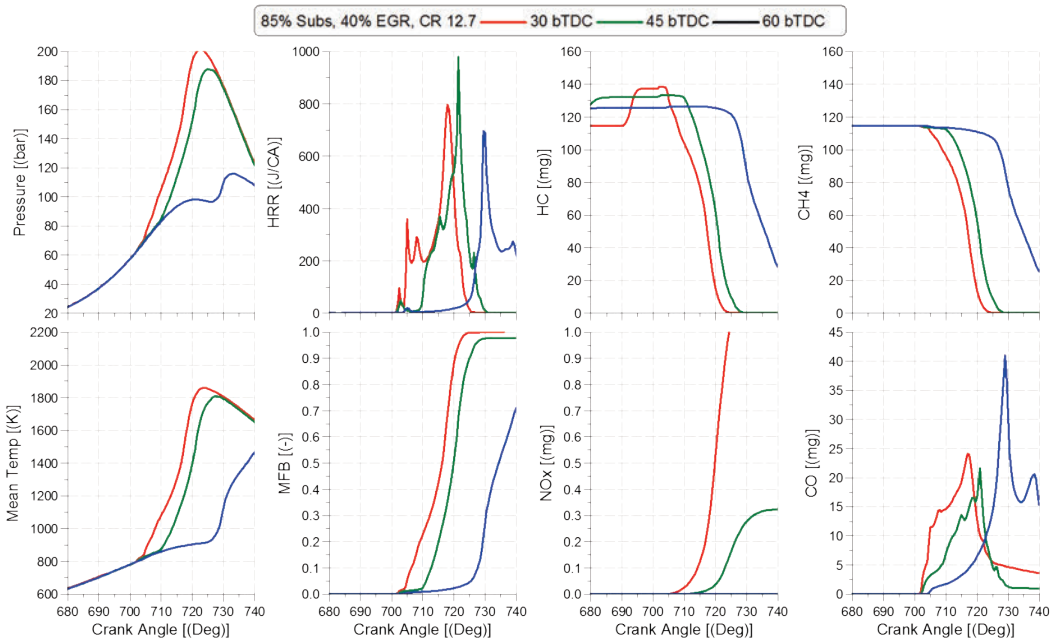

Figure 71 Comparison of performance and emission parameters on a CA basis for different SOI at compression ratio of 12.7 with 40% EGR and 85% CNG substitution for 1500 rpm and 12 bar BMEP using Combined mechanism

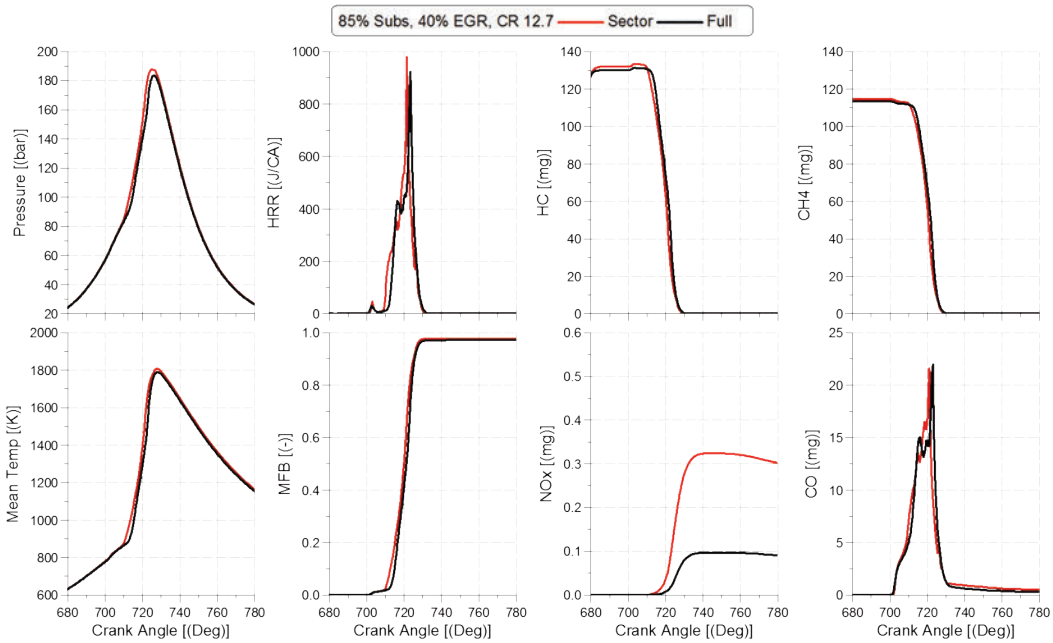

Figure 72 Comparison of performance and emission parameters on a CA basis for sector versus full geometry at compression ratio of 12.7, 40% EGR, 85% CNG substitution and 45 bTDC for 1500 rpm and 12 bar BMEP using Combined mechanism

Table 10 Performance and emission comparison of baseline versus RCCI operation at 1500 rpm and 12 bar BMEP

Parameter	Baseline	RCCI
Speed [rpm]	1500	
BMEP [bar]	12	
Substitution [%]	0	85
EGR [%]	37	40
PCP [bar]	157	184
ISNO$_x$ [g/KW-hr]	0.35	0.09
ISPM [g/KW-hr]	0.394	0.127
ISFC [g/KW-hr]	165	156

6.3 Evaluation of RCCI combustion at 1500 rpm and 20 bar BMEP

In order to evaluate the possibility of a low-NO$_x$ RCCI combustion at 1500 rpm and 20 bar BMEP, the optimum control parameter settings as determined for the 12 bar BMEP case were applied to the 20 bar BMEP load point. This included applying a CR of 12.7:1 with single diesel injection event and 40% EGR. Two different CNG substitutions (90 and 95%) were used for the initial analysis at the 20 bar BMEP operating point. The boundary conditions for both cases were generated using a calibrated GT-Power engine model as outlined in section 5. Table 11 overviews the boost pressure, exhaust pressure and AFR that were generated using the GT-Power engine model. Similar to 12 bar BMEP test point, cold flow CFD simulations were not conducted for each operating point listed in Table 11. However relevant IVC boundary conditions (pressure, temperature and composition) corresponding to the AFR and EGR listed in Table 11 were generated by offsetting existing CFD cold flow results at IVC from the baseline simulation case.

Table 11 Overview of boundary conditions used at 1500 rpm and 20 bar BMEP

	Units	Base	1	2	3
CNG Subs.	%	60	90	95	90
EGR	%	33	40	40	50
SOI	bTDC	1.25	45	45	45
Rail Pressure	bar	1950	1950	1950	1950
Boost Pressure	bar	3.62	4.07	3.79	3.89
Exhaust Pressure	bar	4.33	5.12	4.70	4.49
Air Fuel Ratio	-	21.2	20.6	19.4	16.7

Figure 73 compares the impact of CNG substitution on performance and emission parameters at the 1500 rpm and 20 bar operating point. Referring to Figure 73 we see that at both substitution levels the peak cylinder pressures are close to 300 bar even with the lower compression ratio of 12.7:1. The CA50 retards as the CNG substitution is increased but it also leads to smaller burn duration (CA10-90) which results in higher pressure rise rates leading to high peak cylinder pressures. The GITE improves as the CNG substitution is increased due to the improved CA50 location compared to the 90% CNG substitution case. All emissions including NO_x, CO, PM and THC reduce with increasing substitution to 95%. The PM emissions reduce due to reduction in diesel mass fraction as CNG substitution is increased. The reduction in NO_x emissions stems from the later combustion phasing as shown in Figure 74. However the overall NO_x emission are still higher compared to the requirement of a Low NO_x RCCI combustion system. Along with high NO_x emissions there is also a requirement to reduce the peak cylinder pressures below the baseline hardware limit of 190 bar.

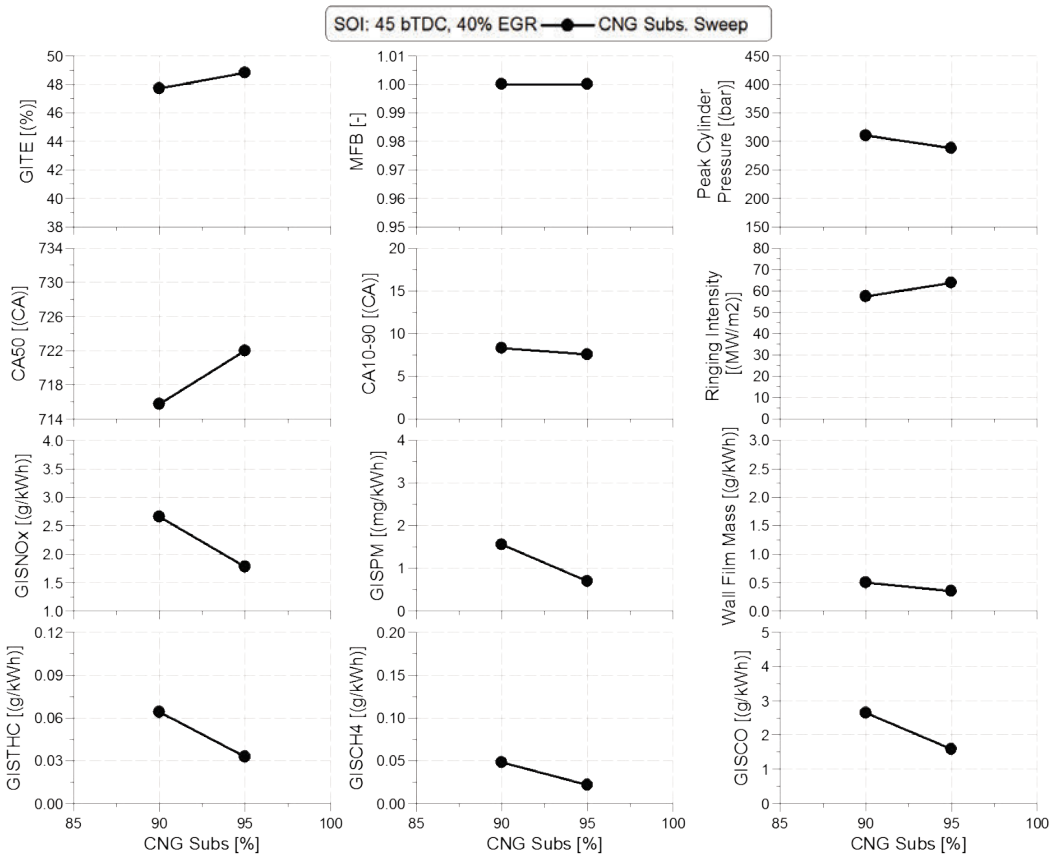

Figure 73 Impact of CNG Substitution on performance and emission parameters at 12.7:1 CR, 40% EGR and 45bTDC SOI for 1500 rpm and 20 bar BMEP using Combined mechanism

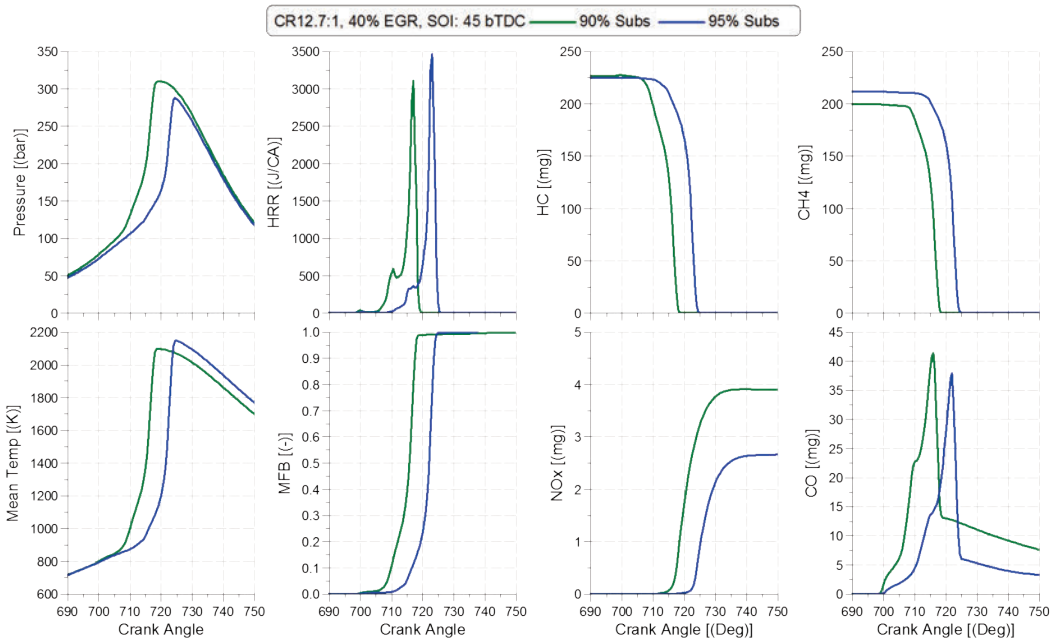

Figure 74 Comparison of performance and emission parameters on a CA basis for different CNG substitutions at 12.7:1 CR, 40% EGR and 45bTDC SOI for 1500 rpm and 20 bar BMEP using Combined mechanism

To lower the NO_x emissions and retard combustion phasing, a higher EGR rate of 50% was applied to the 90% CNG substitution case as shown in Figure 75. The application of higher EGR rate (50%) at 90% CNG substitution results in a retarded combustion phasing similar to 95% CNG substitution case at 40% EGR as highlighted in Figure 76. The higher EGR rate also results in longer burn duration which combined with the retarded combustion phasing results in lower peak cylinder pressure and pressure rise rates, refer Figure 75. The application of higher EGR rate results in near zero NO_x emissions however the application of higher EGR rate negatively impacts the GITE along with higher THC, CO and PM emissions. The application of higher EGR rate resolves the issue of high NO_x emissions but the peak cylinder pressure are still higher than the baseline hardware limit. To reduce the peak cylinder pressure a study was done with lower compression ratio of 11.7:1 as shown in Figure 77. At the lower compression ratio of 11.7:1 the peak cylinder pressures are below 200 bar with a retarded combusting phasing (734 CA) and longer burn duration, refer Figure 78. The retarded combustion phasing results in 9% reduction in GITE. Due to the significant drop in GITE with lower compression ratio it was concluded that the further studies to reduce peak cylinder pressures at 20 bar BMEP would be conducted at compression ratio of 12.7:1.

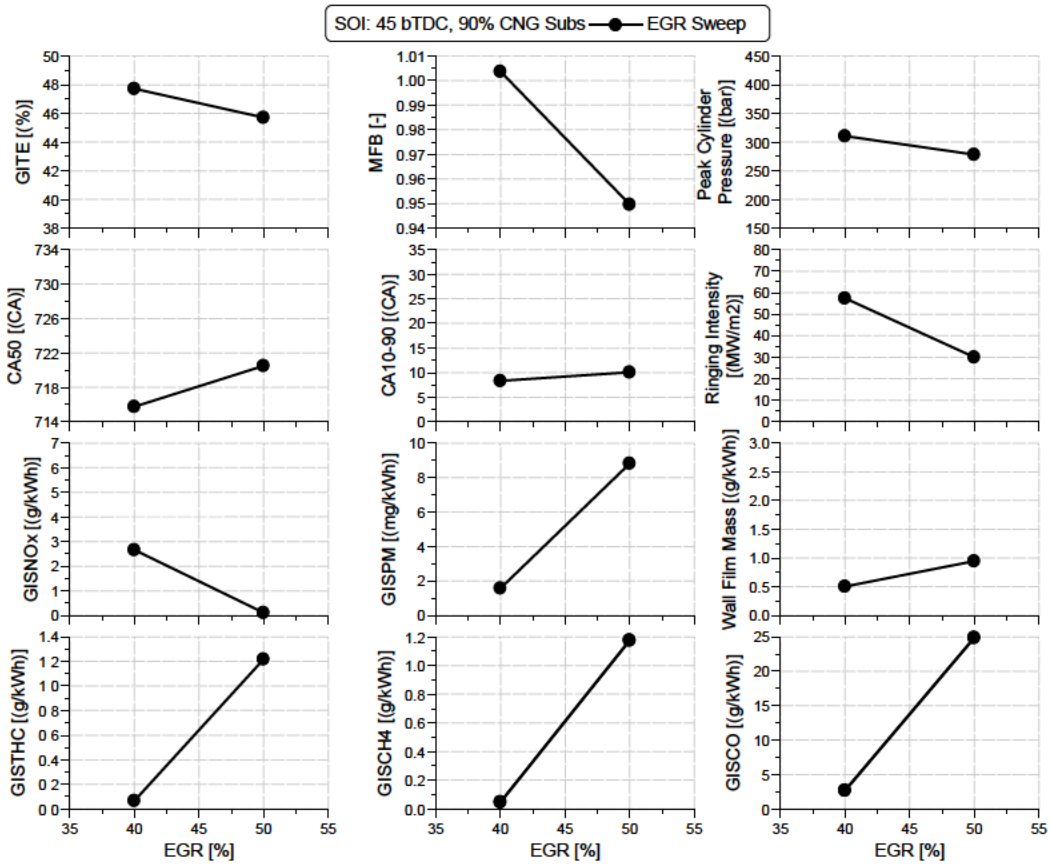

Figure 75 Impact of EGR percentage on performance and emission parameters at 12.7:1 CR, 90% CNG substitution and 45bTDC SOI for 1500 rpm and 20 bar BMEP using Combined mechanism

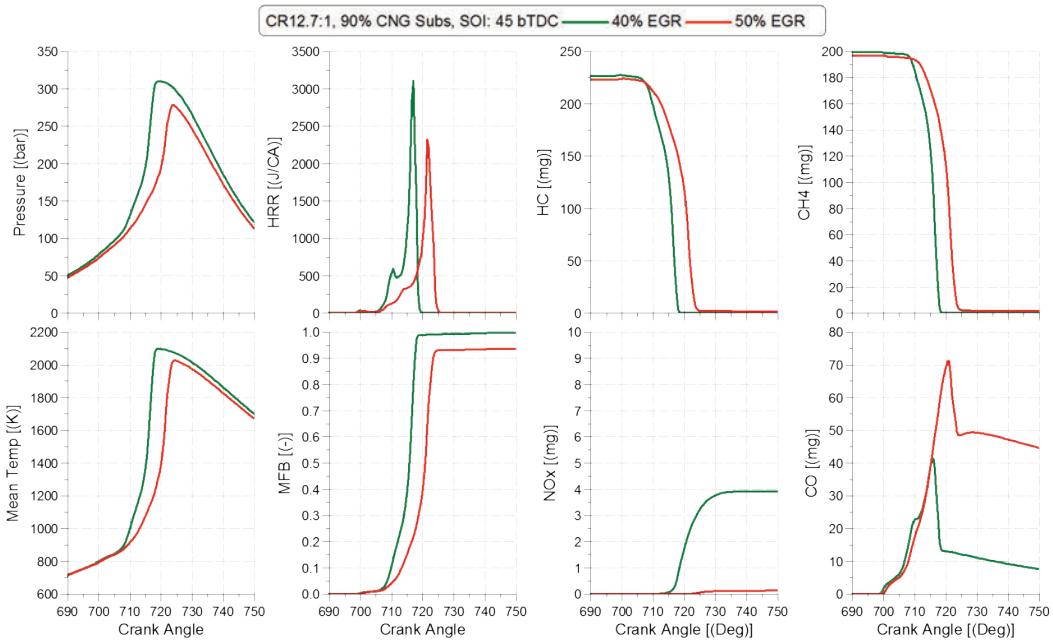

Figure 76 Comparison of performance and emission parameters on a CA basis for different EGR% at 12.7:1 CR, 90% CNG Substitution and 45bTDC SOI for 1500 rpm and 20 bar BMEP using Combined mechanism

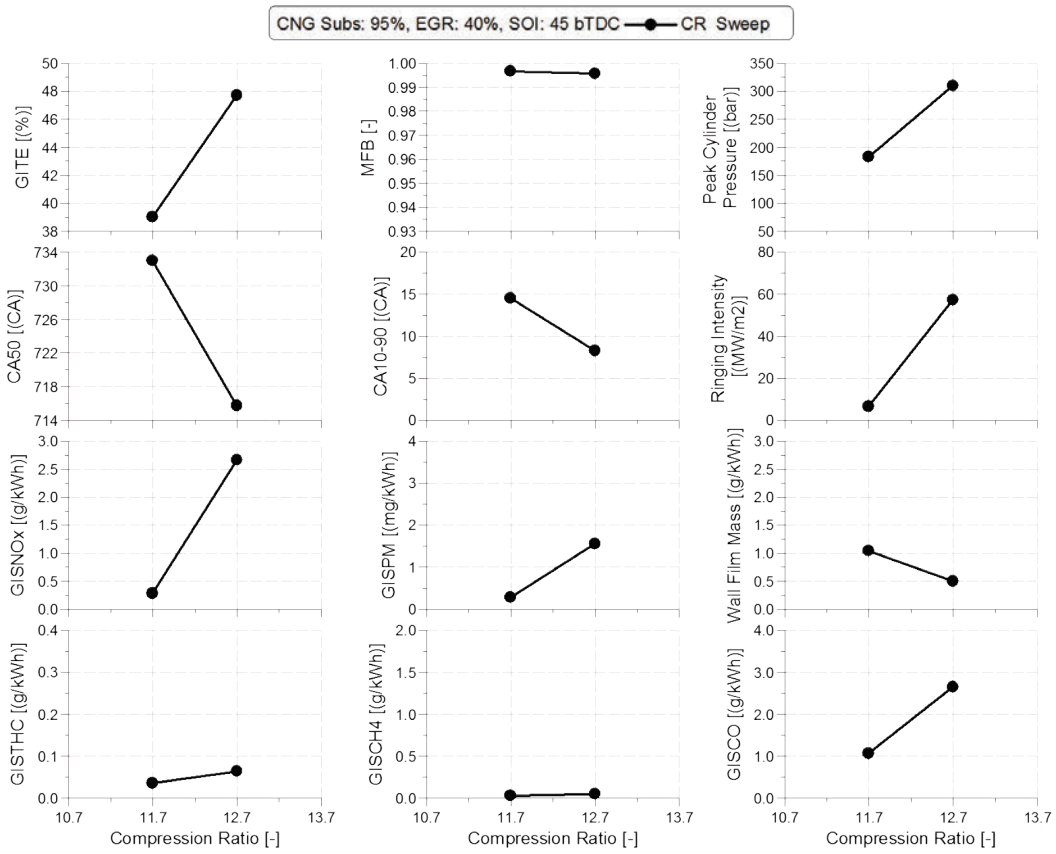

Figure 77 Impact of CR on performance and emission parameters at 95% CNG substitution, 40% EGR and 45bTDC SOI for 1500 rpm and 20 bar BMEP using Combined mechanism

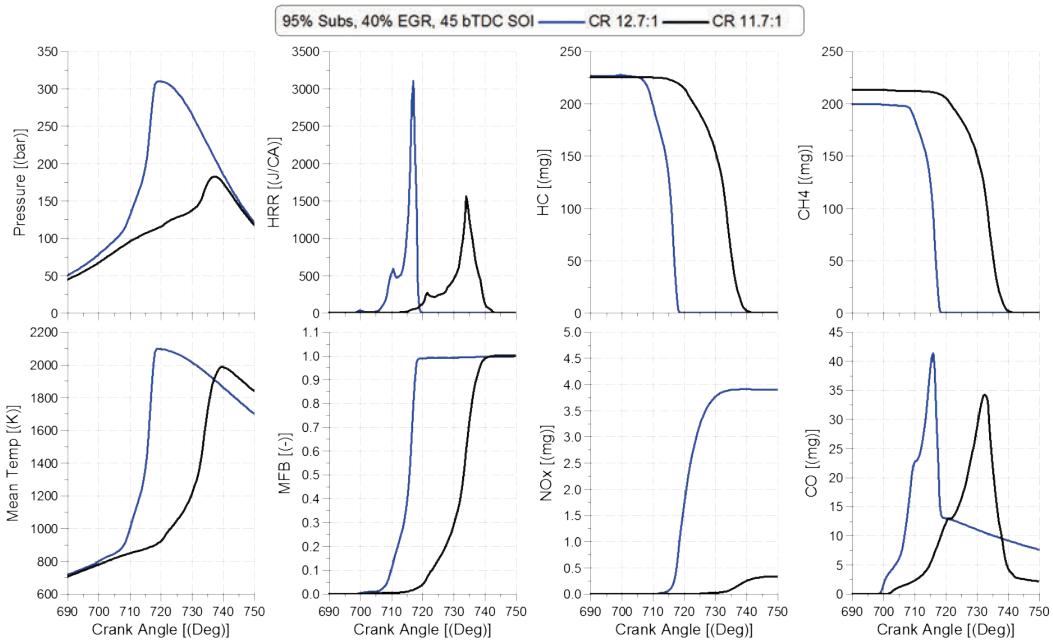

Figure 78 Comparison of performance and emission parameters on a CA basis for different compression ratios at 40% EGR, 90% CNG Substitution and 45bTDC SOI for 1500 rpm and 20 bar BMEP using Combined mechanism

Degree of premixing of the injected diesel mass is another control parameter that can varied for controlling combustion phasing. This can be achieved by using a spilt injection strategy where a certain portion of the diesel fuel is injected early in the compression stroke (e.g.: 60 deg bTDC) and remaining diesel fuel is injected closer to the TDC location. At 12 bar BMEP the Low NO_x RCCI combustion was possible without requiring the application of a spilt injection strategy. However the same control parameter setting at 20 bar BMEP resulted in much higher NO_x emission and peak cylinder pressures. Before the degree of premixing can be evaluated we need to determine which mechanism – Rahimi or Combined – is better suited for evaluating a spilt injection strategy.

Referring to Table 7, the Rahimi mechanism is well suited when the diesel injection timing is closer to the TDC location where as the Combined mechanism is better suited for predicting early diesel injection event. In case of a spilt injection strategy that applies one early injection event and another injection event closer to the TDC location it would be important to determine which mechanism would be better suited to predict the combustion behavior. In order to make this determination a split injection case from the earlier testing evaluation was simulated with both reaction mechanisms as shown in Figure 79. As explained earlier in section 4, during the experimental investigations the rated point (20 bar BMEP) was running very close to the peak cylinder pressure limit and hence did not provide much opportunity to advance injection timing or evaluate a spilt injection strategy. However the evaluation of split injection strategy was possible at a slighter lower BMEP of 17 bar without exceeding the peak cylinder pressure limit of the

baseline hardware as shown in Figure 79. The evaluation at 17 bar BMEP was conducted using a 50/50 spilt of the total diesel injection quantity with the first injection event occurring at 70 deg bTDC and the subsequent injection event at 3.2 deg bTDC. For this evaluation the CNG substitution was fixed to 90% with 30% EGR.

From Figure 79 we can see that the experimental cylinder pressure and HRR are better matched with the Rahimi mechanism compared to the Combined mechanism for the spilt injection case. Referring to the experimental results in Figure 79 we can see that the heat release starts to occur after the second injection event starts. In other words the combustion phasing is controlled by the second diesel injection event. This is well predicted by the Rahimi mechanism as demonstrated with close to the TDC diesel injection events evaluated in Section 6.1. The Combined mechanism predicts a much earlier start of combustion with a subsequent higher peak cylinder pressure compared to the experimental results. From this study it is evident that while evaluating a spilt injection strategy at 20 bar BMEP with the second diesel injection event closer to TDC it is appropriate to use the Rahimi mechanism as opposed to the Combined mechanism which has been used extensively in this study at 12 bar BMEP for evaluating different control parameters setting with relatively early diesel injection events (≥ 30 bTDC).

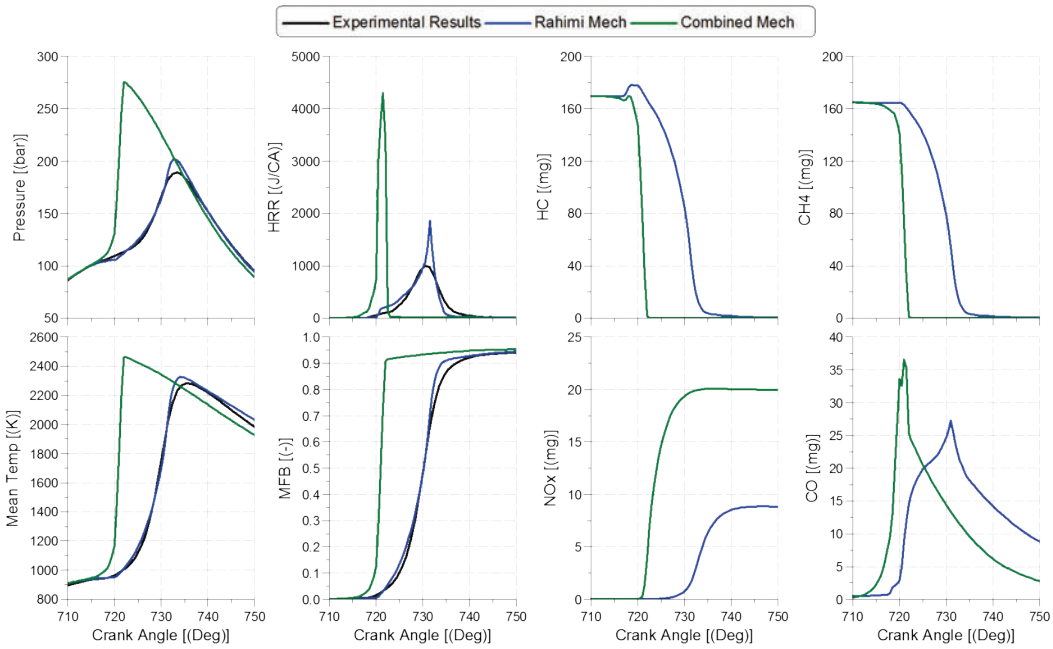

Figure 79 Comparison of performance and emissions predictions on a CA basis with two different reaction mechanisms at 1500 rpm and 17 bar BMEP – 90% CNG Subs., 30% EGR, Split SOI – 70bTDC/3.2 bTDC, CR: 16.7:1

For the split injection case at 20 bar BMEP, similar control parameters setting as applied for the single diesel injection case were used as outlined in Table 12. For the split injection case the first injection was targeted at 60 bTDC while the second injection was applied at 20 bTDC. The location of first diesel injection event was determined based on

the prior single injection timing studies conducted at 12 bar BMEP while the location of the second diesel injection event was inferred from the optimization study conducted by ref [13] at 23 bar BMEP. The 50/50 mass split was determined based on the experimental investigations conducted at 17 bar BMEP as well as the observations made by ref [13].

Table 12 Comparison of control parameters setting for the single injection vs. spilt injection case at 1500 rpm and 20 bar BMEP

Parameter	Single Injection	Split Injection
Speed [rpm]	1500	
BMEP [bar]	20	
Substitution [%]	90	
EGR [%]	40	
CR [-]	12.7:1	
Rail Pressure [bar]	1955	
First Injection timing [bTDC]	45	60
Second Injection timing [bTDC]	-	20
Diesel fraction in First Injection [%]	100	50
Mechanism	Combined	Rahimi

Figure 80 compares two cases – Case#1 uses a single diesel injection event while the Case#2 uses a split injection strategy as outlined in Table 12. We can see that for the spilt injection case the peak cylinder pressures are lower along with a more favorable CA50 location which results in higher thermal efficiency. The retarded combustion phasing supported by a longer burn duration results in lower pressure rise rates as shown in Figure 81. The early diesel injection event for the spilt injection case does lead to higher wall film fraction but the favorable combustion phasing still results in improved thermal efficiency. The retarded combustion phasing also results in lower NO_x emissions while the longer burn duration most probably helps reduce the PM emissions. The use of spilt injection does bring down the peak cylinder pressure from 310 bar to 230 bar but is still higher than the baseline limit of 190 bar. In order to understand the impact of spilt injection timing and mass fraction split on the peak cylinder pressure a three variable DOE was conducted as shown in Table 13. The test plan, as outlined in Table 14, was developed using xCAL DOE tool developed by FEV [42]. The DOE tool uses a space filling algorithm to determine the input set points for the test plan. CFD simulations were conducted at all #19 test points as shown in Table 14

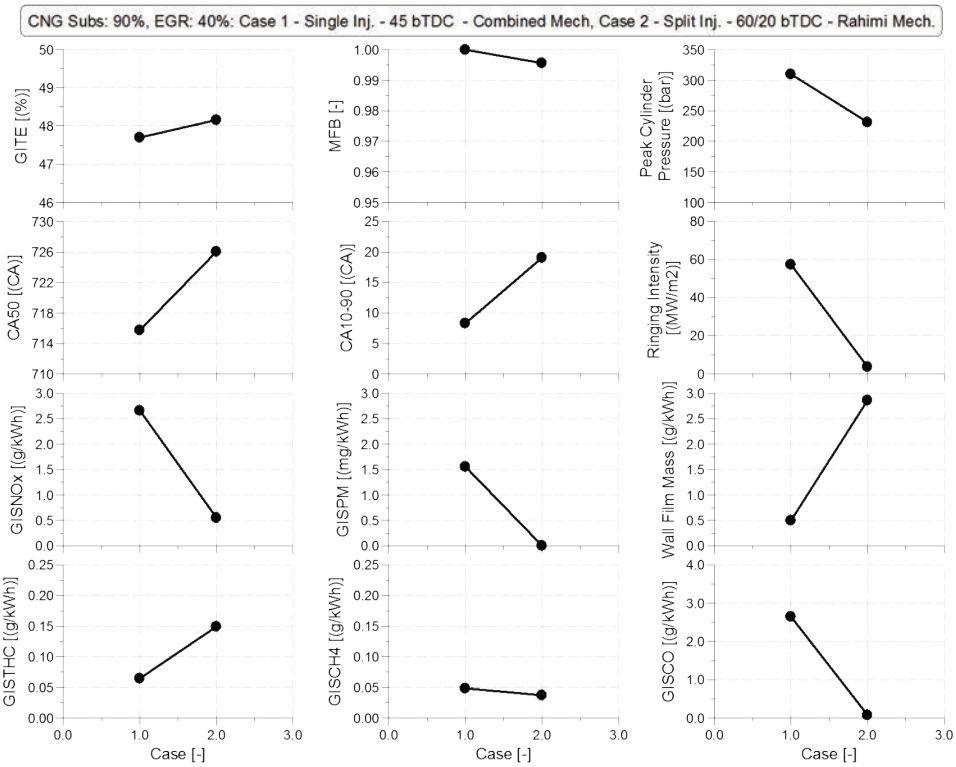

Figure 80 Impact of injection strategy on performance and emission parameters at 90% CNG substitution, 40% EGR and CR of 12.7:1 for 1500 rpm and 20 bar BMEP

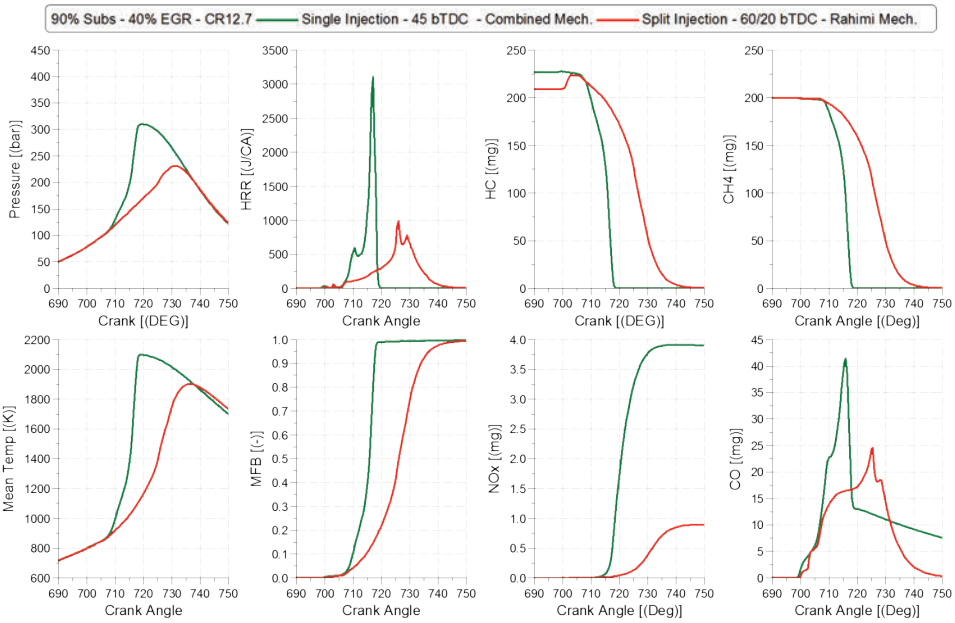

Figure 81 Comparison of performance and emission parameters on a CA basis for single vs. split injection strategy at 40% EGR, 90% CNG substitution and CR 12.7:1 for 1500 rpm and 20 bar BMEP

Table 13 Parameter limits for setting up a three variable DOE using FEV xCAL DOE Tool with Rahimi Mechanism

Parameter	Min	Max
First Injection timing [bTDC]	80	40
Second Injection timing [bTDC]	30	-10
Diesel fraction in First Injection [%]	10	95

Table 14 DOE test plan for evaluating impact of spilt injection and diesel mass fraction on peak cylinder pressure at 1500 rpm and 20 bar BMEP

Sr#	First Injection timing	Second Injection timing	Diesel fraction in First Injection
	bTDC	bTDC	%
1	70	0	72.5
2	50	20	27.5
3	55	5	61.25
4	65	5	38.75
5	45	25	83.75
6	55	-5	61.25
7	75	25	16.25
8	52.5	2.5	21.875
9	72.5	22.5	66.875
10	62.5	-7.5	89.375
11	42.5	12.5	44.375
12	77.5	-2.5	33.125
13	57.5	17.5	78.125
14	47.5	7.5	55.625
15	67.5	27.5	10.625
16	73.75	8.75	25.5
17	66.25	16.25	49.75

18	56.25	26.25	75.3125
19	78.75	13.75	92.1875

Figure 82 shows the intersection plots for peak cylinder pressure, indicated thermal efficiency and NO_x emissions against the three input variables used for the DOE study. As seen from the intersection plots the maximum pressure reduces as the first injection timing is advanced. However this also leads to lower thermal efficiency as a larger portion of the injected fuel forms a wall film as shown in Figure 83. Referring to Figure 82 we see that as the timing of the second injection event is advanced the peak cylinder pressure increases. At close to TDC (0 deg) injection timings we see very low peak cylinder pressure due to partial combustion with very low thermal efficiency indicating that timing of the second injection event needs to be suitably defined to maintain high efficiency and low peak cylinder pressures. Finally the intersection plots for the diesel mass fraction indicates that the peak cylinder pressures as well as NO_x emissions reduces as higher fraction of the total fuel is injected in the first injection event. The thermal efficiency remains relatively unaffected till about 60% mass fraction beyond which a drop in efficiency is seen due to sharp increase in the wall film mass as well as retarded combustion phasing (CA50). Figure 84 shows the tradeoff plot of peak cylinder pressure versus thermal efficiency and NO_x emissions. The blue dots in the figure represent the modeled point while the light green dots in the figure represent the random points that are generated by the Gaussian process (GP) model based on the modeled points. The thermal efficiency as well as NO_x emissions increase with increase in peak cylinder pressure. For the baseline peak cylinder pressure limit of 190 bar the model shows that there a possible combinations that can lead to low NO_x emissions (< 0.2 g/kWh) at a reduced thermal efficiency (<48%).

To determine the optimal settings an optimization run was setup in the DOE model with the aim to maximize thermal efficiency and minimize NO_x emissions. The upper limit for the peak cylinder pressure was fixed to 190 bar while a lower limit of 24 bar was provided for the gross IMEP value. Figure 85 shows the results from the optimized test point determined by the DOE tool based on the provided constraints. Table 15 overviews the resultant input parameter settings and corresponding output predictions for the optimized test points. As inferred from the intersection plots the optimized settings limit the diesel mass fraction in the first injection event to about 63% to avoid the drop in thermal efficiency. The timing of the first injection timing is optimized with the aim of limiting wall film mass while the second injection timing is used to control peak cylinder pressures and resultant NO_x emissions. A CFD simulation was than conducted with the optimum control parameters to verify these conclusions. Table 15 shows the predictions from the CFD model. The peak cylinder pressures as well as the $ISNO_x$ emissions predicted by the DOE model compare well to the CFD model predictions. The IMEP is over predicted by the DOE model compared to the CFD results which results in higher ISFC predictions in the CFD results. With the optimized control parameter settings the

target of demonstrating a Low NO_x RCCI combustion at 20 bar BMEP with peak cylinder pressure below the baseline hardware limit have been achieved.

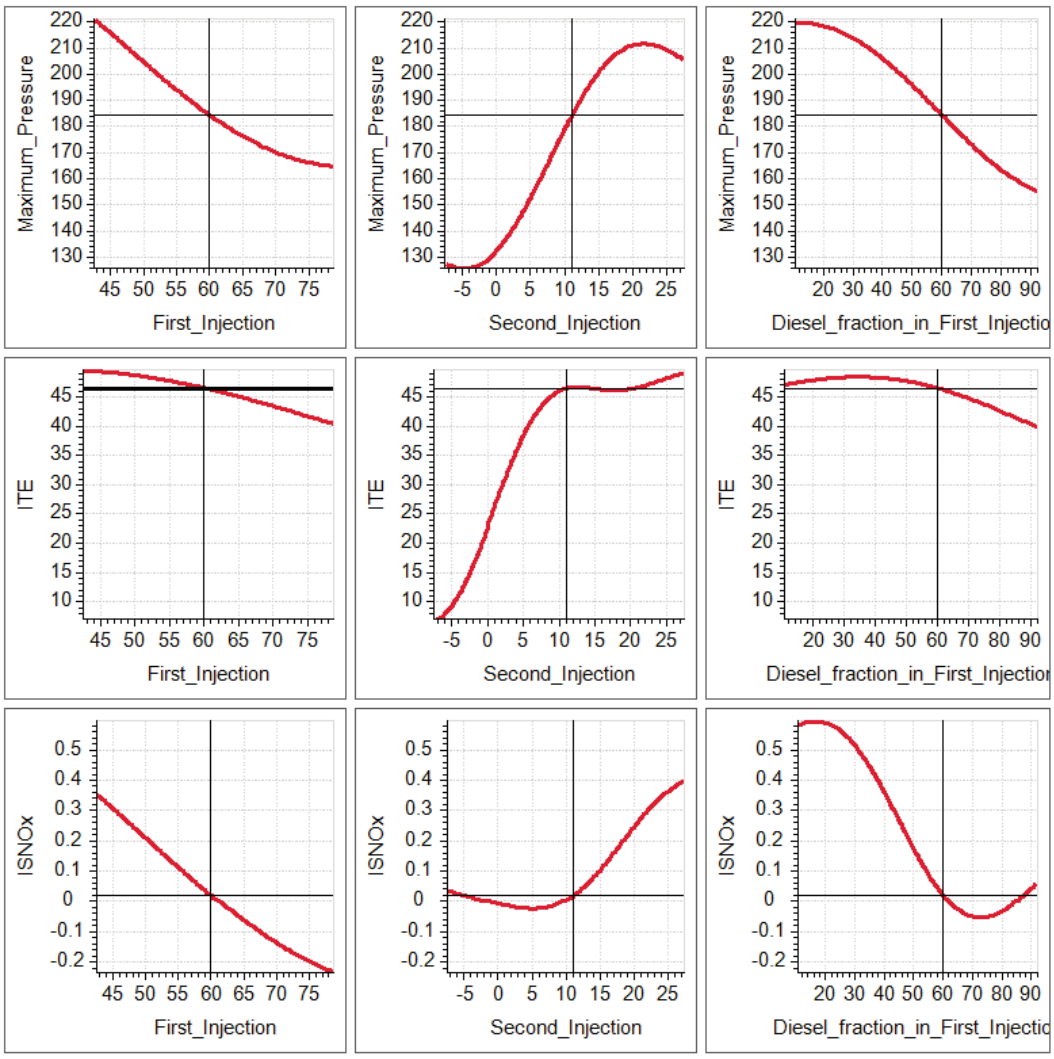

Figure 82 Intersection plots showing the impact of three input DOE variables on maximum cylinder pressure (bar), indicated thermal efficiency (ITE -%) and NO_x emissions ($ISNO_x$ – g/kWh) at 40% EGR, 90% CNG substitution and CR 12.7:1 for 1500 rpm and 20 bar BMEP

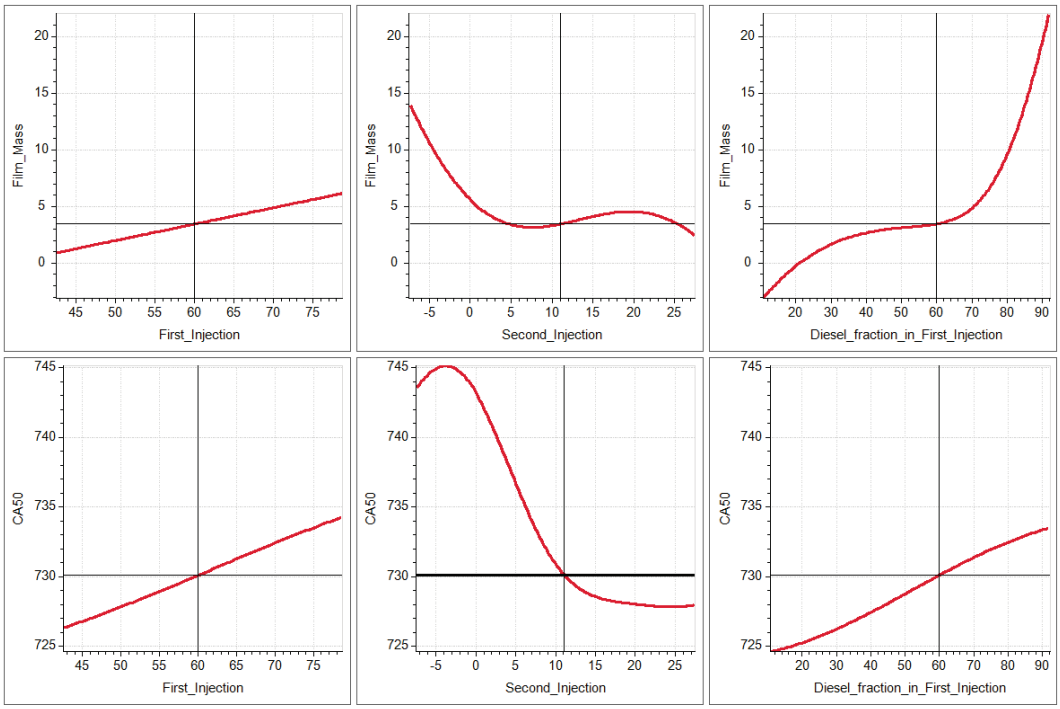

Figure 83 Intersection plots showing the impact of three input DOE variables on Film mass (g/kWh) on the liner and CA50 at 40% EGR, 90% CNG substitution and CR 12.7:1 for 1500 rpm and 20 bar BMEP

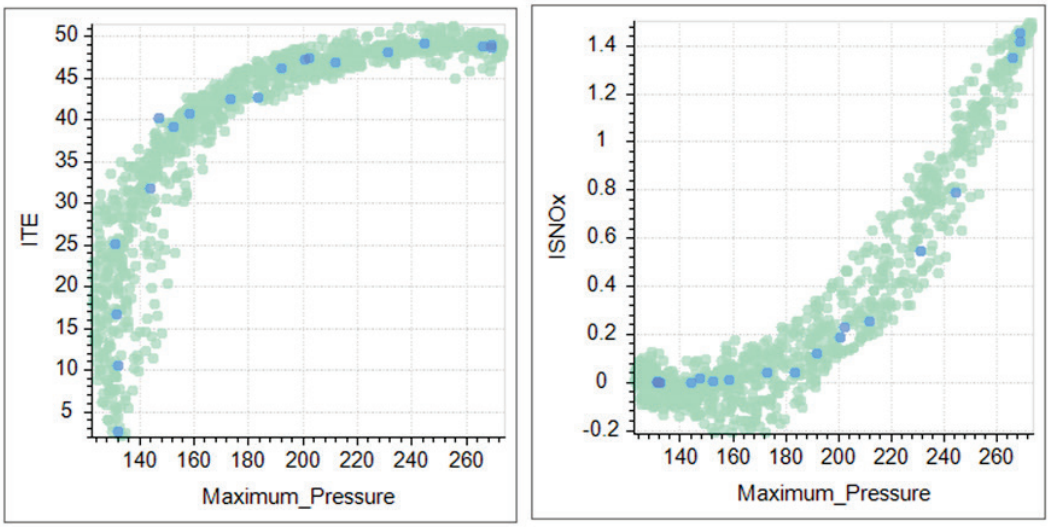

Figure 84 Trade off plots for indicated thermal efficiency (ITE -%) and NO_x emissions ($ISNO_x$ – g/kWh) versus maximum cylinder pressure (bar) for all DOE test points at 40% EGR, 90% CNG substitution and CR 12.7:1 for 1500 rpm and 20 bar BMEP

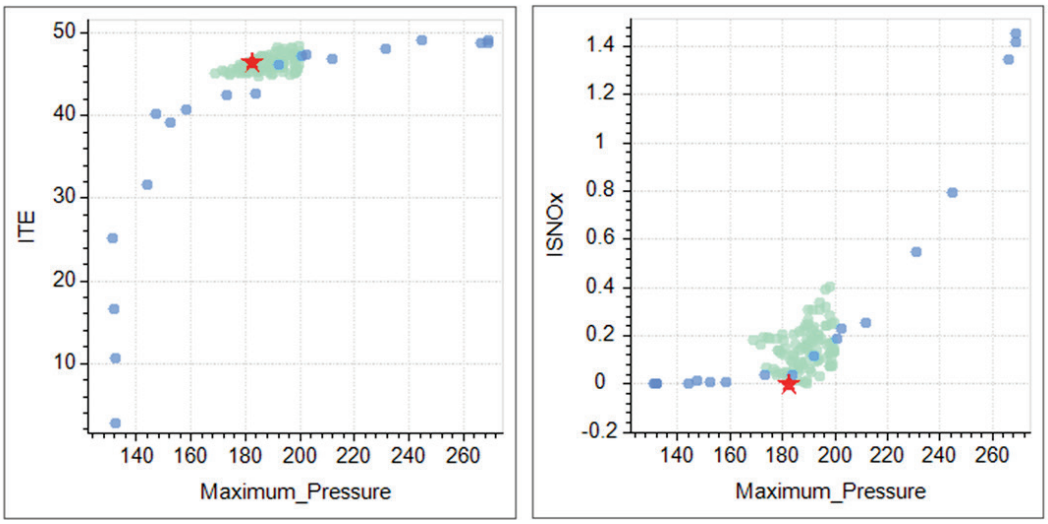

Figure 85 Optimized test point plotted on trade off plots for indicated thermal efficiency (ITE -%) and NO_x emissions ($ISNO_x$ – g/kWh) versus maximum cylinder pressure (bar) at 40% EGR, 90% CNG substitution and CR 12.7:1 for 1500 rpm and 20 bar BMEP

Table 15 Comparison of results from optimum parameter setting from the DOE study using FEV xCAL DOE Tool vs CFD simulations

Parameter	**DOE Model**	**CFD Model**
First injection timing [bTDC]	59.5	
Second injection timing [bTDC]	11.25	
Diesel fraction in first injection [%]	63	
Gross IMEP (bar)	24.8	23.7
Peak cylinder pressure (bar)	182.6	182.5
GITE (%)	46.3	44.3
CA50 (aTDC)	10.3	11.5
$ISNO_x$ (g/kWh)	<0.05	0.043
Wall film mass (g/kWh)	3.65	3.67

With the control parameters defined at 20 bar BMEP, a comparison was made of the results between the sector simulations and the full geometry simulations. The control parameter setting used for this comparison included 40% EGR, 90% CNG substitution, first diesel injection timing of 59.5 bTDC, second diesel injection timing of 11.25 bTDC, 63% mass fraction in first injection at a compression ratio of 12.7. Referring to the heat release trace in Figure 86 we see that the initial heat release rate predictions from the full

geometry simulation is higher compared to the sector simulation case. However the subsequent peak from the main combustion event is lower which results in similar peak cylinder pressures between the sector and full geometry cases. The differences in the initial and peak heat release rate between the sector and full geometry cases could be result of the assumption made in setting up the sector simulations. One key assumption that is made while simulating a sector case is in regards to the fuel mass that leaves the boundary of the sector. This fuel mass is assumed to enter the sector geometry from the other end to mimic spray to spray interactions that would be seen in the full geometry case. This assumes that all sprays in the full geometry behave identical. This assumption has its limitation and may lead to unfavorable fuel to fuel interaction resulting in fuel rich regions which, in our sector case, might have impeded the initial heat release rate and subsequent oxidation of this region might have contributed to the higher heat release rates. Overall good match in the cylinder pressures and temperature traces is seen between the sector and full geometry simulations. The MFB and the resultant NO_x, HC, CH4 and CO emissions also correlate well between the sector and full geometry simulations. The predicted peak cylinder pressures and resultant NO_x emissions from the full geometry simulation confirm the possibility of achieving a low NO_x RCCI combustion at 20 bar BMEP and 1500 rpm. Compared to the baseline experimental results at 20 bar BMEP with diesel only operation, the proposed low NO_x RCCI combustion strategy resulted in 87.5% reduction in NO_x emissions with 2% improvement in fuel consumption as shown in Table 16. Significant reduction (>95%) in PM emissions was also achieved.

Comparing the current work to previous CFD study conducted by Nieman et al. [13] at 23 bar gross IMEP, it was observed that higher levels of EGR were required to increase ignition delay at 20 bar BMEP compared to the baseline diesel operation. This observations were similar to the findings reported by authors in ref [13]. In the study by ref [13] the genetic algorithm also recommended to apply a split injection strategy to control maximum pressure rise rates at 23 bar gross IMEP. Similar observations were also seen in this study where a split injection was required to control the combustion phasing as well as the maximum pressure rise rates. The authors in ref [13] also did a sensitivity analysis on the diesel mass fraction in the first injection and noted that a more equal spilt would be favorable to control the pressure rise rates and maximum pressure at 23 bar gross IMEP. In this study it was observed that increasing the diesel mass fraction in the first injection resulted in lowering of the peak cylinder pressures, refer Figure 82, and along with a reduction in the GITE as the combustion phasing was more retarded as shown in Figure 83. The authors in ref [13] argued that if the diesel mass fraction in the first injection is increased it would result in an earlier combustion phasing and higher pressure rise rates. This was not observed in our study. One possible reason could be the lower compression ratio applied in this study which reduced the compression temperature and the combustion phasing was primarily controlled by the second diesel injection event. Other contributing factor might be the reaction mechanism which was shown in this study to be sensitive to the diesel injection timing event. In the current study the optimum mass fraction was chosen to maximize GITE (reduce wall film mass) while minimizing NO_x emissions (CA50 phasing). In the study by ref [13] it is shown that the

RCCI combustion at 23 bar gross IMEP can be achieved with higher CR of 16.1:1 by application of higher EGR levels (48%) compared to the current study where a lower EGR was applied (40%). In the current study with single diesel injection event it was shown that higher EGR levels were very effective in reducing NO_x emissions but did not impact the peak cylinder pressures significantly, refer Figure 75. Higher EGR levels were not tested with the spilt injection strategy due to the deterioration of combustion efficiency and increase in unburnt hydrocarbon emissions which was also observed by ref [13].

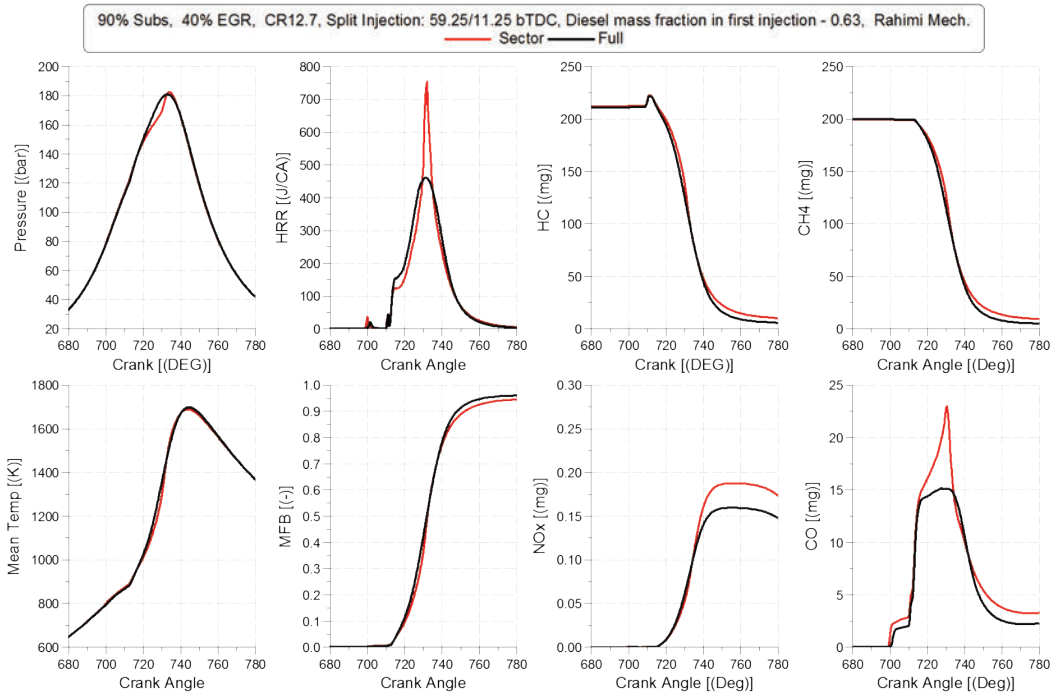

Figure 86 Comparison of performance and emission parameters on a CA basis for sector versus full geometry at compression ratio of 12.7, 40% EGR, 90% CNG substitution and optimized split injection strategy for 1500 rpm and 20 bar BMEP using Rahimi mechanism

Table 16 Performance and emission comparison of baseline versus RCCI operation at 1500 rpm and 20 bar BMEP

Parameter	Baseline	RCCI
Speed [rpm]	1500	
BMEP [bar]	20	
Substitution [%]	0	90
EGR [%]	30	40
PCP [bar]	183	180.9
$ISNO_x$ [g/KW-hr]	0.40	0.05
ISPM [mg/KW-hr]	0.245	0.01
ISFC [g/KW-hr]	167.9	164.6

7 Summary and Conclusion

Experimental and computational studies were conducted to explore the feasibility of a Low NO_x RCCI combustion across the complete engine operating range. The experimental studies were conducted on a 13 liter heavy duty diesel engine. The engine was operated in dual fuel mode through intake fumigation of CNG after the high pressure charge air cooler. The CNG substitution was controlled on an energy equivalence basis. The experimental study was conducted at #12 operating points. All test points were initially evaluated in conventional dual fuel combustion mode. The studies showed that with optimized control strategies (injection timing + substitution) on an average 49% substitution could be achieved across the complete engine operating map. The operation of engine in conventional dual fuel combustion mode resulted in 15% reduction in NO_x and 43% reduction in PM emissions. Experimental evaluation of RCCI combustion was limited to low (5 bar) and mid (12 bar) loads operating points due to the baseline hardware peak cylinder pressure limitation of 190 bar. Evaluation of RCCI combustion at high loads required application of higher EGR levels to limit peak cylinder pressure which was not feasible with the production hardware. At 5 bar BMEP it was observed that for achieving a low NO_x RCCI combustion, along with diesel injection timing, both CNG substitution and EGR rate had to be optimized. At 12 bar BMEP RCCI combustion with low NO_x emissions could not be achieved below 1800 rpm due to peak cylinder pressure limitations. It was observed that maximum pressure rise rates were sensitive to boost pressure as well as EGR levels. Spilt injection was also effective in controlling maximum pressure rise rates at 12 bar BMEP.

Computational investigation were initially carried out at 1500 rpm and 5 bar BMEP using Converge CFD software. The combustion simulation were conducted using the SAGE combustion solver in Converge with the application of Rahimi mechanism. The Rahimi mechanism consisted of 76 species and 464 reactions. The CFD study was focused on the RCCI test points at 5 bar BMEP to establish an initial baseline correlation between simulation results and test data. During the CFD study it was found that the Rahimi mechanism, which consist of combination of GRI Mech 3.0 and Valeri mechanism, was not able to predict the combustion behavior for diesel injection timings advanced beyond 30 bTDC. This behavior was validated at multiple speed and load points. To resolve this shortcoming a new reaction mechanism was proposed. It included combining the original GRI Mech 3.0 mechanism with the Chalmers mechanism. The mechanism was termed as Combined mechanism and included 76 species and 424 reactions as compared to the 76 species and 464 reactions included in the Rahimi mechanism. This mechanism was capable of predicting combustion behavior with early diesel injection timing events (>30 bTDC). For retarded injection timing (<30 bTDC) it was found that the mechanism over predicted the heat release rate. Hence an injection timing boundary with respect to the reaction mechanism was established for this study. When evaluating diesel injection timing closer to TDC (30 bTDC and retarded timing) the Rahimi mechanism was applied while for evaluating advanced diesel injection timing before 30 bTDC the Combined mechanism was applied.

After the baseline correlation was established at 5 bar BMEP and 1500 rpm, a parametric study using Combined mechanism was then conducted at 12 bar BMEP and 1500 rpm. The key parameters that were varied in this study included CNG substitution, EGR rate, diesel injection timing, fuel rail pressure, injector spray angle and geometric compression ratio. The variation in main injection timing was limited to CA before 30 bTDC due to the use of the Combined mechanism. The main challenge that was identified at this load point during testing, was the high pressure rise rates and corresponding higher NOx emissions. Through the CFD study it was found that using high CNG substitution (>85%) and EGR rates (>40%) was very effective in controlling the NO_x emissions. However the resultant boost pressure that was required to hold the AFR above stoichiometry resulted in much higher peak cylinder pressures (>250 bar) than the baseline hardware limit of 190 bar. Changes in rail pressure or injector spray angle did not show a significant impact on the combustion phasing and hence resulted in similar peak cylinder pressures. Finally reducing the geometric compression ratio by 4 points from 16.7:1 to 12.7:1 was found to be very effective in reducing the peak cylinder pressures below the baseline hardware limit of 190 bar. The 4 point change in compression ratio was selected based on existing two step variable compression ratio connecting rod marketed by FEV. This system is capable of reducing the geometric compression ratio by 3 to 4 points for a heavy duty application. Using the lower compression ratio of 12.7:1 along with application of appropriate CNG substitution, EGR rate and injection timing, the target of a low NO_x RCCI combustion was achieved at 12 bar BMEP. The final optimized conditions showed a 75% improvement in NO_x emissions along with 5.5% improvement in ISFC compared to the baseline diesel case. The PM emissions were also reduced by 68% with the optimized case when compared to the baseline diesel case.

As a next step CFD studies were then conducted at 20 bar BMEP and 1500 rpm using the lower compression ratio of 12.7:1. At this load point it was found that the peak cylinder pressures were much higher (>250 bar) than the baseline hardware limitations. A sweep on CNG substitution and EGR rate showed similar behavior as at 12 bar BEMP, where an increase in either parameter resulted in reduced NO_x emissions without significantly impacting the peak cylinder pressures. In order to limit the peak cylinder pressures a spilt injection strategy was then investigated at 20 bar BMEP. After promising initial results a detailed DOE study was conducted on three control parameters – first injection timing, second injection timing and diesel mass fraction in the first injection. The Rahimi mechanism was used for this study as the timings applied for the second diesel injection were closer to the TDC location. A Gaussian process model was then created from the DOE results and was used to determine the optimized parameter settings with the aim to limit peak cylinder pressures below 190 bar. CFD simulations conducted with the optimized configuration from the DOE study resulted in peak cylinder pressures below 190 bar along with lower NO_x emissions than the baseline case. Overall application of a spilt injection strategy along with lower compression ratio was successful in achieving the target of a Low NO_x RCCI combustion at 20 bar BMEP and 1500 rpm. The final simulation results showed a 2% improvement in ISFC compared to the baseline diesel case. Both NO_x and PM emission were simultaneously reduced by 87.5% and 95% respectively compared to the baseline diesel case.

Figure 87 overviews a causality diagram representing the impact of different control parameters in achieving a Low NOx RCCI combustion based on the experimental and computational studies conducted as part of the current study. The diagram highlights pathways through which peak cylinder pressure and NOx emission can be controlled to achieve a Low NOx RCCI across the complete load range (5 bar to 20 bar) at 1500 rpm.

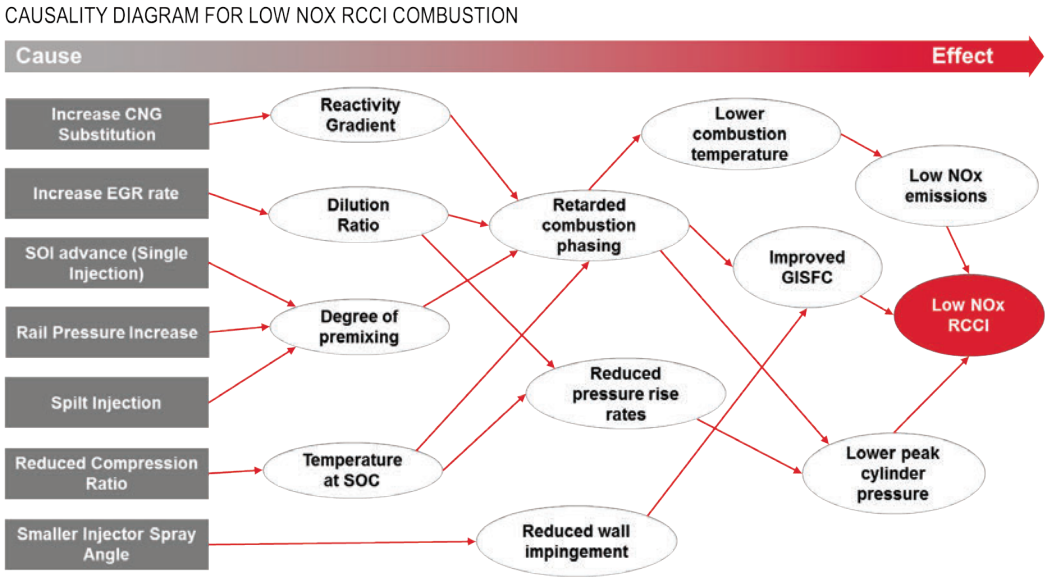

Figure 87 Comparison of performance and emission parameters on a CA basis for sector versus full geometry at compression ratio of 12.7, 40% EGR, 90% CNG substitution and optimized split injection strategy for 1500 rpm and 20 bar BMEP using Rahimi mechanism

In summary the experimental and computational studies demonstrate that a Low NO_x RCCI combustion can be achieved across the complete load range at 1500 rpm from 5 bar to 20 bar BEMP. At all three load points investigated in this study the RCCI combustion strategy results in improved ISFC along with simultaneously reduction in NO_x and PM emissions. For the case of mid and high load points where high CNG substitution (>90%) are applied the resulting PM emissions are very low (>99% reduction). The improved ISFC with RCCI combustion can help engine OEM meet the upcoming Phase II greenhouse gas emission legislations [43] while reduced engine out NO_x emissions can be a significant benefit to reduce aftertreatment complexity with the expected implementation of the ultra-low NOx emission regulations [44].

For future work it is recommended that control parameter settings identified for mid (12 bar BMEP) and high (20 bar BMEP) loads at 1500 rpm should be applied at other engine speeds (e.g. 1200 rpm and 1800 rpm) to verify that a low NO_x RCCI combustion can be achieved across the complete engine operating speed range with the proposed four point reduction in compression ratio at mid and high loads. Experimental verification of the proposed low NO_x RCCI combustion strategy would be a helpful next step in gaining further confidence in the proposed control strategy. There still exists a need to develop a

more comprehensive reaction mechanism that can be used for RCCI investigation with diesel and natural gas across a wider range of injection timings. The current approach of using different reaction mechanism based on injection timing has some limitations especially when injection timings applied are close to the switching boundary as well as with spilt injection studies.

8 Reference List

1. US Energy Information Administration, “Natural Gas,” http://www.eia.gov/naturalgas/, Aug 2013.
2. Ribas X., “Heavy Duty liquefied Natural Gas engine developments to meet future emissions requirements, methodology and real application,” FISITA paper F2010F013, 2010.
3. Ouellette, P., “Cummins Westport Spark-Ignited (SI) and High Pressure Direct Injection (HPDI) Natural Gas Engines,” presented at NGVTF 2003, USA, January 28-29, 2003.
4. Guzman, P., Ribas, X., Garcia Sr, J., and Pita Sr, M., "PM and CO2 Reduction in a Dual-fuel Heavy-duty Diesel Engine during the Freeway Part of Transient Worldwide Emission Tests,” SAE Technical Paper 2013-01-2759, doi:10.4271/2013-01-2759
5. Dronniou, N., Kashdan, J., Lecointe, B., Sauve, K. et al., "Optical Investigation of Dual-fuel CNG/Diesel Combustion Strategies to Reduce CO2 Emissions," SAE Int. J. Engines 7(2):2014, doi:10.4271/2014-01-1313.
6. Weaver, C. and Turner, S., “Dual Fuel Natural Gas/Diesel Engines: Technology, Performance, and Emissions,” SAE Technical Paper 940548, 1994, doi:10.4271/940548.
7. Karim, G., Liu, Z., and Jones, W., “Exhaust Emissions from Dual Fuel Engines at Light Load,” SAE Technical Paper 932822, 1993, doi:10.4271/932822.
8. Abd Alla, G. H., Soliman, H. A., Badr, O. A. and Abd Rabbo, M. F., “Effect of Pilot Fuel Quantity on the Performance of a Dual Fuel Engine.” Energy Conversion and Management, 41 (6): 559-572, 2000, ISSN: 01968904
9. Gebert, K., Beck, N., Barkhimer, R., and Wong, H., “Strategies to Improve Combustion and Emission Characteristics of Dual-Fuel Pilot Ignited Natural Gas Engines,” SAE Technical Paper 971712, 1997, doi: 10.4271/971712
10. Abd Alla, G. H., Soliman, H. A., Badr, O. A. and Abd Rabbo, M. F., “Effect of Injection Timing on the Performance of a Dual Fuel Engine” Energy Conversion and Management, 43:269-277, 2002
11. Dishy, A., You, T., Iwashiro, Y., Nakayama, S. et al., “Controlling Combustion and Exhaust Emissions in a Direct-Injection Diesel Engine Dual-Fueled with Natural Gas,” SAE Technical Paper 952436, 1995, doi:10.4271/952436
12. Dahodwala, M., Joshi, S., Koehler, E., and Franke, M., "Investigation of Diesel and CNG Combustion in a Dual Fuel Regime and as an Enabler to Achieve RCCI Combustion," SAE Technical Paper 2014-01-1308, 2014, doi:10.4271/2014-01-1308
13. Nieman, D., Dempsey, A., and Reitz, R., "Heavy-Duty RCCI Operation Using CNG and Diesel," SAE Int. J. Engines 5(2):270-285, 2012, doi:10.4271/2012-01-0379
14. Zoldak, P., Sobiesiak, A., Bergin, M., and Wickman, D., "Computational Study of Reactivity Controlled Compression Ignition (RCCI) Combustion in a Heavy-Duty

Diesel Engine Using Natural Gas," SAE Technical Paper 2014-01-1321, 2014, doi:10.4271/2014-01-1321.
15. Doosje, E., Willems, F., and Baert, R., "Experimental Demonstration of RCCI in Heavy-Duty Engines usingDiesel and Natural Gas," SAE Technical Paper 2014-01-1318, 2014, doi:10.4271/2014-01-1318.
16. Jia, Z. and Denbratt, I., "Experimental Investigation of Natural Gas-Diesel Dual-Fuel RCCI in a Heavy-Duty Engine," SAE Int. J. Engines 8(2):2015, doi:10.4271/2015-01-0838.
17. Dahodwala, M., Joshi, S., Koehler, E., Franke, M. et al., "Experimental and Computational Analysis of Diesel-Natural Gas RCCI Combustion in Heavy-Duty Engines," SAE Technical Paper 2015-01-0849, 2015, doi:10.4271/2015-01-0849.
18. Zoldak, P., Sobiesiak, A., Wickman, D., and Bergin, M., "Combustion Simulation of Dual Fuel CNG Engine Using Direct Injection of Natural Gas and Diesel," SAE Int. J. Engines 8(2):2015, doi:10.4271/2015-01-0851.
19. Bekdemir, C., Baert, R., Willems, F., and Somers, B., "Towards Control-Oriented Modeling of Natural Gas-Diesel RCCI Combustion," SAE Technical Paper 2015-01-1745, 2015, doi:10.4271/2015-01-1745.
20. Garcia, P. and Tunestal, P., "Experimental Investigation on CNG-Diesel Combustion Modes under Highly Diluted Conditions on a Light Duty Diesel Engine with Focus on Injection Strategy," SAE Int. J. Engines 8(5):2015, doi:10.4271/2015-24-2439.
21. Walker, R., Wissink, M. et al., “Natural Gas for High Load Dual-Fuel Reactivity Controlled Compression Ignition in Heavy-Duty Engines,” Journal of Energy Resources Technology, JULY 2015, Vol. 137 / 042202-1
22. Kakaee, A., Rahnama, P. and Paykani, A., “Influence of fuel composition on combustion and emissions characteristics of natural gas/diesel RCCI engine,” Journal of Natural Gas Science and Engineering 25 (2015) 58-65
23. May, I., Pedrozo, V., Zhao, H., Cairns, A. et al., "Characterization and Potential of Premixed Dual-Fuel Combustion in a Heavy Duty Natural Gas/Diesel Engine," SAE Technical Paper 2016-01-0790, 2016, doi:10.4271/2016-01-0790.
24. Hanson, R., Ickes, A., and Wallner, T., "Comparison of RCCI Operation with and without EGR over the Full Operating Map of a Heavy-Duty Diesel Engine," SAE Technical Paper 2016-01-0794, 2016, doi:10.4271/2016-01-0794.
25. Hanson, R., Ickes, A., and Wallner, T., "Use of adaptive injection strategies to increase the full load limit of RCCI operation," Journal of Engineering for Gas Turbines and Power, GTP-16-1034.
26. Kakaee, A., Nasiri-Toosi, A., Partovi, B. and Paykani, A., “Effects of piston bowl geometry on combustion and emissions characteristics of a natural gas/diesel RCCI engine,” Applied Thermal Engineering 102 (2016) 1462–1472.
27. Khatamnejad, H., Khalilarya, S., Jafarmadar, S., Mirsalim, M. et al., "Influence of Blend Ratio and Injection Parameters on Combustion and Emissions Characteristics of Natural Gas-Diesel RCCI Engine," SAE Technical Paper 2017-24-0083, 2017, doi:10.4271/2017-24-0083.

28. Poorghasemi, K. et al., “Effect of diesel injection strategies on natural gas/diesel RCCI combustion characteristics in a light duty diesel engine”, Journal of Applied Energy, MAY 2017, doi: http://dx.doi.org/10.1016/j.apenergy.2017.05.011
29. Zhang, Y., Sagalovich, I., De Ojeda, W., Ickes, A. et al., "Development of Dual-Fuel Low Temperature Combustion Strategy in a Multi-Cylinder Heavy-Duty Compression Ignition Engine Using Conventional and Alternative Fuels," SAE Int. J. Engines 6(3):1481-1489, 2013, doi:10.4271/2013-01-2422.
30. Joo, S., Alger, T., Chadwell, C., De Ojeda, W. et al., "A High Efficiency, Dilute Gasoline Engine for the Heavy-Duty Market," SAE Int. J. Engines 5(4):1768-1789, 2012, doi:10.4271/2012-01-1979.
31. Splitter, D., Hanson, R., Kokjohn, S., and Reitz, R., "Reactivity Controlled Compression Ignition (RCCI) Heavy-Duty Engine Operation at Mid- and High-Loads with Conventional and Alternative Fuels," SAE Technical Paper 2011-01-0363, 2011, doi:10.4271/2011-01-0363.
32. Maxey, C., Kalaskar, V., Kang, D., and Boehman, A., "Impact of Supplemental CNG on Engine Efficiency, Performance, and Emissions," SAE Technical Paper 2013-01-0847, 2013, doi:10.4271/2013-01-0847.
33. Sun, L., liu, Y., Zhou, L., and Zeng, K., "Experimental Investigation of Cycle-by-Cycle Variations in a CNG/Diesel Dual Fuel Engine with EGR," SAE Technical Paper 2013-01-0853, 2013, doi:10.4271/2013-01-0853.
34. Aroonsrisopon, T., Salad, M., Wirojsakunchai, E., Wannatong, K. et al., “Injection Strategies for Operational Improvement of Diesel Dual Fuel Engines under Low Load Conditions,” SAE Technical Paper 2009-01-1855, 2009, doi:10.4271/2009-01-1855.
35. Kowalewicz A., and Woloszyn R., “Comparison of performance end emissions of turbocharged CI engine fuelled either with diesel fuel or CNG and diesel fuel,” Combustion Engines, PTNSS-2011-SC-117, 2011.
36. Papagiannakis, R., Hountalas, D., Rakopoulos, C., and Rakopoulos, D., “Experimental and Theoretical Analysis of the Combustion and Pollutants Formation Mechanisms in Dual Fuel DI Diesel Engines,” SAE Technical Paper 2005-01-1726, 2005, doi:10.4271/2005-01-1726.
37. Papagiannakis, R., Hountalas, D., and Kotsiopoulos, P., “Combustion and Performance Characteristics of a DI Diesel Engine Operating from Low to High Natural Gas Supplement Ratios at Various Operating Conditions,” SAE Technical Paper 2008-01-1392, 2008,
38. Rahimi, A., Fatehifar, E., and Khoshbakhti Saray, R., “Development of an optimized chemical kinetic mechanism for homogeneous charge compression ignition combustion of a fuel blend of n-heptane and natural gas using a genetic algorithm,” Proceedings of the Institution of Mechanical Engineers, Part D: Journal of Automobile Engineering 2010 224: 1141, doi: 10.1243/09544070JAUTO1343.
39. Gregory P. Smith, David M. Golden, Michael Frenklach, Nigel W. Moriarty, Boris Eiteneer, Mikhail Goldenberg, C. Thomas Bowman, Ronald K. Hanson, Soonho Song, William C. Gardiner, Jr., Vitali V. Lissianski, and Zhiwei Qin http://www.me.berkeley.edu/gri_mech/

40. Edman, J., 3D Modeling of Conventional and HCCI Diesel Combustion, Chalmers University of Technology, PhD dissertation (2005)
41. Joshi, S., Dahodwala, M., Koehler, E., Franke, M., "Engine Strategies to Meet Phase-2 Greenhouse Gas Emission Legislation for Heavy-Duty Diesel Engines," ICEF2017-3552.
42. https://www.fev-sts.com/what-we-do/products/calibration/calibration-platform-xcal.html
43. Federal Register / Vol. 81, No. 206 / Tuesday, October 25, 2016 / Rules and Regulations Greenhouse Gas Emissions and Fuel Efficiency Standards for Medium- and Heavy-Duty Engines and Vehicles— Phase 2
44. Memorandum in Response to Petition for Rulemaking to Adopt Ultra-Low NO_x Standards for On-Highway Heavy-Duty Trucks and Engines, EPA, December 2016

A Calculation for CNG Substitution and Brake Specific Cost

A.1 CNG Substitution Calculation

$$CNG\ SUB\ [\%] = \frac{\dot{m}_{cng} \times QLHV_{cng}}{\dot{m}_{cng} \times QLHV_{cng} + \dot{m}_{diesel} \times QLHV_{diesel}}$$

Where,

$\dot{m}_{cng}$ = Mass flow rate of CNG

$QLHV_{cng}$ = Lower heating value of CNG

$\dot{m}_{diesel}$ = Mass flow rate of diesel

A.2 Brake Specific Cost Calculation

Brake specific cost is a parameter that accounts for the amount of cost savings that one can get through CNG substitution. The average national cost of CNG (2.09$/GGE) and Diesel (3.84$/Gallon) in May 2013 were used for this calculation.

$$BSC\ \left[\frac{\$}{kWh}\right] = \frac{\dot{m}_{cng} \times C_{cng} + \dot{m}_{diesel} \times C_{diesel}}{P}$$

Where,

C_{cng} = Average National Cost of CNG in $/Kg (1 GGE CNG = 2.567 Kg CNG)

C_{diesel} = Average National Cost of Diesel in $/Kg (1 US Gallon Diesel = 3.149 Kg Diesel)

B Rahimi Mechanism

Reactions 1 to 325 (the GRI-Mech 3.0 mechanism) describe the NG oxidation reactions, and reactions 326 to 464 (the Valeri mechanism) describe the n-heptane oxidation reactions

The rate coefficients are expressed in the form

$$K = AT^{b}\exp(-\frac{E}{RT})$$

The units for the concentrations are moles per cubic centimeter and for the time are seconds.

The species considered are as follows:

C7H16, O2, N2, CO, CO2, H, H2, O, H2O, OH, HO2, H2O2, CH4, CH3, CH3O, CH2CO, CH2, CH2O, CH3O2, CH4O2, HCO, HCCO, C7H15-1, C7H15-2, C7H15O2, C7H14O2H, C7H14O2HO2, C7KET21, C6H12, C5H11CHO, C5H11CO, C5H11, C4H9, C4H, C4H2, C4H3, C3H7, C3H6, C3H5, C3H4, C3H3, C3H2, C2H, C2H2, C2H3, C2H4, C2H5, C2H6, N2O, NO, N, C3H8, CH2CHO, CH3CHO, CH3CO, CH2OH, C, CH, HCCOH, CH3OH, CH2(S), NH, NH2, NH3, NNH, NO2, HNO, CN, HCN, H2CN, HCNN, HCNO, HOCN, HNCO, NCO, and Ar.

#	REACTION	A	b	E (cal/mole)
1	2O+M<=>O2+M	1.20E+17	-1.03	0
2	O+H+M<=>OH+M	4.96E+17	-0.99	0
3	O+H2<=>H+OH	3.90E+04	2.7	6210
4	O+HO2<=>OH+O2	2.08E+13	0	0
5	O+H2O2<=>OH+HO2	9.21E+06	2.09	4080
6	O+CH<=>H+CO	5.73E+13	0	0
7	O+CH2<=>H+HCO	7.61E+13	0	0
8	O+CH2(S)<=>H2+CO	1.56E+13	0	0
9	O+CH2(S)<=>H+HCO	1.55E+13	0	0
10	O+CH3<=>H+CH2O	5.06E+13	0	0
11	O+CH4<=>OH+CH3	1.01E+09	1.53	8590
12	O+CO(+M)<=>CO2(+M)	1.83E+10	0	2430
13	O+HCO<=>OH+CO	2.95E+13	0	0
14	O+HCO<=>H+CO2	3.06E+13	0	0
15	O+CH2O<=>OH+HCO	3.92E+13	0	3610
16	O+CH2OH<=>OH+CH2O	9.64E+12	0	0
17	O+CH3O<=>OH+CH2O	9.67E+12	0	0
18	O+CH3OH<=>OH+CH2OH	3.81E+05	2.39	3190
19	O+CH3OH<=>OH+CH3O	1.32E+05	2.56	4810

20	O+C2H<=>CH+CO	5.01E+13	0	0
21	O+C2H2<=>H+HCCO	1.31E+07	2.04	1940
22	O+C2H2<=>OH+C2H	4.57E+19	-1.43	28700
23	O+C2H2<=>CO+CH2	6.60E+06	1.99	1970
24	O+C2H3<=>H+CH2CO	2.88E+13	0	0
25	O+C2H4<=>CH3+HCO	1.28E+07	1.88	229
26	O+C2H5<=>CH3+CH2O	2.25E+13	0	0
27	O+C2H6<=>OH+C2H5	9.21E+07	1.93	5470
28	O+HCCO<=>H+2CO	9.99E+13	0	0
29	O+CH2CO<=>OH+HCCO	9.52E+12	0	8080
30	O+CH2CO<=>CH2+CO2	1.82E+12	0	1320
31	O2+CO<=>O+CO2	2.46E+12	0	48400
32	O2+CH2O<=>HO2+HCO	9.51E+13	0	38500
33	H+O2+M<=>HO2+M	2.75E+18	-0.9	0
34	H+2O2<=>HO2+O2	1.98E+19	-1.26	0
35	H+O2+H2O<=>HO2+H2O	1.16E+19	-0.73	0
36	H+O2+N2<=>HO2+N2	2.70E+19	-1.22	0
37	H+O2+AR<=>HO2+AR	6.94E+17	-0.81	0
38	H+O2<=>O+OH	2.61E+16	-0.7	16400
39	2H+M<=>H2+M	1.01E+18	-10	0
40	2H+H2<=>2H2	9.24E+16	-0.6	0
41	2H+H2O<=>H2+H2O	5.81E+19	-1.26	0
42	2H+CO2<=>H2+CO2	5.54E+20	-1.95	0
43	H+OH+M<=>H2O+M	2.27E+22	-1.91	0
44	H+HO2<=>O+H2O	4.11E+12	0	680
45	H+HO2<=>O2+H2	4.28E+13	0	1050
46	H+HO2<=>2OH	8.08E+13	0	629
47	H+H2O2<=>HO2+H2	1.23E+07	1.96	5270
48	H+H2O2<=>OH+H2O	1.04E+13	0	3640
49	H+CH<=>C+H2	1.69E+14	0	0
50	H+CH2(+M)<=>CH3(+M)	6.00E+14	0	0
51	H+CH2(S)<=>CH+H2	3.06E+13	0	0
52	H+CH3(+M)<=>CH4(+M)	1.45E+16	-0.54	546
53	H+CH4<=>CH3+H2	6.63E+08	1.57	10300
54	H+HCO(+M)<=>CH2O(+M)	1.05E+12	0.47	-253
55	H+HCO<=>H2+CO	7.32E+13	0	0
56	H+CH2O(+M)<=>CH2OH(+M)	5.34E+11	0.46	3690
57	H+CH2O(+M)<=>CH3O(+M)	5.31E+11	0.44	2530
58	H+CH2O<=>HCO+H2	5.46E+07	1.97	2850
59	H+CH2OH(+M)<=>CH3OH(+M)	1.10E+12	0.5	85.4
60	H+CH2OH<=>H2+CH2O	2.01E+13	0	0
61	H+CH2OH<=>OH+CH3	1.62E+11	0.63	-284
62	H+CH2OH<=>CH2(S)+H2O	3.13E+13	-0.09	599
63	H+CH3O(+M)<=>CH3OH(+M)	2.49E+12	0.53	48.5
64	H+CH3O<=>H+CH2OH	4.33E+07	1.58	2000

65	H+CH3O<=>H2+CH2O	1.94E+13	0	0
66	H+CH3O<=>OH+CH3	1.54E+12	0.51	-106
67	H+CH3O<=>CH2(S)+H2O	2.69E+14	-0.22	1030
68	H+CH3OH<=>CH2OH+H2	1.65E+07	2.12	4900
69	H+CH3OH<=>CH3O+H2	4.01E+06	2.13	4770
70	H+C2H(+M)<=>C2H2(+M)	1.05E+17	-0.96	0
71	H+C2H2(+M)<=>C2H3(+M)	5.86E+12	0	2510
72	H+C2H3(+M)<=>C2H4(+M)	6.30E+12	0.26	284
73	H+C2H3<=>H2+C2H2	3.10E+13	0	0
74	H+C2H4(+M)<=>C2H5(+M)	5.66E+11	0.46	1810
75	H+C2H4<=>C2H3+H2	1.36E+06	2.57	12600
76	H+C2H5(+M)<=>C2H6(+M)	5.07E+17	-0.97	1500
77	H+C2H5<=>H2+C2H4	2.05E+12	0	0
78	H+C2H6<=>C2H5+H2	1.16E+08	1.9	7540
79	H+HCCO<=>CH2(S)+CO	1.00E+14	0	0
80	H+CH2CO<=>HCCO+H2	4.76E+13	0	7630
81	H+CH2CO<=>CH3+CO	1.14E+13	0	3400
82	H+HCCOH<=>H+CH2CO	1.04E+13	0	0
83	H2+CO(+M)<=>CH2O(+M)	4.17E+07	1.56	77700
84	OH+H2<=>H+H2O	2.10E+08	1.44	3490
85	2OH(+M)<=>H2O2(+M)	7.37E+13	-0.37	0
86	2OH<=>O+H2O	3.70E+04	2.4	-2140
87	OH+HO2<=>O2+H2O	1.42E+13	0	-501
88	OH+H2O2<=>HO2+H2O	2.09E+12	0	419
89	OH+H2O2<=>HO2+H2O	1.62E+18	0	29000
90	OH+C<=>H+CO	5.14E+13	0	0
91	OH+CH<=>H+HCO	3.13E+13	0	0
92	OH+CH2<=>H+CH2O	2.05E+13	0	0
93	OH+CH2<=>CH+H2O	1.07E+07	1.93	3000
94	OH+CH2(S)<=>H+CH2O	2.99E+13	0	0
95	OH+CH3(+M)<=>CH3OH(+M)	2.67E+18	-1.38	1340
96	OH+CH3<=>CH2+H2O	5.58E+07	1.64	5540
97	OH+CH3<=>CH2(S)+H2O	6.49E+17	-1.27	1380
98	OH+CH4<=>CH3+H2O	9.72E+07	1.53	3150
99	OH+CO<=>H+CO2	4.59E+07	1.28	66.8
100	OH+HCO<=>H2O+CO	4.80E+13	0	0
101	OH+CH2O<=>HCO+H2O	3.30E+09	1.17	-428
102	OH+CH2OH<=>H2O+CH2O	5.12E+12	0	0
103	OH+CH3O<=>H2O+CH2O	4.81E+12	0	0
104	OH+CH3OH<=>CH2OH+H2O	1.42E+06	2	-881
105	OH+CH3OH<=>CH3O+H2O	6.12E+06	1.97	1470
106	OH+C2H<=>H+HCCO	1.96E+13	0	0
107	OH+C2H2<=>H+CH2CO	2.24E-04	4.32	-1030
108	OH+C2H2<=>H+HCCOH	4.80E+05	2.23	13900
109	OH+C2H2<=>C2H+H2O	3.27E+07	2.07	13700

110	OH+C2H2<=>CH3+CO	4.60E-04	3.81	-2020
111	OH+C2H3<=>H2O+C2H2	5.15E+12	0	0
112	OH+C2H4<=>C2H3+H2O	3.74E+06	2.01	2600
113	OH+C2H6<=>C2H5+H2O	3.62E+06	2.21	868
114	OH+CH2CO<=>HCCO+H2O	7.19E+12	0	2020
115	2HO2<=>O2+H2O2	1.35E+11	0	-1660
116	2HO2<=>O2+H2O2	4.06E+14	0	11800
117	HO2+CH2<=>OH+CH2O	2.07E+13	0	0
118	HO2+CH3<=>O2+CH4	1.00E+12	0	0
119	HO2+CH3<=>OH+CH3O	3.82E+13	0	0
120	HO2+CO<=>OH+CO2	1.45E+14	0	24000
121	HO2+CH2O<=>HCO+H2O2	5.55E+06	2.02	12100
122	C+O2<=>O+CO	5.95E+13	0	562
123	C+CH2<=>H+C2H	4.80E+13	0	0
124	C+CH3<=>H+C2H2	5.11E+13	0	0
125	CH+O2<=>O+HCO	6.83E+13	0	0
126	CH+H2<=>H+CH2	1.13E+14	0	3230
127	CH+H2O<=>H+CH2O	5.73E+12	0	-771
128	CH+CH2<=>H+C2H2	4.14E+13	0	0
129	CH+CH3<=>H+C2H3	2.95E+13	0	0
130	CH+CH4<=>H+C2H4	5.80E+13	0	0
131	CH+CO(+M)<=>HCCO(+M)	5.13E+13	0	0
132	CH+CO2<=>HCO+CO	1.88E+14	0	15800
133	CH+CH2O<=>H+CH2CO	9.28E+13	0	-496
134	CH+HCCO<=>CO+C2H2	5.16E+13	0	0
135	CH2+O2<=>OH+H+CO	5.21E+12	0	1510
136	CH2+H2<=>H+CH3	4.96E+05	2.1	7010
137	2CH2<=>H2+C2H2	1.56E+15	0	11500
138	CH2+CH3<=>H+C2H4	4.01E+13	0	0
139	CH2+CH4<=>2CH3	2.52E+06	2.04	8030
140	CH2+CO(+M)<=>CH2CO(+M)	8.24E+11	0.48	4610
141	CH2+HCCO<=>C2H3+CO	2.99E+13	0	0
142	CH2(S)+N2<=>CH2+N2	1.46E+13	0	595
143	CH2(S)+AR<=>CH2+AR	9.08E+12	0	587
144	CH2(S)+O2<=>H+OH+CO	2.82E+13	0	0
145	CH2(S)+O2<=>CO+H2O	1.15E+13	0	0
146	CH2(S)+H2<=>CH3+H	7.00E+13	0	0
147	CH2(S)+H2O(+M)<=>CH3OH(+M)	4.87E+17	-1.21	1200
148	CH2(S)+H2O<=>CH2+H2O	3.07E+13	0	0
149	CH2(S)+CH3<=>H+C2H4	1.24E+13	0	-541
150	CH2(S)+CH4<=>2CH3	1.58E+13	0	-588
151	CH2(S)+CO<=>CH2+CO	9.07E+12	0	0
152	CH2(S)+CO2<=>CH2+CO2	6.74E+12	0	0
153	CH2(S)+CO2<=>CO+CH2O	1.43E+13	0	0
154	CH2(S)+C2H6<=>CH3+C2H5	3.86E+13	0	-543

155	CH3+O2<=>O+CH3O	3.56E+13	0	29500
156	CH3+O2<=>OH+CH2O	2.28E+12	0	21200
157	CH3+H2O2<=>HO2+CH4	2.43E+04	2.37	5380
158	2CH3(+M)<=>C2H6(+M)	6.97E+16	-1.13	685
159	2CH3<=>H+C2H5	7.03E+12	0.1	11100
160	CH3+HCO<=>CH4+CO	2.53E+13	0	0
161	CH3+CH2O<=>HCO+CH4	3.47E+03	2.82	5640
162	CH3+CH3OH<=>CH2OH+CH4	3.14E+07	1.51	9860
163	CH3+CH3OH<=>CH3O+CH4	1.04E+07	1.48	10300
164	CH3+C2H4<=>C2H3+CH4	2.28E+05	1.99	9410
165	CH3+C2H6<=>C2H5+CH4	6.14E+06	1.8	10100
166	HCO+H2O<=>H+CO+H2O	1.57E+18	-1.03	16200
167	HCO+M<=>H+CO+M	1.80E+17	-0.98	16600
168	HCO+O2<=>HO2+CO	1.36E+13	0	409
169	CH2OH+O2<=>HO2+CH2O	1.77E+13	0	923
170	CH3O+O2<=>HO2+CH2O	4.33E-13	7.67	-3570
171	C2H+O2<=>HCO+CO	1.04E+13	0	-782
172	C2H+H2<=>H+C2H2	5.47E+10	0.92	1920
173	C2H3+O2<=>HCO+CH2O	4.76E+16	-1.33	975
174	C2H4(+M)<=>H2+C2H2(+M)	7.78E+12	0.44	86400
175	C2H5+O2<=>HO2+C2H4	8.74E+11	0	3860
176	HCCO+O2<=>OH+2CO	3.21E+12	0	851
177	2HCCO<=>2CO+C2H2	9.72E+12	0	0
178	N+NO<=>N2+O	2.65E+13	0	351
179	N+O2<=>NO+O	8.79E+09	1.03	6630
180	N+OH<=>NO+H	3.47E+13	0	368
181	N2O+O<=>N2+O2	1.41E+12	0	10500
182	N2O+O<=>2NO	3.01E+13	0	22100
183	N2O+H<=>N2+OH	3.97E+14	0	19000
184	N2O+OH<=>N2+HO2	1.97E+12	0	22000
185	N2O(+M)<=>N2+O(+M)	7.75E+10	0	54500
186	HO2+NO<=>NO2+OH	2.13E+12	0	-469
187	NO+O+M<=>NO2+M	1.07E+20	-1.37	0
188	NO2+O<=>NO+O2	3.82E+12	0	-236
189	NO2+H<=>NO+OH	1.29E+14	0	358
190	NH+O<=>NO+H	4.19E+13	0	0
191	NH+H<=>N+H2	3.19E+13	0	339
192	NH+OH<=>HNO+H	2.08E+13	0	0
193	NH+OH<=>N+H2O	2.05E+09	1.25	0
194	NH+O2<=>HNO+O	4.62E+05	1.96	6420
195	NH+O2<=>NO+OH	1.26E+06	1.5	96.5
196	NH+N<=>N2+H	1.47E+13	0	0
197	NH+H2O<=>HNO+H2	1.99E+13	0	13800
198	NH+NO<=>N2+OH	2.20E+13	-0.23	0
199	NH+NO<=>N2O+H	3.54E+14	-0.45	0

200	NH2+O<=>OH+NH	3.11E+12	0	0
201	NH2+O<=>H+HNO	3.76E+13	0	0
202	NH2+H<=>NH+H2	3.98E+13	0	3760
203	NH2+OH<=>NH+H2O	9.18E+07	1.47	-453
204	NNH<=>N2+H	3.39E+08	0	0
205	NNH+M<=>N2+H+M	1.28E+14	-0.11	4950
206	NNH+O2<=>HO2+N2	4.85E+12	0	0
207	NNH+O<=>OH+N2	2.38E+13	0	0
208	NNH+O<=>NH+NO	7.32E+13	0	0
209	NNH+H<=>H2+N2	5.22E+13	0	0
210	NNH+OH<=>H2O+N2	1.97E+13	0	0
211	NNH+CH3<=>CH4+N2	2.47E+13	0	0
212	H+NO+M<=>HNO+M	4.26E+19	-1.34	742
213	HNO+O<=>NO+OH	2.55E+13	0	0
214	HNO+H<=>H2+NO	8.86E+11	0.72	632
215	HNO+OH<=>NO+H2O	1.31E+07	1.81	-936
216	HNO+O2<=>HO2+NO	9.60E+12	0	13300
217	CN+O<=>CO+N	7.95E+13	0	0
218	CN+OH<=>NCO+H	3.97E+13	0	0
219	CN+H2O<=>HCN+OH	8.40E+12	0	7710
220	CN+O2<=>NCO+O	6.14E+12	0	-419
221	CN+H2<=>HCN+H	2.87E+05	2.35	2260
222	NCO+O<=>NO+CO	2.41E+13	0	0
223	NCO+H<=>NH+CO	5.15E+13	0	0
224	NCO+OH<=>NO+H+CO	2.57E+12	0	0
225	NCO+N<=>N2+CO	2.05E+13	0	0
226	NCO+O2<=>NO+CO2	1.97E+12	0	19600
227	NCO+M<=>N+CO+M	3.01E+14	0	53400
228	NCO+NO<=>N2O+CO	1.85E+17	-1.54	771
229	NCO+NO<=>N2+CO2	3.98E+18	-2.07	807
230	HCN+M<=>H+CN+M	1.01E+29	-3.26	131000
231	HCN+O<=>NCO+H	2.08E+04	2.62	4780
232	HCN+O<=>NH+CO	5.23E+03	2.58	5170
233	HCN+O<=>CN+OH	3.78E+09	1.54	25500
234	HCN+OH<=>HOCN+H	1.10E+06	2.06	13700
235	HCN+OH<=>HNCO+H	4.33E+03	2.28	6480
236	HCN+OH<=>NH2+CO	1.63E+02	2.64	8710
237	H+HCN(+M)<=>H2CN(+M)	3.37E+13	0	0
238	H2CN+N<=>N2+CH2	6.07E+13	0	400
239	C+N2<=>CN+N	6.45E+13	0	45200
240	CH+N2<=>HCN+N	3.03E+09	0.92	19400
241	CH+N2(+M)<=>HCNN(+M)	3.11E+12	0.14	0
242	CH2+N2<=>HCN+NH	1.00E+13	0	77400
243	CH2(S)+N2<=>NH+HCN	9.78E+10	0	68000
244	C+NO<=>CN+O	1.95E+13	0	0

245	C+NO<=>CO+N	3.01E+13	0	0
246	CH+NO<=>HCN+O	4.00E+13	0	0
247	CH+NO<=>H+NCO	1.59E+13	0	0
248	CH+NO<=>N+HCO	2.53E+13	0	0
249	CH2+NO<=>H+HNCO	3.22E+17	-1.37	1320
250	CH2+NO<=>OH+HCN	2.87E+14	-0.67	751
251	CH2+NO<=>H+HCNO	3.62E+13	-0.38	566
252	CH2(S)+NO<=>H+HNCO	3.18E+17	-1.36	1300
253	CH2(S)+NO<=>OH+HCN	2.94E+14	-0.68	772
254	CH2(S)+NO<=>H+HCNO	3.71E+13	-0.35	597
255	CH3+NO<=>HCN+H2O	9.73E+13	0	29800
256	CH3+NO<=>H2CN+OH	1.05E+12	0	22000
257	HCNN+O<=>CO+H+N2	2.30E+13	0	0
258	HCNN+O<=>HCN+NO	2.01E+12	0	0
259	HCNN+O2<=>O+HCO+N2	1.19E+13	0	0
260	HCNN+OH<=>H+HCO+N2	1.22E+13	0	0
261	HCNN+H<=>CH2+N2	1.03E+14	0	0
262	HNCO+O<=>NH+CO2	9.65E+07	1.44	8480
263	HNCO+O<=>HNO+CO	1.43E+08	1.6	44000
264	HNCO+O<=>NCO+OH	2.16E+06	2.19	11100
265	HNCO+H<=>NH2+CO	2.24E+07	1.72	3930
266	HNCO+H<=>H2+NCO	1.05E+05	2.51	13200
267	HNCO+OH<=>NCO+H2O	3.19E+07	1.43	3710
268	HNCO+OH<=>NH2+CO2	3.41E+06	1.47	3710
269	HNCO+M<=>NH+CO+M	1.16E+16	0	83800
270	HCNO+H<=>H+HNCO	2.20E+15	-0.71	2860
271	HCNO+H<=>OH+HCN	2.66E+11	0.18	2050
272	HCNO+H<=>NH2+CO	1.75E+14	-0.72	3000
273	HOCN+H<=>H+HNCO	1.98E+07	1.98	2100
274	HCCO+NO<=>HCNO+CO	8.69E+12	0	0
275	CH3+N<=>H2CN+H	5.93E+14	-0.3	279
276	CH3+N<=>HCN+H2	3.62E+12	0.16	-86.4
277	NH3+H<=>NH2+H2	5.19E+05	2.51	10000
278	NH3+OH<=>NH2+H2O	5.03E+07	1.59	912
279	NH3+O<=>NH2+OH	9.38E+06	1.95	6620
280	NH+CO2<=>HNO+CO	9.66E+12	0	13900
281	CN+NO2<=>NCO+NO	6.29E+15	-0.77	342
282	NCO+NO2<=>N2O+CO2	3.37E+12	0	-682
283	N+CO2<=>NO+CO	3.01E+12	0	11300
284	O+CH3<=>H+H2+CO	3.47E+13	0	0
285	O+C2H4<=>H+CH2CHO	6.95E+06	1.8	225
286	O+C2H5<=>H+CH3CHO	1.05E+14	0	0
287	OH+HO2<=>O2+H2O	5.15E+15	0	17100
288	OH+CH3<=>H2+CH2O	8.08E+09	0.49	-1750
289	CH+H2(+M)<=>CH3(+M)	1.99E+12	0.43	2375

290	CH2+O2<=>2H+CO2	5.96E+12	0	1530
291	CH2+O2<=>O+CH2O	2.40E+12	0	1490
292	CH2+CH2<=>2H+C2H2	1.98E+14	0	10700
293	CH2(S)+H2O<=>H2+CH2O	6.85E+10	0.24	-937
294	C2H3+O2<=>O+CH2CHO	3.11E+11	0.3	10.5
295	C2H3+O2<=>HO2+C2H2	1.29E+06	1.68	-392
296	O+CH3CHO<=>OH+CH2CHO	2.95E+12	0	1880
297	O+CH3CHO<=>OH+CH3+CO	2.91E+12	0	1850
298	O2+CH3CHO<=>HO2+CH3+CO	3.15E+13	0	38700
299	H+CH3CHO<=>CH2CHO+H2	2.07E+09	1.17	2380
300	H+CH3CHO<=>CH3+H2+CO	2.07E+09	1.19	2510
301	OH+CH3CHO<=>CH3+H2O+CO	2.33E+10	0.74	-1150
302	HO2+CH3CHO<=>CH3+H2O2+CO	3.08E+12	0	11500
303	CH3+CH3CHO<=>CH3+CH4+CO	2.74E+06	1.79	6000
304	H+CH2CO(+M)<=>CH2CHO(+M)	4.73E+11	0.44	-1800
305	O+CH2CHO<=>H+CH2+CO2	1.52E+14	0	0
306	O2+CH2CHO<=>OH+CO+CH2O	1.86E+10	0	0
307	O2+CH2CHO<=>OH+2HCO	2.34E+10	0	0
308	H+CH2CHO<=>CH3+HCO	2.25E+13	0	0
309	H+CH2CHO<=>CH2CO+H2	1.09E+13	0	0
310	OH+CH2CHO<=>H2O+CH2CO	1.25E+13	0	0
311	OH+CH2CHO<=>HCO+CH2OH	2.99E+13	0	0
312	CH3+C2H5(+M)<=>C3H8(+M)	9.24E+12	0	0
313	O+C3H8<=>OH+C3H7	2.03E+05	2.71	3820
314	H+C3H8<=>C3H7+H2	1.36E+06	2.59	6800
315	OH+C3H8<=>C3H7+H2O	3.10E+07	1.79	945
316	C3H7+H2O2<=>HO2+C3H8	3.60E+02	2.7	1480
317	CH3+C3H8<=>C3H7+CH4	8.67E-01	3.7	7090
318	CH3+C2H4(+M)<=>C3H7(+M)	2.45E+06	1.65	5740
319	O+C3H7<=>C2H5+CH2O	1.01E+14	0	0
320	H+C3H7(+M)<=>C3H8(+M)	3.48E+13	0	0
321	H+C3H7<=>CH3+C2H5	4.13E+06	2.18	853
322	OH+C3H7<=>C2H5+CH2OH	2.44E+13	0	0
323	HO2+C3H7<=>O2+C3H8	2.59E+10	0.27	-899
324	HO2+C3H7<=>OH+C2H5+CH2O	2.29E+13	0	0
325	CH3+C3H7<=>2C2H5	2.02E+13	-0.29	0
326	C7H16+O2<=>C7H15-1+HO2	2.58E+13	0	45800
327	C7H16+O2<=>C7H15-2+HO2	2.69E+14	0	48600
328	C7H16+H<=>C7H15-1+H2	5.64E+07	1.95	7770
329	C7H16+H<=>C7H15-2+H2	4.78E+07	1.9	4610
330	C7H16+OH<=>C7H15-1+H2O	8.91E+09	1.11	1820
331	C7H16+OH<=>C7H15-2+H2O	4.95E+09	1.19	629
332	C7H16+HO2<=>C7H15-1+H2O2	7.50E+12	0	17500
333	C7H16+HO2<=>C7H15-2+H2O2	9.10E+12	0	18600
334	C7H16+CH3<=>C7H15-1+CH4	1.20E+12	0	12700

335	C7H16+CH3<=>C7H15-2+CH4	7.89E+11	0	9310
336	C7H16<=>C7H15-1+H	4.32E+19	-0.97	95300
337	C7H16<=>C7H15-2+H	1.20E+21	-1.45	107000
338	C7H16<=>C4H9+C3H7	2.15E+16	0	76200
339	C7H15-1+O2<=>C7H15O2	1.83E+12	0	0
340	C7H15-2+O2<=>C7H15O2	1.95E+12	0	0
341	C7H15O2<=>C7H14O2H	6.32E+11	0	19000
342	C7H14O2H+O2<=>C7H14O2HO2	2.56E+11	0	0
343	C7H14O2HO2<=>C7KET21+OH	3.11E+13	0	27600
344	C7KET21<=>C5H11CO+CH2O+OH	1.10E+16	0	40100
345	C5H11CHO+O2<=>C5H11CO+HO2	2.13E+13	0.53	38100
346	C5H11CHO+OH<=>C5H11CO+H2O	9.71E+12	0	0
347	C5H11CHO+H<=>C5H11CO+H2	4.25E+13	0	4270
348	C5H11CHO+O<=>C5H11CO+OH	4.81E+12	0	1900
349	C5H11CHO+HO2<=>C5H11CO+H2O2	2.94E+12	0	13900
350	C5H11CHO+CH3<=>C5H11CO+CH4	1.57E+12	0	9250
351	C5H11CHO+CH3O2<=>C5H11CO+CH3O2H	1.03E+12	0	8550
352	C5H11CO<=>C5H11+CO	9.66E+10	0	8710
353	C5H11<=>C2H5+C3H6	3.22E+13	0	28300
354	C7H15-1<=>C2H4+C5H11	2.52E+13	0	30600
355	C7H15-2<=>CH3+C6H12	2.73E+13	0	27700
356	C6H12<=>C3H7+C3H5	9.62E+15	0	63400
357	C7H15-2<=>C4H9+C3H6	1.27E+13	0	30900
358	C7H15-1<=>C7H15-2	1.95E+11	0	19800
359	C4H9<=>C3H6+CH3	2.41E+17	-1.33	32800
360	C4H9<=>C2H5+C2H4	2.61E+13	0	29700
361	C3H7<=>C2H4+CH3	9.03E+13	0	31500
362	C3H7<=>C3H6+H	1.32E+14	0	34400
363	C3H7+O2<=>C3H6+HO2	1.01E+12	0	4920
364	C3H6<=>C2H3+CH3	6.04E+15	0	78400
365	C3H6+H<=>C3H5+H2	5.49E+12	0	1580
366	C3H6+CH3<=>C3H5+CH4	8.37E+12	0	8230
367	C3H6+O2<=>C3H5+HO2	4.07E+12	0	40400
368	C3H6+OH<=>CH3CHO+CH3	3.34E+11	0	0
369	C3H5<=>C3H4+H	4.32E+13	0	68900
370	C3H5+H<=>C3H4+H2	9.90E+12	0	0
371	C3H5+O2<=>C3H4+HO2	5.57E+11	0	10700
372	C3H4+OH<=>C2H3+CH2O	9.85E+11	0	0
373	C3H4+OH<=>C2H4+HCO	1.01E+12	0	0
374	C3H4+O2<=>C3H3+HO2	3.64E+13	0	36600
375	C2H4+HO2<=>CH3CHO+OH	2.23E+13	0	18900
376	C2H4+CH3O<=>CH3CHO+CH3	3.30E+13	0	15800
377	C2H4+CH3O2<=>CH3CHO+CH3O	7.47E+13	0	14100
378	CH3CHO<=>CH3+HCO	6.48E+15	0	86500
379	CH3CO+M<=>CH3+CO+M	1.94E+16	0	14900

380	CH3CHO+O2<=>CH3CO+HO2	1.95E+13	0.55	42600
381	CH3CHO+H<=>CH3CO+H2	4.43E+13	0	4580
382	CH3CHO+OH<=>CH3CO+H2O	9.76E+12	0	0
383	CH3CHO+O<=>CH3CO+OH	6.30E+12	0	1710
384	CH3CHO+CH3<=>CH3CO+CH4	1.58E+12	0	7700
385	CH3CHO+CH2<=>CH3CO+CH3	1.63E+12	0	3380
386	CH3CHO+HO2<=>CH3CO+H2O2	1.77E+12	0	11700
387	CH3CHO+CH3O2<=>CH3CO+CH3O2H	1.26E+11	0	10000
388	CH3CO+O<=>CH3+CO2	1.09E+13	0	0
389	CH3CO+H<=>CH3+HCO	1.04E+14	0	0
390	CH3CO+OH<=>CH3+CO+OH	3.11E+13	0	0
391	CH3CO+HO2<=>CH3+CO2+OH	2.90E+13	0	0
392	CH3CO+CH3<=>C2H6+CO	4.73E+13	0	0
393	CH3O+CO<=>CH3+CO2	1.59E+14	0	12000
394	CH3+O2<=>CH3O2	3.05E+59	-16.44	17300
395	CH3O2+HO2<=>CH3O2H+O2	4.70E+11	0	-2590
396	CH3O2+CH4<=>CH3O2H+CH3	1.93E+11	0	20300
397	CH3O2+CH3<=>CH3O+CH3O	2.51E+13	0	0
398	CH3O2+O<=>CH3O+O2	3.82E+13	0	0
399	CH3O2+H<=>CH3O+OH	9.37E+13	0	0
400	CH3O2+CH2O<=>CH3O2H+HCO	9.74E+11	0	12800
401	CH3O2+C2H6<=>CH3O2H+C2H5	3.18E+11	0	14300
402	CH3O2+CH3O2<=>CH3O+CH3O+O2	2.57E+11	0	-794
403	CH3O2+H2O2<=>CH3O2H+HO2	2.30E+12	0	9130
404	CH3O2H<=>CH3O+OH	3.15E+16	0	46000
405	CH3O2+C2H4<=>C2H3+CH3O2H	7.37E+11	0	16200
406	CH3O2H+OH<=>CH3O2+H2O	9.56E+12	0	-248
407	CH3O2H+O<=>CH3O2+OH	2.06E+13	0	4890
408	H2+O2<=>OH+OH	1.59E+13	0	43000
409	O+OH+M<=>HO2+M	1.01E+16	0	0
410	H2O2+O<=>H2O+O2	8.21E+11	0	4180
411	HO2+H2<=>H2O+OH	5.89E+11	0	20300
412	HCO+HCO<=>CH2O+CO	3.08E+13	0	0
413	HCO+HO2<=>CO2+OH+H	2.98E+13	0	0
414	CH3+H<=>CH4	1.95E+36	-6.61	9870
415	CH3+CH3O<=>CH4+CH2O	3.27E+14	0	0
416	CH2+O2<=>HCO+OH	4.12E+10	0	-549
417	CH2+O2<=>CO2+H2	6.83E+11	0	549
418	CH2+O2<=>CO+H2O	2.18E+10	0	-906
419	CH2+CO2<=>CH2O+CO	9.55E+10	0	933
420	CH3+HCO<=>CH2O+CH2	3.09E+13	0	0
421	CH3+CH3<=>C2H4+H2	1.00E+15	0	29600
422	C2H4+O<=>CH2O+CH2	2.82E+04	1.97	191
423	C2H4+O<=>C2H3+OH	1.51E+07	1.95	3880
424	C2H4+OH<=>CH2O+CH3	6.51E+13	0	110

425	C2H4+HO2<=>C2H3+H2O2	7.39E+11	0	16000
426	C2H4+H<=>C2H5	2.77E+43	-8.85	54000
427	C2H6+O2<=>C2H5+HO2	1.01E+13	0	48300
428	C2H4+O2<=>C2H3+HO2	3.92E+14	0	62800
429	C2H4+C2H4<=>C2H5+C2H3	5.14E+14	0	58900
430	C2H5+HO2<=>C2H4+H2O2	2.94E+11	0	0
431	C2H2+O2<=>HCO+HCO	3.71E+12	0	28900
432	C2H3+CH2<=>C2H2+CH3	2.85E+13	0	0
433	C2H3+HCO<=>C2H4+CO	6.01E+13	0	0
434	C2H3+C2H3<=>C2H2+C2H4	1.46E+13	0	0
435	C2H3+O<=>C2H2+OH	1.06E+13	0	0
436	C2H2+CH2<=>H+C3H3	1.22E+13	0	6390
437	C3H3+OH<=>C3H2+H2O	9.42E+12	0	0
438	C3H3+O<=>CH2O+C2H	9.26E+12	0	0
439	C2H3<=>C2H2+H	4.87E+40	-8.75	48000
440	C2H2<=>C2H+H	2.25E+32	-5.67	123000
441	C2H2+C2H<=>C4H2+H	1.00E+14	0	0
442	C3H4+O<=>C2H3+HCO	3.08E+12	0	2020
443	C3H4+O<=>C2H4+CO	3.25E+12	0	2120
444	C3H4+O<=>HCCO+CH3	5.97E+12	0	2090
445	C4H+H2<=>H+C4H2	4.76E+05	2.44	552
446	C4H2+OH<=>C4H+H2O	3.58E+07	1.99	15400
447	C4H2+O<=>C3H2+CO	2.62E+13	0	1620
448	C3H2+O<=>C2H2+CO	6.56E+13	0	0
449	C3H2+OH<=>HCO+C2H2	6.75E+13	0	0
450	C2H2+C2H<=>N-C4H3	4.71E+37	-7.21	7250
451	C3H2+CH2<=>N-C4H3+H	5.13E+13	0	0
452	C4H2+H<=>N-C4H3	1.14E+42	-8.44	16000
453	N-C4H3+H<=>C2H2+C2H2	5.89E+25	-3.55	9800
454	N-C4H3+H<=>C4H2+H2	1.45E+13	0	0
455	N-C4H3+OH<=>C4H2+H2O	2.35E+12	0	0
456	C2H2+HCCO<=>C3H3+CO	1.09E+11	0	3090
457	C3H2+O2<=>HCCO+CO+H	4.59E+13	0	0
458	C3H3+O2<=>CH2CO+HCO	2.78E+10	0	3130
459	N-C4H3+O2<=>HCCO+CH2CO	8.14E+16	-1.67	0
460	C3H8+C2H5<=>C3H7+C2H6	8.81E-01	3.36	8580
461	C3H8+C2H3<=>C3H7+C2H4	6.54E+02	3.51	10700
462	C3H7+CH3<=>CH4+C3H6	1.11E+13	0	0
463	C3H6+C2H5<=>C3H5+C2H6	2.01E+00	3.54	7100
464	C3H6+O<=>CH3+CH3CO	7.27E+04	2.42	-1190

C Combined Reaction Mechanism

Reactions 1 to 325 (the GRI-Mech 3.0 mechanism) describe the NG oxidation reactions, and reactions 326 to 424 (the Chalmers mechanism) describe the n-heptane oxidation reactions

The rate coefficients are expressed in the form

$$K = AT^{b}\exp(-\frac{E}{RT})$$

The species considered are as follows:

H2, H, O, O2, OH, H2O, HO2, H2O2, C, CH, CH2, CH2(S), CH3, CH4, CO, CO2, HCO, CH2O, CH2OH, CH3O, CH3OH, C2H, C2H2, C2H3, C2H4, C2H5, C2H6, HCCO, CH2CO, HCCOH, N, NH, NH2, NH3, NNH, NO, NO2, N2O, HNO, CN, HCN, H2CN, HCNN, HCNO, HOCN, HNCO, NCO, N2, Ar, C3H7, C3H8, CH2CHO, CH3CHO, CH3O2, CH4O2, C3H2, C3H6, C4H, C4H2, N-C4H3, C3H3, C3H4, C3H5, C5H11CO, C4H9, C5H11, C6H12, C7H15-1, C7H15-2, C7H16, C7KET12, C5H11CHO, C7H15O2, C7H14O2H, C7H14O2HO2, CH3CO

#	REACTION	A	b	E (Cal/mole)
1	2O+M<=>O2+M	1.20E+17	-1	0
2	O+H+M<=>OH+M	5.00E+17	-1	0
3	O+H2<=>H+OH	3.87E+04	2.7	6260
4	O+HO2<=>OH+O2	2.00E+13	0	0
5	O+H2O2<=>OH+HO2	9.63E+06	2	4000
6	O+CH<=>H+CO	5.70E+13	0	0
7	O+CH2<=>H+HCO	8.00E+13	0	0
8	O+CH2(S)<=>H2+CO	1.50E+13	0	0
9	O+CH2(S)<=>H+HCO	1.50E+13	0	0
10	O+CH3<=>H+CH2O	5.06E+13	0	0
11	O+CH4<=>OH+CH3	1.02E+09	1.5	8600
12	O+CO(+M)<=>CO2(+M)	1.80E+10	0	2385
13	O+HCO<=>OH+CO	3.00E+13	0	0
14	O+HCO<=>H+CO2	3.00E+13	0	0
15	O+CH2O<=>OH+HCO	3.90E+13	0	3540
16	O+CH2OH<=>OH+CH2O	1.00E+13	0	0
17	O+CH3O<=>OH+CH2O	1.00E+13	0	0
18	O+CH3OH<=>OH+CH2OH	3.88E+05	2.5	3100
19	O+CH3OH<=>OH+CH3O	1.30E+05	2.5	5000
20	O+C2H<=>CH+CO	5.00E+13	0	0
21	O+C2H2<=>H+HCCO	1.35E+07	2	1900
22	O+C2H2<=>OH+C2H	4.60E+19	-1.41	28950

23	O+C2H2<=>CO+CH2	6.94E+06	2	1900
24	O+C2H3<=>H+CH2CO	3.00E+13	0	0
25	O+C2H4<=>CH3+HCO	1.25E+07	1.83	220
26	O+C2H5<=>CH3+CH2O	2.24E+13	0	0
27	O+C2H6<=>OH+C2H5	8.98E+07	1.92	5690
28	O+HCCO<=>H+2CO	1.00E+14	0	0
29	O+CH2CO<=>OH+HCCO	1.00E+13	0	8000
30	O+CH2CO<=>CH2+CO2	1.75E+12	0	1350
31	O2+CO<=>O+CO2	2.50E+12	0	47800
32	O2+CH2O<=>HO2+HCO	1.00E+14	0	40000
33	H+O2+M<=>HO2+M	2.80E+18	-0.86	0
34	H+2O2<=>HO2+O2	2.08E+19	-1.24	0
35	H+O2+H2O<=>HO2+H2O	1.13E+19	-0.76	0
36	H+O2+N2<=>HO2+N2	2.60E+19	-1.24	0
37	H+O2+AR<=>HO2+AR	7.00E+17	-0.8	0
38	H+O2<=>O+OH	2.65E+16	-0.67	17041
39	2H+M<=>H2+M	1.00E+18	-1	0
40	2H+H2<=>2H2	9.00E+16	-0.6	0
41	2H+H2O<=>H2+H2O	6.00E+19	-1.25	0
42	2H+CO2<=>H2+CO2	5.50E+20	-2	0
43	H+OH+M<=>H2O+M	2.20E+22	-2	0
44	H+HO2<=>O+H2O	3.97E+12	0	671
45	H+HO2<=>O2+H2	4.48E+13	0	1068
46	H+HO2<=>2OH	8.40E+13	0	635
47	H+H2O2<=>HO2+H2	1.21E+07	2	5200
48	H+H2O2<=>OH+H2O	1.00E+13	0	3600
49	H+CH<=>C+H2	1.65E+14	0	0
50	H+CH2(+M)<=>CH3(+M)	6.00E+14	0	0
51	H+CH2(S)<=>CH+H2	3.00E+13	0	0
52	H+CH3(+M)<=>CH4(+M)	1.39E+16	-0.53	536
53	H+CH4<=>CH3+H2	6.60E+08	1.62	10840
54	H+HCO(+M)<=>CH2O(+M)	1.09E+12	0.48	-260
55	H+HCO<=>H2+CO	7.34E+13	0	0
56	H+CH2O(+M)<=>CH2OH(+M)	5.40E+11	0.45	3600
57	H+CH2O(+M)<=>CH3O(+M)	5.40E+11	0.45	2600
58	H+CH2O<=>HCO+H2	5.74E+07	1.9	2742
59	H+CH2OH(+M)<=>CH3OH(+M)	1.06E+12	0.5	86
60	H+CH2OH<=>H2+CH2O	2.00E+13	0	0
61	H+CH2OH<=>OH+CH3	1.65E+11	0.65	-284
62	H+CH2OH<=>CH2(S)+H2O	3.28E+13	-0.09	610
63	H+CH3O(+M)<=>CH3OH(+M)	2.43E+12	0.52	50
64	H+CH3O<=>H+CH2OH	4.15E+07	1.63	1924
65	H+CH3O<=>H2+CH2O	2.00E+13	0	0
66	H+CH3O<=>OH+CH3	1.50E+12	0.5	-110
67	H+CH3O<=>CH2(S)+H2O	2.62E+14	-0.23	1070

68	H+CH3OH<=>CH2OH+H2	1.70E+07	2.1	4870
69	H+CH3OH<=>CH3O+H2	4.20E+06	2.1	4870
70	H+C2H(+M)<=>C2H2(+M)	1.00E+17	-1	0
71	H+C2H2(+M)<=>C2H3(+M)	5.60E+12	0	2400
72	H+C2H3(+M)<=>C2H4(+M)	6.08E+12	0.27	280
73	H+C2H3<=>H2+C2H2	3.00E+13	0	0
74	H+C2H4(+M)<=>C2H5(+M)	5.40E+11	0.45	1820
75	H+C2H4<=>C2H3+H2	1.32E+06	2.53	12240
76	H+C2H5(+M)<=>C2H6(+M)	5.21E+17	-0.99	1580
77	H+C2H5<=>H2+C2H4	2.00E+12	0	0
78	H+C2H6<=>C2H5+H2	1.15E+08	1.9	7530
79	H+HCCO<=>CH2(S)+CO	1.00E+14	0	0
80	H+CH2CO<=>HCCO+H2	5.00E+13	0	8000
81	H+CH2CO<=>CH3+CO	1.13E+13	0	3428
82	H+HCCOH<=>H+CH2CO	1.00E+13	0	0
83	H2+CO(+M)<=>CH2O(+M)	4.30E+07	1.5	79600
84	OH+H2<=>H+H2O	2.16E+08	1.51	3430
85	2OH(+M)<=>H2O2(+M)	7.40E+13	-0.37	0
86	2OH<=>O+H2O	3.57E+04	2.4	-2110
87	OH+HO2<=>O2+H2O	1.45E+13	0	-500
89	OH+H2O2<=>HO2+H2O	1.70E+18	0	29410
90	OH+C<=>H+CO	5.00E+13	0	0
91	OH+CH<=>H+HCO	3.00E+13	0	0
92	OH+CH2<=>H+CH2O	2.00E+13	0	0
93	OH+CH2<=>CH+H2O	1.13E+07	2	3000
94	OH+CH2(S)<=>H+CH2O	3.00E+13	0	0
95	OH+CH3(+M)<=>CH3OH(+M)	2.79E+18	-1.43	1330
96	OH+CH3<=>CH2+H2O	5.60E+07	1.6	5420
97	OH+CH3<=>CH2(S)+H2O	6.44E+17	-1.34	1417
98	OH+CH4<=>CH3+H2O	1.00E+08	1.6	3120
99	OH+CO<=>H+CO2	4.76E+07	1.23	70
100	OH+HCO<=>H2O+CO	5.00E+13	0	0
101	OH+CH2O<=>HCO+H2O	3.43E+09	1.18	-447
102	OH+CH2OH<=>H2O+CH2O	5.00E+12	0	0
103	OH+CH3O<=>H2O+CH2O	5.00E+12	0	0
104	OH+CH3OH<=>CH2OH+H2O	1.44E+06	2	-840
105	OH+CH3OH<=>CH3O+H2O	6.30E+06	2	1500
106	OH+C2H<=>H+HCCO	2.00E+13	0	0
107	OH+C2H2<=>H+CH2CO	2.18E-04	4.5	-1000
108	OH+C2H2<=>H+HCCOH	5.04E+05	2.3	13500
109	OH+C2H2<=>C2H+H2O	3.37E+07	2	14000
110	OH+C2H2<=>CH3+CO	4.83E-04	4	-2000
111	OH+C2H3<=>H2O+C2H2	5.00E+12	0	0
112	OH+C2H4<=>C2H3+H2O	3.60E+06	2	2500
113	OH+C2H6<=>C2H5+H2O	3.54E+06	2.12	870

114	OH+CH2CO<=>HCCO+H2O	7.50E+12	0	2000
116	2HO2<=>O2+H2O2	4.20E+14	0	12000
117	HO2+CH2<=>OH+CH2O	2.00E+13	0	0
118	HO2+CH3<=>O2+CH4	1.00E+12	0	0
119	HO2+CH3<=>OH+CH3O	3.78E+13	0	0
120	HO2+CO<=>OH+CO2	1.50E+14	0	23600
121	HO2+CH2O<=>HCO+H2O2	5.60E+06	2	12000
122	C+O2<=>O+CO	5.80E+13	0	576
123	C+CH2<=>H+C2H	5.00E+13	0	0
124	C+CH3<=>H+C2H2	5.00E+13	0	0
125	CH+O2<=>O+HCO	6.71E+13	0	0
126	CH+H2<=>H+CH2	1.08E+14	0	3110
127	CH+H2O<=>H+CH2O	5.71E+12	0	-755
128	CH+CH2<=>H+C2H2	4.00E+13	0	0
129	CH+CH3<=>H+C2H3	3.00E+13	0	0
130	CH+CH4<=>H+C2H4	6.00E+13	0	0
131	CH+CO(+M)<=>HCCO(+M)	5.00E+13	0	0
132	CH+CO2<=>HCO+CO	1.90E+14	0	15792
133	CH+CH2O<=>H+CH2CO	9.46E+13	0	-515
134	CH+HCCO<=>CO+C2H2	5.00E+13	0	0
135	CH2+O2<=>OH+H+CO	5.00E+12	0	1500
136	CH2+H2<=>H+CH3	5.00E+05	2	7230
137	2CH2<=>H2+C2H2	1.60E+15	0	11944
138	CH2+CH3<=>H+C2H4	4.00E+13	0	0
139	CH2+CH4<=>2CH3	2.46E+06	2	8270
140	CH2+CO(+M)<=>CH2CO(+M)	8.10E+11	0.5	4510
141	CH2+HCCO<=>C2H3+CO	3.00E+13	0	0
142	CH2(S)+N2<=>CH2+N2	1.50E+13	0	600
143	CH2(S)+AR<=>CH2+AR	9.00E+12	0	600
144	CH2(S)+O2<=>H+OH+CO	2.80E+13	0	0
145	CH2(S)+O2<=>CO+H2O	1.20E+13	0	0
146	CH2(S)+H2<=>CH3+H	7.00E+13	0	0
147	CH2(S)+H2O(+M)<=>CH3OH(+M)	4.82E+17	-1.16	1145
148	CH2(S)+H2O<=>CH2+H2O	3.00E+13	0	0
149	CH2(S)+CH3<=>H+C2H4	1.20E+13	0	-570
150	CH2(S)+CH4<=>2CH3	1.60E+13	0	-570
151	CH2(S)+CO<=>CH2+CO	9.00E+12	0	0
152	CH2(S)+CO2<=>CH2+CO2	7.00E+12	0	0
153	CH2(S)+CO2<=>CO+CH2O	1.40E+13	0	0
154	CH2(S)+C2H6<=>CH3+C2H5	4.00E+13	0	-550
155	CH3+O2<=>O+CH3O	3.56E+13	0	30480
156	CH3+O2<=>OH+CH2O	2.31E+12	0	20315
157	CH3+H2O2<=>HO2+CH4	2.45E+04	2.47	5180
158	2CH3(+M)<=>C2H6(+M)	6.77E+16	-1.18	654
159	2CH3<=>H+C2H5	6.84E+12	0.1	10600

160	CH3+HCO<=>CH4+CO	2.65E+13	0	0
161	CH3+CH2O<=>HCO+CH4	3.32E+03	2.81	5860
162	CH3+CH3OH<=>CH2OH+CH4	3.00E+07	1.5	9940
163	CH3+CH3OH<=>CH3O+CH4	1.00E+07	1.5	9940
164	CH3+C2H4<=>C2H3+CH4	2.27E+05	2	9200
165	CH3+C2H6<=>C2H5+CH4	6.14E+06	1.74	10450
166	HCO+H2O<=>H+CO+H2O	1.50E+18	-1	17000
167	HCO+M<=>H+CO+M	1.87E+17	-1	17000
168	HCO+O2<=>HO2+CO	1.34E+13	0	400
169	CH2OH+O2<=>HO2+CH2O	1.80E+13	0	900
170	CH3O+O2<=>HO2+CH2O	4.28E-13	7.6	-3530
171	C2H+O2<=>HCO+CO	1.00E+13	0	-755
172	C2H+H2<=>H+C2H2	5.68E+10	0.9	1993
173	C2H3+O2<=>HCO+CH2O	4.58E+16	-1.39	1015
174	C2H4(+M)<=>H2+C2H2(+M)	8.00E+12	0.44	86770
175	C2H5+O2<=>HO2+C2H4	8.40E+11	0	3875
176	HCCO+O2<=>OH+2CO	3.20E+12	0	854
177	2HCCO<=>2CO+C2H2	1.00E+13	0	0
178	N+NO<=>N2+O	2.70E+13	0	355
179	N+O2<=>NO+O	9.00E+09	1	6500
180	N+OH<=>NO+H	3.36E+13	0	385
181	N2O+O<=>N2+O2	1.40E+12	0	10810
182	N2O+O<=>2NO	2.90E+13	0	23150
183	N2O+H<=>N2+OH	3.87E+14	0	18880
184	N2O+OH<=>N2+HO2	2.00E+12	0	21060
185	N2O(+M)<=>N2+O(+M)	7.91E+10	0	56020
186	HO2+NO<=>NO2+OH	2.11E+12	0	-480
187	NO+O+M<=>NO2+M	1.06E+20	-1.41	0
188	NO2+O<=>NO+O2	3.90E+12	0	-240
189	NO2+H<=>NO+OH	1.32E+14	0	360
190	NH+O<=>NO+H	4.00E+13	0	0
191	NH+H<=>N+H2	3.20E+13	0	330
192	NH+OH<=>HNO+H	2.00E+13	0	0
193	NH+OH<=>N+H2O	2.00E+09	1.2	0
194	NH+O2<=>HNO+O	4.61E+05	2	6500
195	NH+O2<=>NO+OH	1.28E+06	1.5	100
196	NH+N<=>N2+H	1.50E+13	0	0
197	NH+H2O<=>HNO+H2	2.00E+13	0	13850
198	NH+NO<=>N2+OH	2.16E+13	-0.23	0
199	NH+NO<=>N2O+H	3.65E+14	-0.45	0
200	NH2+O<=>OH+NH	3.00E+12	0	0
201	NH2+O<=>H+HNO	3.90E+13	0	0
202	NH2+H<=>NH+H2	4.00E+13	0	3650
203	NH2+OH<=>NH+H2O	9.00E+07	1.5	-460
204	NNH<=>N2+H	3.30E+08	0	0

205	NNH+M<=>N2+H+M	1.30E+14	-0.11	4980
206	NNH+O2<=>HO2+N2	5.00E+12	0	0
207	NNH+O<=>OH+N2	2.50E+13	0	0
208	NNH+O<=>NH+NO	7.00E+13	0	0
209	NNH+H<=>H2+N2	5.00E+13	0	0
210	NNH+OH<=>H2O+N2	2.00E+13	0	0
211	NNH+CH3<=>CH4+N2	2.50E+13	0	0
212	H+NO+M<=>HNO+M	4.48E+19	-1.32	740
213	HNO+O<=>NO+OH	2.50E+13	0	0
214	HNO+H<=>H2+NO	9.00E+11	0.72	660
215	HNO+OH<=>NO+H2O	1.30E+07	1.9	-950
216	HNO+O2<=>HO2+NO	1.00E+13	0	13000
217	CN+O<=>CO+N	7.70E+13	0	0
218	CN+OH<=>NCO+H	4.00E+13	0	0
219	CN+H2O<=>HCN+OH	8.00E+12	0	7460
220	CN+O2<=>NCO+O	6.14E+12	0	-440
221	CN+H2<=>HCN+H	2.95E+05	2.45	2240
222	NCO+O<=>NO+CO	2.35E+13	0	0
223	NCO+H<=>NH+CO	5.40E+13	0	0
224	NCO+OH<=>NO+H+CO	2.50E+12	0	0
225	NCO+N<=>N2+CO	2.00E+13	0	0
226	NCO+O2<=>NO+CO2	2.00E+12	0	20000
227	NCO+M<=>N+CO+M	3.10E+14	0	54050
228	NCO+NO<=>N2O+CO	1.90E+17	-1.52	740
229	NCO+NO<=>N2+CO2	3.80E+18	-2	800
230	HCN+M<=>H+CN+M	1.04E+29	-3.3	126600
231	HCN+O<=>NCO+H	2.03E+04	2.64	4980
232	HCN+O<=>NH+CO	5.07E+03	2.64	4980
233	HCN+O<=>CN+OH	3.91E+09	1.58	26600
234	HCN+OH<=>HOCN+H	1.10E+06	2.03	13370
235	HCN+OH<=>HNCO+H	4.40E+03	2.26	6400
236	HCN+OH<=>NH2+CO	1.60E+02	2.56	9000
237	H+HCN(+M)<=>H2CN(+M)	3.30E+13	0	0
238	H2CN+N<=>N2+CH2	6.00E+13	0	400
239	C+N2<=>CN+N	6.30E+13	0	46020
240	CH+N2<=>HCN+N	3.12E+09	0.88	20130
241	CH+N2(+M)<=>HCNN(+M)	3.10E+12	0.15	0
242	CH2+N2<=>HCN+NH	1.00E+13	0	74000
243	CH2(S)+N2<=>NH+HCN	1.00E+11	0	65000
244	C+NO<=>CN+O	1.90E+13	0	0
245	C+NO<=>CO+N	2.90E+13	0	0
246	CH+NO<=>HCN+O	4.10E+13	0	0
247	CH+NO<=>H+NCO	1.62E+13	0	0
248	CH+NO<=>N+HCO	2.46E+13	0	0
249	CH2+NO<=>H+HNCO	3.10E+17	-1.38	1270

250	CH2+NO<=>OH+HCN	2.90E+14	-0.69	760
251	CH2+NO<=>H+HCNO	3.80E+13	-0.36	580
252	CH2(S)+NO<=>H+HNCO	3.10E+17	-1.38	1270
253	CH2(S)+NO<=>OH+HCN	2.90E+14	-0.69	760
254	CH2(S)+NO<=>H+HCNO	3.80E+13	-0.36	580
255	CH3+NO<=>HCN+H2O	9.60E+13	0	28800
256	CH3+NO<=>H2CN+OH	1.00E+12	0	21750
257	HCNN+O<=>CO+H+N2	2.20E+13	0	0
258	HCNN+O<=>HCN+NO	2.00E+12	0	0
259	HCNN+O2<=>O+HCO+N2	1.20E+13	0	0
260	HCNN+OH<=>H+HCO+N2	1.20E+13	0	0
261	HCNN+H<=>CH2+N2	1.00E+14	0	0
262	HNCO+O<=>NH+CO2	9.80E+07	1.41	8500
263	HNCO+O<=>HNO+CO	1.50E+08	1.57	44000
264	HNCO+O<=>NCO+OH	2.20E+06	2.11	11400
265	HNCO+H<=>NH2+CO	2.25E+07	1.7	3800
266	HNCO+H<=>H2+NCO	1.05E+05	2.5	13300
267	HNCO+OH<=>NCO+H2O	3.30E+07	1.5	3600
268	HNCO+OH<=>NH2+CO2	3.30E+06	1.5	3600
269	HNCO+M<=>NH+CO+M	1.18E+16	0	84720
270	HCNO+H<=>H+HNCO	2.10E+15	-0.69	2850
271	HCNO+H<=>OH+HCN	2.70E+11	0.18	2120
272	HCNO+H<=>NH2+CO	1.70E+14	-0.75	2890
273	HOCN+H<=>H+HNCO	2.00E+07	2	2000
274	HCCO+NO<=>HCNO+CO	9.00E+12	0	0
275	CH3+N<=>H2CN+H	6.10E+14	-0.31	290
276	CH3+N<=>HCN+H2	3.70E+12	0.15	-90
277	NH3+H<=>NH2+H2	5.40E+05	2.4	9915
278	NH3+OH<=>NH2+H2O	5.00E+07	1.6	955
279	NH3+O<=>NH2+OH	9.40E+06	1.94	6460
280	NH+CO2<=>HNO+CO	1.00E+13	0	14350
281	CN+NO2<=>NCO+NO	6.16E+15	-0.75	345
282	NCO+NO2<=>N2O+CO2	3.25E+12	0	-705
283	N+CO2<=>NO+CO	3.00E+12	0	11300
284	O+CH3<=>H+H2+CO	3.37E+13	0	0
285	O+C2H4<=>H+CH2CHO	6.70E+06	1.83	220
286	O+C2H5<=>H+CH3CHO	1.10E+14	0	0
288	OH+CH3<=>H2+CH2O	8.00E+09	0.5	-1755
289	CH+H2(+M)<=>CH3(+M)	1.97E+12	0.43	-370
290	CH2+O2<=>2H+CO2	5.80E+12	0	1500
291	CH2+O2<=>O+CH2O	2.40E+12	0	1500
292	CH2+CH2<=>2H+C2H2	2.00E+14	0	10989
293	CH2(S)+H2O<=>H2+CH2O	6.82E+10	0.25	-935
294	C2H3+O2<=>O+CH2CHO	3.03E+11	0.29	11
295	C2H3+O2<=>HO2+C2H2	1.34E+06	1.61	-384

296	O+CH3CHO<=>OH+CH2CHO	2.92E+12	0	1808
297	O+CH3CHO<=>OH+CH3+CO	2.92E+12	0	1808
298	O2+CH3CHO<=>HO2+CH3+CO	3.01E+13	0	39150
299	H+CH3CHO<=>CH2CHO+H2	2.05E+09	1.16	2405
300	H+CH3CHO<=>CH3+H2+CO	2.05E+09	1.16	2405
301	OH+CH3CHO<=>CH3+H2O+CO	2.34E+10	0.73	-1113
302	HO2+CH3CHO<=>CH3+H2O2+CO	3.01E+12	0	11923
303	CH3+CH3CHO<=>CH3+CH4+CO	2.72E+06	1.77	5920
304	H+CH2CO(+M)<=>CH2CHO(+M)	4.86E+11	0.42	-1755
305	O+CH2CHO<=>H+CH2+CO2	1.50E+14	0	0
306	O2+CH2CHO<=>OH+CO+CH2O	1.81E+10	0	0
307	O2+CH2CHO<=>OH+2HCO	2.35E+10	0	0
308	H+CH2CHO<=>CH3+HCO	2.20E+13	0	0
309	H+CH2CHO<=>CH2CO+H2	1.10E+13	0	0
310	OH+CH2CHO<=>H2O+CH2CO	1.20E+13	0	0
311	OH+CH2CHO<=>HCO+CH2OH	3.01E+13	0	0
312	CH3+C2H5(+M)<=>C3H8(+M)	9.43E+12	0	0
313	O+C3H8<=>OH+C3H7	1.93E+05	2.68	3716
314	H+C3H8<=>C3H7+H2	1.32E+06	2.54	6756
315	OH+C3H8<=>C3H7+H2O	3.16E+07	1.8	934
316	C3H7+H2O2<=>HO2+C3H8	3.78E+02	2.72	1500
317	CH3+C3H8<=>C3H7+CH4	9.03E-01	3.65	7154
318	CH3+C2H4(+M)<=>C3H7(+M)	2.55E+06	1.6	5700
319	O+C3H7<=>C2H5+CH2O	9.64E+13	0	0
320	H+C3H7(+M)<=>C3H8(+M)	3.61E+13	0	0
321	H+C3H7<=>CH3+C2H5	4.06E+06	2.19	890
322	OH+C3H7<=>C2H5+CH2OH	2.41E+13	0	0
323	HO2+C3H7<=>O2+C3H8	2.55E+10	0.26	-943
324	HO2+C3H7<=>OH+C2H5+CH2O	2.41E+13	0	0
325	CH3+C3H7<=>2C2H5	1.93E+13	-0.32	0
326	C7H16+H<=>C7H15-1+H2	5.60E+07	2	7667
327	C7H16+H<=>C7H15-2+H2	4.38E+07	2	4750
328	C7H16+OH<=>C7H15-1+H2O	8.61E+09	1.1	1815
329	C7H16+OH<=>C7H15-2+H2O	4.50E+09	1.3	690.5
330	C7H16+HO2<=>C7H15-1+H2O2	1.12E+13	0	19300
331	C7H16+HO2<=>C7H15-2+H2O2	1.65E+13	0	16950
332	C7H16+O2<=>C7H15-1+HO2	2.50E+13	0	48810
333	C7H16+O2<=>C7H15-2+HO2	2.00E+14	0	47380
334	C7H15-1+O2<=>C7H15O2	2.00E+12	0	0
335	C7H15-2+O2<=>C7H15O2	2.00E+12	0	0
336	C7H15O2<=>C7H14O2H	6.00E+11	0	20380
337	C7H14O2H+O2<=>C7H14O2HO2	4.60E+11	0	0
338	C7H14O2HO2<=>C7KET12+OH	1.00E+09	0	7480
339	C7KET12<=>C5H11CHO+CH2O+O	1.05E+16	0	41100
340	C5H11CHO+O2<=>C5H11CO+HO2	2.00E+13	0.5	42200

341	C5H11CHO+OH<=>C5H11CO+H2O	1.00E+13	0	0
342	C5H11CHO+H<=>C5H11CO+H2	4.00E+13	0	4200
343	C5H11CHO+O<=>C5H11CO+OH	5.00E+12	0	1790
344	C5H11CHO+HO2<=>C5H11CO+H2O2	2.80E+12	0	13600
345	C5H11CHO+CH3<=>C5H11CO+CH4	1.70E+12	0	8440
346	C5H11CHO+CH3O2<=>C5H11CO+CH4O2	1.00E+12	0	9500
347	C5H11CO<=>C5H11+CO	1.00E+11	0	9600
348	C5H11<=>C2H4+C3H7	3.20E+13	0	28300
349	C7H15-1<=>C2H4+C5H11	2.50E+13	0	28810
350	C7H15-2<=>C4H9+C3H6	2.20E+13	0	28100
351	C7H15-1<=>C7H15-2	3.60E+16	0	80700
352	C4H9<=>C2H5+C2H4	2.50E+13	0	28810
353	C3H7<=>C2H4+CH3	9.60E+13	0	30950
354	C3H7<=>C3H6+H	1.25E+14	0	36900
355	C3H7+O2<=>C3H6+HO2	1.00E+12	0	4980
356	C3H6<=>C2H3+CH3	3.15E+15	0	85500
357	C3H6+H<=>C3H5+H2	5.00E+12	0	1500
358	C3H6+CH3<=>C3H5+CH4	9.00E+12	0	8480
359	C3H5<=>C3H4+H	4.00E+13	0	69760
360	C3H5+H<=>C3H4+H2	1.00E+13	0	0
361	C3H5+O2<=>C3H4+HO2	6.00E+11	0	10000
362	C3H4+OH<=>C2H3+CH2O	1.00E+12	0	0
363	C3H4+OH<=>C2H4+HCO	1.00E+12	0	0
364	CH3O+CO<=>CH3+CO2	1.57E+14	0	11800
365	CH3+O2<=>CH3O2	3.02E+59	-15	17204
366	CH3O2+HO2<=>CH4O2+O2	4.63E+11	0	-2583
367	CH3O2+CH4<=>CH4O2+CH3	1.81E+11	0	18480
368	CH3O2+CH3<=>CH3O+CH3O	2.41E+13	0	0
369	CH3O2+O<=>CH3O+O2	3.61E+13	0	0
370	CH3O2+H<=>CH3O+OH	9.64E+13	0	0
371	CH3O2+CH2O<=>CH4O2+HCO	1.00E+12	0	11665
372	CH3O2+C2H6<=>CH4O2+C2H5	2.95E+11	0	14944
373	CH3O2+CH3O2<=>CH3O+CH3O+O2	2.80E+11	0	-780
374	CH3O2+H2O2<=>CH4O2+HO2	2.40E+12	0	10000
375	CH4O2<=>CH3O+OH	3.00E+16	0	42920
376	CH3O2+C2H4<=>C2H3+CH4O2	7.10E+11	0	17110
377	CH4O2+OH<=>CH3O2+H2O	1.00E+13	0	-258
378	CH4O2+O<=>CH3O2+OH	2.00E+13	0	4750
379	CH3+OH<=>CH2O+H2	4.00E+12	0	0
380	CO+O2<=>CO2+O	1.60E+13	0	41000
381	H2+O2<=>OH+OH	1.70E+13	0	47780
382	O+OH+M<=>HO2+M	1.00E+16	0	0
383	H+HO2<=>OH+OH	1.70E+14	0	875
384	OH+OH<=>O+H2O	6.00E+08	1.3	0
385	H+H+M<=>H2+M	1.00E+18	-1	0

386	H+H+H2<=>H2+H2	9.20E+16	-0.6	0
387	H+H+H2O<=>H2+H2O	6.00E+19	-1.25	0
388	H+H+CO2<=>H2+CO2	5.49E+20	-2	0
389	O+O+M<=>O2+M	1.89E+13	0	-1788
390	HO2+HO2<=>H2O2+O2	2.00E+12	0	0
391	H2O2+M<=>OH+OH+M	4.30E+16	0	45500
392	H2O2+O<=>H2O+O2	8.40E+11	0	4260
393	H2+HO2<=>H2O+OH	6.50E+11	0	18800
394	HCO+HCO<=>CH2O+CO	3.01E+13	0	0
395	HCO+HO2<=>CO2+OH+H	3.00E+13	0	0
396	CH4+CH2<=>CH3+CH3	4.00E+12	0	-570
397	CH3+H<=>CH4	1.90E+36	-7	9050
398	CH3+CH3O<=>CH4+CH2O	4.30E+14	0	0
399	CH3+CH3<=>C2H6	2.70E+53	-12	19400
400	CH3+CH3<=>C2H5+H	4.99E+12	0.1	10600
401	CH2+O2<=>HCO+OH	4.30E+10	0	-500
402	CH2+O2<=>CO2+H2	6.90E+11	0	500
403	CH2+O2<=>CO+H2O	2.00E+10	0	-1000
404	CH2+O2<=>CO2+H+H	1.60E+12	0	1000
405	CH2+CH2<=>C2H2+H2	1.20E+13	0	800
406	CH2+CH2<=>C2H2+H+H	1.20E+14	0	800
407	CH2+CO2<=>CH2O+CO	1.00E+11	0	1000
408	CH3+HCO<=>CH2O+CH2	3.00E+13	0	0
409	CH3+CH3<=>C2H4+H2	1.00E+15	0	31000
410	C2H4+O<=>CH2O+CH2	3.00E+04	1.88	180
411	C2H4+O<=>C2H3+OH	1.51E+07	1.91	3790
412	C2H4+OH<=>CH2O+CH3	6.00E+13	0	960
413	C2H4+HO2<=>C2H3+H2O2	7.10E+11	0	17110
414	C2H4+H<=>C2H5	2.60E+43	-9.25	52580
415	C2H6+O2<=>C2H5+HO2	1.00E+13	0	48960
416	C2H4+O2<=>C2H3+HO2	4.20E+14	0	57590
417	C2H4+C2H4<=>C2H5+C2H3	5.00E+14	0	64700
418	C2H5+HO2<=>C2H4+H2O2	3.00E+11	0	0
419	C2H2+O2<=>HCO+HCO	4.00E+12	0	28000
420	C2H3+CH2<=>C2H2+CH3	3.00E+13	0	0
421	C2H3+HCO<=>C2H4+CO	6.03E+13	0	0
422	C2H3+C2H3<=>C2H2+C2H4	1.45E+13	0	0
423	C2H3+O<=>C2H2+OH	1.00E+13	0	0
424	C2H3<=>C2H2+H	4.60E+40	-8.8	46200

D Methane Fuel Analysis

DTE Energy

DTE Gas
Laboratory Services
Gas Analysis Report

17150 Allen Road
Melvindale, MI 48122
P: (313) 389-7354 F: (313) 389-7757

Customer:
FEV, Inc.
4554 Glenmeade Lane
Auburn Hills, MI 48326
(248) 802-2301

Date Analyzed:	2/12/2015		
Lab Run No.:	GQR_FEV Inc Auburn Hills_021015		
LOCATION:	FEV Inc. Auburn Hills	**DATE SAMPLED:**	2/10/2015
REQUESTOR:	[redacted]	**DATE RECEIVED:**	2/10/2015
METER NO.:	FEV	**GAS TEMP. (°F):**	N/A
FORMATION:	Niagaran	**GAS PRESSURE (psig):**	220
SAMPLE PT.:	CNG Gas	**SAMPLED BY:**	DO

ANALYTICAL RESULTS

GAS ANALYSIS

	MOL %
Nitrogen	0.665
Methane	95.537
Carbon Dioxide	1.432
Ethane	2.131
Propane	0.156
I-Butane	0.025
N-Butane	0.030
I-Pentane	0.010
N-Pentane	0.007
Hexanes	0.007
Heptanes	<0.001
Octanes	<0.001
Nonane	<0.001
TOTAL:	**100.000**

GROSS HEATING VALUE (BTU/SCF)

	14.65 DRY	14.73 DRY
Calculated (Real)	1008	1014

SPECIFIC GRAVITY

Calculated (Real)	0.5846

REMARKS: Gas Sampling Method: GPA 2166 / API 14.1 Section 1
Gas Analysis Method: GPA 2286

ANALYZED BY: [redacted]
AUTHOR : [redacted]
APPROVED BY: [redacted]

A2LA ACCREDITED
Testing Cert. No. 2811.01

E Copyright documentation

E.1 SAE Technical Paper 2014-01-1308

SAE International LICENSE TERMS AND CONDITIONS

Oct 05, 2018

This is a License Agreement between Mufaddel Z Dahodwala ("You") and SAE International ("SAE International") provided by Copyright Clearance Center ("CCC"). The license consists of your order details, the terms and conditions provided by SAE International, and the payment terms and conditions.

All payments must be made in full to CCC. For payment instructions, please see information listed at the bottom of this form.

License Number	4442540417698
License date	Sep 22, 2018
Licensed content publisher	SAE International
Licensed content title	Experimental and Computational Analysis of Diesel-Natural Gas RCCI Combustion in Heavy-Duty Engines
Licensed content date	Jan 1, 2015
Type of Use	Thesis/Dissertation
Requestor type	Author of requested content
Format	Print, Electronic
Portion	chapter/article
The requesting person/organization is:	Mufaddel Dahodwala
Title or numeric reference of the portion(s)	Text from Results and Discussion section, Table 3, Table 4, Figure 4, Figure 5, Figure 6, Figure 7, Figure 8, Figure 9, Figure 10, Figure 11, Figure 21, Figure 22, Figure 23, Figure 24, Figure 25, Figure 26, Figure 27
Title of the article or chapter the portion is from	Experimental and Computational Analysis of Diesel-Natural Gas RCCI Combustion in Heavy-Duty Engines
Editor of portion(s)	Mufaddel Dahodwala
Author of portion(s)	Mufaddel Dahodwala
Volume of serial or monograph.	NA

Page range of the portion	
Publication date of portion	04/14/2015
Rights for	Main product
Duration of use	Life of current and all future editions
Creation of copies for the disabled	no
With minor editing privileges	no
For distribution to	Worldwide
In the following language(s)	Original language of publication
With incidental promotional use	no
The lifetime unit quantity of new product	Up to 499
Title	EXPERIMENTAL AND COMPUTATIONAL INVESTIGATION OF DUAL FUEL DIESEL- NATURAL GAS RCCI COMBUSTION IN A HEAVY-DUTY DIESEL ENGINE
Instructor name	Dr. Jeffrey Naber
Institution name	Michigan Technological University
Expected presentation date	Nov 2018
Attachment	CCC- Order 501430624.pdf
Billing Type	Invoice
Billing Address	Mufaddel Z Dahodwala 7334 CREEK VIEW CT West Bloomfield, MI 48322 United States Attn: Mufaddel Z Dahodwala
Total (may include CCC user fee)	0.00 USD
Terms and Conditions	

TERMS AND CONDITIONS

The following terms are individual to this publisher:

None

Other Terms and Conditions:

STANDARD TERMS AND CONDITIONS

1. Description of Service; Defined Terms. This Republication License enables the User to obtain licenses for republication of one or more copyrighted works as described in detail on the relevant Order Confirmation (the "Work(s)"). Copyright Clearance Center, Inc. ("CCC") grants licenses through the Service on behalf of the rightsholder identified on the Order Confirmation (the "Rightsholder"). "Republication", as used herein, generally means the inclusion of a Work, in whole or in part, in a new work or works, also as described on the Order Confirmation. "User", as used herein, means the person or entity making such republication.

2. The terms set forth in the relevant Order Confirmation, and any terms set by the Rightsholder with respect to a particular Work, govern the terms of use of Works in connection with the Service. By using the Service, the person transacting for a republication license on behalf of the User represents and warrants that he/she/it (a) has been duly authorized by the User to accept, and hereby does accept, all such terms and conditions on behalf of User, and (b) shall inform User of all such terms and conditions. In the event such person is a "freelancer" or other third party independent of User and CCC, such party shall be deemed jointly a "User" for purposes of these terms and conditions. In any event, User shall be deemed to have accepted and agreed to all such terms and conditions if User republishes the Work in any fashion.

3. Scope of License; Limitations and Obligations.

3.1 All Works and all rights therein, including copyright rights, remain the sole and exclusive property of the Rightsholder. The license created by the exchange of an Order Confirmation (and/or any invoice) and payment by User of the full amount set forth on that document includes only those rights expressly set forth in the Order Confirmation and in these terms and conditions, and conveys no other rights in the Work(s) to User. All rights not expressly granted are hereby reserved.

3.2 General Payment Terms: You may pay by credit card or through an account with us payable at the end of the month. If you and we agree that you may establish a standing account with CCC, then the following terms apply: Remit Payment to: Copyright Clearance Center, 29118 Network Place, Chicago, IL 60673-1291. Payments Due: Invoices are payable upon their delivery to you (or upon our notice to you that they are available to you for downloading). After 30 days, outstanding amounts will be subject to a service charge of 1-1/2% per month or, if less, the maximum rate allowed by applicable law. Unless otherwise specifically set forth in the Order Confirmation or in a separate written agreement signed by CCC, invoices are due and payable on "net 30" terms. While User may exercise the rights licensed immediately upon issuance of the Order Confirmation, the license is automatically revoked and is null and void, as if it had never been

issued, if complete payment for the license is not received on a timely basis either from User directly or through a payment agent, such as a credit card company.

3.3 Unless otherwise provided in the Order Confirmation, any grant of rights to User (i) is "one-time" (including the editions and product family specified in the license), (ii) is non-exclusive and non-transferable and (iii) is subject to any and all limitations and restrictions (such as, but not limited to, limitations on duration of use or circulation) included in the Order Confirmation or invoice and/or in these terms and conditions. Upon completion of the licensed use, User shall either secure a new permission for further use of the Work(s) or immediately cease any new use of the Work(s) and shall render inaccessible (such as by deleting or by removing or severing links or other locators) any further copies of the Work (except for copies printed on paper in accordance with this license and still in User's stock at the end of such period).

3.4 In the event that the material for which a republication license is sought includes third party materials (such as photographs, illustrations, graphs, inserts and similar materials) which are identified in such material as having been used by permission, User is responsible for identifying, and seeking separate licenses (under this Service or otherwise) for, any of such third party materials; without a separate license, such third party materials may not be used.

3.5 Use of proper copyright notice for a Work is required as a condition of any license granted under the Service. Unless otherwise provided in the Order Confirmation, a proper copyright notice will read substantially as follows: "Republished with permission of [Rightsholder's name], from [Work's title, author, volume, edition number and year of copyright]; permission conveyed through Copyright Clearance Center, Inc. " Such notice must be provided in a reasonably legible font size and must be placed either immediately adjacent to the Work as used (for example, as part of a by-line or footnote but not as a separate electronic link) or in the place where substantially all other credits or notices for the new work containing the republished Work are located. Failure to include the required notice results in loss to the Rightsholder and CCC, and the User shall be liable to pay liquidated damages for each such failure equal to twice the use fee specified in the Order Confirmation, in addition to the use fee itself and any other fees and charges specified.

3.6 User may only make alterations to the Work if and as expressly set forth in the Order Confirmation. No Work may be used in any way that is defamatory, violates the rights of third parties (including such third parties' rights of copyright, privacy, publicity, or other tangible or intangible property), or is otherwise illegal, sexually explicit or obscene. In addition, User may not conjoin a Work with any other material that may result in damage to the reputation of the Rightsholder. User agrees to inform CCC if it becomes aware of any infringement of any rights

in a Work and to cooperate with any reasonable request of CCC or the Rightsholder in connection therewith.

4. Indemnity. User hereby indemnifies and agrees to defend the Rightsholder and CCC, and their respective employees and directors, against all claims, liability, damages, costs and expenses, including legal fees and expenses, arising out of any use of a Work beyond the scope of the rights granted herein, or any use of a Work which has been altered in any unauthorized way by User, including claims of defamation or infringement of rights of copyright, publicity, privacy or other tangible or intangible property.

5. Limitation of Liability. UNDER NO CIRCUMSTANCES WILL CCC OR THE RIGHTSHOLDER BE LIABLE FOR ANY DIRECT, INDIRECT, CONSEQUENTIAL OR INCIDENTAL DAMAGES (INCLUDING WITHOUT LIMITATION DAMAGES FOR LOSS OF BUSINESS PROFITS OR INFORMATION, OR FOR BUSINESS INTERRUPTION) ARISING OUT OF THE USE OR INABILITY TO USE A WORK, EVEN IF ONE OF THEM HAS BEEN ADVISED OF THE POSSIBILITY OF SUCH DAMAGES. In any event, the total liability of the Rightsholder and CCC (including their respective employees and directors) shall not exceed the total amount actually paid by User for this license. User assumes full liability for the actions and omissions of its principals, employees, agents, affiliates, successors and assigns.

6. Limited Warranties. THE WORK(S) AND RIGHT(S) ARE PROVIDED “AS IS”. CCC HAS THE RIGHT TO GRANT TO USER THE RIGHTS GRANTED IN THE ORDER CONFIRMATION DOCUMENT. CCC AND THE RIGHTSHOLDER DISCLAIM ALL OTHER WARRANTIES RELATING TO THE WORK(S) AND RIGHT(S), EITHER EXPRESS OR IMPLIED, INCLUDING WITHOUT LIMITATION IMPLIED WARRANTIES OF MERCHANTABILITY OR FITNESS FOR A PARTICULAR PURPOSE. ADDITIONAL RIGHTS MAY BE REQUIRED TO USE ILLUSTRATIONS, GRAPHS, PHOTOGRAPHS, ABSTRACTS, INSERTS OR OTHER PORTIONS OF THE WORK (AS OPPOSED TO THE ENTIRE WORK) IN A MANNER CONTEMPLATED BY USER; USER UNDERSTANDS AND AGREES THAT NEITHER CCC NOR THE RIGHTSHOLDER MAY HAVE SUCH ADDITIONAL RIGHTS TO GRANT.

7. Effect of Breach. Any failure by User to pay any amount when due, or any use by User of a Work beyond the scope of the license set forth in the Order Confirmation and/or these terms and conditions, shall be a material breach of the license created by the Order Confirmation and these terms and conditions. Any breach not cured within 30 days of written notice thereof shall result in immediate termination of such license without further notice. Any unauthorized (but licensable) use of a Work that is terminated immediately upon notice thereof may

be liquidated by payment of the Rightsholder's ordinary license price therefor; any unauthorized (and unlicensable) use that is not terminated immediately for any reason (including, for example, because materials containing the Work cannot reasonably be recalled) will be subject to all remedies available at law or in equity, but in no event to a payment of less than three times the Rightsholder's ordinary license price for the most closely analogous licensable use plus Rightsholder's and/or CCC's costs and expenses incurred in collecting such payment.

8. **Miscellaneous.**

8.1 User acknowledges that CCC may, from time to time, make changes or additions to the Service or to these terms and conditions, and CCC reserves the right to send notice to the User by electronic mail or otherwise for the purposes of notifying User of such changes or additions; provided that any such changes or additions shall not apply to permissions already secured and paid for.

8.2 Use of User-related information collected through the Service is governed by CCC's privacy policy, available online here: http://www.copyright.com/content/cc3/en/tools/footer/privacypolicy.html.

8.3 The licensing transaction described in the Order Confirmation is personal to User. Therefore, User may not assign or transfer to any other person (whether a natural person or an organization of any kind) the license created by the Order Confirmation and these terms and conditions or any rights granted hereunder; provided, however, that User may assign such license in its entirety on written notice to CCC in the event of a transfer of all or substantially all of User's rights in the new material which includes the Work(s) licensed under this Service.

8.4 No amendment or waiver of any terms is binding unless set forth in writing and signed by the parties. The Rightsholder and CCC hereby object to any terms contained in any writing prepared by the User or its principals, employees, agents or affiliates and purporting to govern or otherwise relate to the licensing transaction described in the Order Confirmation, which terms are in any way inconsistent with any terms set forth in the Order Confirmation and/or in these terms and conditions or CCC's standard operating procedures, whether such writing is prepared prior to, simultaneously with or subsequent to the Order Confirmation, and whether such writing appears on a copy of the Order Confirmation or in a separate instrument.

8.5 The licensing transaction described in the Order Confirmation document shall be governed by and construed under the law of the State of New York, USA, without regard to the principles thereof of conflicts of law. Any case, controversy, suit, action, or proceeding arising out of, in connection with, or related to such licensing transaction shall be brought, at CCC's sole discretion, in any federal or

state court located in the County of New York, State of New York, USA, or in any federal or state court whose geographical jurisdiction covers the location of the Rightsholder set forth in the Order Confirmation. The parties expressly submit to the personal jurisdiction and venue of each such federal or state court.If you have any comments or questions about the Service or Copyright Clearance Center, please contact us at 978-750-8400 or send an e-mail to info@copyright.com.

v 1.1

Questions? customercare@copyright.com or +1-855-239-3415 (toll free in the US) or +1-978-646-2777.

E.2 SAE Technical Paper 2015-01-0849

SAE International LICENSE TERMS AND CONDITIONS

Oct 05, 2018

This is a License Agreement between Mufaddel Z Dahodwala ("You") and SAE International ("SAE International") provided by Copyright Clearance Center ("CCC"). The license consists of your order details, the terms and conditions provided by SAE International, and the payment terms and conditions.

All payments must be made in full to CCC. For payment instructions, please see information listed at the bottom of this form.

License Number	4442540289925
License date	Sep 22, 2018
Licensed content publisher	SAE International
Licensed content title	Investigation of Diesel and CNG Combustion in a Dual Fuel Regime and as an Enabler to Achieve RCCI Combustion
Licensed content date	Jan 1, 2014
Type of Use	Thesis/Dissertation
Requestor type	Author of requested content

Format	Print, Electronic
Portion	chapter/article
The requesting person/organization is:	Mufaddel Dahodwala
Title or numeric reference of the portion(s)	Text from 'Results and Discussions' section, Figure 3, Figure 4, Figure 6, Figure 8, Figure 10, Figure 11, Figure 12, Figure 13, Figure 14, Figure 15, Figure 16, Figure 17, Figure 18, Figure 19, Table 1
Title of the article or chapter the portion is from	Investigation of Diesel and CNG Combustion in a Dual Fuel Regime and as an Enabler to Achieve RCCI Combustion
Editor of portion(s)	Mufaddel Dahodwala
Author of portion(s)	Mufaddel Dahodwala
Volume of serial or monograph.	NA
Page range of the portion	
Publication date of portion	04/01/2014
Rights for	Main product
Duration of use	Life of current and all future editions
Creation of copies for the disabled	no
With minor editing privileges	no
For distribution to	Worldwide
In the following language(s)	Original language of publication
With incidental promotional use	no
The lifetime unit quantity of new product	Up to 499
Title	EXPERIMENTAL AND COMPUTATIONAL INVESTIGATION OF DUAL FUEL DIESEL- NATURAL GAS RCCI COMBUSTION IN A HEAVY-DUTY DIESEL ENGINE
Instructor name	Dr. Jeffrey Naber
Institution name	Michigan Technological University
Expected presentation date	Nov 2018
Attachment	CCC- Order 501430624.pdf
Billing Type	Invoice
Billing Address	Mufaddel Z Dahodwala 7334 CREEK VIEW CT West Bloomfield, MI 48322 United States Attn: Mufaddel Z Dahodwala

Total (may include CCC user fee) 0.00 USD

Terms and Conditions

TERMS AND CONDITIONS

The following terms are individual to this publisher:

None

Other Terms and Conditions:

STANDARD TERMS AND CONDITIONS

1. Description of Service; Defined Terms. This Republication License enables the User to obtain licenses for republication of one or more copyrighted works as described in detail on the relevant Order Confirmation (the "Work(s)"). Copyright Clearance Center, Inc. ("CCC") grants licenses through the Service on behalf of the rightsholder identified on the Order Confirmation (the "Rightsholder"). "Republication", as used herein, generally means the inclusion of a Work, in whole or in part, in a new work or works, also as described on the Order Confirmation. "User", as used herein, means the person or entity making such republication.

2. The terms set forth in the relevant Order Confirmation, and any terms set by the Rightsholder with respect to a particular Work, govern the terms of use of Works in connection with the Service. By using the Service, the person transacting for a republication license on behalf of the User represents and warrants that he/she/it (a) has been duly authorized by the User to accept, and hereby does accept, all such terms and conditions on behalf of User, and (b) shall inform User of all such terms and conditions. In the event such person is a "freelancer" or other third party independent of User and CCC, such party shall be deemed jointly a "User" for purposes of these terms and conditions. In any event, User shall be deemed to have accepted and agreed to all such terms and conditions if User republishes the Work in any fashion.

3. Scope of License; Limitations and Obligations.

3.1 All Works and all rights therein, including copyright rights, remain the sole and exclusive property of the Rightsholder. The license created by the exchange of an Order Confirmation (and/or any invoice) and payment by User of the full amount set forth on that document includes only those rights expressly set forth in the Order Confirmation and in these terms and conditions, and conveys no other rights in the Work(s) to User. All rights not expressly granted are hereby reserved.

3.2 General Payment Terms: You may pay by credit card or through an account with us payable at the end of the month. If you and we agree that you may establish a standing account with CCC, then the following terms apply: Remit Payment to: Copyright Clearance Center, 29118 Network Place, Chicago, IL 60673-1291. Payments Due: Invoices are payable upon their delivery to you (or upon our notice to you that they are available to you for downloading). After 30 days, outstanding amounts will be subject to a service charge of 1-1/2% per month or, if less, the maximum rate allowed by applicable law. Unless otherwise specifically set forth in the Order Confirmation or in a separate written agreement signed by CCC, invoices are due and payable on "net 30" terms. While User may exercise the rights licensed immediately upon issuance of the Order Confirmation, the license is automatically revoked and is null and void, as if it had never been issued, if complete payment for the license is not received on a timely basis either from User directly or through a payment agent, such as a credit card company.

3.3 Unless otherwise provided in the Order Confirmation, any grant of rights to User (i) is "one-time" (including the editions and product family specified in the license), (ii) is non-exclusive and non-transferable and (iii) is subject to any and all limitations and restrictions (such as, but not limited to, limitations on duration of use or circulation) included in the Order Confirmation or invoice and/or in these terms and conditions. Upon completion of the licensed use, User shall either secure a new permission for further use of the Work(s) or immediately cease any new use of the Work(s) and shall render inaccessible (such as by deleting or by removing or severing links or other locators) any further copies of the Work (except for copies printed on paper in accordance with this license and still in User's stock at the end of such period).

3.4 In the event that the material for which a republication license is sought includes third party materials (such as photographs, illustrations, graphs, inserts and similar materials) which are identified in such material as having been used by permission, User is responsible for identifying, and seeking separate licenses (under this Service or otherwise) for, any of such third party materials; without a separate license, such third party materials may not be used.

3.5 Use of proper copyright notice for a Work is required as a condition of any license granted under the Service. Unless otherwise provided in the Order Confirmation, a proper copyright notice will read substantially as follows: "Republished with permission of [Rightsholder's name], from [Work's title, author, volume, edition number and year of copyright]; permission conveyed through Copyright Clearance Center, Inc. " Such notice must be provided in a reasonably legible font size and must be placed either immediately adjacent to the Work as used (for example, as part of a by-line or footnote but not as a separate electronic link) or in the place where substantially all other credits or notices for the new work containing the republished Work are located. Failure to include the required

notice results in loss to the Rightsholder and CCC, and the User shall be liable to pay liquidated damages for each such failure equal to twice the use fee specified in the Order Confirmation, in addition to the use fee itself and any other fees and charges specified.

3.6 User may only make alterations to the Work if and as expressly set forth in the Order Confirmation. No Work may be used in any way that is defamatory, violates the rights of third parties (including such third parties' rights of copyright, privacy, publicity, or other tangible or intangible property), or is otherwise illegal, sexually explicit or obscene. In addition, User may not conjoin a Work with any other material that may result in damage to the reputation of the Rightsholder. User agrees to inform CCC if it becomes aware of any infringement of any rights in a Work and to cooperate with any reasonable request of CCC or the Rightsholder in connection therewith.

4. Indemnity. User hereby indemnifies and agrees to defend the Rightsholder and CCC, and their respective employees and directors, against all claims, liability, damages, costs and expenses, including legal fees and expenses, arising out of any use of a Work beyond the scope of the rights granted herein, or any use of a Work which has been altered in any unauthorized way by User, including claims of defamation or infringement of rights of copyright, publicity, privacy or other tangible or intangible property.

5. Limitation of Liability. UNDER NO CIRCUMSTANCES WILL CCC OR THE RIGHTSHOLDER BE LIABLE FOR ANY DIRECT, INDIRECT, CONSEQUENTIAL OR INCIDENTAL DAMAGES (INCLUDING WITHOUT LIMITATION DAMAGES FOR LOSS OF BUSINESS PROFITS OR INFORMATION, OR FOR BUSINESS INTERRUPTION) ARISING OUT OF THE USE OR INABILITY TO USE A WORK, EVEN IF ONE OF THEM HAS BEEN ADVISED OF THE POSSIBILITY OF SUCH DAMAGES. In any event, the total liability of the Rightsholder and CCC (including their respective employees and directors) shall not exceed the total amount actually paid by User for this license. User assumes full liability for the actions and omissions of its principals, employees, agents, affiliates, successors and assigns.

6. Limited Warranties. THE WORK(S) AND RIGHT(S) ARE PROVIDED “AS IS”. CCC HAS THE RIGHT TO GRANT TO USER THE RIGHTS GRANTED IN THE ORDER CONFIRMATION DOCUMENT. CCC AND THE RIGHTSHOLDER DISCLAIM ALL OTHER WARRANTIES RELATING TO THE WORK(S) AND RIGHT(S), EITHER EXPRESS OR IMPLIED, INCLUDING WITHOUT LIMITATION IMPLIED WARRANTIES OF MERCHANTABILITY OR FITNESS FOR A PARTICULAR PURPOSE. ADDITIONAL RIGHTS MAY BE REQUIRED TO USE ILLUSTRATIONS, GRAPHS, PHOTOGRAPHS, ABSTRACTS, INSERTS OR OTHER PORTIONS

OF THE WORK (AS OPPOSED TO THE ENTIRE WORK) IN A MANNER CONTEMPLATED BY USER; USER UNDERSTANDS AND AGREES THAT NEITHER CCC NOR THE RIGHTSHOLDER MAY HAVE SUCH ADDITIONAL RIGHTS TO GRANT.

7. Effect of Breach. Any failure by User to pay any amount when due, or any use by User of a Work beyond the scope of the license set forth in the Order Confirmation and/or these terms and conditions, shall be a material breach of the license created by the Order Confirmation and these terms and conditions. Any breach not cured within 30 days of written notice thereof shall result in immediate termination of such license without further notice. Any unauthorized (but licensable) use of a Work that is terminated immediately upon notice thereof may be liquidated by payment of the Rightsholder's ordinary license price therefor; any unauthorized (and unlicensable) use that is not terminated immediately for any reason (including, for example, because materials containing the Work cannot reasonably be recalled) will be subject to all remedies available at law or in equity, but in no event to a payment of less than three times the Rightsholder's ordinary license price for the most closely analogous licensable use plus Rightsholder's and/or CCC's costs and expenses incurred in collecting such payment.

8. **Miscellaneous.**

8.1 User acknowledges that CCC may, from time to time, make changes or additions to the Service or to these terms and conditions, and CCC reserves the right to send notice to the User by electronic mail or otherwise for the purposes of notifying User of such changes or additions; provided that any such changes or additions shall not apply to permissions already secured and paid for.

8.2 Use of User-related information collected through the Service is governed by CCC's privacy policy, available online here: http://www.copyright.com/content/cc3/en/tools/footer/privacypolicy.html.

8.3 The licensing transaction described in the Order Confirmation is personal to User. Therefore, User may not assign or transfer to any other person (whether a natural person or an organization of any kind) the license created by the Order Confirmation and these terms and conditions or any rights granted hereunder; provided, however, that User may assign such license in its entirety on written notice to CCC in the event of a transfer of all or substantially all of User's rights in the new material which includes the Work(s) licensed under this Service.

8.4 No amendment or waiver of any terms is binding unless set forth in writing and signed by the parties. The Rightsholder and CCC hereby object to any terms contained in any writing prepared by the User or its principals, employees, agents or affiliates and purporting to govern or otherwise relate to the licensing transaction

described in the Order Confirmation, which terms are in any way inconsistent with any terms set forth in the Order Confirmation and/or in these terms and conditions or CCC's standard operating procedures, whether such writing is prepared prior to, simultaneously with or subsequent to the Order Confirmation, and whether such writing appears on a copy of the Order Confirmation or in a separate instrument.

8.5 The licensing transaction described in the Order Confirmation document shall be governed by and construed under the law of the State of New York, USA, without regard to the principles thereof of conflicts of law. Any case, controversy, suit, action, or proceeding arising out of, in connection with, or related to such licensing transaction shall be brought, at CCC's sole discretion, in any federal or state court located in the County of New York, State of New York, USA, or in any federal or state court whose geographical jurisdiction covers the location of the Rightsholder set forth in the Order Confirmation. The parties expressly submit to the personal jurisdiction and venue of each such federal or state court.If you have any comments or questions about the Service or Copyright Clearance Center, please contact us at 978-750-8400 or send an e-mail to info@copyright.com.

v 1.1

Questions? customercare@copyright.com or +1-855-239-3415 (toll free in the US) or +1-978-646-2777.